INSIGHT INTO STRUCTURE-REACTIVITY RELATIONSHIPS AND REACTION PATHWAYS FOR HIGHER ALCOHOL SYNTHESIS FROM SYNGAS OVER POTASSIUM PROMOTED MOLYBDENUM SULFIDE SUPPORTED CATALYSTS

A Dissertation
Presented to
The Academic Faculty

By

Micaela Taborga Claure

In Partial Fulfillment
of the Requirements for the Degree
Doctor of Philosophy in Chemical Engineering

Georgia Institute of Technology

August 2016

INSIGHT INTO STRUCTURE-REACTIVITY RELATIONSHIPS AND REACTION PATHWAYS FOR HIGHER ALCOHOL SYNTHESIS FROM SYNGAS OVER POTASSIUM PROMOTED MOLYBDENUM SULFIDE SUPPORTED CATALYSTS

Approved by:

Dr. Christopher W. Jones, Co-Advisor
School of Chemical & Biomolecular Engineering
Georgia Institute of Technology

Dr. Pradeep K. Agrawal, Co-Advisor
School of Chemical & Biomolecular Engineering
Georgia Institute of Technology

Dr. David S. Sholl
School of Chemical & Biomolecular Engineering
Georgia Institute of Technology

Dr. Michael A. Filler
School of Chemical & Biomolecular Engineering
Georgia Institute of Technology

Dr. Faisal M. Alamgir
School of Materials Science and Engineering
Georgia Institute of Technology

Date Approved: May 23, 2016

ACKNOWLEDGEMENTS

I would like to express my sincere gratitude to my thesis advisors, Dr. Christopher W. Jones and Dr. Pradeep K. Agrawal for taking the risk to bring me into their groups. I came to Georgia Tech with a B.S. in Engineering Management and a limited Chemical Engineering foundation, eager to learn. Their constant support, technical guidance, and encouragement led me through the past four challenging years of my Ph.D. I would also like to express my sincere appreciation to Dr. Paul Blowers at the University of Arizona for giving me the confidence and encouragement to pursue a Ph.D. in Chemical Engineering.

I would like to express appreciation to my thesis committee members- Dr. David S. Sholl, Dr. Faisal M. Alamgir, and Dr. Michael A. Filler for their invaluable insight and input on my thesis. I would like to thank Dr. Alamgir for helping me analyze and understand my XAS data. I would also like to thank Dr. Leslie T. Gelbaum for fruitful discussions regarding my ^{13}C-NMR data and help with experimental setup. Additionally, I would like to thank Dr. Kinga A. Unocic at Oak Ridge National Laboratory, Dr. Sungsik Lee at Argonne National Laboratory, and Dr. Syed Khalid at Brookhaven National Laboratory for their assistance and instruction.

I also express gratitude to the Center for Understanding and Control of Acid Gas Evolution of Materials for Energy (UNCAGE-ME EFRC), an Energy Frontier Research Center, via contract DE-SC0012577 for partial financial support of my work.

I would like to thank the Jones group members for constant feedback and support. In particular, I would like to thank Dr. Michael R. Morrill, who trained me how to operate the high-pressure reactor system I used to conduct the work presented in this thesis and helped me get started on my research. Dr. Li-Chen Lee, whom I collaborated

with on the ^{13}C-NMR liquid sample experiments discussed in Chapter 4. I also would like to thank Taylor Sulmonetti for helping me conduct the in situ XAS experiments discussed in Appendix 2.C at Argonne National Laboratory. Additionally, I would like to thank Dr. Heng Shou from Dr. Robert Davis' Group at University of Virginia for teaching me the basics regarding XAS experimental setup and data analysis. I also would like to thank Dr. Liwei Li from Dr. Sholl's Group for productive discussions regarding reaction pathways over Mo based catalysts.

Finally, I would like to thank my family from the bottom of my heart for their continuous support and understanding. In particular, I would like to thank William P. Mounfield, III, who has been there with me every step of the way these past four years- balancing effort with ease!

Micaela Taborga Claure, 04/30/2016

TABLE OF CONTENTS

LIST OF TABLES

LIST OF FIGURES

LIST OF SYMBOLS AND ABBREVIATIONS

ANL	Argonne National Member
BET	Brunauer-Emett-Teller
BJH	Barret-Joyner Halenda Model
C	Mesoporous activated carbon
DFT	Density Functional Theory
EXAFS	X-ray Absorption Near Edge Fine Structure
GC	Gas Chromatograph
HAS	Higher Alcohol Synthesis
HDS	Hydrodesulfurization
HER	Hydrogen Evolution Reaction
HYD	Hydrogenation
IR	Infrared Spectroscopy
MMO	Mixed Metal Oxide
NMR	Nuclear Magnetic Resonance
ORNL	Oak Ridge National Laboratory
P&ID	Plumbing and Istrumentation Diagram
STEM	Scanning Transmission Electron Microscopy
TEM	Transmission Electron Microscopy
TPD	Temperature Programmed Desorption
XAS	X-ray Absorption Spectroscopy
XANES	X-ray Absorption Near Edge Spectroscopy
XPS	X-ray Photonelectron Spectroscopy
XRD	X-ray Diffraction

SUMMARY

K/MoS_2 supported on MgAl oxide (MMO) yields high C_{3+} alcohol selectivity and K/MoS_2 supported on carbon yields greater alcohol productivity; however, both the active sites and reaction pathways involved in these outcomes are not yet well understood. A comprehensive study to understand the structure-reactivity relationships for supported K/MoS_2 catalysts is presented as a basis for the elucidation of reaction pathways via proposed alcohol and olefin co-feed experiments, and ^{13}C labeled co-feed experiments. A summary of the contents in later chapters is given below.

In Chapter 2, an investigation of structure-reactivity relationships is provided with an emphasis on tuning higher alcohol selectivity and productivity. Detailed catalyst characterization via STEM and XAS was used to probe the effect of catalyst structure on selectivity by preparing an array of mixed carbon (C) and MMO supported K/MoS_2 catalysts. MoS_2 domain structures (characterized via STEM) were correlated with the selectivity of the catalysts ($C_{3+}OH$ ~ double MoS_2 layers, total hydrocarbon selectivity ~ single MoS_2 layers). A hybrid catalyst, where Mo is initially contained on the carbon support and ground with MMO, was demonstrated to show high $C_{3+}OH$ selectivity and productivity due to migration of Mo species from the carbon to MMO support.

In Chapter 3, changes in product distribution over K/MoS_2 carbon and MMO supported catalysts are explored via methanol, ethanol, and ethylene co-feed experiments. K/bulk-MoS_2 was used as a control catalyst to investigate reaction pathways associated with the MMO and C support. C supports facilitate alcohol dehydration/hydrogenation to produce hydrocarbons, while MMO influences methanol and 1-propanol coupling to form isobutyl alcohol. A methanol co-feed results in an increase in ethanol and methane production for the catalysts studied. Ethanol and ethylene co-feeds yield increased $C_{3+}OH$ and $C_{2+}HC$ over the supported catalysts. It was

observed that ethylene and ethanol co-feeds yield similar $C_{3+}OH$ production rates over the MMO K/MoS_2 supported catalyst, indicating that alcohol formation likely proceeds primarily via the same acyl intermediate as olefin carbonylation.

In Chapter 4, C-C bond formation pathways are elucidated via $^{13}C_2$-C_2H_5OH, and $^{13}C_2$-C_2H_4 co-feed experiments. The fate of the labeled ^{13}C was tracked using ^{13}C-NMR. As hypothesized, the $^{13}C_2$-C_2H_5OH, and $^{13}C_2$-C_2H_4 co-feed resulted in preferential ^{13}C enrichment of the terminal carbons of the C_3-C_4 alcohols, suggesting that the formation of alcohols occurs via the same acyl precursor in the CO insertion pathway as olefin carbonylation. While CO insertion is the primary pathway to higher alcohols, $^{13}C_2$-C_2H_5OH co-feeds conclusively show that ethanol self-coupling to C_4-1-butanol is a secondary pathway over the MMO supported K/MoS_2 catalyst. It was also observed that only the alkoxy group is preferentially enriched for ethyl acetate and propyl acetate. It can therefore be concluded that hydrogenation of an acetyl species (CH_3CO*) to the ethoxy intermediate (C_2H_5O*) is largely irreversible as there is no preferential enrichment of the acetyl group in ethyl acetate and propyl acetate.

Finally, the major results in this thesis are summarized, and challenges and opportunities are outlined for future work of this research area in Chapter 5.

CHAPTER 1

INTRODUCTION

Even though global oil production has boomed in the recent months resulting in low oil prices, the need for petroleum-free routes to value-added chemicals will continue to intensify as crude oil becomes exhausted and carbon building blocks become increasingly scarce. Lower olefins (C_2-C_4), primarily produced by steam cracking, are the key building blocks in the chemical industry, with ethylene being the largest volume petrochemical produced worldwide at approximately 80 million metric tons per year.[1] Ethylene is commonly used in polymers, solvents, drugs, cosmetics, and detergents.[2, 3] Another versatile petrochemical that has even more derivatives than ethylene is propylene, with poly(propylene) accounting for 55% of the consumption of the 40 million metric tons produced every year. Also, C_4 olefins are used as raw materials for the production of common products, such as synthetic rubber and ABS plastic. With a constantly growing demand for olefins, the global production capacity has doubled over the past 15 years.[1] The demand for olefins will continue to increase, with propylene demand expected to exceed production capacity, inevitably requiring the development of processes utilizing alternative feedstocks to olefins.[1]

Another driver of the search for alternative routes is that one of the top ten energy-consuming processes of the petrochemical industry is olefin production via steam cracking, accounting for 40% of the total energy consumption every year.[4] There is also a pressing need to decrease CO_2 emissions and explore alternative feedstocks, such as biomass, with lower net CO_2 contribution than from conventional oil.[1] Research

into developing synthetic fuel and chemical technology using alternative energy sources is vital to energy security and air quality improvement.

1.1 Higher Alcohols from Syngas

Syngas is a versatile chemical feedstock that can be produced from coal, biomass, natural gas and mixtures thereof with commercial technologies. Syngas-based processes to olefins include long chain hydrocarbon cracking, methanol to olefin conversion (MTO), and higher alcohol (C_2-C_4) dehydration. Two of these building blocks are currently commercially available from syngas: methanol over Cu based catalysts[1, 5] and long chain hydrocarbons over Fischer-Tropsch (FT) catalysts.[6] However, there is no commercially viable catalyst to produce higher alcohols from syngas.

Higher alcohol (intermediate length alcohols such as ethanol, propanol, and butanol) synthesis from syngas has been investigated with different families of catalysts including, heterogeneous,[1, 7-9] molecular[10-14] and biological catalysts.[15-20] The most widely studied noble metal catalysts among the heterogeneous catalysts for CO hydrogenation are rhodium based. Supported rhodium catalysts are known for their selectivity towards ethanol and other C_2 oxygenates, though methane formation is significant on these catalysts and their cost is significant.[7, 9, 21-27] Other well studied non-noble metal catalysts are modified methanol[8, 28-31] and modified FT synthesis catalysts.[9, 32-34] Methanol synthesis catalysts, which are typically Cu-based, are modified with an alkali promoter to increase higher alcohol production; however, methanol remains the dominant product.[9] Fischer-Tropsch catalysts based on Co, Ru, and Fe modified with Ir and supported on SiO_2 have been reported to shift the product distribution from hydrocarbons to higher alcohols with moderate ethanol selectivity, but methanol selectivity is high and methane is a dominant product.[9]

A particularly promising non-noble metal family of catalysts is modified MoS_2 based catalysts promoted with potassium. This is due to its resistance to sulfur poisoning, less severe coke deposition, and ability to form higher alcohols with high ethanol selectivity.[35-37] However, MoS_2 based catalysts are less active than noble metal catalysts and require higher pressures to achieve working productivities. Supported MoS_2 catalysts have also been widely studied as a means to improve higher alcohol selectivity and productivity. Early studies were performed using SiO_2, TiO_2, MgO, Al_2O_3, CeO_2, and a variety of carbons as supports.[38-41] Further studies were performed using activated carbon[42-47] and multi-walled carbon nanotubes (MWCNT)[48-54] as supports that enhanced productivity due to higher dispersion of MoS_2 domains. These studies showed that catalytic activity is enhanced by dispersing the MoS_2 over the support and that Mo-support interactions can affect the reactivity and product distribution of the catalyst by facilitating alcohol reaction pathways. Recently, Morrill et al.[55, 56] developed new potassium promoted MoS_2 catalysts supported on Mg/Al oxide (MMO) derived from hydrotalcites that strongly perturbed the product distribution to higher alcohols, due to the intrinsically basic properties of the support that promotes alcohol-forming reactions, unlike commonly acidic γ-alumina[57-60] known to promote alcohol dehydration and subsequent hydrocarbon formation.

1.2. K/MoS_2 carbon and MMO supported catalysts

Higher alcohol synthesis from syngas with MMO and carbon supported MoS_2 catalysts promoted with K_2CO_3 was previously studied by Dr. Morrill using the high pressure reactor system built at Georgia Tech with the support of the Dow Chemical company, which facilitates investigations of sulfide catalysts under high pressure reaction conditions with a packed bed reactor (Appendix 1.A). The studies showed that unsupported bulk MoS_2 promoted with potassium had excellent alcohol selectivity over hydrocarbons, but methanol was the main product. Both MMO and carbon (benchmark support) supported catalysts effectively shifted the alcohol distribution from C_1-C_2 to C_2-C_4 (Table 1.1).[55, 56]

Table 1.1: Reaction results of supported and unsupported MoS_2 catalysts. Elevated higher alcohol selectivity was obtained over MgAl oxide supported potassium promoted MoS_2 catalysts. Selectivities shown are CO_2 free, with CO_2 selectivities being typically 40-50%.[i]

Catalyst (K:Mo ratio 1:1)	CO Conv. %	Sel. MeOH	Sel. EtOH	Sel. nPrOH	Sel. BuOHs	Sel. $C_{2+}OH$	Sel. Total Oxy	Sel. CH_4	Sel. Total HC	$C_{2+}OH$ Prod. ($g/g_{Mo}/h$)
Bulk K/MoS_2	8	34.1	32.9	5.5	0.9	39.3	77.8	19.6	22.2	0.23
MgAlOx-K/MoS_2 (5% Mo)	8	4.5	25.9	18.7	10.9	55.5	63.0	13.9	37.0	0.23
MgAlOx-K/MoS_2 (15% Mo)	9	28.9	33.9	13.3	3.2	50.4	83.2	14.9	16.8	0.34
Carbon-K/MoS_2 (5% Mo)	8	14.2	33.5	13.6	4.6	51.7	68.0	15.7	32.0	0.88

[i] Adapted from Catalysis Letters, "Mixed MgAl Oxide Supported Potassium Promoted Molybdenum Sulfide as a Selective Catalyst for Higher Alcohol Synthesis from Syngas," 142, 2012, 875-881,M.R. Morrill, N.T. Thao, P.K. Agrawal, C.W. Jones, R.J. Davis, H. Shou, D.G. Barton, D. Ferrari, © Springer Science +Business Media, LLC 2012. DOI: 10.1007/s10562-012-0827-z
Adapted from M. R. Morrill, N. T. Thao, H. Shou, R. J. Davis, D. G. Barton, D. Ferrari, P. K. Agrawal and C. W. Jones, "Origins of Unusual Alcohol Selectivities over Mixed MgAl Oxide Supported K/MoS_2 Catalysts for Higher Alcohol Synthesis from Syngas," ACS Catal., 2013, 3, 1665-1675, Copyright © 2013 American Chemical Society. DOI: 10.1021/cs400147d

The key findings from these studies include:

(i) K/MoS_2 carbon supported catalysts improved ethanol selectivity, but produced mainly methanol and ethanol.[55]

(ii) K/MoS_2 MMO supported catalysts yield significantly enhanced ethanol and C_{3+} alcohol selectivities.[55]

(iii) The Mo loading on the support significantly affects alcohol selectivity. Low Mo loading resulting in enhanced C_{2+} alcohol selectivity was hypothesized to correlate with smaller MoS_2 domain size. At higher Mo loading, the number of MoS_2 stacked layers increased (Figure 1.1) and had significant methanol and ethanol production.[56]

(iv) The nature of the Mo phase (oxide vs. carbide) precursors prior to sulfidation did not affect product selectivity, indicating that Mo was highly mobile during sulfidation and that Mo:MMO ratio greatly affects selectivity, as it influences the MoS_2 domain size.[61]

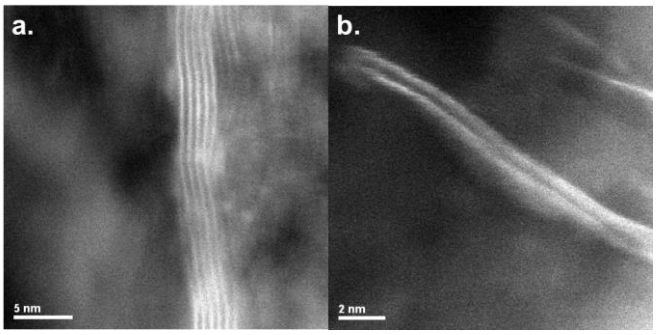

Figure 1.1: TEM images of MgAl supported, potassium-promoted MoS_2 catalysts: (a) 15 wt% Mo catalyst showed numerous stacked layers of MoS_2 and had signifcant methanol and ethanol production, (b) 5 wt% Mo catalyst had more dispersed MoS_2, with fewer stacked layers, and was selective to ethanol, propanol and butanols.[ii]

[ii] Reproduced from M. R. Morrill, N. T. Thao, H. Shou, R. J. Davis, D. G. Barton, D. Ferrari, P. K. Agrawal, C. W. Jones, "Origins of Unusual Alcohol Selectivities over Mixed MgAl Oxide Supported K/MoS_2 Catalysts for Higher Alcohol Synthesis from Syngas," ACS Catal., 2013, 3, 1665-1675, Copyright © 2013 American Chemical Society. DOI**:** 10.1021/cs400147d

Additionally, K/MoS_2 supported on carbon was shown to have higher C_{2+} alcohol productivity compared to the MMO counterpart. A high surface area mesoporous activated carbon was obtained via collaboration with Dr. Sheng Dai at Oak Ridge National Laboratory (ORNL), that when used as a support, was confirmed to show greater alcohol productivity than commercial activated carbon (Figure 1.2).[62-64]

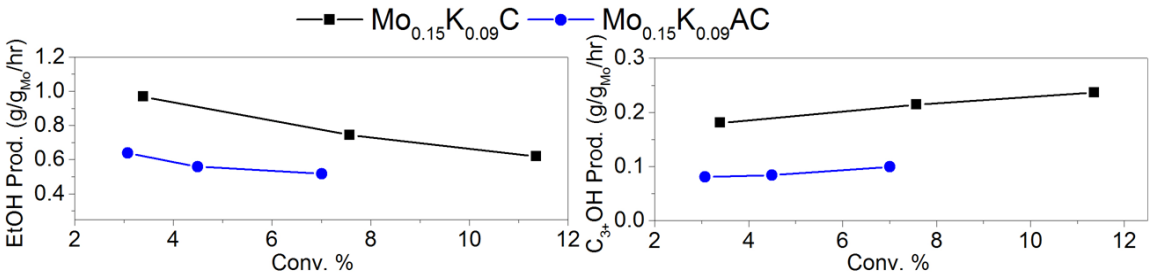

Figure 1.2: Ethanol and C_{3+} alcohol productivity as a function of conversion for ORNL carbon (C) and activated carbon (AC) MoS_2 supported catalysts with a 15 wt. % Mo, and 9 wt. % K loading.

1.3 Background

The optimization of the catalysts used for a specific catalytic process requires fundamental knowledge of reaction pathways and active sites involved in the catalytic reaction. The elucidation of reaction pathways based on product distribution, reaction rates, and intermediates as well as the identification of the nature of the active site(s), turnover rates of the sites and their interaction with reactants, intermediates and products, are critical, necessary steps in developing the understanding necessary for designing improved catalysts. The active sites and reaction pathways involved in higher alcohol synthesis from syngas over potassium promoted molybdenum sulfide based catalysts are not well-established in the literature. This may be primarily due to the complexity of the catalyst and reactions, as interactions of the promoter, MoS_2 phase, and support may all be important and reactions need to be conducted at high pressures with hazardous gases present in the syngas composition. The elucidation of structure-

reactivity properties, active sites and reaction pathways for higher alcohol synthesis is critical to the advancement of MoS_2 based catalysts. To this end, the current state of knowledge about the nature of the active sites and reaction pathways in MoS_2 based catalysts is reviewed below.

1.3.1 Limited Fundamental Knowledge of the Nature of the Active Sites in K/MoS_2 Higher Alcohol Synthesis Catalysts

Identification of active sites involved in different reaction pathways in molybdenum sulfide based catalysts has been of particular interest for hydrodesulfurization (HDS) reactions over the past 50 years. MoS_2 has a sandwich-like layer structure (Figures 1.3), comprised of Mo atoms surrounded by six sulfur atoms, with weak S-S interactions between layers. The potential importance of "edge" sites along the sides of stacked MoS_2 layers originated from the work of Voorhoeve,[65] who proposed that catalysis on MoS_2 materials occurs at the edges and at corner sites and not on basal planes, as sulfur ions in the MoS_2 basal plane are more strongly bound to Mo than sulfur atoms at the edges. Tanaka et al. observed that hydrogenation (HYD) and hydrogen exchange activity in the conversion of olefins increased with an enlargement of the edge surface area, suggesting that hydrogen dissociation and hydrogenation reactions occur at the edges of stacked MoS_2 slabs, where Mo is in a doubly uncoordinated state.[66]

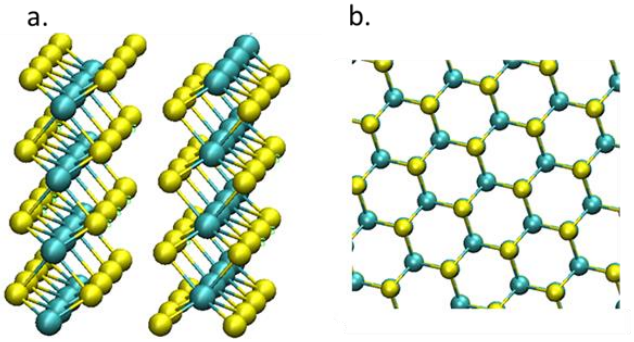

Figure 1.3: Atomic level view of the layered structure of MoS_2 (a) perpendicular to the c-axis and (b) top view.

Probe molecules have been used extensively to provide insight into the MoS_2 active sites responsible for HDS reactions, as transmission electron microscopy (TEM) studies showed that MoS_2 domain edges are reactive toward oxygen.[67] Linear correlations of oxygen chemisorption and HDS activity have been achieved for unpromoted MoS_2, and alumina-supported MoS_2 catalysts.[68-70] In contrast to unpromoted catalysts, no simple relations were found between O_2 chemisorption and HDS activity for Co-promoted catalysts to further elucidate the nature of the Co-Mo-S site.[71, 72] However, *in-situ* IR spectroscopic studies of NO adsorption facilitated the identification of promoted and unpromoted edge sites.[70] Topsøe et al. found that the increase in Co concentration resulted in a decrease of NO adsorption on the Mo atoms, indicating that Co is located at edge positions on the MoS_2 support, which is now widely accepted.[70, 73]

Chianelli et al. further studied the effect of the MoS_2 structure on the HYD and HDS selectivity of dibenzothiophene (DBT) conversion.[74] They suggested that there was a direct correlation between the degree of MoS_2 stacking determined by XRD and the selectivity of the HYD of DBT through the "rim-edge" model shown in Figure 1.4 that describes the catalyst as a stack of several disks. The top and bottom disks were associated with rim sites, the disks in between were associated with edge sites and the top surface of the disk is the inert basal plane. The total rim and edge site density was then calculated based on the total number of stacked layers, with the aim of finding a correlation between the site density and activity for HDS and HYD of DBT. The results suggested that sulfur liberation via hydrogenolysis occurred at both the rim and edge sites, and DBT hydrogenation occurred on rim sites only. Based on this model, it is hypothesized that CO hydrogenation reactions over K/MoS_2 supported on MMO should primarily occur on rim sites, as it was observed that low Mo loading with small MoS_2 domains (few stacked layers) results in enhanced higher alcohol selectivity.

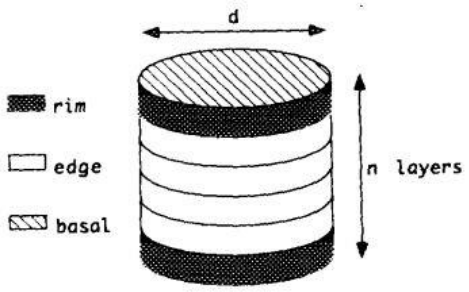

Figure 1.4: Molybdenum sulfide consisting of MoS_2 stacked, with active sites existing on the rim/edges of the layers, according to the "Rim – Edge" model.[iii]

Recently, there has been a similar focus placed on understanding the effect of catalyst structure for alcohol synthesis, though relatively little has been done compared to the HDS case. For γ–alumina supported MoS_2 catalysts, a linear relationship was observed between the methane production rate and oxygen uptake in work by Fu et al.[75] They suggested that CO and H_2 were not adsorbed on the same site, as the O_2 uptake on a catalyst saturated with pre-adsorbed H_2 was very close to that for a sample without pre-adsorption, whereas the O_2 uptake changed for the sample with pre-adsorbed CO. Jiang et al. observed that chemisorptive O_2 and CO uptakes decreased upon sulfidation of the oxide precursor with K addition, suggesting that the aggregation of MoS_2 species may be correlated to a decrease in coordinatively unsaturated Mo sites (CUS) sites, as discussed above for the case of cobalt promotion. It was further inferred that the Mo based CUS may be responsible for hydrocarbon formation, as a correlation was observed for methane activities with O_2 chemisorption uptake.[76] Thus, early studies aimed at elucidating the nature of the active sites in alkali-promoted MoS_2 catalysts for higher alcohol synthesis have shown important differences from the HDS cases discussed above. Alkali promoters are essential for shifting the product distribution from

[iii] Reprinted from Journal of Catalysis, 149, M. Daage, R.R. Chianelli, "Structure-Function Relations in Molybdenum Sulfide Catalysts: The "Rim-Edge" Model", 414-427, Copyright © 1994, with permission from Elsevier. DOI:10.1006/jcat.1994.1308

hydrocarbons to higher alcohol over a MoS_2 catalyst, creating different types of sites compared to typical MoS_2 phase in hydrodesulfurization (HDS) catalysts. A recent study by Gascon et al. determined that potassium stabilizes alkoxy species, which are key intermediates in CO insertion reaction pathway from syngas to higher alcohols, as discussed below.[77] Potassium is thought to poison the hydrogenation activity of MoS_2 toward hydrocarbons.

Overall, structure-reactivity relationships and the location of active sites in molybdenum sulfide catalysts for alcohol synthesis is still unclear and needs to be explored to work towards closing the fundamental knowledge gaps necessary for the rational optimization of molybdenum sulfide based catalysts.

1.3.2 Reaction Mechanisms for syngas conversion to alcohols

Although the active sites for CO hydrogenation reactions might be hypothesized to be similar to those in HDS catalysts, knowledge about the pathways and sites required for the C-C bond forming reactions to higher alcohols is limited. The most frequently discussed mechanisms for carbon-carbon bond formation are CO insertion and Guerbet coupling pathways. CO insertion is the addition of CO to an alkyl group ($C_nH_{2n+1}^*$) to form an acyl species ($C_nH_{2n+1}CO^*$), which is then hydrogenated to form an alcohol (depicted in Figure 1.5).[36]

In Guerbet coupling reactions, an alcohol with a C-H group on the beta carbon is coupled with another alcohol on a base site, suggesting that methanol can be coupled with ethanol to form 1-propanol, methanol can be coupled with 1-propanol to form isobutyl alcohol, or 1-butanol can be formed by ethanol self-coupling of ethanol.[78]

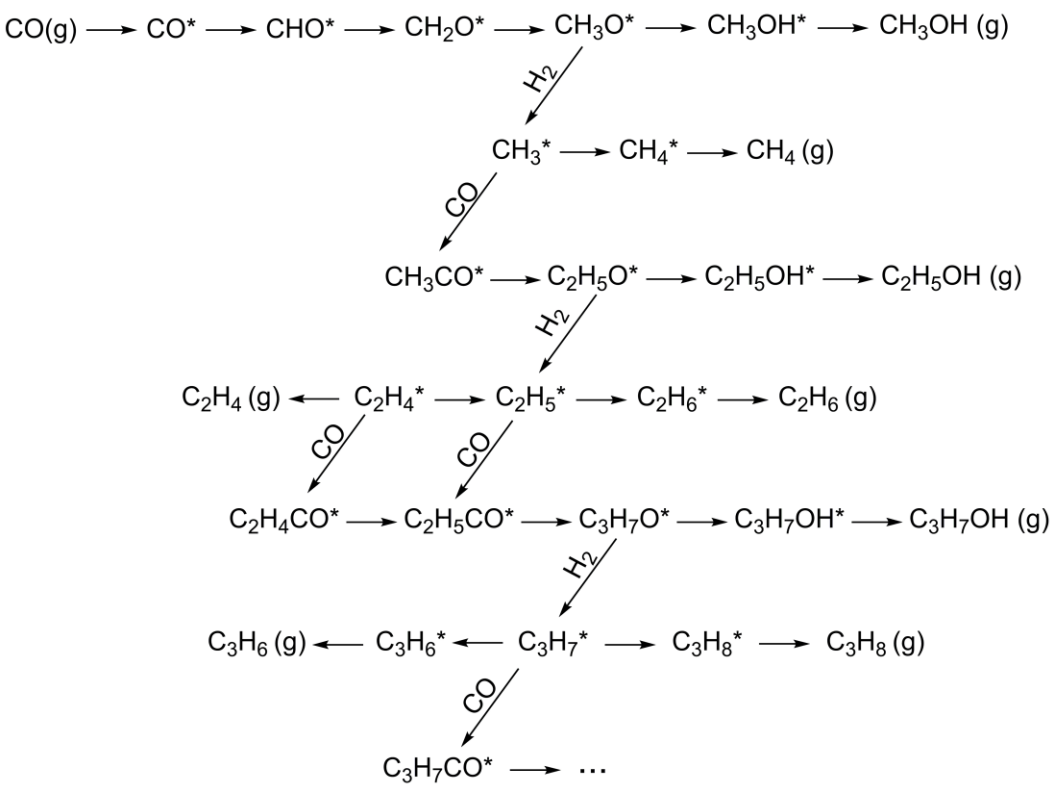

Figure 1.5: CO insertion mechanism over K/MoS_2 based catalysts.[iv]

Co-feeding of olefins/alcohols along with syngas has been used to analyse the influence of these species on product distributions in higher alcohol synthesis over various catalysts.[35, 79-82] Specifically, alcohol co-feeds have been used as a means to experimentally probe the mechanisms of carbon-carbon bond formation for higher alcohol synthesis. Early studies by Santiesteban et al. demonstrated with ^{13}C-methanol that higher alcohols were formed via classical CO insertion pathways over alkali/MoS_2 and alkali/Co/MoS_2.[36] However, recent studies showed that coupling reactions may also be important. Using an ethanol co-feed with K_2CO_3 promoted Co-MoS_2 catalysts supported on carbon, Christensen et al. observed that the production of 1-propanol increased with the ethanol fraction in the feed; however, the production of 1-butanol was more strongly enhanced,

[iv] Reproduced from Taborga Claure, M. et al., Catal Sci Technol, 2016,6, 1957-1966 by permission from The Royal Society of Chemistry. DOI: 10.1039/C5CY01587A.

suggesting that not only is CO insertion important for chain growth, but also that self-coupling ethanol or ethanol-derived species leads to higher alcohols.[83] In other work, addition of acetaldehyde to the syngas feed over K_2CO_3 promoted Co-MoS_2 catalysts not only enhanced higher alcohol production, but influenced the product distribution towards 1-butanol production, also suggesting that coupling reactions are important over these catalysts.[84] As explained above, Gascon et al. suggested that the formation of higher alcohols proceeds through CO insertion via stabilization of alkoxy species on the surface by K and to a small extent, by base catalysed aldol condensation over K_2CO_3/bulk-MoS_2 catalysts using operando infrared spectroscopy, and ethanol co-feed experiments, respectively.[77]

In addition to experimental work, kinetic models have been developed to evaluate reaction mechanisms to higher alcohols over K/MoS_2 based catalysts. Smith et al. found that linear alcohols are predominantly formed by CO insertion over alkali/MoS_2 rather than Guerbet coupling by comparing their kinetic model with their product distribution.[85] More recently, Park et al. developed a kinetic model on the basis of a CO insertion mechanism and predicted the formation and distribution of products within a range of experimental conditions (T=250-350 °C, P=15-90 atm, H_2/CO molar feed ratio=0.5-4).[86]

Whereas there has been some effort into investigating reaction pathways to higher alcohols over K_2CO_3 promoted MoS_2 catalysts, reaction pathways over K/MoS_2 supported catalysts remain poorly elucidated, where Mo-support interactions are shown to affect alcohol product distribution.[55, 56, 87]

1.4 References

(1) H. M. Torres Galvis and K. P. de Jong, *ACS Catal.*, 2013, **3**, 2130-2149.

(2) H. M. Torres Galvis, J. H. Bitter, C. B. Khare, M. Ruitenbeek, A. I. Dugulan and K. P. de Jong, *Science*, 2012, **335**, 835-838.

(3) P. Lanzafame, G. Centi and S. Perathoner, *Chem. Soc. Rev.*, 2014, **43**, 7562-7580.

(4) N. Rahimi and R. Karimzadeh, *Appl. Catal., A*, 2011, **398**, 1-17.

(5) P. Tian, Y. Wei, M. Ye and Z. Liu, *ACS Catal.*, 2015, **5**, 1922-1938.

(6) A. Y. Khodakov, W. Chu and P. Fongarland, *Chem. Rev.*, 2007, **107**, 1692-1744.

(7) V. Subramani and S. K. Gangwal, *Energy Fuels*, 2008, **22**, 814-839.

(8) M. Gupta, M. L. Smith and J. J. Spivey, *ACS Catal.*, 2011, **1**, 641-656.

(9) J. J. Spivey and A. Egbebi, *Chem. Soc. Rev.*, 2007, **36**, 1514-1528.

(10) Y. Xiang, V. Chitry, P. Liddicoat, P. Felfer, J. Cairney, S. Ringer and N. Kruse, *J. Am. Chem. Soc.*, 2013, **135**, 7114-7117.

(11) B. K. Warren and B. D. Dombek, *J. Catal.*, 1983, **79**, 334-347.

(12) D. R. Fahey, *J. Am. Chem. Soc.*, 1981, **103**, 136-141.

(13) J. S. Bradley, *J. Am. Chem. Soc.*, 1979, **101**, 7419-7421.

(14) B. D. Dombek, *J. Organomet. Chem.*, 1983, **250**, 467-483.

(15) H. N. Abubackar, M. C. Veiga and C. Kennes, *Biofpr.*, 2011, **5**, 93-114.

(16) V. G. Debabov, *Appl. Biochem. Microbiol.*, 2013, **49**, 619-628.

(17) P. C. Munasinghe and S. K. Khanal, *Bioresour. Technol.*, 2010, **101**, 5013-5022.

(18) S. Rajagopalan, R. P. Datar and R. S. Lewis, *Biomass Bioenergy*, 2002, **23**, 487-493.

(19) J. Vega, S. Prieto, B. Elmore, E. Clausen and J. Gaddy, *Appl. Biochem. Biotechnol.*, 1989, **20**, 781-797.

(20) R. M. Worden, A. J. Grethlein, M. K. Jain and R. Datta, *Fuel*, 1991, **70**, 615-619.

(21) M. A. Haider, M. R. Gogate and R. J. Davis, *J. Catal.*, 2009, **261**, 9-16.

(22) M. R. Gogate and R. J. Davis, *ChemCatChem*, 2009, **1**, 295-303.

(23) J. Gao, X. H. Mo, A. C. Y. Chien, W. Torres and J. G. Goodwin, *J. Catal.*, 2009, **262**, 119-126.

(24) Y. Choi and P. Liu, *J. Am. Chem. Soc.*, 2009, **131**, 13054-13061.

(25) D. H. Mei, R. Rousseau, S. M. Kathmann, V. A. Glezakou, M. H. Engelhard, W. L. Jiang, C. M. Wang, M. A. Gerber, J. F. White and D. J. Stevens, *J. Catal.*, 2010, **271**, 325-342.

(26) S. F. Zaman and K. J. Smith, *Catal. Today*, 2011, **171**, 266-274.

(27) M. M. Bhasin and P. C. Ellgen, *US Patent 4096164 A, to Union Carbide Corporation, 1978*.

(28) J. C. Slaa, J. G. van Ommen and J. R. H. Ross, *Catal. Today*, 1992, **15**, 129-148.

(29) J. G. Nunan, R. G. Herman and K. Klier, *J. Catal.*, 1989, **116**, 222-229.

(30) G. B. Hoflund, W. S. Epling and D. M. Minahan, *Catal. Lett.*, 1997, **45**, 135-138.

(31) K. J. Smith and R. B. Anderson, *Can. J. Chem. Eng.*, 1983, **61**, 40-45.

(32) A. Razzaghi, J.-P. Hindermann and A. Kiennemanna, *Appl. Catal.*, 1984, **13**, 193-210.

(33) K. Takeuchi, T. Matsukaki, H. Arakawa and Y. Sugi, *Appl. Catal.*, 1985, **18**, 325-334.

(34) K. Fujimoto and T. Oba, *Appl. Catal.*, 1985, **13**, 289-293.

(35) C. B. Murchinson, M. M. Conway, R. R. Stevens and G. J. Quarderer, *In 9th Annual Congress on Catalysis, Calgary, Alberta, Canada*, 1988, 626-633.

(36) J. G. Santiesteban, C. E. Bogdan, R. G. Herman and K. Klier, *in: M.J. Philips, M. Ternan (Eds.), vol. 2, 9th Annual Congress on Catalysis, Chemical Institute of Canada, Calgary, 1988, pp. 561-568.*

(37) J. M. Christensen, P. M. Mortensen, R. Trane, P. A. Jensen and A. D. Jensen, *Appl. Catal., A*, 2009, **366**, 29-43.

(38) T. Tatsumi, A. Muramats and H.-o. Tominaga, *Chem. Lett.*, 1985, **14**, 593-594.

(39) B. E. Concha, G. L. Bartholomew and C. H. Bartholomew, *J. Catal.*, 1984, **89**, 536-541.

(40) T. Tatsumi, A. Muramatsu and H.-o. Tominaga, *Appl. Catal.*, 1987, **34**, 77-88.

(41) T. Tatsumi, A. Muramatsu and H.-o. Tominaga, *Appl. Catal.*, 1986, **27**, 69-82.

(42) J. C. Duchet, E. M. van Oers, V. H. J. de Beer and R. Prins, *J. Catal.*, 1983, **80**, 386-402.

(43) L. Gang, Z. Chengfang, C. Yanqing, Z. Zhibin, N. Yianhui, C. Linjun and Y. Fong, *Appl. Catal., A*, 1997, **150**, 243-252.

(44) J. Iranmahboob and D. Hill, *Catal. Lett.*, 2002, **78**, 49-55.

(45) Z.-r. Li, Y.-l. Fu, M. Jiang, T.-d. Hu, T. Liu and Y.-n. Xie, *J. Catal.*, 2001, **199**, 155-161.

(46) X. Li, L. Feng, Z. Liu, B. Zhong, D. B. Dadyburjor and E. L. Kugler, *Ind. Eng. Chem. Res.*, 1998, **37**, 3853-3863.

(47) X. Li, L. Feng, L. Zhang, D. Dadyburjor and E. Kugler, *Molecules*, 2003, **8**, 13-30.

(48) V. R. Surisetty, I. Eswaramoorthi and A. K. Dalai, *Fuel*, 2012, **96**, 77-84.

(49) V. R. Surisetty, A. K. Dalai and J. Kozinski, *Appl. Catal., A*, 2011, **393**, 50-58.

(50) V. R. Surisetty, A. K. Dalai and J. Kozinski, *Appl. Catal., A*, 2010, **385**, 153-162.

(51) V. R. Surisetty, A. K. Dalai and J. Kozinski, *Ind. Eng. Chem. Res.*, 2010, **49**, 6956-6963.

(52) V. R. Surisetty, A. Tavasoli and A. K. Dalai, *Appl. Catal., A*, 2009, **365**, 243-251.

(53) X. Ma, G. Lin and H. Zhang, *Chinese J. Catal.*, 2006, **27**, 1019-1027.

(54) X.-M. Ma, G.-D. Lin and H.-B. Zhang, *Catal. Lett.*, 2006, **111**, 141-151.

(55) M. R. Morrill, N. T. Thao, P. K. Agrawal, C. W. Jones, R. J. Davis, H. Shou, D. G. Barton and D. Ferrari, *Catal. Lett.*, 2012, **142**, 875-881.

(56) M. R. Morrill, N. T. Thao, H. Shou, R. J. Davis, D. G. Barton, D. Ferrari, P. K. Agrawal and C. W. Jones, *ACS Catal.*, 2013, **3**, 1665-1675.

(57) G.-z. Bian, Y.-l. Fu and Y.-s. Ma, *Catal. Today*, 1999, **51**, 187-193.

(58) Y.-l. Fu, K. Fujimoto, P.-y. Lin, K. Omata and Y.-s. Yu, *Appl. Catal., A*, 1995, **126**, 273-285.

(59) Z.-r. Li, Y.-l. Fu, M. Jiang, M. Meng, Y.-n. Xie, T.-d. Hu and T. Liu, *Catal. Lett.*, 2000, **65**, 43-48.

(60) Z.-r. Li, Y.-l. Fu and M. Jiang, *Appl. Catal., A*, 1999, **187**, 187-198.

(61) H. Okatsu, M. Morrill, H. Shou, D. Barton, D. Ferrari, R. Davis, P. Agrawal and C. Jones, *Catal. Lett.*, 2014, **144**, 825-830.

(62) E. T. Liakakou, E. Heracleous, K. S. Triantafyllidis and A. A. Lemonidou, *Appl. Catal., B*, 2015, **165**, 296-305.

(63) S.-H. Chai, J. Y. Howe, X. Wang, M. Kidder, V. Schwartz, M. L. Golden, S. H. Overbury, S. Dai and D.-e. Jiang, *Carbon*, 2012, **50**, 1574-1582.

(64) S.-H. Chai, V. Schwartz, J. Y. Howe, X. Wang, M. Kidder, S. H. Overbury, S. Dai and D.-e. Jiang, *Microporous Mesoporous Mater.*, 2013, **170**, 141-149.

(65) R. J. H. Voorhoeve and J. C. M. Stuiver, *J. Catal.*, 1971, **23**, 243-252.

(66) K.-i. Tanaka and T. Okuhara, *J. Catal.*, 1982, **78**, 155-164.

(67) R. R. Chianelli, A. F. Ruppert, S. K. Behal, B. H. Kear, A. Wold and R. Kershaw, *J. Catal.*, 1985, **92**, 56-63.

(68) J. Bachelier, J. Duchet and D. Cornet, *Bull. Soc. Chim. Belg*, 1981, **90**, 1301.

(69) S. J. Tauster, T. A. Pecoraro and R. R. Chianelli, *J. Catal.*, 1980, **63**, 515-519.

(70) H. Topsoe and B. S. Clausen, *Appl. Catal.*, 1986, **25**, 273-293.

(71) R. Burch and A. Collins, *Appl. Catal.*, 1985, **17**, 273-308.

(72) W. Zmierczak, G. MuraliDhar and F. E. Massoth, *J. Catal.*, 1982, **77**, 432-438.

(73) N. Y. Topsoe and H. Topsoe, *J. Catal.*, 1983, **84**, 386-401.

(74) M. Daage and R. R. Chianelli, *J. Catal.*, 1994, **149**, 414-427.

(75) F. Yilu, T. Xibai, H. Zhigang, F. Chongzheng, J. Mingrong and W. Jianxin, *Appl. Catal.*, 1989, **55**, 11-20.

(76) M. Jiang, G.-Z. Bian and Y.-L. Fu, *J. Catal.*, 1994, **146**, 144-154.

(77) V. P. Santos, B. van der Linden, A. Chojecki, G. Budroni, S. Corthals, H. Shibata, G. R. Meima, F. Kapteijn, M. Makkee and J. Gascon, *ACS Catal.*, 2013, **3**, 1634-1637.

(78) J. T. Kozlowski and R. J. Davis, *ACS Catal.*, 2013, **3**, 1588-1600.

(79) G. J. Quarderer, R. R. Stevens, G. A. Cochran and C. B. Murchison, *US Patent 4825013 A, to The Dow Chemical Company, 1989.*

(80) B. Temel, P. E. H. Nielsen and P. Beato, *US Patent 0225879A1, to Haldor Topsoe A/S*, 2013.

(81) P. E. H. Nielsen, B. Temel and P. Beato, *US Patent 8637580B2, to Haldor Toposoe A/S*, 2014.

(82) N. E. Kinkade, *US Patent WO1985003073 A1, to Union Carbide Corp*, 1985.

(83) J. M. Christensen, P. A. Jensen, N. C. Schiødt and A. D. Jensen, *ChemCatChem*, 2010, **2**, 523-526.

(84) L. W. Bolton and B. P. Gracey, *US 20110281961 A1, 2007*.

(85) K. J. Smith, R. G. Herman and K. Klier, *Chem. Eng. Sci.*, 1990, **45**, 2639-2646.

(86) T. Y. Park, I.-S. Nam and Y. G. Kim, *Ind. Eng. Chem. Res.*, 1997, **36**, 5246-5257.

(87) M. Taborga Claure, S.-H. Chai, S. Dai, K. A. Unocic, F. M. Alamgir, P. K. Agrawal and C. W. Jones, *J. Catal.*, 2015, **324**, 88-97.

APPENDIX 1.A

HIGH PRESSURE REACTOR SYSTEM

The unique custom-designed high pressure reactor system shown below was built at Georgia Tech in 2008 with support of the Dow Chemical Company with all the safety measures necessary to handle flammable/toxic gas components of the syngas and high pressure reactions required to study MoS_2 based catalysts. The reactor system is comprised of toxic/flammable cabinets, sensors and alarms for detection of CO, and H_2S leaks, and automated operation. Reactions operate at high temperatures (250-500 °C) and very high pressures (1000-2500 psig).

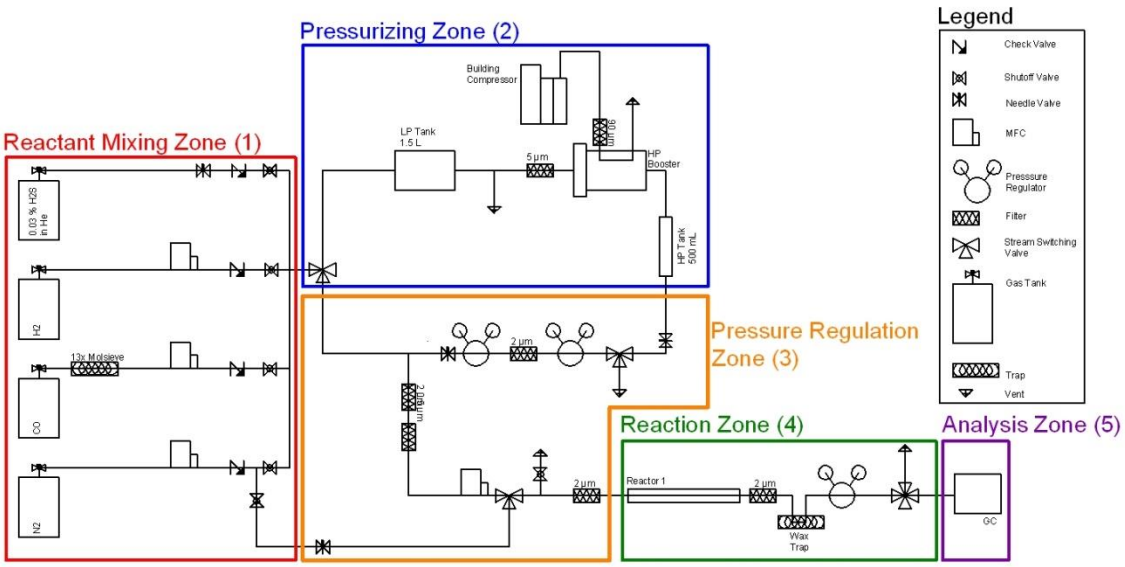

Figure 1.A.1: A simplified plumbing and instrumentation diagram (P&ID) of the high pressure reactor system.[v]

[v] Reproduced from M. R. Morrill, "Higher Alcohol Synthesis on Magnesium/Aluminum Mixed Metal Oxide Supported Potassium Carbonate Promoted Molybdenum Sulfide," Georgia Institute of Technology, Copyright © 2013 by Michael R. Morrill.

CHAPTER 2

SUPPORTED K/MoS_2 DOMAIN STRUCTURE-REACTIVITY RELATIONSHIP

This Chapter was adapted from Journal of Catalysis, 324, M. Taborga Claure, S.-H. Chai, S. Dai., K.A. Unocic, F.M. Alamgir, P.K. Agrawal, C.W. Jones "Tuning of higher alcohol selectivity and productivity in CO hydrogenation reactions over K/MoS_2 domains supported on mesoporous activated carbon and mixed MgAl oxide", 88-97, Copyright 2015, with permission from Elsevier. DOI: 10.1016/j.jcat.2015.01.015

As noted in Chapter 1, ORNL high surface area carbon (denoted "carbon" hereafter) is confirmed to show greater alcohol productivity over commercial activated carbon in preliminary experiments.[1-3] Also, hydrotalcite-derived MMO yields high C_{3+}OH selectivity, influenced by Mo-MMO interactions, but generally yields low productivity.[4, 5] The intrinsically basic properties of the MMO support were suggested to promote alcohol-forming reactions, unlike common acidic γ-alumina[6-9] known to promote alcohol dehydration and subsequent hydrocarbon formation. It has also been noted that the Mo:MMO ratio greatly affects selectivity, while catalyst preparation methods had little impact on this parameter.[5] Furthermore, it has been shown that Mo is highly mobile during sulfidation and potentially during reaction as well.[10]

A series of K/MoS_2 domains supported on mesoporous carbon (C), mixed MgAl oxide (MMO), or mixtures thereof are studied for higher alcohol synthesis from syngas. The hypothesis that molybdenum supported on a family of MMO and carbon mixed supports may allow tuning of higher alcohol productivity (due to the carbon support) and selectivity (due to the MMO support) was evaluated, with an emphasis on understanding

the MoS_2 structure-reactivity relationships over the carbon and MMO supported catalysts. A particular focus is placed on determining the effect of the support on MoS_2 structure, as well as the mobility of Mo species on the two supports under reaction conditions.

2.1 Experimental Section

Mesoporous activated carbon was prepared via a published procedure developed at ORNL. Mesoporous carbon was synthesized by carbonization of nanostructured polymeric species, obtained by self-assembly of block copolymer and phenolic resin under acidic conditions *via* soft-template method, under flowing N_2 at 850 °C for 2h. The mesoporous carbon was then activated with KOH and subsequently washed by dilute HCl to remove residual KOH. For KOH activation, a physical mixture of solid KOH (16 g) and mesoporous carbon (4 g) was loaded to a quartz tube in a nickel crucible and heated under flowing N_2 to 900 °C and held for 2h. The resulting material was washed with deionized water and then mixed with a ~0.2 M HCl solution that was then heated up to 80 °C with stirring for 30 min. The activated mesoporous carbon was collected by filtration, washed with deionized water, and dried at 100 °C.[11] MMO was synthesized using the same method described in our previous studies[4, 5] by coprecipitation of magnesium nitrate hexahydrate (Alfa Aesar, 98-102%), and aluminum nitrate nonahydrate (Alfa Aesar, 98-102%) aqueous solutions with a Mg:Al molar ratio of 7:3 (0.6 M in metal ions) together with a 1.2 M NaOH (EMD, 97.0%) and 0.15 M Na_2CO_3 (Aldrich, 99.5+%) at 65 °C and a pH of 9.5. The resulting solution was stirred for 48 h, filtered, washed with deionized water, dried overnight at 105 °C, and then calcined at 450 °C for 2 h.

A set of four catalysts using a mixture of mesoporous activated carbon and MMO supports were synthesized with an approximate Mo loading of 5 wt.%, K loading of 3

wt.%, and a molar ratio of Mo:K of 1. The parent catalysts in this Chapter, which are derived from a single support, are referred to as MoKMMO and MoKC. The mixed supported catalysts in this Chapter are referred as MoKC-MMO and MoKMMO-C, where the parent catalyst is first prepared and then is ground with the bare secondary support in a mass ratio of MMO:C of 3.6 to yield the final precatalysts (Figure 2.1). $Mo_{0.15}K_{0.09}C$ was used as the parent catalyst for MoKC-MMO, and $Mo_{0.06}K_{0.04}MMO$ was used as the parent catalyst of MoKMMO-C, so that when ground with the secondary support the desired Mo and K loadings were achieved. The precatalysts were then pressed into pellets for catalyst testing in the fixed bed reactor. MoKMMO was pelletized to ~3000 psig, whereas mixed supported catalysts (MoKMMO-C and MoKC-MMO) were pelletized at ~6000 psig to obtain self-supporting pellets. In Table 2.A.1 in Appendix 2.A, it is shown that upon pelletization the MMO and MMO-C supports lose ~20% of their surface area, and ~10% of their pore volume. Therefore, there is no considerable decrease in porosity upon pelletization.

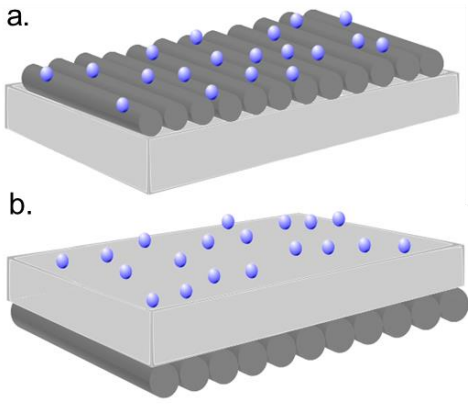

Figure 2.1: Catalyst schematic for (a) MoKC-MMO and (b) MoKMMO-C precatalysts with Mo oxide domains represented by spheres, mesoporous activated carbon represented by cylinders, and MMO represented by a rectangular box.

Mo was added to the supports via incipient wetness impregnation using ammonium molybdate tetrahydrate (AMT) (Sigma-Aldrich, ACS Reagent) dissolved in DMSO for the MMO support (the solution was stirred for 12 h until AMT was dissolved) and water for the carbon support. DMSO was used as the impregnation solvent for MMO instead of water to limit the recrystallization of the hydrotalcite phase, which can be induced by water, thereby "burying" the potassium promoter.[12-14] The resulting materials were dried in open atmosphere at 135 °C for 12 h for the MMO support and at 100 °C for 12 h for the carbon support, and then placed in a quartz tube, whereby the AMT was decomposed via heating to 200 °C for 6 h at 5 °C /min, followed by further heating to 450 °C for 2 h at 5 °C/min under 40 mL/min of flowing N_2. After the decomposition step, the parent oxide precatalysts were physically ground for 15 min with K_2CO_3 (Aldrich, 99%, stored in an oven at 105 °C).[15] For the mixed supported catalysts, the parent catalyst was ground for an additional 15 min with the secondary support to create the precatalysts with mixed supports.

The prepared precatalysts containing MMO were pelletized, crushed, and sieved through 20-40 mesh prior to loading in the reactor, while for the MoKC catalyst, silicon carbide (Alfa Aesar, 46 grit SiC) was mixed with the powder catalyst (but not ground) in a 5:1 SiC:catalyst mass ratio to minimize plugging and hot spots, as self-supporting pellets could not be made with the carbon-rich catalyst. It is important to note that SiC is inert under the reaction conditions, as verified with a blank, SiC-only, reaction. The precatalysts were then loaded into a 6.35 mm steel tube reactor (1 g for MoKMMO, 0.8 g for the mixed supported catalysts, and 0.4 g for MoKC) for catalytic evaluation.

The precatalyst bed was then pretreated with 10% H_2S/H_2 (Matheson Tri-Gas, UHP) at 450 °C at a heating rate of 5 °C/min and then held at 450 °C for 2 h with a flow rate of 20 mL/min to reduce the oxide precatalyst to the sulfide phase, in situ. After in situ sulfidation, the reactions with syngas, 45% H_2 (Airgas, UHP), 45% CO (Airgas, UHP,

purified with 5A molecular sieve carbonyl trap), 10% N_2 (Airgas, UHP) as an internal standard, and 50 ppm H_2S (from 5000 ppm H_2S in He, Matheson Tri-Gas, UHP) were carried out at 310 °C and 1500 psig at flow rates 10-60 mL/min (700-6500 $mL/g_{catalyst}/h$) to reach 3-4 different steady-state, isothermal CO conversion levels for a total of ~12 days of time on-stream. All the catalysts studied reached the first isothermal CO conversion after 3 days of reaction, as shown in Figure 2.B.1. For the 2-3 additional isothermal CO conversion levels studied in each run, reactions were carried out until the productivity and product selectivity were stabilized for ~3 days. H_2S was added to the syngas feed to prevent sulfur leaching and maintain steady-state sulfur levels on the surface of the catalyst to ensure catalyst stability. No major change in activity was observed during ~12 days of reaction, with less than 10% change in the CO conversion observed over this period. Please note that significant safety precautions are required to study toxic (CO, H_2S) and flammable (H_2, CO, H_2S) gases under high pressure and temperature.

The main reaction products were quantified with an Agilent 7890 gas chromatograph (methane, ethane, ethylene, carbon dioxide, propane/propylene, methanol, ethanol, 1-propanol, 1-butanol, isobutyl alcohol, acetaldehyde, methyl formate, methyl acetate, ethyl acetate, methyl propionate, and ethyl propionate) using single point calibration curves. CO conversion, productivity and reaction selectivity were calculated from pseudo-steady-state data.

At the completion of the reactions, all catalysts were passivated in situ with 1% O_2 in He (Matheson Trigas, UHP) for 8 h at room temperature at 20 mL/min. Catalysts were then placed in a vial under argon and stored in a desiccator. The reaction-aged catalysts were characterized ex situ via elemental analysis, nitrogen physisorption, X-ray diffraction (XRD), Raman spectroscopy, X-ray absorption spectroscopy (XAS) including the near-edge and extended X-ray absorption fine structure (XANES and EXAFS), and

scanning transmission electron microscopy (STEM). In addition, the carbon and MMO supports were characterized with nitrogen physisorption, ammonia and carbon dioxide temperature programmed desorption (TPD) experiments.

Elemental analysis was performed at ALS Environmental; for carbon analysis, the samples were directly analyzed using Perkin Elmer 2400 II (combustion/ thermal conductivity), and for metal analysis the samples were first digested in a microwave (Anton Paar Multiwave 3000) with nitric, hydrochloric, hydrofluoric, and peroxide, and the analysis was performed with inductively coupled plasma optical emission spectroscopy (ICP-OES) using Perkin Elmer Optima 3000 DV. Nitrogen physisorption isotherms were collected at -196 °C using Micromeritics Tristar II after being heated to 200 °C under vacuum for 10 h prior to the analysis. Ammonia and carbon dioxide Temperature Program Desorption (TPD) experiments were conducted on an AutoChem II 2920 instrument from Micromeritics. Approximately 35 mg of the sample was placed in a quartz U-tube, which was mounted on the instrument. For Ammonia TPD experiments, the sample was pretreated under a helium atmosphere by heating to 500 °C at a heating rate of 10 °C/min. Ammonia gas (1984 ppm in He) was introduced into the tube for one hour after cooling the sample to 120 °C. The system was then purged with helium for one hour at 120 °C. The TPD profile was recorded until the temperature reached 800 °C in helium flow at a heating rate of 10 °C/min. A similar procedure was followed for carbon dioxide TPD experiments; the sample (~ 35 mg) was pretreated under a helium atmosphere by heating to 700°C at a heating rate of 10°C/min. CO_2 gas (99.99%) was introduced into the tube for one hour after cooling down the sample to 50°C. The system was then purged with helium for 30 min at 50°C. The TPD profile was recorded to 700°C in helium flow at a heating rate of 10°C/min. XRD was performed using a Philips X-pert diffractometer using Cu-Kα radiation. A Witec confocal Raman microscope (Alpha 300R) was used to obtain Raman spectra for the reaction-aged catalysts with an Ar^+ ion laser

(λ=513.998 nm) with 1.5 mW excitation source intensity and 1800 grading with <0.9 cm^{-1} pixel resolution. Bulk MoS_2, molybdenum (IV) sulfide, purum, powder (Aldrich) was used as a reference material. Samples for STEM imaging were prepared by dispersing the particles in methanol and dropping them on a lacy carbon coated Cu grid. Images were collected on an aberration-corrected JEOL 2200FS STEM operated at 200 kV at ORNL.

X-ray absorption spectroscopy (EXAFS and XANES) was performed at beamlines 10-BM-A, and 12-BM of the Advanced Photon Source (APS), Argonne National Laboratory, and beamline X18B of the National Synchrotron Light Source (NSLS), Brookhaven National Laboratory. The XAS data were obtained in transmission mode at the Mo K-edge (20 keV) with a spot size of 0.5 mm x 1.2 mm at APS and 0.5 mm x 5 mm at NSLS. The Mo K-edge spectra were measured at room temperature in air with Mo foil as an energy reference. The reaction-aged catalysts were ground with boron nitride (99%, Sigma-Aldrich) and loaded into a polyamide tube (0.16 in. I.D.) to obtain an attenuation length of approximately one. Two scans from 19800 to 21000 eV were collected for each sample. The XAS data were then processed with Athena software for background removal, edge-step normalization, and Fourier transform.

2.2 Results and Discussion

2.2.1 XRD Patterns of Reaction-aged Catalysts

XRD patterns of the reaction-aged catalysts after passivation are shown in Figure 2.2. Small, relatively broad peaks for the MoS_2 [101] (33°) and, [110] (58°) planes were observed in all of the reaction-aged catalysts. The MoS_2 [002] plane at 14° was observed for the MoKC, MoKC-MMO, and MoKMMO-C catalysts, but was absent in the MoKMMO catalyst. The presence of the [002] plane in the carbon containing catalysts could be indicative of a higher degree of MoS_2 stacking compared to the MoKMMO catalyst.[16] Diffraction lines characteristic of the MgO at 44° and 64° were apparent in all

MMO containing catalysts. It is important to note that the carbon-containing catalysts exhibited a diffraction line at 26°, corresponding to MoO_2 domains. Additional peaks at 37°, 44°, 53° were also characteristic of MoO_2 domains in the MoKC catalyst. The presence of MoO_2 domains in carbon-containing catalysts are most likely attributed to incomplete reduction during in situ sulfidation.

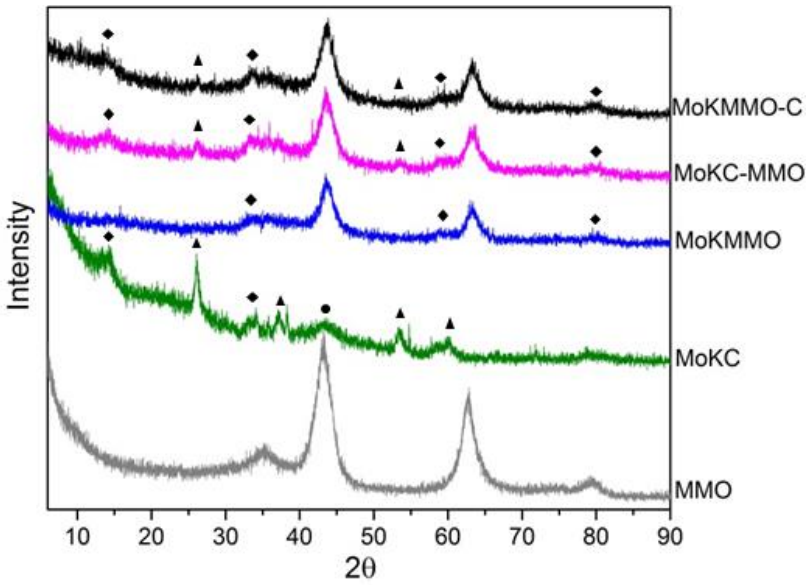

Figure 2.2: XRD patterns of MMO (gray) standard and reaction-aged MoKC (green), MoKMMO (blue), MoKC-MMO (magenta), MoKC-MMO (black) catalysts.(♦) MoS_2 (▲) MoO_2 (●) MoO_3.

2.2.2 N_2 Physisorption and Elemental Analysis of Reaction-aged Catalysts

N_2 physisorption isotherms of the mixed supported reaction-aged catalysts shown in Figure 2.A.2 depict a double hysteresis due to a bimodal pore-size distribution (~34 nm due to the macroporous MMO support and ~10 nm due to the mesoporous carbon support) calculated with the Barret-Joyner Halenda (BJH) model. The Brunauer-Emmett-Teller (BET) surface areas calculated from the nitrogen physisorption data of the mixed supported catalysts were substantially smaller than those from the carbon supported catalyst due to the presence of the relatively low surface area MMO support (Table 2.A.1). This observation is consistent with the work of Dalai et al., where they observed a

significant decrease in porosity upon binder incorporation into the $CoRhMoS_2$, MWCNT-supported catalysts as means of enhancing pelletization for industrial applications.[17]

Elemental analysis results shown in Table 2.1 confirm that the catalysts were prepared within 10% of the target Mo and K wt. % loadings. It has been previously observed that the Mo:MMO mass ratio greatly affected catalyst selectivity.[5] Therefore, maintaining the Mo:MMO mass ratio for the MMO supported catalysts allows for meaningful comparison of the catalytic performance across the family of catalysts. Similarly, a constant MMO:C mass ratio for the mixed supported catalysts was used to shed light into the Mo mobility between the two support phases in the mixed supported catalysts, as it is thought that Mo species are highly mobile during sulfidation and possibly the early stages of the catalytic reaction.[10] It should also be noted that the mass ratio of Mo/S was similar among all the catalysts and minor deviations did not follow any specific trend for the catalysts studied.

Table 2.1: BET surface area and composition for MMO and C supports and reaction-aged MoKC, MoKC-MMO, MoKMMO-C, MoKMMO catalysts.

Sample	BET Surface Area (m^2/g)	Mo wt. %	K wt. %	C wt. %	Mo/Mg mass ratio	Mo/S mass ratio
MMO	180	-	-	-	-	-
C	1989	-	-	-	-	-
MoKC	1263	5.3	2.3	74.1	-	1.60
MoKC-MMO	237	4.5	2.3	16.5	0.21	1.30
MoKMMO-C	266	5.6	2.4	15.6	0.24	1.97
MoKMMO	45	5.3	2.5	-	0.19	1.63

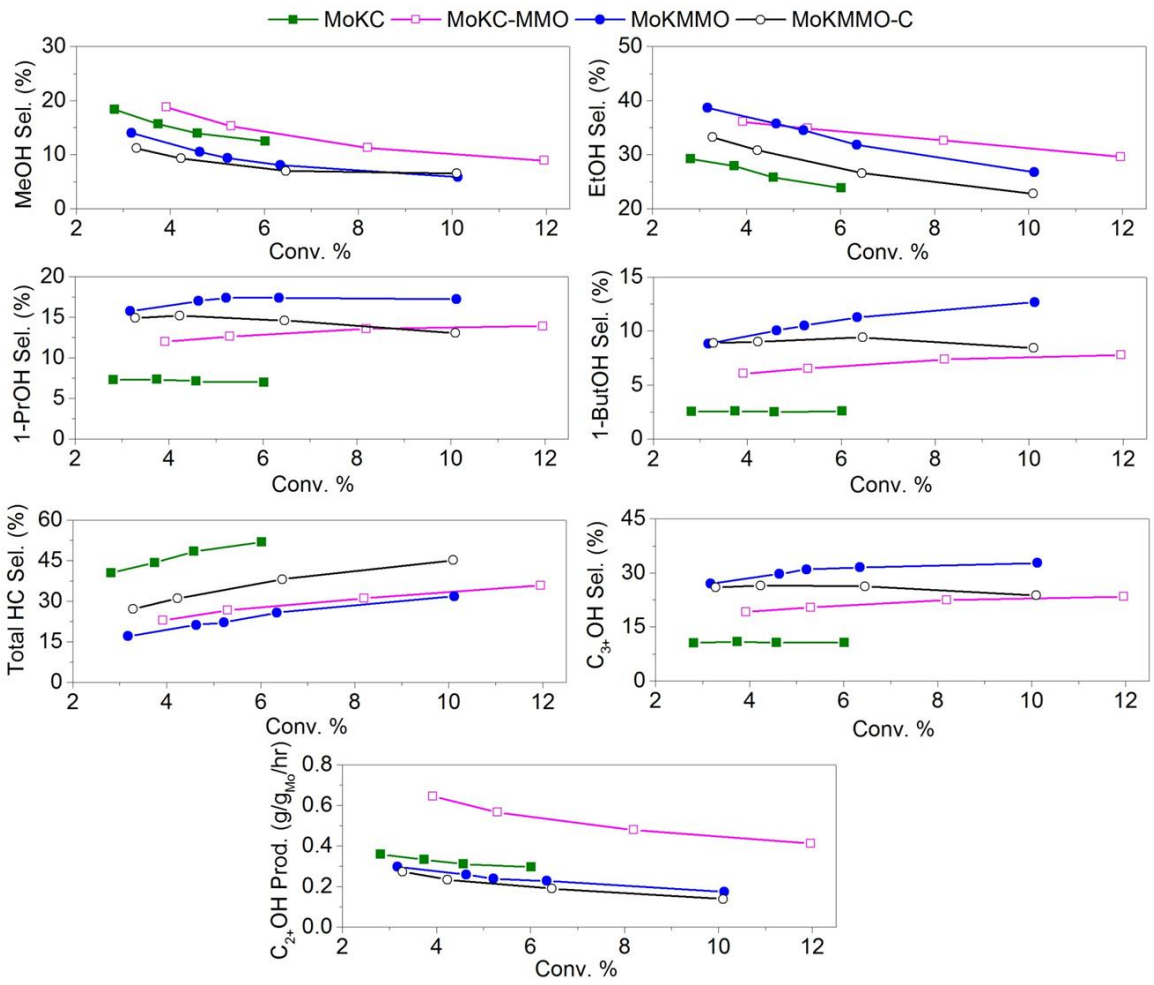

Figure 2.3: C_1-C_4 linear alcohols, total hydrocarbons (HC) and C_{3+}OH selectivity (CO_2-free), as well as C_{2+}OH productivity vs. CO conversion over MoKC, MoKC-MMO, MoKMMO, MoKMMO-C catalysts. Reaction conditions: 310 °C and 1500 psig. All reaction results are given after ~3 days of time on-stream at steady state.

2.2.3 Reactivity Results

The reactivity results for the family of carbon and MMO supported K/MoS_2 catalysts are shown in Figure 2.3. Linear alcohol and total hydrocarbon selectivity, as well as C_{2+} alcohol productivity (C_{2+}OH) are plotted against CO conversion. Selectivities are quantified on a CO_2-free basis for a clear depiction of higher alcohol synthesis, since CO_2 selectivities over these catalysts are high, due to water-gas shift reactions facilitated over MoS_2 based catalysts (Table 2.B.1). [18-21] The total non-alcohol oxygenate (acetaldehyde, methyl formate, methyl acetate, ethyl acetate, methyl propionate, and

ethyl propionate) selectivities for all the catalysts in this study were less than 3% (Table 2.B.1), indicating that primarily linear alcohols were the oxygenates formed over these catalysts. A second set of catalysts prepared from different batches of MMO and C supports were prepared and reacted to ensure the reactivity trends were consistent and reproducible. The second set of catalyst's reactivity trends are shown in Figure 2.B.2.

As previously observed, the MoKC catalyst was primarily selective towards methanol and ethanol, whereas the MoKMMO catalyst shifted the product distribution from C_1-C_2 to C_2-C_4 linear alcohols.[4] It is observed in this work that the MoKMMO catalyst had the highest C_{3+}OH selectivity, as expected, whereas the MoKC catalyst had the lowest C_{3+}OH selectivity but showed improved C_{2+}OH productivity compared to the MoKMMO catalyst. The enhanced C_{2+}OH productivity over the MoKC catalyst may be associated to the acidic nature of the carbon support as suggested from NH_3 TPD (Figure 2.A.3a), supported by the work of Liakakou et al. correlating increased CO conversion with increased acidity of a similar catalyst (K-NiMo supported on acid pretreated activated carbon).[3]

The C_{3+}OH selectivity trend for the MoKC-MMO catalyst was between that of the MoKMMO and MoKC parent catalysts (Figure 2.3), suggesting that some of the Mo was able to move from the originally (Mo) impregnated carbon support to the MMO support during sulfidation and reaction, creating a catalyst that was more selective towards C_{3+}OH, characteristic of the Mo domains on the MMO support. Unlike what was observed in the work by Dalai et al. upon binder incorporation to a CoRhMoS_2/MWCNT catalyst, the addition of the intrinsically basic MMO support to MoKC over the MoKC-MMO catalyst resulted in increased C_{3+}OH selectivity instead of a significant reduction of total alcohol selectivity.[17] It is particularly striking to note that the MoKC-MMO catalyst gave the highest alcohol productivity in this family of catalysts with more than a two-fold

increase in $C_{2+}OH$ productivity compared to that of the related MoKMMO and MoKMMO-C catalysts.

In contrast, the MoKMMO-C catalyst had selectivity and productivity trends similar to the MoKMMO catalyst, suggesting that the strong Mo-MMO interactions created when Mo was originally impregnated on MMO limited the ability of Mo to migrate to the carbon support under reaction conditions. It is important to note that the MoKMMO-C catalyst had a slightly higher total hydrocarbon selectivity, resulting in slightly lower $C_{2+}OH$ selectivity when compared to the MoKMMO catalyst. The addition of acidic carbon support to MoKMMO over the MoKMMO-C catalyst results in increased hydrocarbon formation by promoting dehydration/hydrogenation reactions.[3, 22]

2.2.3.1 Anderson-Shulz-Flory distribution

The Anderson-Schulz-Flory (ASF) distribution for linear alcohols and linear hydrocarbons is shown in Figure 2.B.3. Consistent with the selectivity trends, the catalysts where the Mo is initially contained on the MMO (MoKMMO and MoKMMO-C) have higher linear alcohol chain growth probabilities (α=0.49) followed by the MoKC-MMO and MoKC catalysts. The MoKMMO catalyst had the lowest alpha value for linear hydrocarbons, whereas carbon containing catalysts (MoKC, MoKMMO-C, and MoKC-MMO) had increased alpha values. The MoKMMO-C catalyst had the highest alpha value (0.41) for linear hydrocarbons consistent with higher hydrocarbon formation due to the acidic nature of the carbon support, as discussed above.

2.2.3.2 Approximate Turnover Frequencies

Approximate turnover frequencies (TOFs) for $C_{2+}OH$, and total hydrocarbons (HC) based on CO conversions are provided in Figure 2.B.4 and Table 2.B.2. A lower bound (LB) TOF estimate is provided, assuming all Mo atoms are active sites. In addition, a middle estimate (ME) of the TOF is provided, assuming only edge Mo atoms are active. Consistent with the productivity trends, the catalysts where the Mo was

initially contained on the MMO (MoKMMO and MoKMMO-C) have lower ME TOFs at 5% CO conversion (5.0 and 5.7, respectively) compared to catalysts whereby Mo was initially contained on the carbon support (MoKC (11.1) and MoKC-MMO (13.7)). These values are an order of magnitude lower than values obtained for rhodium catalysts at similar reaction conditions, shown in Table 2.B.3, as expected.

2.2.3.3 Reaction Pathways

Mo-support interactions not only seem to affect Mo mobility, but also may facilitate certain reaction pathways. Mg/Al mixed oxides (MMO) can facilitate Guerbet coupling reactions due to their acid-base pairs, where the Lewis acidic Al is thought to stabilize the aldehyde and ketone intermediates.[23] It can be observed in Figure 2.3 that in MMO containing catalysts, ethanol selectivity decreased with increasing conversion, while 1-butanol selectivities increased, suggesting that ethanol self-coupling may be an important secondary reaction over these catalysts. Even though MoS_2 is acidic in nature and the presence of potassium increases the basicity of the catalyst (creating the possibility of having both acid and base sites), the carbon support lacks the base sites present in MMO (Figure A5b), and therefore, this trend was not observed over MoKC. Furthermore, isobutyl alcohol selectivity, an indicator of methanol + 1-propanol coupling reactions, was measurably lower over the MoKC catalyst than over the MoKMMO catalyst, as shown in Table 2.B.1. Further experiments need to be conducted to investigate the importance of coupling pathways over these catalysts, which will be the focus of the subsequent chapters.

2.2.4 Structural Properties of Reaction-aged Catalysts

2.2.4.1 Role of K

To gain a deeper understanding of these reactivity trends it is necessary to explore the structural properties of the catalysts and how these properties affect the productivity and selectivity. The modification of MoS_2 based catalysts with potassium is well known to shift the product distribution from hydrocarbons to alcohols by inhibiting hydrocarbon formation, as shown in Figure 2.B.5a.[24] Unpromoted MoC and MoMMO catalysts were compared to promoted MoKC and MoKMMO catalysts. The MoC and MoMMO catalysts were mainly selective towards hydrocarbons and upon K promotion their selectivity shifted from hydrocarbons to higher alcohols. The MoC catalyst was not active towards higher alcohols ($C_{2+}OH$ productivity was close to zero), whereas the MoMMO catalyst showed $C_{2+}OH$ productivity similar to the MoKMMO catalyst, as the intrinsically basic MMO support facilitates higher alcohol formation. Therefore, modification with potassium over MMO supported catalysts affects only the selectivity of the catalyst by inhibiting hydrocarbon formation. Additionally, potassium is thought to play a role in the active sites for production of alcohols.[25-29] X-ray photoelectron spectroscopy (XPS) analysis shown in Table 2.A.3 demonstrates that there is a decrease in sulfur content between MoMMO and MoKMMO, which may be attributed to sulfur vacancies created when potassium intercalates in the MoS_2 stacked layer that may inhibit hydrocarbon formation. This hypothesis is supported by Beltrami et al. work, where they correlated the sulfur loss (anionic vacancies) observed over an unsupported Ni/MoS_2 catalyst to the promotion of higher alcohol formation.[30] It has also been observed in the literature that alkali metal intercalates between the layers of MoS_2,[31-35] which are held together by van der Waals forces, and this weak binding force allows the interlayer gap to increase to accept alkali metal ions.

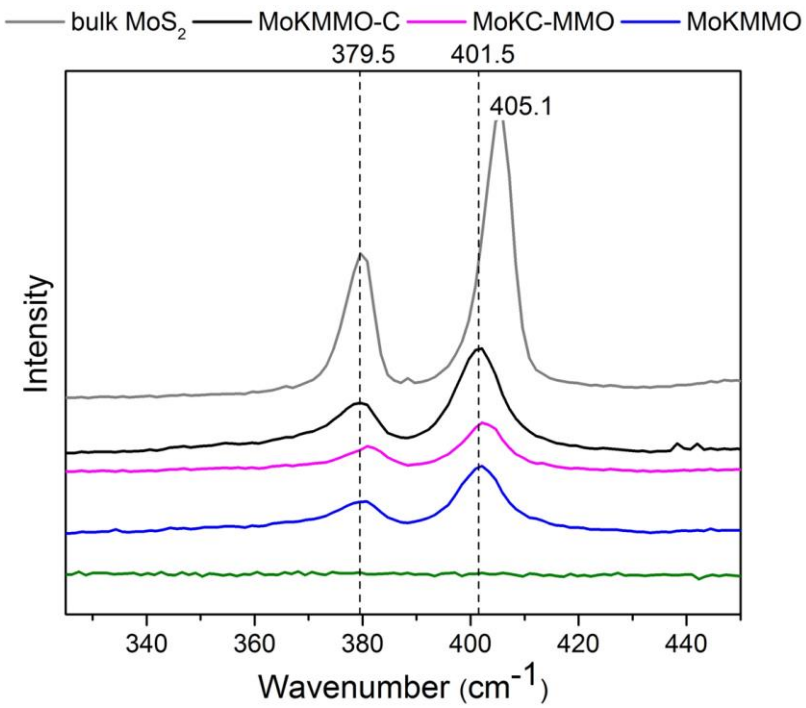

Figure 2.4: Raman spectra of bulk MoS_2 and reaction-aged MoKC, MoKMMO, MoKMMO-C, and MoKC-MMO catalysts.

2.2.4.2 Raman Results

Raman spectra shown in Figure 2.4 of the MoKMMO and MoKMMO-C catalysts depict two bands at 379.5 and 401.5 cm^{-1}, which correspond to $v(E^1_{2g})$ and $v(A_{1g})$ MoS_2 vibrational modes, respectively. The MoKC-MMO catalyst showed similar bands shifted to higher frequencies, 380.6 cm^{-1} for $v(E^1_{2g})$ and 402.4 cm^{-1} for $v(A_{1g})$ vibrational modes. Similar to the MoKMMO and MoKMMO-C catalyst, the bulk MoS_2 commercial standard had a band at 379.5 cm^{-1} corresponding to $v(E^1_{2g})$, but the $v(A_{1g})$ band was shifted to 405.1 cm^{-1}, suggesting that the interlayer distance between the MoS_2 stacked layers was smaller than the MMO and carbon supported MoS_2 catalysts.[36] This difference may be caused by a lesser degree of MoS_2 stacking in the supported catalysts compared to the bulk MoS_2 material, resulting in a less compact MoS_2 domain[37] and/or by K intercalation between the MoS_2 stacked layers.[33] Figure 2.B.5b shows that promoted catalysts have a longer induction period compared to unpromoted catalyst, which may be attributed to K

intercalating in the MoS_2 structure.[25] The shift to higher frequencies observed in the MoKC-MMO catalyst compared to the MoKMMO and MoKMMO-C catalysts can be attributed to the increased number of MoS_2 domains with 3+ layers, as observed from STEM (Figure 2.6a) and discussed below, that have smaller interlayer distance compared to MoS_2 domains with mainly double layers (larger interlayer distance) present in the MoKMMO and MoKMMO-C catalysts.[37] In contrast to the above materials, the Raman spectra for the MoKC catalyst showed no Mo-S vibration bands, as the MoKC catalyst was mainly comprised of single layers with highly dispersed Mo, as observed by STEM imaging, and described below. Additionally, it should be noted that the lack of Mo-S vibration bands for the MoKC catalyst is likely not associated with spectral fluorescence because a higher Mo content supported on the carbon showed these bands clearly (data not shown).

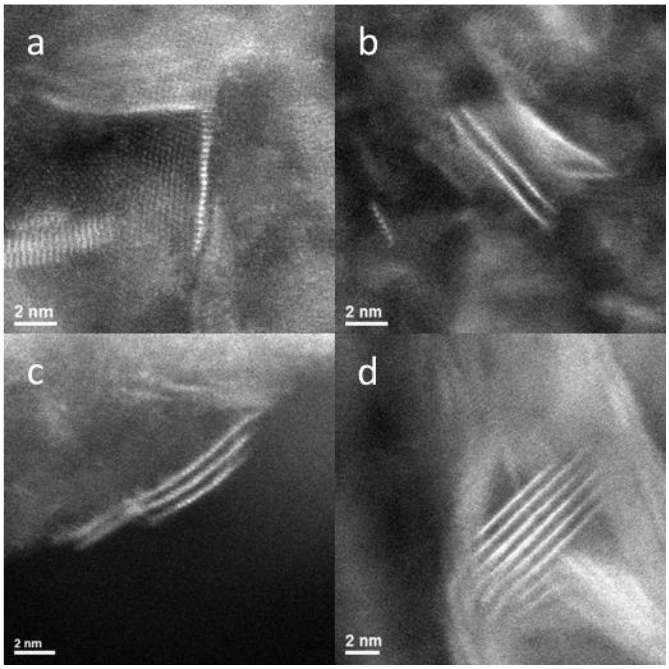

Figure 2.5: Dark field STEM images of single layer (a), double layer (b), triple layer (c) and 3+ layer (d) examples of MoS_2 [002] stacking of the reaction-aged catalysts in this study.

2.2.4.3 STEM Results

High-angle annular dark field (HAADF) STEM imaging was used as the primary means to characterize the MoS_2 domain size and [002] layer stacking in the various catalysts. A total of 790 STEM images were analyzed to determine the fraction of MoS_2 stacked layers in each catalyst of this family of catalysts, taking into account over 240 MoS_2 domains for the each of the MoKC, MoKC-MMO, and MoKMMO-C catalysts and 150 MoS_2 domains for the MoKMMO catalyst (a similar MoKMMO catalyst was previously characterized by STEM[5]). The number of MoS_2 [002] stacked layers was quantified as single, double, triple and 3+ layers, as exemplified in Figure 2.5, and the percentage of MoS_2 [002] layers as a function of number of layers for each catalyst is quantified in Figure 2.6a.It should be noted that domains with fewer MoS_2 stacked layers (1-3 layers) were generally shorter in length than the domains with 3+ layers, among all the catalysts studied.

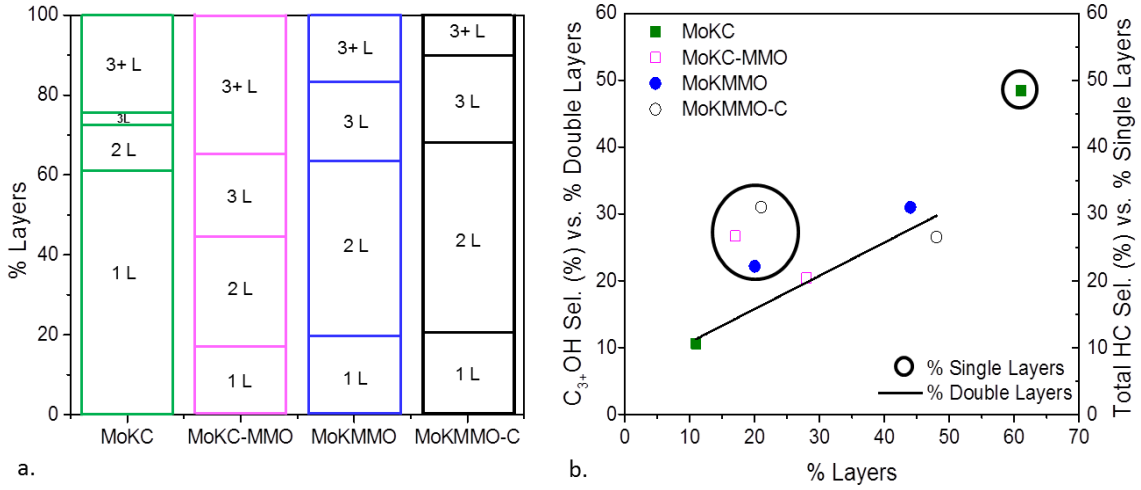

Figure 2.6: (a) Layer distribution of MoS_2 stacked layers for the reaction-aged catalysts in this study (b) $C_{3+}OH$ selectivity (CO_2-free) vs. % double layers (solid line) and total hydrocarbon selectivity (CO_2-free) vs. % single layers (circles) determined from Figure 2.6a.

2.2.4.4 Structure Reactivity Relationships

Analogous to the MoKMMO sample and consistent with the work of Morrill et al.,[5] the MoKMMO-C catalyst contained mainly double MoS_2 layers (Figure 2.6a), consistent with reactivity trends selective toward C_{3+} alcohols, as described above. Figure 2.6b shows that as the number of double layers increases, the $C_{3+}OH$ selectivity increases. Dorokhov et al. observed a similar trend over K/MoS_2 supported on γ-Al_2O_3-SiO_2, where the total alcohol yield increased with an increasing fraction of 2+ layers, with double layers being the dominant domain size.[34] The MoKMMO and MoKMMO-C catalysts have the highest fraction of double layers with correspondingly higher $C_{3+}OH$ selectivity, followed by the MoKC-MMO, and MoKC catalysts having the lowest $C_{3+}OH$ selectivity with lowest fraction of double layers. This trend suggests that K/MoS_2 interactions with MMO play an important role in the formation of higher alcohols, as strong support-Mo interactions limit the growth of the number of MoS_2 stacked layers, compared to carbon supported MoKC and MoKC-MMO catalysts that have a significant amount of 3+ layers due to weaker Mo-carbon interactions.

It can be further inferred that the MoKC catalyst had predominately single layers (without potassium intercalation, which is not possible for a single layer), which facilitate hydrocarbon formation. This is in agreement with the Rim-Edge model, where rim sites are responsible for hydrocarbon formation and single layers only possess rim sites.[38] Figure 2.6b further supports that single Mo rim sites correlate with production of hydrocarbons, as the selectivity for total hydrocarbons increased with an increase in the percentage of single layers present in the catalysts, as also observed by Dorokhov et al.[34] The MMO-containing catalysts had a significantly lower fraction of single layers, supporting the low selectivity of these catalysts towards hydrocarbons.

Additionally, it should be noted that the MoKC-MMO catalst had a more even distribution of 2, 3, and 3+ MoS_2 stacked layers, supporting the observation that the

selectivity trends for this catalyst were in between that of the MoKMMO and MoKC catalysts, as noted above, yielding a catalyst that was both active and selective to higher alcohols. This is consistent with our original hypothesis, whereby the MMO supported domains were suggested to provide sites that could yield good higher alcohol selectivity due to strong Mo-MMO interactions that limit the growth of stacked layers, and carbon supported domains would more effectively activate the hydrogen and carbon monoxide, yielding higher reaction rates due to weak Mo-C interactions that facilitate Mo dispersion across the supports. It should be noted that these correlating observations, however, do not necessarily prove causality, and it is unclear at this stage if reaction intermediates from carbon-supported domains migrate and further react on MMO supported domains. As mentioned below, $Mo_{0.15}K_{0.09}C$ catalyst showed increased MoS_2 [002] stacking with an increase in loading compared to $Mo_{0.05}K_{0.03}C$. This increase in stacking resulted in an increase in $C_{2+}OH$ selectivity and productivity, as shown in Table 2.B.4. MMO supported catalysts showed an increase in stacking with increase in loading, similar to the C support. However, the catalyst with a lower Mo loading with fewer stacked layers was more selective towards $C_{2+}OH$ and more productive towards $C_{3+}OH$.[5] It is hypothesized that intimate contact between the K/MoS_2 domains and MMO has a synergistic effect in the formation of higher alcohols.

2.2.4.5 Single Layer Correlation to Hydrocarbon Formation

A detailed analysis of domains comprised of 3+ layers and the MoO_2 domains, which were also present over the MoKC catalyst, was necessary to provide further insight into the single layer domain formation and their effect on hydrocarbon formation. Figure 2.A.7a shows that MoKC formed domains with 3+ layers in the proximity of MoO_2 domains, suggesting that MoO_2 domains supply Mo species for growth of nearby domains of 3+ MoS_2 layers. However, not all the MoO_2 domains were fully reduced to form MoS_2 stacked layers under the conditions used, as further supported by the peaks

associated with crystalline MoO_2 domains observed in the XRD pattern of the MoKC catalyst (Figure 2.2). Increasing the Mo and K loading to 15 and 9 wt.%, respectively, over a carbon support ($Mo_{0.15}K_{0.09}C$), resulted in the formation of predominantly domains with 3+ layers, as shown in Figure 2.A.10, suggesting that clustering of Mo species is necessary for the formation of highly stacked MoS_2 domains. Therefore, it is hypothesized that single layers over the MoKC catalyst are formed due to the highly dispersed Mo species across the support (due to low Mo, K loading) that do not agglomerate to grow beyond the critical nucleus size necessary for growth of MoS_2 stacked layers, compared to the $Mo_{0.15}K_{0.09}C$ catalyst with higher Mo and K loading. The XRD pattern of the higher loading $Mo_{0.15}K_{0.09}C$ catalyst, shown in Figure 2.A.11, exhibited a MoO_2 diffraction line at 26°, also present in MoKC, further supporting that the presence of MoO_2 domains contribute to the formation of MoS_2 stacked layers and likely not single layers. In addition, the MoKC precatalyst in oxide form, without undergoing in situ sulfidation, was selective towards methanol and ethanol (see Table 2.B.1) when reacted, supporting the notion that the MoO_2 domains do not strongly influence hydrocarbon formation under the conditions employed, and that single layer MoS_2 domains were likely responsible for hydrocarbon formation.

2.2.4.6 Structure as a Function of Reaction Time

To further investigate the reactivity trends observed for the mixed supported catalysts, the MoKC-MMO and MoKMMO-C catalysts were subjected to different reaction times on-stream followed by STEM characterization to quantify changes of MoS_2 domain size as a function of reaction time. The MoKC-MMO catalyst underwent a significant change in the layer distribution as shown in Figure 2.7a. After ex situ sulfidation before undergoing catalytic reaction, the catalyst possessed mainly double layers. During the transient period at the initial stages of the catalytic reaction, the layer distribution shifted to 3 and 3+ layers, and the catalyst was comprised of mainly 3+ layers when the catalyst

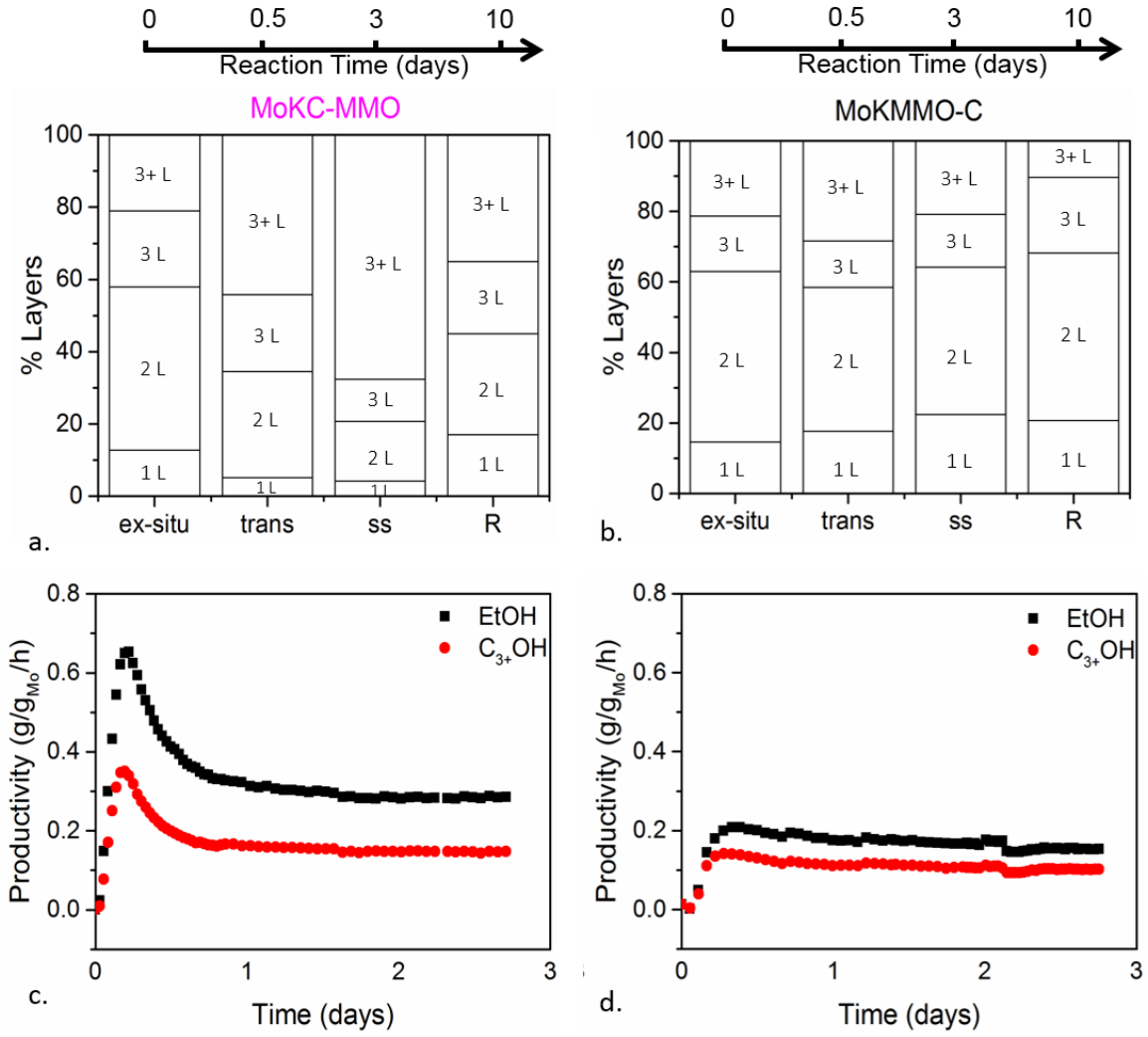

Figure 2.7: Layer distribution of MoS_2 stacked layers with different reaction times on-stream: ex situ- 0 days, transient period (trans)- 0.5 days, steady state (ss)- 3 days, reaction-aged (R)- 12 days for MoKC-MMO (a) and MoKMMO-C (b) catalysts. EtOH and $C_{3+}OH$ Productivity as a function of time for MoKC-MMO (c) and MoKMMO-C (d) catalysts.

reached steady-state. It is important to note that the layer distribution of the MoKC-MMO catalyst at steady-state was similar to that of the reaction-aged $Mo_{0.15}K_{0.09}C$ catalyst shown in Figure 2.A.10, which suggests the majority of the Mo species formed large clusters (3+ layers) on the carbon when the reaction approached steady-state. This observation is consistent with the MoKC-MMO preparation, where the $Mo_{0.15}K_{0.09}C$ oxide precatalyst was ground with the bare MMO. This suggests that the MoKC-MMO catalyst will possess largely 3+ layers, similar to the $Mo_{0.15}K_{0.09}C$ catalyst, before the bulk of the Mo species redistribution across the supports occurs (if the Mo species were mobile during reaction). The drastic shift in layer distribution observed for the reaction-aged MoKC-MMO catalyst indicates that the Mo species were in fact highly mobile during the reaction and redistributed between the carbon and MMO supports, as there was an even distribution of 1, 2, 3, and 3+ layer domains in the reaction-aged catalyst. The Mo species were able to redistribute effectively because they (relatively) weakly interacted with the parent carbon support compared to the MMO support. This Mo redistribution may allow vacancies or defects to be created on the MoS_2 domains, resulting in higher productivity, as discussed above.

On the other hand, the MoKMMO-C catalyst did not undergo any significant change in the layer distribution as the reaction progressed, as shown in Figure 2.7b. This observation further supports the idea that when Mo was impregnated on the parent MMO support, the Mo species were more strongly bound to the MMO and were not significantly redistributed between the carbon and MMO supports during reaction, as with the MoKC-MMO counterpart. Additionally, Figure 2.7c shows that the significant change in productivity over the MoKC-MMO catalyst during the first three days of reaction can be attributed to the growth of MoS_2 stacking. On the other hand, the MoKMMO-C catalyst had no significant change in higher alcohol productivity (Figure 2.7d) over the first three days of reaction, from ex situ to steady-state, compared to the

MoKC-MMO catalyst, consistent with the lack of a change in layer distribution throughout the reaction.

It is also interesting to note that the layer distributions for both the MoKC-MMO and MoKMMO-C catalysts that were ex situ sulfided but not reacted with syngas were comparably similar (Figure 2.7a and 2.7b), indicating that the sulfidation process led to similar arrays of MoS_2 domains in the absence of syngas. However, specific Mo-support interactions affected the spontaneous growth of the Mo domains under syngas conversion conditions. In the case of the MoKMMO-C catalyst, strong Mo-MMO interactions prevented significant redistribution of the array of MoS_2 stacked layers. In contrast, comparably weak Mo-C interactions in the MoKC-MMO catalyst facilitated significant redistribution of Mo and changed the array of MoS_2 stacked layers.

2.2.4.7 EXAFS Results

EXAFS spectroscopy was also used to shed light into the structure of the MoS_2 layers present over the family of carbon and MMO supported catalysts. The Fourier transform k^3-weighted Mo K-edge EXAFS spectra show that the supported catalysts had lower Mo-Mo coordination numbers compared to bulk MoS_2, as the Mo-Mo peak intensity was far lower than the bulk MoS_2 counterpart, as also observed by Morrill et al.[5] Lower Mo-Mo coordination numbers compared to the bulk MoS_2 may indicate monolayer defects created during the sulfidation and reaction. Among the catalysts studied, the MoKC catalyst seemed to have the smallest Mo-Mo coordination number (Figure 2.A.12), as expected due to high dispersion of Mo species on the carbon support, which contained many single layer domains. The mixed supported catalysts (MoKC-MMO, MoKMMO-C) appeared to have Mo-Mo coordination numbers in between that of the MoKMMO and MoKC catalysts, with the MoKMMO catalyst having the highest Mo-Mo coordination number due strong Mo-MMO interactions that limited the dispersion of the Mo species on the support.

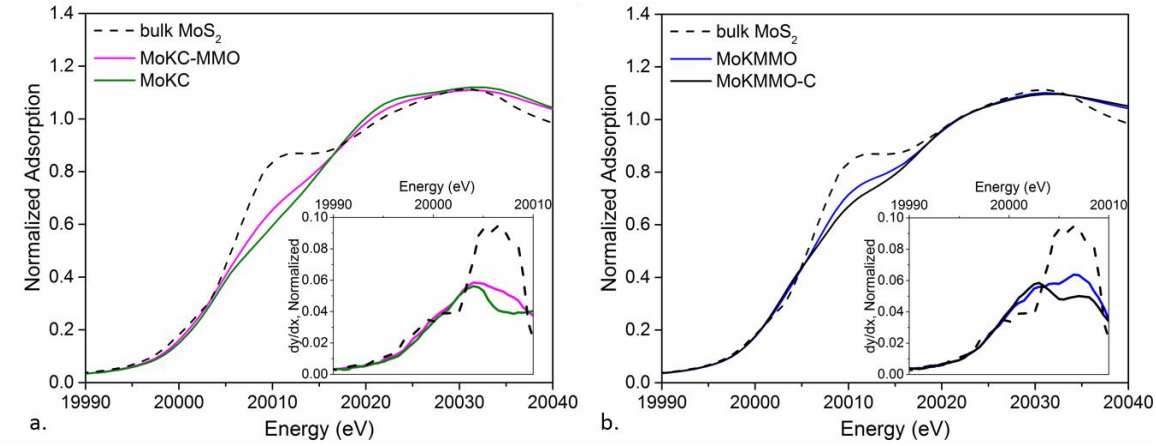

Figure 2.8: XANES Mo K-edge spectra of bulk MoS_2, and reaction-aged (a) MoKC, MoKC-MMO, and (b) MoKMMO, MoKMMO-C catalysts; (inset) first derivative of the Mo K-edge spectra.

An assessment of the electronic structure of the MoS_2 domains was inferred from XANES spectroscopy, as shown in Figure 2.8.[39] Specifically, isosbestic points where the reaction-aged catalysts intersected bulk MoS_2 were an indication that the reaction-aged catalysts had chemical states similar to that of bulk MoS_2. Following the overlay of the XANES edges, it was unsurprising that the catalysts where Mo was originally impregnated on carbon (MoKC and MoKC-MMO in Figure 2.8a) were similar to each other just as those supported on MMO (MoKMMO and MoKMMO-C in Figure 2.8b) were similar as well. What is clear, however, is that the support interaction was quite subtle and that even though the MoKC and MoKC-MMO catalysts had different isosbestic points from the MoKMMO and MoKMMO-C catalysts (at 20015 eV and 20005 eV, respectively), with both sets being slightly different from bulk MoS_2, all the catalysts studied had overall similar chemical signatures to that of the bulk MoS_2. In addition, the normalized first derivative, shown in the inset of Figure 2.8, offers further insight into the catalysts' chemical state. The adsorption edge energy of the MoKC and MoKC-MMO catalysts shifted to higher values compared to that of the MoKMMO and MoKMMO-C catalysts, suggesting a higher average Mo oxidation state for the catalysts where Mo

was originally impregnated on carbon. The shift in adsorption energy of the MoKC and MoKC-MMO catalysts may be associated with the MoO_2 domains present after reaction, as seen in the XRD patterns in Figure 2.2 and STEM images (Figure 2.A.7). In addition, the spectra of the MoKC and MoKC-MMO catalysts, shown in Figure 2.8, differed from that of bulk MoS_2 in that they did not show the sharp feature at 20010 eV characteristic of bulk MoS_2, and there was an increase of intensity in the tail of the edge just before the white line at (20025 eV). These differences further suggest that both the MoKC and MoKC-MMO catalysts were not fully reduced from the oxide phase to the sulfide phase.[40, 41]

2.3 Conclusions

Two distinct supports, a layered MMO material and a mesoporous activated carbon, were combined to tune the higher alcohol selectivity and productivity of K/MoS_2 domains during syngas conversion. The reactivity and structural data compiled here are consistent with the hypothesis that Mo had the ability to migrate from the carbon support (where mobility was high) to the MMO support (where mobility was lower), creating in the case of MoKC-MMO, a hybrid catalyst that was both productive and selective towards higher alcohols. In contrast, when Mo was originally impregnated on the MMO support, Mo migration under reaction conditions was decreased, yielding a less active catalyst that behaved more like the parent MoKMMO catalyst. The $C_{3+}OH$ selectivity over the family of catalysts was shown to correlate with the percentage of double [002] MoS_2 layers present in reaction-aged catalysts. Strong Mo-MMO interactions in the MoKMMO and MoKMMO-C catalysts, which contained mainly double layers, were thought to limit the growth of MoS_2 stacked layers, resulting in the highest observed $C_{3+}OH$ selectivity over the catalysts studied. On the other hand, catalysts that contained many single [002] MoS_2 layers, without potassium intercalation, were shown to be more

selective towards hydrocarbons, with the MoKC catalyst having the highest total hydrocarbon selectivity. The structure-reactivity relationships (MoS_2 domain stacking vs. selectivity) explored in this work provide the basis for further investigations focused on understanding reaction pathways over these interesting catalysts.

2.4 References

(1) S.-H. Chai, J. Y. Howe, X. Wang, M. Kidder, V. Schwartz, M. L. Golden, S. H. Overbury, S. Dai and D.-e. Jiang, *Carbon*, 2012, **50**, 1574-1582.

(2) S.-H. Chai, V. Schwartz, J. Y. Howe, X. Wang, M. Kidder, S. H. Overbury, S. Dai and D.-e. Jiang, *Microporous Mesoporous Mater.*, 2013, **170**, 141-149.

(3) E. T. Liakakou, E. Heracleous, K. S. Triantafyllidis and A. A. Lemonidou, *Appl. Catal., B*, 2015, **165**, 296-305.

(4) M. R. Morrill, N. T. Thao, P. K. Agrawal, C. W. Jones, R. J. Davis, H. Shou, D. G. Barton and D. Ferrari, *Catal. Lett.*, 2012, **142**, 875-881.

(5) M. R. Morrill, N. T. Thao, H. Shou, R. J. Davis, D. G. Barton, D. Ferrari, P. K. Agrawal and C. W. Jones, *ACS Catal.*, 2013, **3**, 1665-1675.

(6) G.-z. Bian, Y.-l. Fu and Y.-s. Ma, *Catal. Today*, 1999, **51**, 187-193.

(7) Y.-l. Fu, K. Fujimoto, P.-y. Lin, K. Omata and Y.-s. Yu, *Appl. Catal., A*, 1995, **126**, 273-285.

(8) Z.-r. Li, Y.-l. Fu, M. Jiang, M. Meng, Y.-n. Xie, T.-d. Hu and T. Liu, *Catal. Lett.*, 2000, **65**, 43-48.

(9) Z.-r. Li, Y.-l. Fu and M. Jiang, *Appl. Catal., A*, 1999, **187**, 187-198.

(10) H. Okatsu, M. Morrill, H. Shou, D. Barton, D. Ferrari, R. Davis, P. Agrawal and C. Jones, *Catal. Lett.*, 2014, **144**, 825-830.

(11) X. Wang, J. S. Lee, C. Tsouris, D. W. DePaoli and S. Dai, *J. Mater. Chem.*, 2010, **20**, 4602-4608.

(12) J. G. Nunan, R. G. Herman and K. Klier, *J. Catal.*, 1989, **116**, 222-229.

(13) K. Takehira, T. Shishido, D. Shoro, K. Murakami, M. Honda, T. Kawabata and K. Takaki, *Catal. Commun.*, 2004, **5**, 209-213.

(14) J. Pérez-Ramírez, S. Abelló and N. M. van der Pers, *Chem. Eur. J.*, 2007, **13**, 870-878.

(15) D. Ferrari, G. Budroni, L. Bisson, N. J. Rane, B. D. Dickie, J. H. Kang and S. J. Rozeveld, *Appl. Catal., A*, 2013, **462-463**, 302-309.

(16) K. S. Liang, R. R. Chianelli, F. Z. Chien and S. C. Moss, *J. Non-Cryst. Solids*, 1986, **79**, 251-273.

(17) P. E. Boahene, V. R. Surisetty, R. Sammynaiken and A. K. Dalai, *Top. Catal.*, 2014, **57**, 538-549.

(18) M. Kantschewa, F. Delannay, H. Jeziorowski, E. Delgado, S. Eder, G. Ertl and H. Knözinger, *J. Catal.*, 1984, **87**, 482-496.

(19) R. N. Nickolov, R. M. Edreva-Kardjieva, V. J. Kafedjiysky, D. A. Nikolova, N. B. Stankova and D. R. Mehandjiev, *Appl. Catal., A*, 2000, **190**, 191-196.

(20) X.-R. Shi, S.-G. Wang, J. Hu, H. Wang, Y.-Y. Chen, Z. Qin and J. Wang, *Appl. Catal., A*, 2009, **365**, 62-70.

(21) P. Hou, D. Meeker and H. Wise, *J. Catal.*, 1983, **80**, 280-285.

(22) F. M. Bautista and B. Delmon, *Appl. Catal., A*, 1995, **130**, 47-65.

(23) J. T. Kozlowski and R. J. Davis, *ACS Catal.*, 2013, **3**, 1588-1600.

(24) H. Shou and R. J. Davis, *J. Catal.*, 2011, **282**, 83-93.

(25) V. P. Santos, B. van der Linden, A. Chojecki, G. Budroni, S. Corthals, H. Shibata, G. R. Meima, F. Kapteijn, M. Makkee and J. Gascon, *ACS Catal.*, 2013, **3**, 1634-1637.

(26) J. G. Santiesteban, C. E. Bogdan, R. G. Herman and K. Klier, *in: M.J. Philips, M. Ternan (Eds.), vol. 2, 9th Annual Congress on Catalysis, Chemical Institute of Canada, Calgary, 1988, pp. 561-568.*

(27) H. C. Woo, I. S. Nam, J. S. Lee, J. S. Chung and Y. G. Kim, *J. Catal.*, 1993, **142**, 672-690.

(28) J. S. Lee, S. Kim, K. H. Lee, I. S. Nam, J. S. Chung, Y. G. Kim and H. C. Woo, *Appl. Catal., A*, 1994, **110**, 11-25.

(29) D. Li, C. Yang, W. Li, Y. Sun and B. Zhong, *Top. Catal.*, 2005, **32**, 233-239.

(30) M. Konarova, F. Q. Tang, J. L. Chen, G. Wang, V. Rudolph and J. Beltramini, *ChemCatChem*, 2014, **6**, 2394-2402.

(31) R. B. Somoano, V. Hadek, A. Rembaum, S. Samson and J. A. Woollam, *J. Chem. Phys.*, 1975, **62**, 1068-1073.

(32) E. Benavente, M. A. Santa Ana, F. Mendizábal and G. González, *Coord. Chem. Rev.*, 2002, **224**, 87-109.

(33) A. Andersen, S. M. Kathmann, M. A. Lilga, K. O. Albrecht, R. T. Hallen and D. Mei, *J. Phys. Chem. C*, 2012, **116**, 1826-1832.

(34) V. S. Dorokhov, D. I. Ishutenko, P. A. Nikul'shin, K. V. Kotsareva, E. A. Trusova, T. N. Bondarenko, O. L. Eliseev, A. L. Lapidus, N. N. Rozhdestvenskaya and V. M. Kogan, *Kinet. Catal.*, 2013, **54**, 243-252.

(35) F. Wypych, T. Weber and R. Prins, *Chem. Mater.*, 1998, **10**, 723-727.

(36) A. Müller and T. Weber, *Appl. Catal.*, 1991, **77**, 243-250.

(37) H. Li, Q. Zhang, C. C. R. Yap, B. K. Tay, T. H. T. Edwin, A. Olivier and D. Baillargeat, *Adv. Funct. Mater.*, 2012, **22**, 1385-1390.

(38) M. Daage and R. R. Chianelli, *J. Catal.*, 1994, **149**, 414-427.

(39) L. Li, M. R. Morrill, H. Shou, D. G. Barton, D. Ferrari, R. J. Davis, P. K. Agrawal, C. W. Jones and D. S. Sholl, *J. Phys. Chem. C*, 2013, **117**, 2769-2773.

(40) R. G. Leliveld, A. J. van Dillen, J. W. Geus and D. C. Koningsberger, *J. Catal.*, 1997, **171**, 115-129.

(41) R. Cattaneo, T. Shido and R. Prins, *Stu. Surf. Sci. Catal.*, 1999, **127**, 421-425.

APPENDIX 2.A

K/MoS_2 CATALYST CHARACTERIZATION

This appendix includes the supporting characterization of supported K/MoS_2 domain structure via N_2 physisorption, X-ray Diffraction, and High Resolution STEM imaging discussed in this chapter.

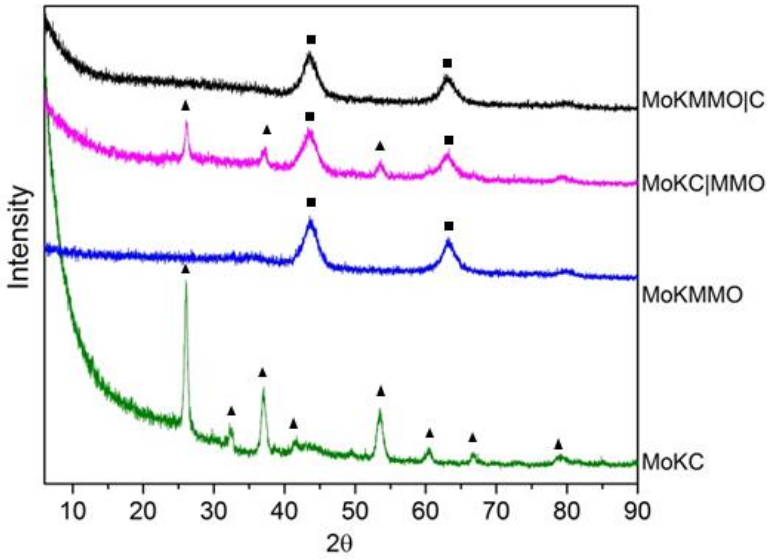

Figure 2.A.1: XRD patterns of the MoKMMO-C (black), MoKC-MMO (magneta), MoKMMO (blue), and MoKC (green) oxide precatalysts. (▲) MoO_2 (■) MgO.

Table 2.A.1: BET surface area and BJH Adsorption Pore Volume changes for MMO and MMO-C upon pelletization (P).

Sample	BET Surface Area (m2/g)	BJH Adsorption Pore Volume (cm^3/g)
MMO	190	0.50
MMO-P	154	0.46
MMO-C	590	0.49
MMO-C-P	457	0.44

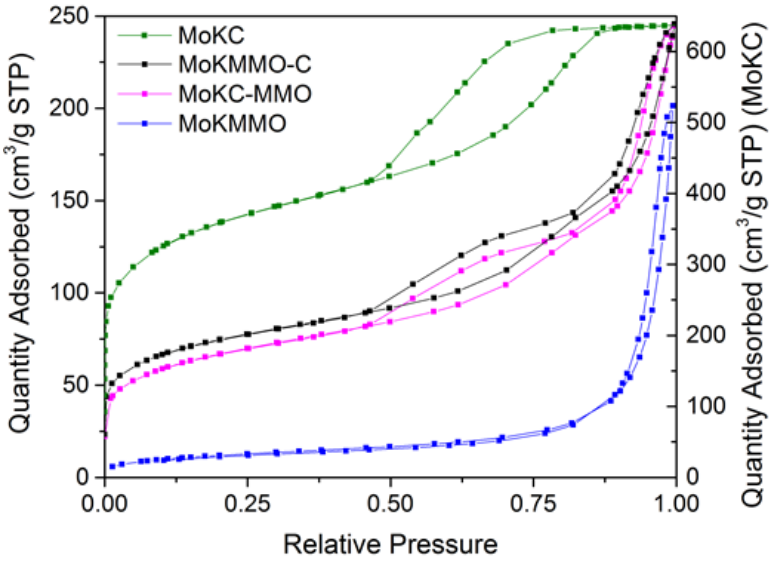

Figure 2.A.2: Adsorption isotherms for the MoKC, MoKMMO-C, MoKC-MMO, and MoKMMO catalysts.

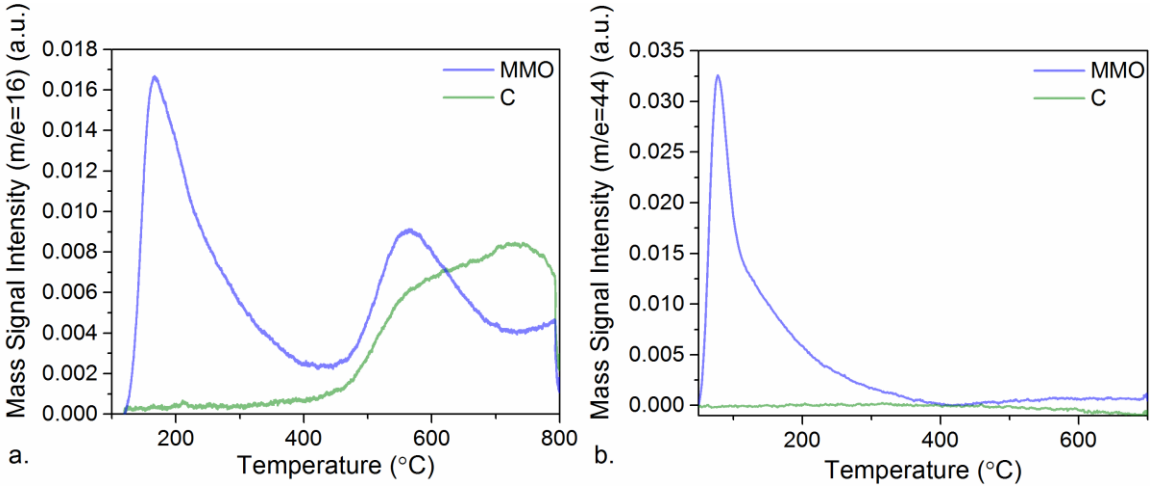

Figure 2.A.3: (a) Ammonia TPD (b) CO_2 TPD of mesoporous activated carbon and MMO supports.

Table 2.A.2: Acid and Base Properties of mesoporous activated carbon and MMO supports.

Total Uptake	Carbon	MMO
NH_3 (μmol/g)	1.3	2.6
CO_2 (μmol/g)	-	1.97

Table 2.A.3: XPS analysis for MMO, MoMMO, and MoKMMO catalysts.

Element (at %)	MMO[a]	MoMMO[b]	MoKMMO[c]
Mo 3p	-	3.44	3.58
S 2p	1.45	4.41	2.09
K 2p/ 3p	-	-	NA
Mg 1s	20.86	19.84	20.39
Al 2p	20.25	17.23	17.4
O 1s	54.49	48.25	52.56
C 2s	2.95	6.82	3.97
XPS data (at%/at%)			
Mo 3p/S 2p	N/A	0.78	1.71
Mg 1s/O 1s	0.38	0.41	0.39
Surface composition	N/A	$MoS_{1.28}$	$MoS_{0.58}$

[a]ex situ sulfided [b]in situ sulfided and reaction-aged until steady-state [c]in situ sulfided and reaction-aged for ~12 days. For the MoKMMO catalyst, K at. % was not able to be determined as K 3p overlapped with O 2s and K 2p overlapped with C 1s.

XANES and XRD results showed that the surface of the catalyst readily oxidizes (specifically the MoKC and MoKC-MMO catalysts were sensitive to oxidation during passivation and storage). As XPS is a surface technique, no accurate depiction of the sulfur species across the whole of the catalyst can be made with this technique alone. The MoMMO catalyst was prepared just before this XPS analysis, whereas the MoKMMO catalyst was prepared months before XPS analysis. Therefore, some of the sulfur loss associated to the MoKMMO catalyst may be due to oxidation of the MoS_2 domain surface during storage, supported by the observation that the MoKMMO catalyst has the lowest atomic ratio of Mg 1s/O 1s as well as the fitting curves of the MoMMO and MoKMMO catalysts (Figure 2.A.4 and 2.A.5) that indicate that Mo^{6+} species are present in the MoKMMO catalyst but not in the MoMMO catalyst, which likely come from MoO_3 domains.

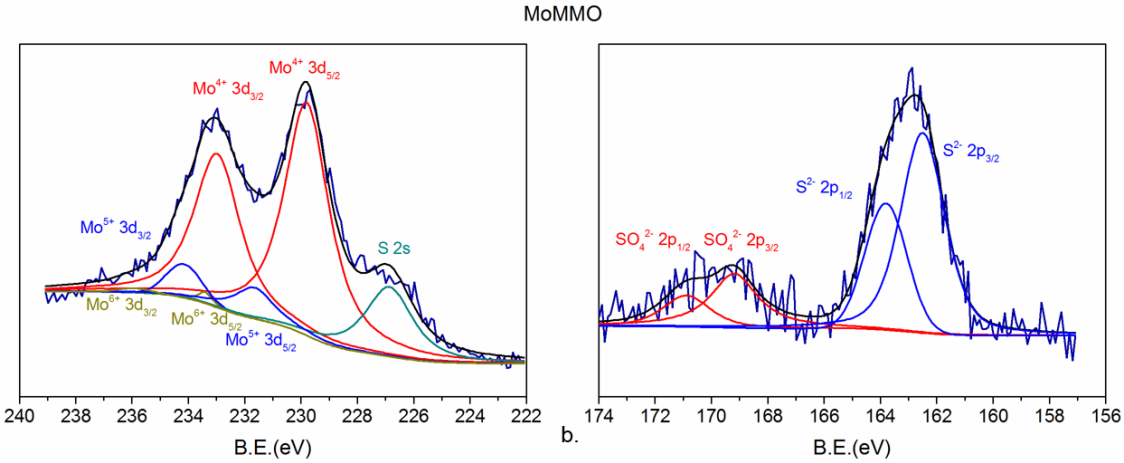

Figure 2.A.4: XPS results and fitting curves for the MoMMO catalyst (a) scan in Mo 3d region (b) scan in S 2p region.

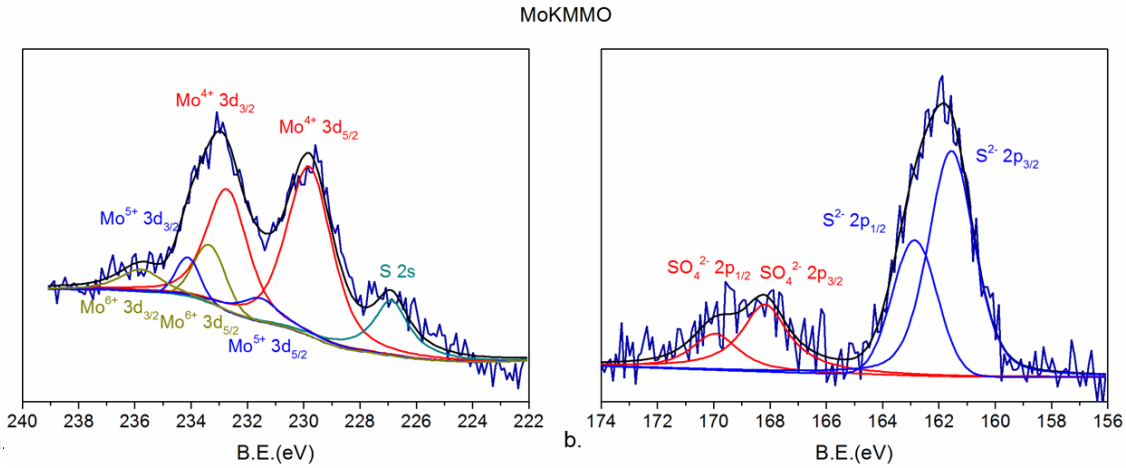

Figure 2.A.5: XPS results and fitting curves for the MoKMMO catalyst (a) scan in Mo 3d region (b) scan in S 2p region.

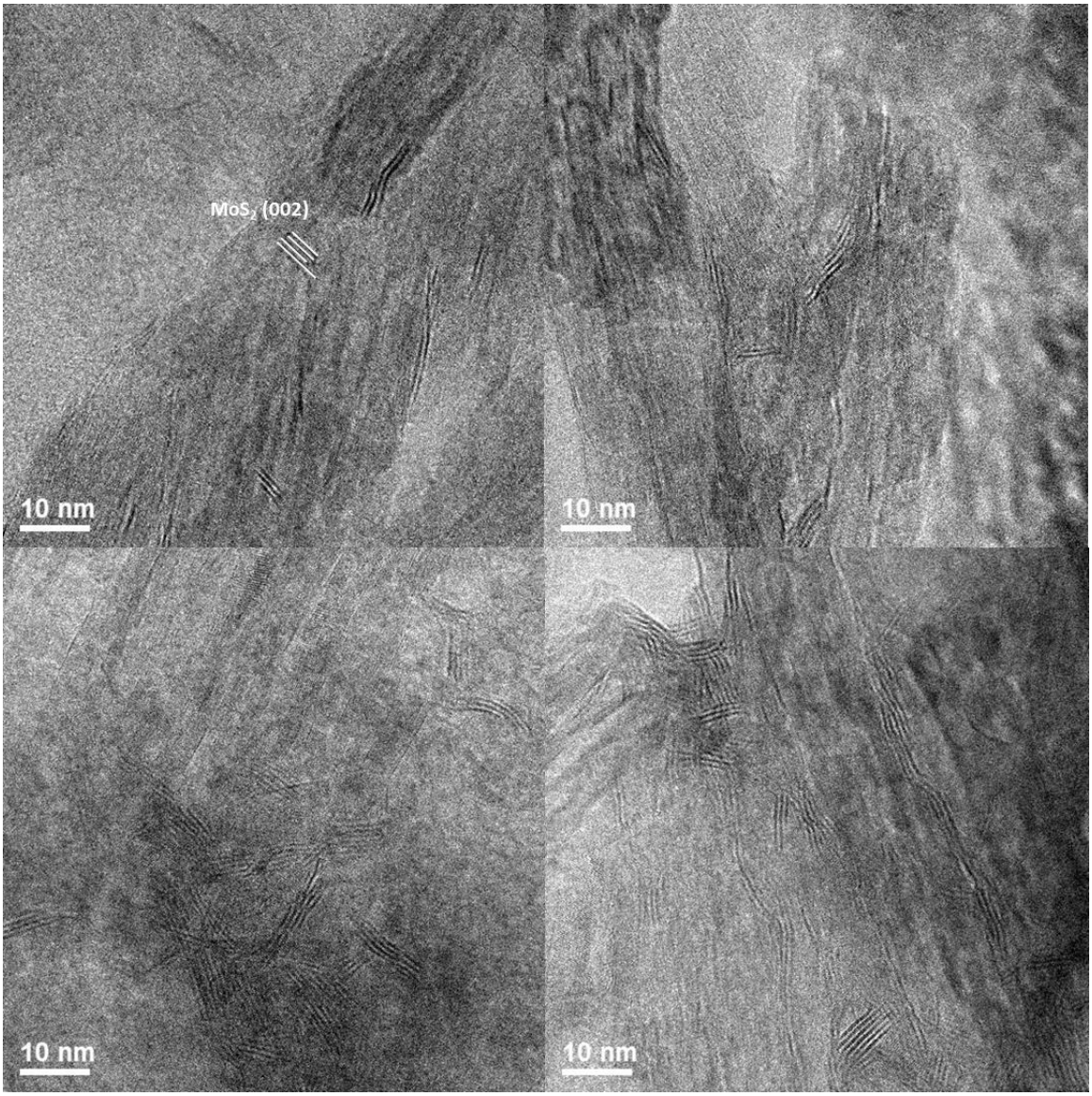

Figure 2.A.6: Representative STEM images of MoS_2 [002] domains over the reaction-aged MoKC-MMO catalyst.

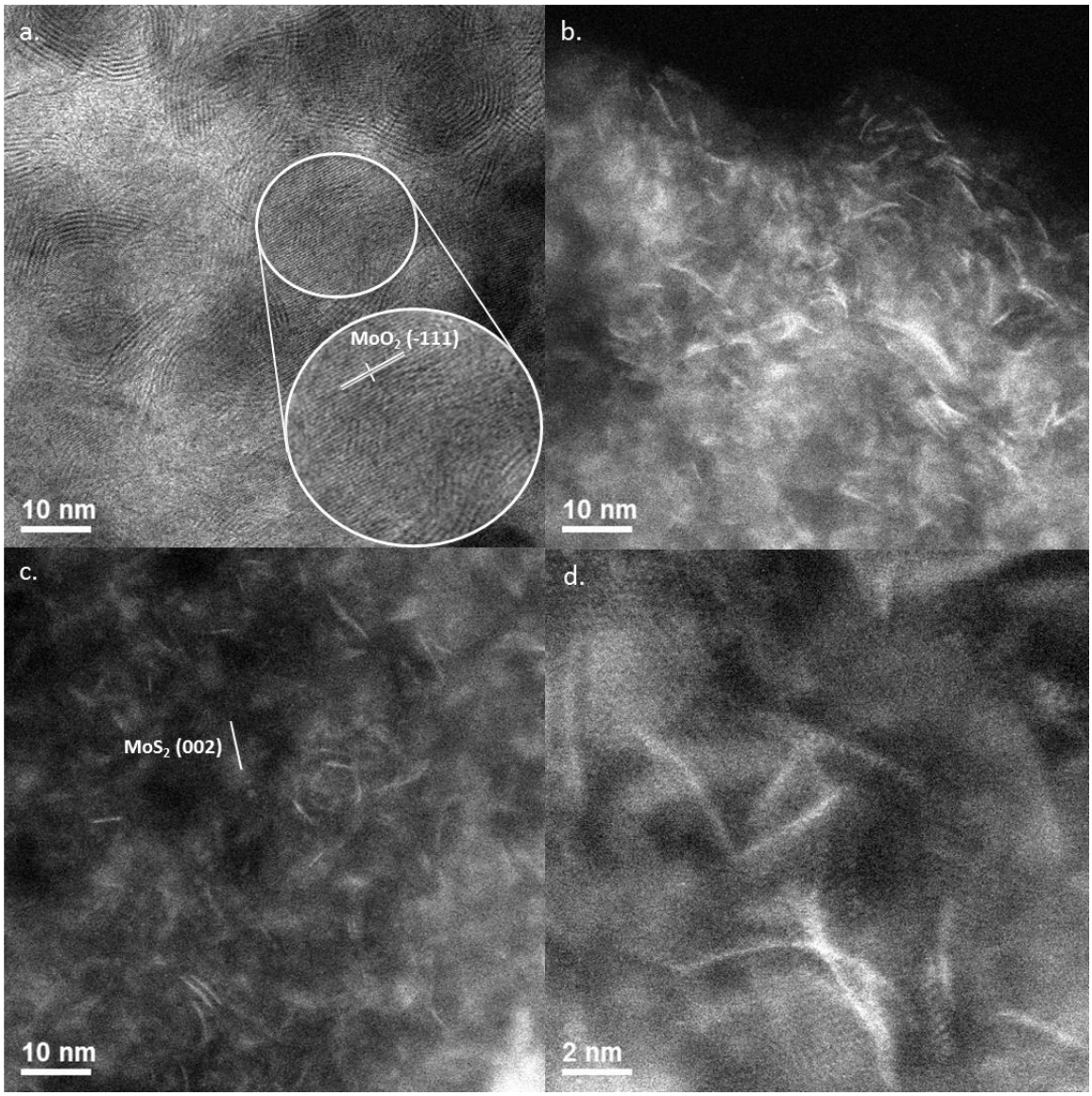

Figure 2.A.7: Representative STEM images of MoS_2 [002] domains over the reaction-aged MoKC catalyst; (a) includes a representative MoO_2 [-111] domain present in the MoKC sample.

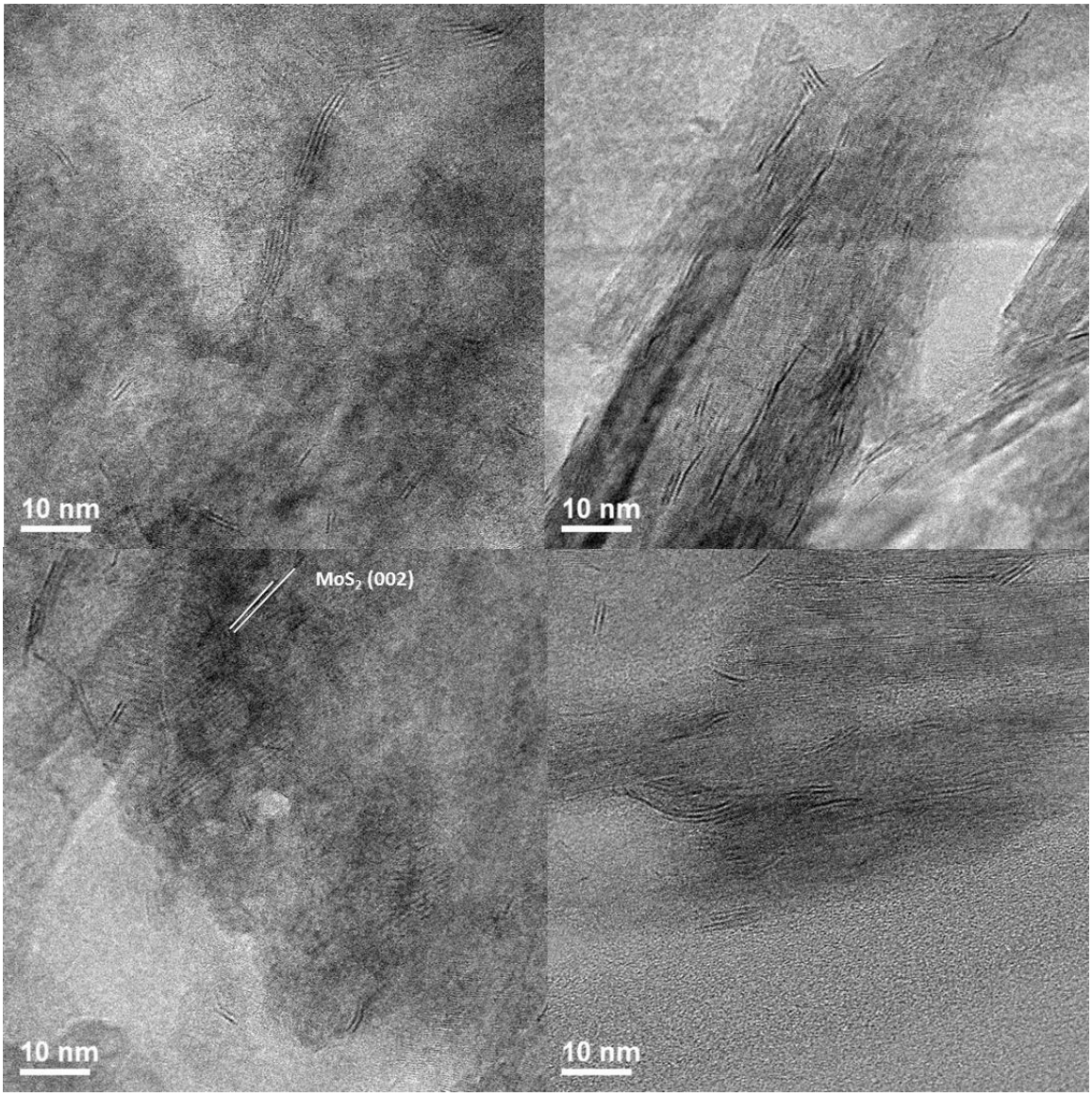

Figure 2.A.8: Representative STEM images of MoS_2 [002] domains over the reaction-aged MoKMMO catalyst.

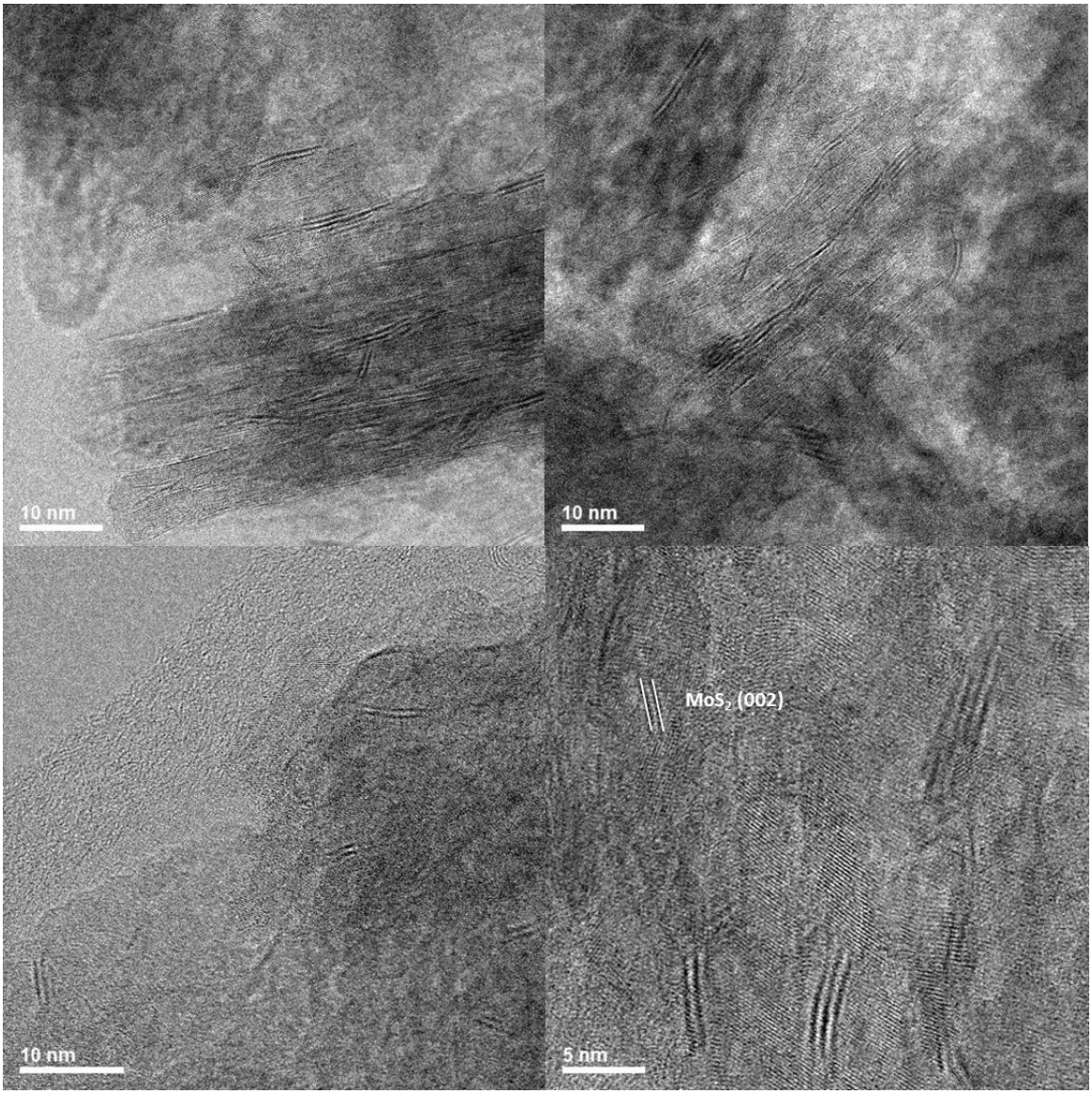

Figure 2.A.9: Representative STEM images of MoS_2 domains over the reaction-aged MoKMMO-C catalyst.

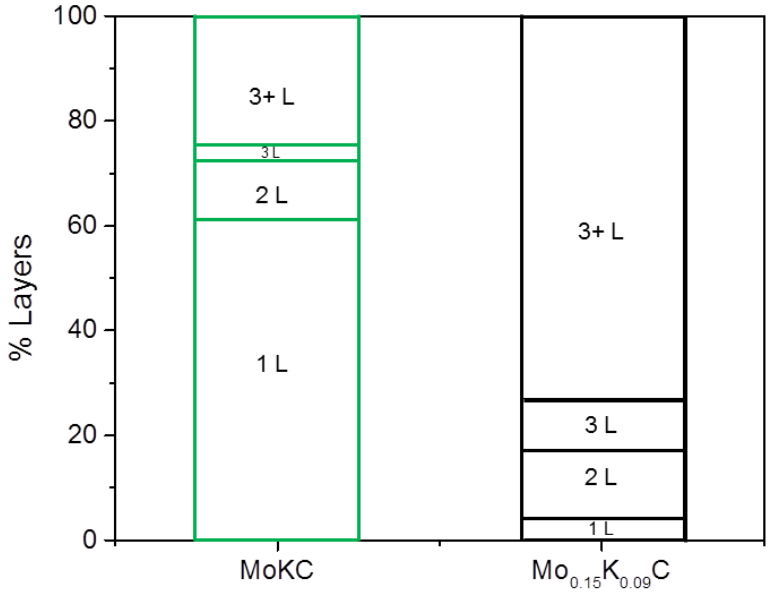

Figure 2.A.10: Layer distribution of MoS_2 stacked layers for MoKC and $Mo_{0.15}K_{0.09}C$ (prepared with a different batch of carbon support).

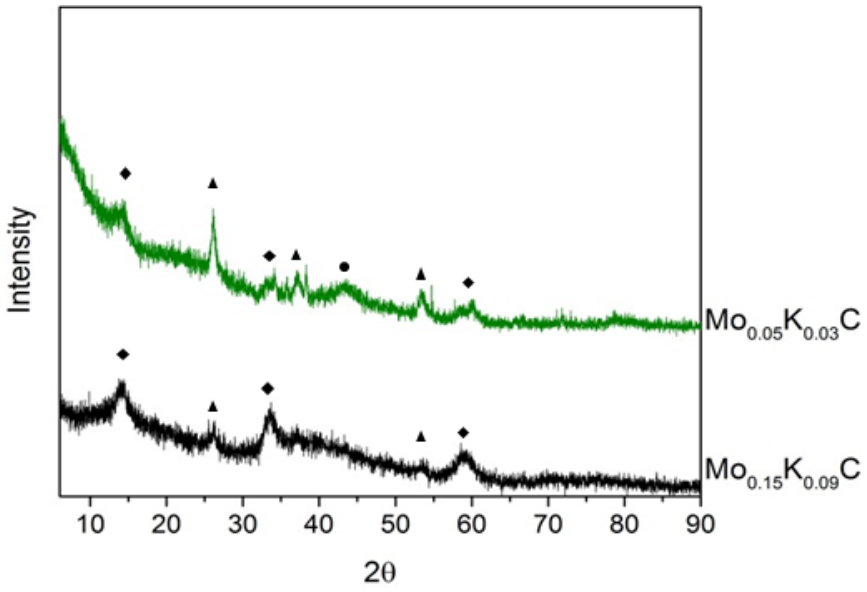

Figure 2.A.11: XRD patterns of the $Mo_{0.15}K_{0.09}C$ (black) (different carbon batch), MoKC (green). (♦) MoS_2 (▲) MoO_2 (●) MoO_3.

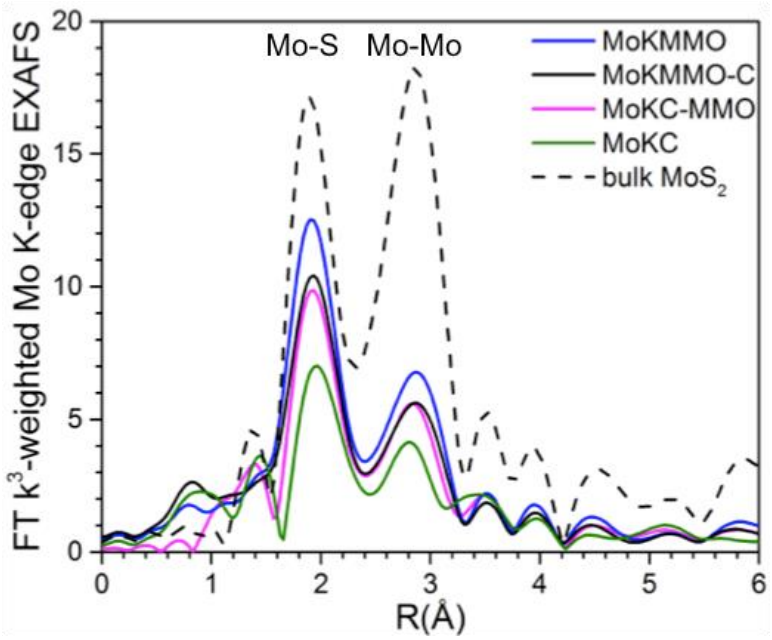

Figure 2.A.12: Fourier transform of k^3-weighted Mo K-edge EXAFS of bulk MoS_2, and reaction-aged MoKMMO, MoKMMO-C, MoKC-MMO, and MoKC catalysts.

Table 2.A.4: Results from the analysis of Mo K edge EXAFS.

Sample	shell	CN	r(Å)	$\Delta\sigma(10^{-3}Å^2)$	ΔE_0(eV)	R factor
bulk MoS_2	Mo-S	6[b]	2.40 ± 0.01	1.0 ± 1.3	2.87 ± 1.2	0.02
	Mo-Mo	6[b]	3.14 ± 0.01	1.0 ± 1.6	-4.5 ± 1.7	
MoKC-MMO	Mo-S	3.9 ± 0.5	2.41 ± 0.02	2.0 ± 1.3	4.0 ± 1.1	0.02
	Mo-Mo	2.8 ± 1.2	3.14 ± 0.01	2.6 ± 2.4	-6.5 ± 2.3	
MoKMMO	Mo-S	4.6 ± 0.7	2.41 ± 0.01	1.6 ± 1.6	3.6 ± 1.4	0.03
	Mo-Mo	2.4 ± 1.6	3.13 ± 0.01	1.0 ± 3.6	-6.9 ± 4.2	
MoKMMO-C	Mo-S	3.8 ± 0.8	2.42 ± 0.02	1.4 ± 2.0	4.7 ± 1.8	0.050
	Mo-Mo	2.2 ± 1.7	3.13 ± 0.01	1.0 ± 4.3	-6.6 ± 4.9	
MoKC	Mo-S	3.8 ± 1.0	2.42 ± 0.02	4.9 ± 3.9	4.6 ± 2.6	0.1
	Mo-Mo	5.2 ± 3.4	3.13 ± 0.01	8.8 ± 5.3	-8.0 ± 3.3	

Fitting parameters: Fourier transform range, Δk, 2-12 $Å^{-1}$, ΔR, 1.2-3.2 Å, weighting, k^1 and k^3, S_0^2(Mo-S)=0.70, S_0^2(Mo-Mo)=0.74

APPENDIX 2.B

K/MoS_2 REACTIVITY DATA

This appendix includes the supporting reactivity data of supported K/MoS_2 domains discussed in this Chapter.

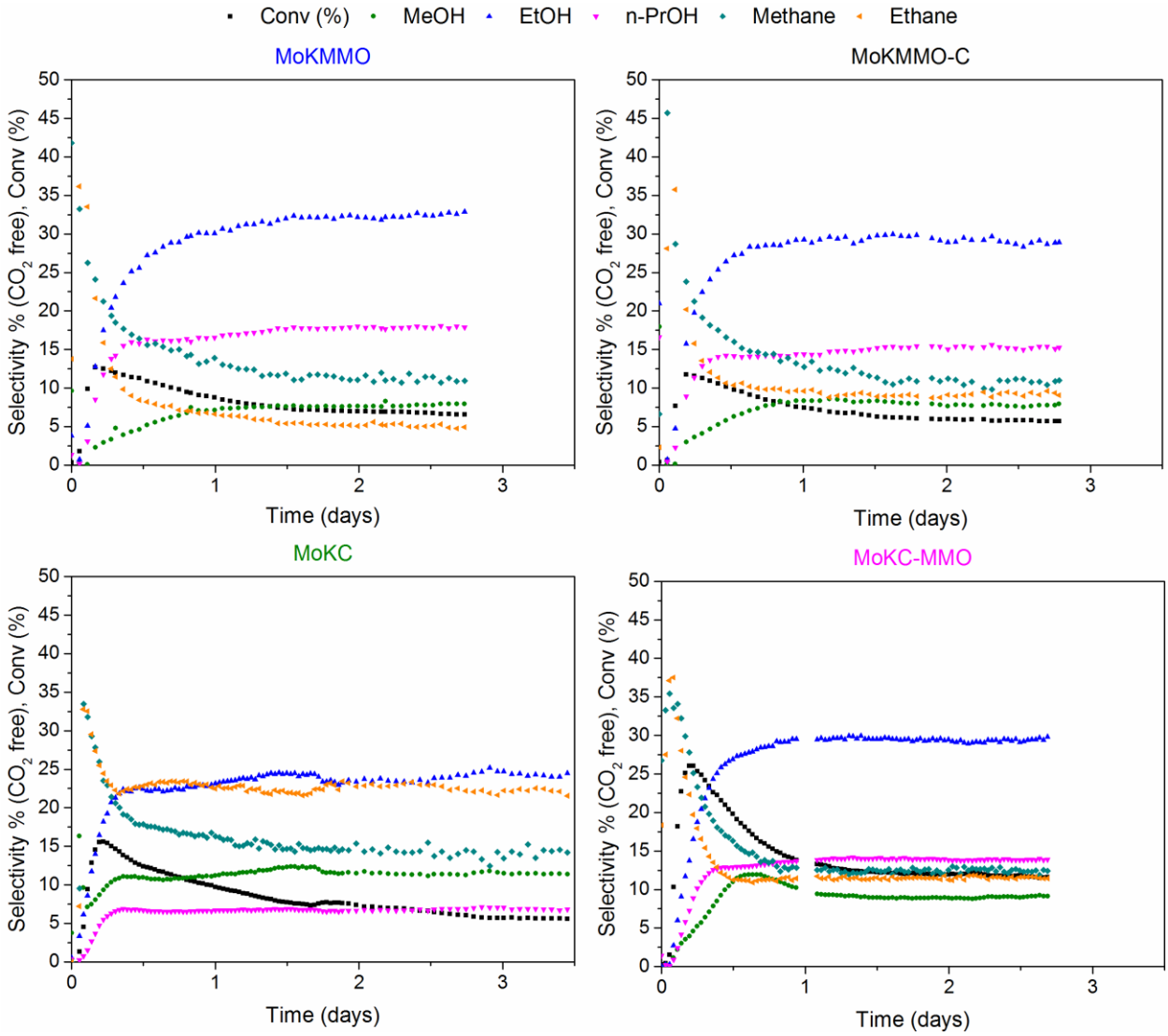

Figure 2.B.1: Transient reactivity data for the MoKC, MoKMMO, MoKC-MMO, and MoKMMO-C catalysts**.** Reaction conditions: 310 °C, 1500 psig.

Table 2.B.1: Reactivity results for MoKC, MoKC-MMO, MoKMMO, MoKMMO-C, and MoKC* catalysts. All reaction results are given after ~3 days of reaction, at steady state.

				Product Selectivity (Carbon % excluding CO_2)												
Catalyst	WHSV (ml/g/hr)	Conv. (% from prod.)	CO2 Sel. (%)	MeOH	EtOH	1-PrOH	1-ButOH	i-ButOH	CH_4	C_2H_6	Prop's	$C_{2+}OH$	$C_{3+}OH$	Total OH	Total HC	Total Non-OH Oxygenates	$C_{2+}OH$ Prod. (g/gMo/hr)
MoKC	3188	6.0	44.8	12.5	23.8	7.0	2.6	1.0	14.0	21.6	13.5	34.4	10.6	46.9	51.9	1.2	0.30
MoKC	3971	4.6	42.4	14.0	25.7	7.1	2.5	1.0	13.3	19.3	12.9	36.3	10.6	50.3	48.4	1.3	0.31
MoKC	4772	3.7	41.3	15.6	27.9	7.4	2.6	0.9	11.9	17.5	11.4	38.8	10.9	54.4	44.2	1.4	0.33
MoKC	6300	2.8	37.6	18.4	29.2	7.3	2.5	0.7	10.8	13.9	12.4	39.7	10.5	58.1	40.4	1.5	0.36
MoKC-MMO	1497	12.0	45.3	8.9	29.6	13.9	7.8	1.8	12.2	11.3	10.2	53.0	23.4	62.1	35.8	2.1	0.41
MoKC-MMO	2322	8.2	42.9	11.3	32.6	13.6	7.4	1.5	11.3	9.5	8.3	55.1	22.5	66.5	31.1	2.4	0.48
MoKC-MMO	3936	5.3	39.1	15.3	34.9	12.6	6.5	1.2	10.7	7.5	6.6	55.2	20.4	70.7	26.7	2.6	0.57
MoKC-MMO	5819	3.9	36.8	18.8	36.1	12.0	6.1	1.1	8.8	6.0	6.0	55.2	19.2	74.3	22.9	2.8	0.65
MoKMMO	706	10.1	48.0	5.9	26.8	17.3	12.7	2.8	14.0	7.0	9.1	59.5	32.8	65.9	31.8	2.3	0.17
MoKMMO	1277	6.3	43.8	8.1	31.8	17.4	11.3	2.9	12.6	5.0	6.6	63.3	31.5	71.9	25.8	2.3	0.23
MoKMMO	1522	5.2	42.3	9.4	34.5	17.4	10.5	3.1	10.7	4.4	5.7	65.5	31.0	75.4	22.1	2.5	0.24
MoKMMO	1829	4.6	41.4	10.5	35.8	17.0	10.0	2.6	9.9	3.8	6.0	65.4	29.7	76.4	21.3	2.3	0.26
MoKMMO	2888	3.2	38.5	14.0	38.7	15.8	8.8	2.5	7.9	2.4	5.0	65.8	27.1	80.3	17.1	2.6	0.30
MoKMMO-C	748	10.1	49.8	6.5	22.8	13.1	8.4	2.3	16.4	12.7	13.8	46.5	23.8	53.2	45.2	1.6	0.14
MoKMMO-C	1340	6.5	47.3	7.0	26.6	14.6	9.4	2.3	12.3	10.7	11.6	52.9	26.3	60.1	38.1	1.8	0.19
MoKMMO-C	2168	4.2	43.8	9.3	30.8	15.2	9.0	2.3	10.3	7.8	9.8	57.3	26.5	66.9	31.0	2.1	0.23
MoKMMO-C	3060	3.3	42.2	11.2	33.2	14.9	8.9	2.2	9.0	6.5	8.7	59.2	26.0	70.7	27.1	2.2	0.27
MoKC*	3024	17.7	36.4	36.6	22.3	5.8	1.8	1.3	15.1	9.9	4.73	31.2	8.9	67.8	30.0	2.2	0.87

***** The MoKC oxide precatalyst was reacted to confirm that the selectivity toward hydrocarbons in MoKC was not caused by the MoO_2 present in the reaction-aged catalyst, as shown in Figure 2.2.

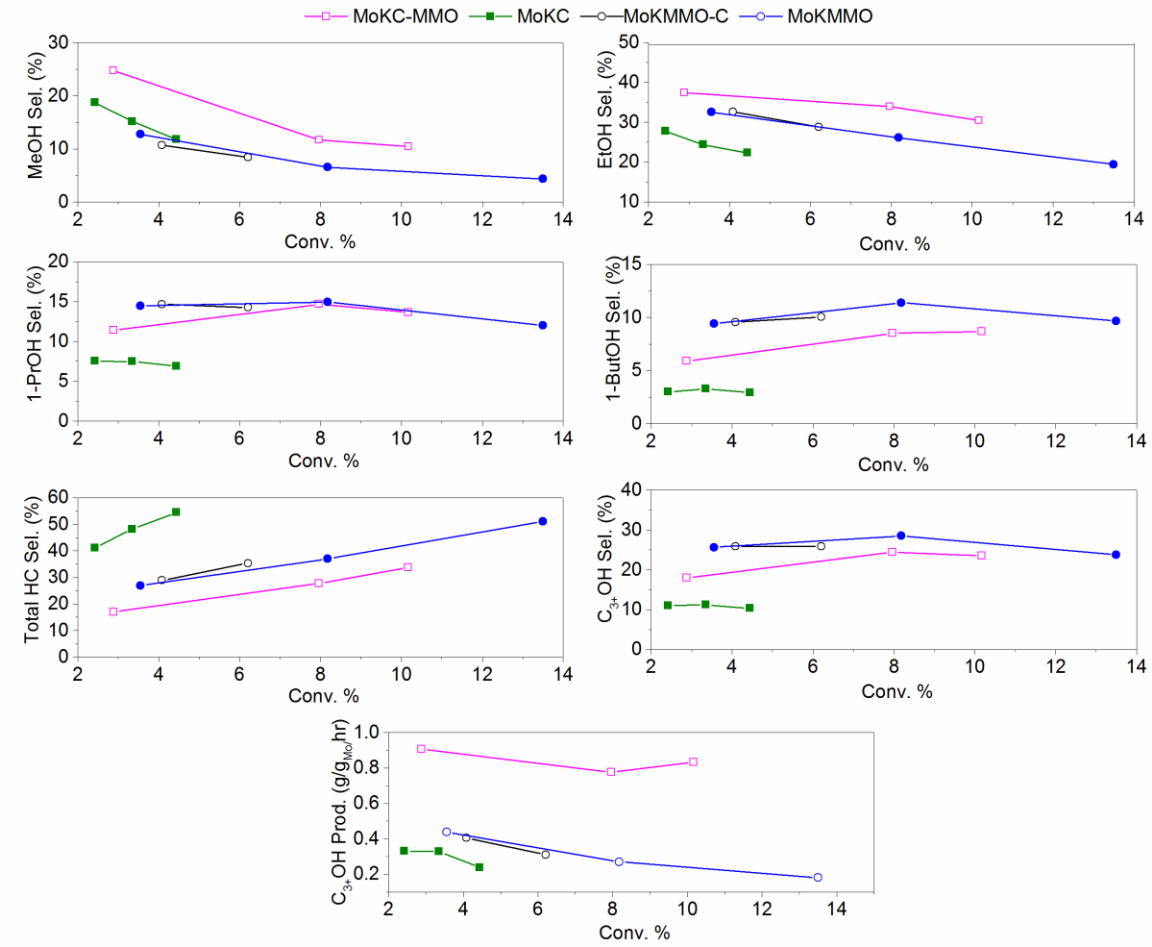

Figure 2.B.2: C_1-C_4 linear alcohols, total hydrocarbons (HC) and C_{3+}OH selectivities (CO_2-free), as well as C_{2+}OH productivity vs. CO conversion over the MoKC, MoKC-MMO, MoKMMO, MoKMMO-C catalysts with other batches of C and MMO supports. Reaction conditions: 310 °C, 1500 psig. All reaction results are given after ~3 days of reaction, at initial steady state.

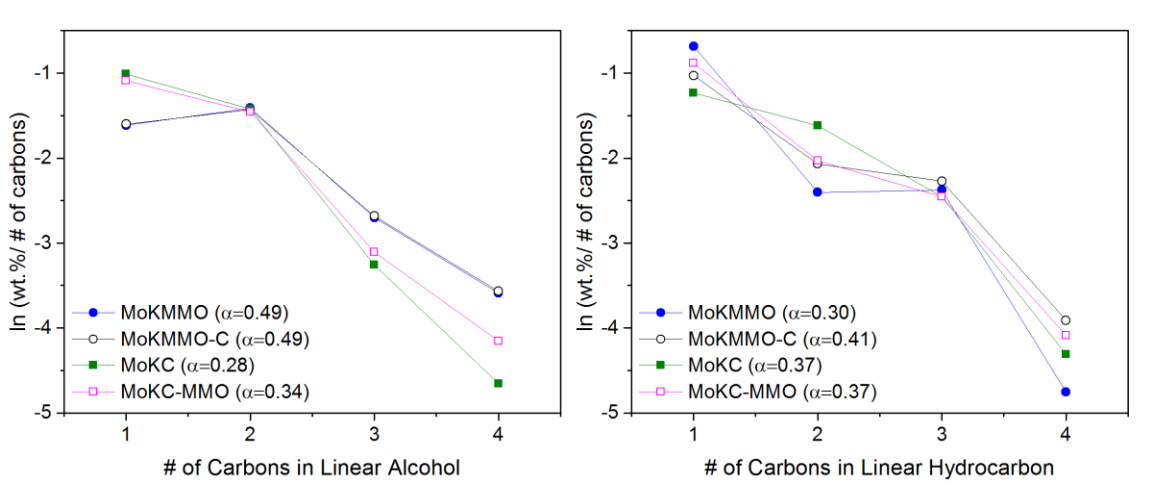

Figure 2.B.3: Anderson-Shulz-Flory (ASF) distribution for linear alcohols and linear hydrocarbons for MoKMMO, MoKMMO-C, MoKC, and MoKC-MMO catalysts at ~4% conversion.

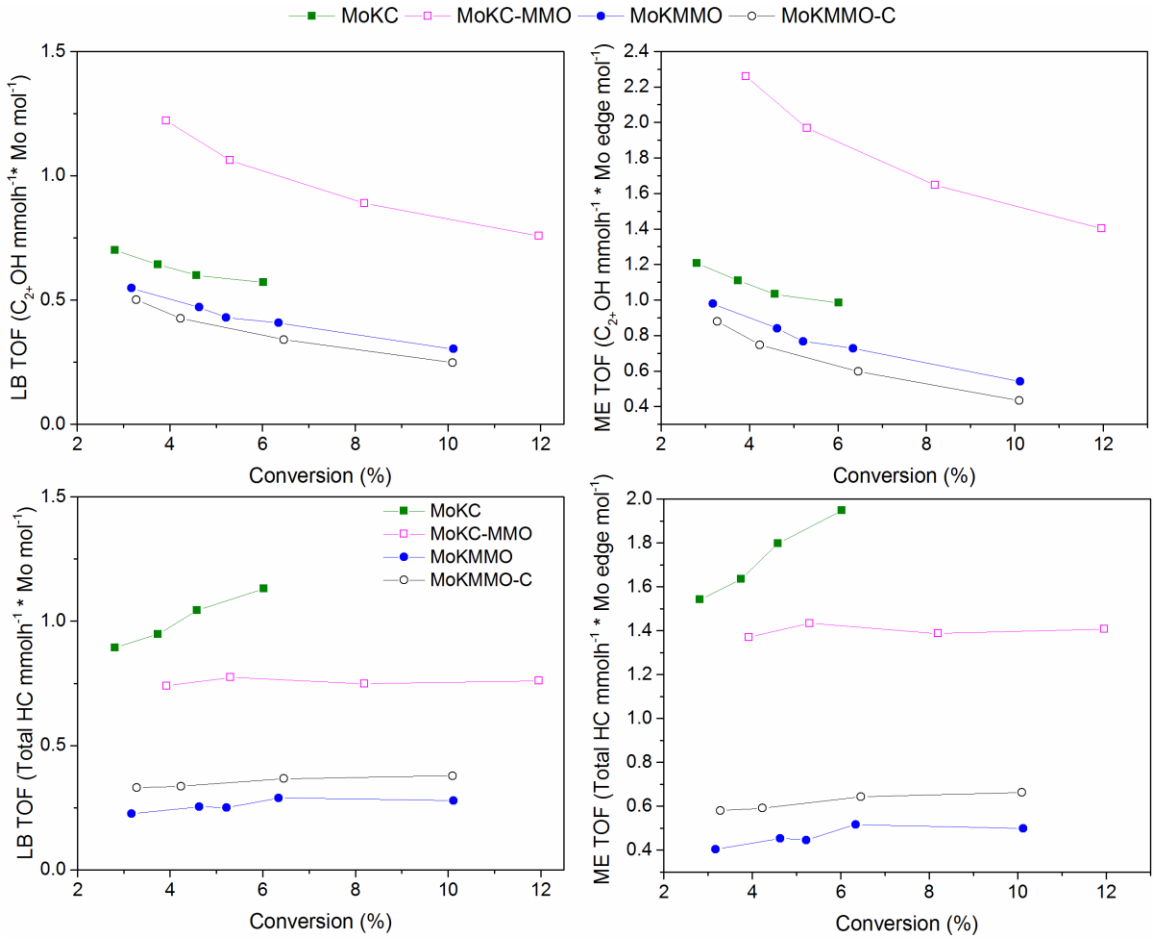

Figure 2.B.4: Lower bound (LB) (where all Mo atoms are assumed to be active) and middle estimate (ME) (where only edge Mo atoms are assumed to be active) TOF for C_{2+}OH and total hydrocarbons (HC) formation for the MoKC, MoKC-MMO, MoKMMO, and MoKMMO-C catalysts.

While accurate TOFs cannot be assessed due to the lack of a suitable probe molecule to titrate the active sites, estimates of TOFs are provided here for comparison to the literature. Ideally, upper bound and lower bound (LB) TOFs would be estimated, to bracket the range of possible TOFs. However, an estimate of the upper bound TOF is a challenge in these materials with a polydisperse array of MoS_2 domain sizes. Thus, here a LB TOF estimate is provided, assuming all Mo atoms are active sites. In addition, a middle estimate (ME) of the TOF is provided, assuming all edge sites are active.

Table 2.B.2: Lower bound (LB) (where all Mo atoms are assumed to be active) and middle estimate (ME) (where only edge Mo atoms are assumed to be active) TOFs based on CO conversion, as well as LB and ME TOF for $C_{2+}OH$ and total hydrocarbon (HC) formation for the MoKC, MoKC-MMO, MoKMMO, and MoKMMO-C catalysts.

		LB TOF (mmol reacted CO/hr*mol^{-1} all Mo)	ME TOF (mmol reacted CO/hr*mol^{-1} Mo edge)	LB TOF (mmol Product/hr*mol^{-1} all Mo)		ME TOF (mmol Product/hr*mol^{-1} Mo edge)	
	Conv. (%)	in CO Conv.%	in CO Conv. %	$C_{2+}OH$	Total HC	$C_{2+}OH$	Total HC
MoKMMO	3.2	3.0	5.8	0.55	0.23	0.98	0.40
MoKMMO	4.6	3.3	5.4	0.47	0.25	0.84	0.45
MoKMMO	5.2	2.9	5.0	0.43	0.25	0.77	0.45
MoKMMO	6.3	2.8	5.1	0.41	0.29	0.73	0.52
MoKMMO	10.1	2.5	4.5	0.30	0.28	0.54	0.50
MoKMMO-C	3.3	3.6	6.2	0.50	0.33	0.88	0.58
MoKMMO-C	4.2	3.3	5.7	0.43	0.34	0.75	0.59
MoKMMO-C	6.5	3.1	5.4	0.34	0.37	0.60	0.64
MoKMMO-C	10.1	2.7	4.7	0.25	0.38	0.43	0.66
MoKC	2.8	6.3	10.9	0.70	0.89	1.21	1.54
MoKC	3.7	6.3	10.9	0.64	0.95	1.11	1.63
MoKC	4.6	6.5	11.1	0.60	1.04	1.03	1.80
MoKC	6.0	6.8	11.8	0.57	1.13	0.98	1.95
MoKC-MMO	3.9	8.1	15.0	1.22	0.74	2.26	1.37
MoKC-MMO	5.3	7.4	13.7	1.06	0.77	1.97	1.43
MoKC-MMO	8.2	6.8	12.5	0.89	0.75	1.65	1.39
MoKC-MMO	12.0	6.4	11.8	0.76	0.76	1.40	1.41

Lower Bound (LB) and Middle Estimate (ME) TOF calculations:

$$\frac{mol\ C_{2+}OH}{mol\ Mo \cdot h} = \frac{n_i}{V} \cdot WGSV \cdot \frac{1}{1000\ mL} \cdot \frac{1}{x_{Mo}} \cdot MW_{Mo}$$

$$\frac{n_i}{V} = \frac{mol\ reacted\ CO\ or\ product}{Volume(L)}\ WGSV[=]\frac{mL}{g \cdot h}\ \ x_{Mo} = mass\ fraction\ Mo\ (0.05\ for\ all\ catalysts)$$

$$ME = \frac{LB}{f_{Mo\ edge}}$$

$$f_{Mo\ edge} = \frac{number\ of\ Mo\ edge\ atoms}{total\ Mo\ atoms}$$

$$No.\ Mo\ edge\ atoms = 2 \cdot \frac{avg\ layer\ length \cdot avg\ stacking}{Mo{-}Mo\ bond\ distance} + 2 \cdot (avg\ layer\ width - 2) \cdot avg\ stacking$$

Average layer width is determined to be 4 Mo atoms from EXAFS. The Mo-Mo CN = ~2 ± 2 as shown in Table 2.A.4.

Table 2.B.3: Literature TOF values at similar reaction conditions.

Catalyst	Conv. (%)	Temp. (°C)	H_2:CO	TOF(s^{-1})	Citation
2% Rh-1%Fe/TiO_2	7.5-9.0	270	1:1	0.0472[a]	R.J. Davis et al., J. Catal. 261 (2009) 9.
Co/Al_2O_3	6.9	280	30:15	0.27[b]	J.G. Goodwin Jr. et al., J. Catal. 285 (2012) 208.
2% Rh/TiO_2	7.89	270	1:1	0.012[c]	R.J. Davis et al., Catal. Commun. 11 (2010) 10.
2% Rh/TiO_2	7.89	270	1:1	0.023[d]	R.J. Davis et al., Catal. Commun. 11 (2010) 10.
2% Rh-2.5% Fe/TiO_2	9.16	270	1:1	0.036[c]	R.J. Davis et al., Catal. Commun. 11 (2010) 10.
2% Rh-2.5% Fe/TiO_2	9.16	270	1:1	0.055[d]	R.J. Davis et al., Catal. Commun. 11 (2010) 10.
RML/SiO_2(SB)[e]	8.2	300	2:1	0.068[f]	G. Lu et al., J. Mol. Cat. A: Chem. 367 (2010).
RML/SiO_2(CM)[e]	6.5	300	2:1	0.028[f]	G. Lu et al., J. Mol. Cat. A: Chem. 367 (2010).

[a]Molecules of CO converted per Rh surface atom per second

[b]Based on SSITKA, calculated as $TOF_{mk}=1/\tau_{CH4}$

[c]Molecules of CO converted per total metal atom per second

[d]Molecules of CO converted per active site counted by H_2 chemisorption per second

[e]RML denotes Rh:Mn:Li = 1.5:1.5:0.07; SB denotes SiO_2 prepared by the Stöber method; CM denotes commercial SiO_2

[f]TOF based on CO conversion and H_2 chemisorption

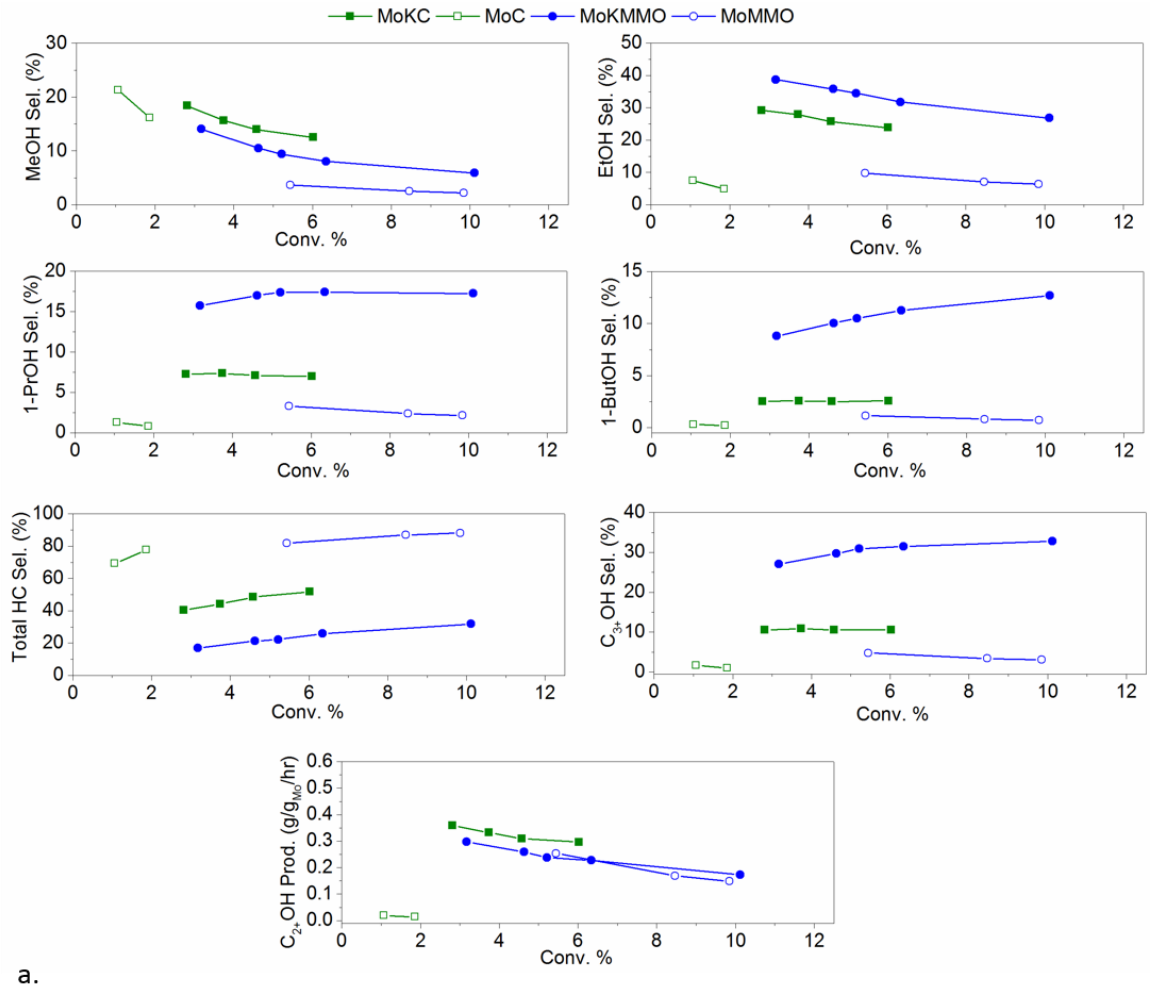

Figure 2.B.5: (a) C_1-C_4 linear alcohols, total hydrocarbons (HC) and C_{3+}OH selectivities (CO_2-free), as well as C_{2+}OH productivity vs. CO conversion as a function of promotion (MoMMO, MoKMMO, MoC, and MoKC). The MoMMO and MoC catalysts have 5 wt. % Mo loading, similar to the MoKMMO and MoKC catalysts, respectively. Reaction conditions: 310 °C, 1500 psig. Reaction results are given after ~2 days of reaction, at steady state, for the MoMMO and MoC catalysts and after ~3 days of reaction for the MoKMMO and MoKC catalysts. (b) Transient reactivity data as a function of promotion (MoC, MoMMO, MoKMMO, and MoKC). Reaction conditions: 310 °C, 1500 psig.

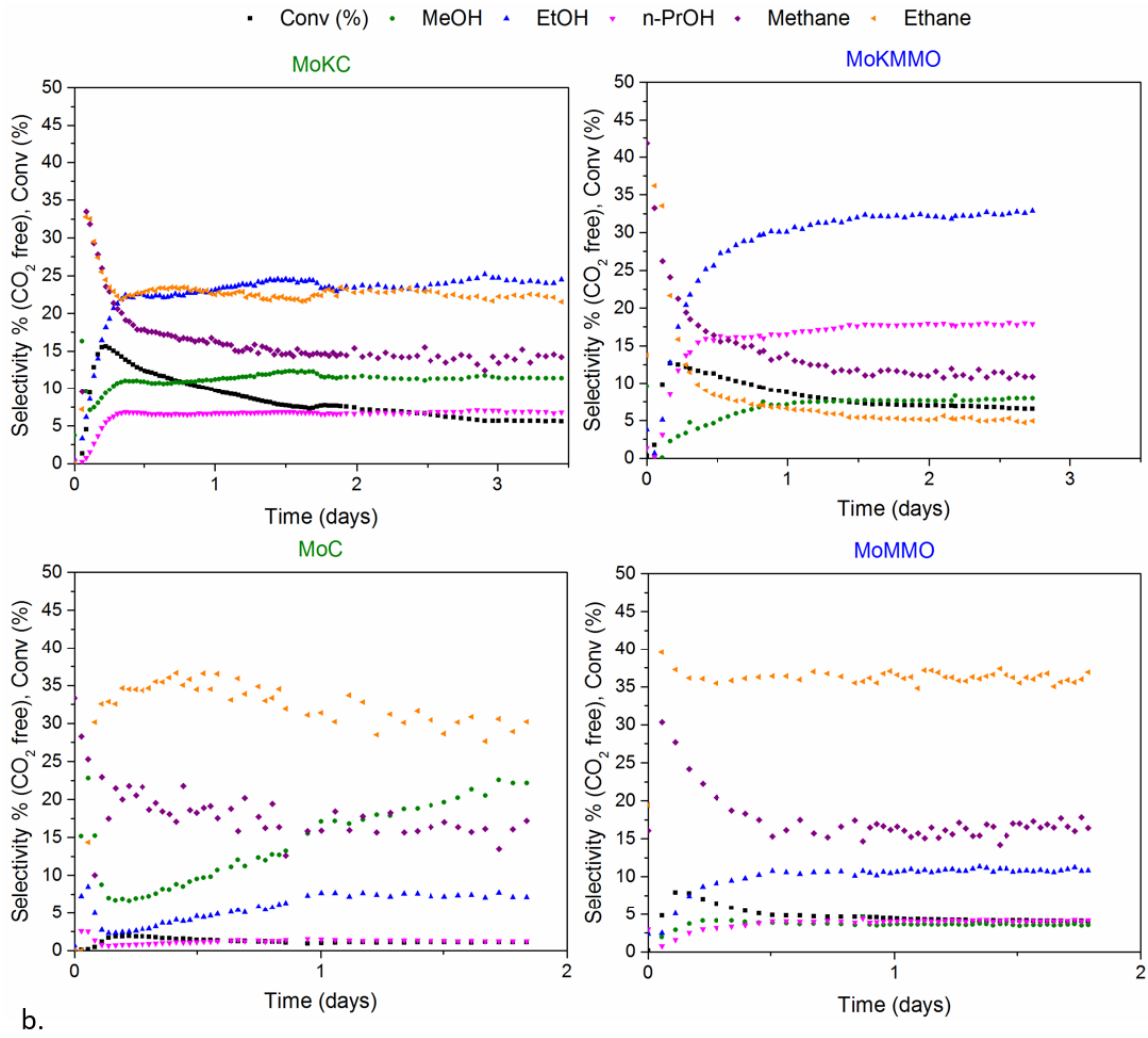

Figure 2.B.5: (continued)

Table 2.B.4: Reactivity data as function of increased Mo, and K loading for MMO and C supports.

Catalyst	WHSV (ml/g/hr)	Conv. (% from prod.)	CO2 Sel. (%)	Product Selectivity (Carbon % excluding CO_2)											EtOH Prod. (g/gMo/hr)	C_{3+}OH Prod. (g/gMo/hr)
				MeOH	EtOH	1-PrOH	1-ButOH	i-ButOH	CH_4	C_2H_6	C_{2+}OH	C_{3+}OH	Total OH	Total HC		
$Mo_{0.05}K_{0.03}C$	4772	3.7	41.3	15.6	27.9	7.4	2.6	0.9	11.9	17.5	38.8	10.9	54.4	44.2	0.25	0.08
$Mo_{0.15}K_{0.09}C$	15122	3.6	31.7	29.7	39.5	7.4	2.2	0.9	8.2	3.5	50	10.5	79.7	15.6	0.42	0.09
$Mo_{0.05}K_{0.03}MMO$[a]	4610	3.3	29.3	14.7	36.3	19	10.2	1.9	6.4	3.2	67.4	31.1	82.7	15	0.32	0.25
$Mo_{0.15}K_{0.09}MMO$[b]	16465	3.5	21.1	53.3	25.1	7.7	0.8	1.2	7	0.4	34.8	9.7	88.2	9.1	0.31	0.1

[a,b]Adapted from M. R. Morrill, N. T. Thao, H. Shou, R. J. Davis, D. G. Barton, D. Ferrari, P. K. Agrawal and C. W. Jones, "Origins of Unusual Alcohol Selectivities over Mixed MgAl Oxide Supported K/MoS_2 Catalysts for Higher Alcohol Synthesis from Syngas," ACS Catal., 2013, 3, 1665-1675, Copyright © 2013 American Chemical Society. **DOI:** 10.1021/cs400147d

APPENDIX 2.C

INSIGHT INTO K/MOS_2 DOMAIN CHANGES VIA IN SITU XAS

In-situ XAS experiments were conducted at the Argonne National Laboratory (ANL) as a means to investigate changes in the K/MoS_2 domains at the monolayer level. The catalysts were pre-reacted at Georgia Tech at 1500 psig and 310 °C for 3 days until pseudo steady state was reached. The pre-reacted catalysts were loaded in the in situ cell at the beamline and a XAS spectrum was collected with flowing He at 5 mL/min, referred to as preR. Then the catalysts were heated to 310 °C for 3 h under flowing syngas at 40 psig and a flow rate of 7 mL/min of syngas with $CO:H_2$ ratio of 1:1 (2 mL/min of 10% CO and 5 mL/min of 4% H_2). In the case of Figure 2.C.1d, the catalyst was pressurized to 500 psig with 10% syngas at a $CO:H_2$ ratio of 1:1 and heated to 310 °C. The catalysts were then cooled down to room temperature gradually under syngas flow. Once room temperature was reached, a XAS spectrum was collected under He flow at 5 mL/min, referred to as R. The samples were then passivated for 1 h with flowing 1% O_2 in He flow at 10 mL/min, referred to as P.

An assessment of the electronic structure of the MoS_2 domains was inferred from XANES spectroscopy, as shown in Figure 2.C.1. The reaction-aged catalysts (reaction time: 10 days) discussed in the main body of this Chapter can be correlated to the pre-reacted catalysts (reaction time: 3 days) in Figure 2.C.1. The preR catalysts had overall similar chemical signatures to that of the bulk MoS_2 (Figure 2.8), similar to the reaction-aged catalysts discussed in this Chapter. The normalized first derivative, shown in the inset of Figure 2.C.1 (a-d) provides insight into the catalysts' chemical state. As expected, upon syngas pretreatment the adsorption edge energy of all reacted (R)

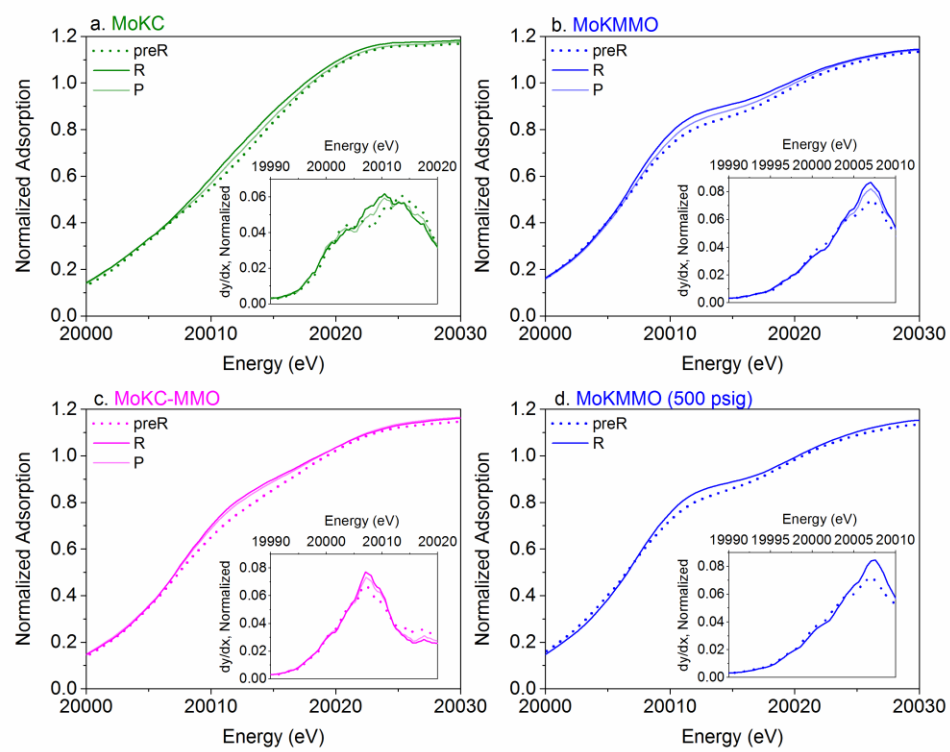

Figure 2.C.1: XANES Mo K-edge spectra of MoKC (a), MoKMMO (b), MoKC-MMO (c), and MoKMMO at 500 psig (d) for the pre-reacted catalyst (preR) at Georgia Tech, the in situ reacted catalyst (R) at the beamline, and the passivated catalyst (P) after in situ experiment; (inset) first derivative of the Mo K-edge spectra.

catalysts shifted to lower values compared to the pre-reacted catalysts (preR), suggesting a lower average Mo oxidation state for the catalysts. After passivation, the adsorption edge energy of the passivated (P) catalysts shifted to higher values compared to the reacted (R) catalysts, supported by the normalized derivative shown in the inset of Figure 2.C.1 (a-d), as the catalyst began to revert to a higher average Mo oxidation state by partial surface oxidation, discussed below. Alamgir et al. showed that a shift in the adsorption energy observed in XANES may not necessarily relate to the oxidation state of the material, but also reflect the shrinkage/expansion of the crystal,[1] supported by theory suggesting that the energy gap between the pre-edge features and the inflection point of the white line depends on the inverse square of the bond length.[2] As discussed below, the Mo-S bond length of the passivated MoKC-MMO catalyst

increased when compared to the reacted catalyst, as the Mo-S peak of the Fourier transform of k^3-weighted Mo K-edge EXAFS shifted to higher R-space (Å) values. Therefore, the increase in the Mo-S bond length may result in an apparent shift to lower adsorption energies over the MoKC-MMO catalyst.

It is expected that upon syngas exposure the pre-reacted catalysts will undergo reconstruction of the active MoS_2 phase, as K migrates/redistributes during the "break-in" induction period.[3] Santos et al. showed that after 3 h of reaction (induction period), vibrational bands associated with the formation of alcohols appear over a K/MoS_2 catalyst using in situ DRIFTS;[3] therefore, a 3 h syngas exposure treatment was conducted for the in situ XAS experiments. Andersen et al. showed that upon loading K atoms in the hexagonal interstitial sites in a (2a x 2a) 2H-MoS_2 supercell cell crystal (K_xMoS_2 with x= 0.125-1) at 0 K electronic ground state, the a (≈b) lattice parameters significantly increases.[4] This lengthening can be explained by repulsive interactions between K^+ ions that are densely packed (in the case of x=1, similar to Mo/K ratio studied with these catalysts) with a near-monolayer population of K atoms that intercalate the MoS_2 structure. The authors also suggested that lengthening Mo-S bond distances can be associated with incremental donation of 4s charges of K atoms added to MoS_2. At higher temperatures, K atoms are expected to readily diffuse in and out of the MoS_2 structure resulting in a higher degree of disorder within the K interstitial layers. It is hypothesized that K mobility will facilitate growth of MoS_2 layers along the a (≈b) plane, as hypothesized by Dorokhov et al. based on the observation that with increasing K loading MoS_2 crystallites join along lateral faces, leading to a linear size increase.[5]

The peak intensity of the Fourier transform k^3-weighted Mo K-edge EXAFS spectra can be contributed to by the number (N) of neighboring atoms, the distance (R) to the neighboring atom, and the disorder in the neighbor distance (σ^2).[6] The full width at half maximum (FWHM) of the Mo-O, Mo-S, and Mo-Mo peaks can provide insight into

which of these parameters is contributing to the peak intensity increase observed when comparing the pre-reacted and reacted catalysts in Figure 2.C.2. If there is no change observed in the FWHM between the pre-reacted and reacted catalyst, a peak intensity increase suggest that the number of neighboring atoms increases (a more coordinated structure). However, if the FWHM becomes narrower, a peak intensity increase suggests that the structure becomes coherent.

Figure 2.C.2 shows that across all catalysts the Mo-S and Mo-Mo peaks intensity increase, when comparing the pre-reacted and reacted catalyts' EXAFS spectra. It is important to note that the Mo-S and Mo-Mo peak intensity over MoKMMO increased significantly more when reacted at 500 psig (relevant to practical reaction conditions) compared to when reacted at 40 psig (Figure 2.C.2d, Figure 2.C.2b, respectively). Even though no experiments at 500 psig were conducted for the MoKC and MoKC-MMO catalysts, the experiments at 40 psig can provide insight into the changes of the MoS_2 structure as similar trends are observed when compared to those of MoKMMO at 40 psig. As shown in Table 2.C.1, the FWHM of the Mo-Mo, and Mo-S peaks for all the catalyst do not change significantly when comparing the pre-reacted vs. reacted catalyst. Therefore, the peak intensity increase for these catalysts can be attributed to an increase in neighboring atoms. As explained above, K is expected to migrate during the 3 h syngas exposure and facilitate growth of the MoS_2 layers in the a (≈b) plane, leading to a more coordinated MoS_2 structure.

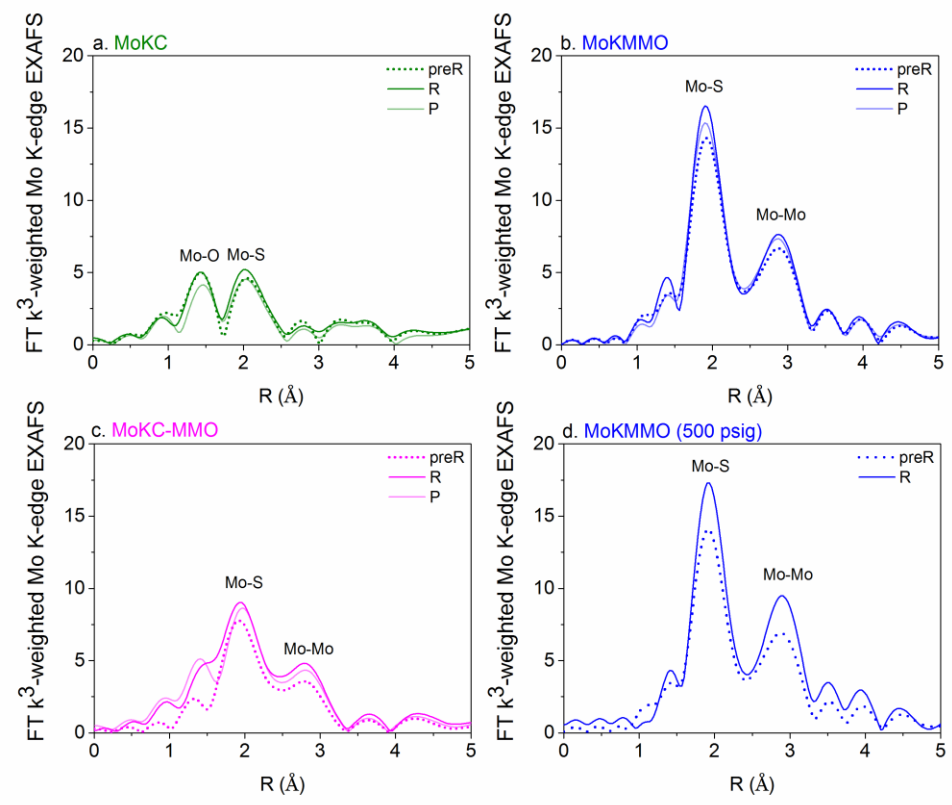

Figure 2.C.2: Fourier transform of k^3-weighted Mo K-edge EXAFS of MoKC (a), MoKMMO (b), MoKC-MMO (c), and MoKMMO at 500 psig (d) for the pre-reacted catalyst (preR) at Georgia Tech, the in situ reacted catalyst (R) at the beamline, and the passivated catalyst (P) after in situ experiment.

After passivation, the intensity of the Mo-Mo and Mo-S peaks of the passivated (P) catalysts decreases when compared to the reacted (R) catalyst, while the FWHM of these catalysts do not significantly change, further supporting that upon passivation the catalysts begin to revert to a lower coordinated MoS_2 structure. As discussed above, the Mo-S bond length also increased for the MoKC, and MoKC-MMO catalyst when comparing the reacted vs. passivated EXAFS spectra. This observation may be attributed to the incorporation of oxygen atoms into the structure creating Mo-O-S groups that would result in an increase of the average Mo-S distances while not changing the average Mo-O distance. Weak Mo-support interactions with the carbon support lead to a more readily oxidized K/MoS_2 structure. In contrast, there are no

changes observed in the Mo-S bond lengths for the MoKMMO catalyst after passivation, which is consistent with the hypothesis that strong Mo-MMO interactions preserve the K/MoS_2 structure. It appears from Figure 2.C.2 that the Mo-O bond length increases for the MoKC catalyst when comparing the reacted vs. passivated EXAFS spectra. However, it would be expected that upon passivation the Mo-O coordination number would increase, indicated by an increase in peak intensity. It is recommended that these reactions are repeated to further investigate the apparent Mo-O bond length increase.

Additionally, computational work on K_xMoS_2 structures at relevant practical reaction temperatures should be conducted. These results can then be used to generate relevant EXAFS models to fit the data of model K/MoS_2 structures to obtain accurate information.

Table 2.C.1: Full width at the half maximum (FWHM) of the Gaussian fitted Mo-O, Mo-S, and Mo-Mo peaks of the Fourier transform of k^3-weighted Mo K-edge EXAFS of MoKC (a), MoKMMO (b), MoKC-MMO (c), and MoKMMO at 500 psig (d).

a. **MoKC**		
	Mo-S peak FWHM	Mo-Mo peak FWHM
preR	0.33	0.43
R	0.35	0.45
P	0.32	0.52
b. **MoKMMO**		
	Mo-S peak FWHM	Mo-Mo peak FWHM
preR	0.48	0.70
R	0.45	0.66
P	0.52	0.64
c. **MoKC-MMO**		
	Mo-S peak FWHM	Mo-Mo peak FWHM
preR	0.55	0.63
R	0.62	0.61
P	0.54	0.58
d. **MoKMMO** (500 psig)		
	Mo-S peak FWHM	Mo-Mo peak FWHM
preR	0.48	0.68
R	0.46	0.69

References

(1) C. F. Petersburg, Z. Li, N. A. Chernova, M. S. Whittingham and F. M. Alamgir, *J. Mater. Chem.*, 2012, **22**, 19993-20000.

(2) A. Bianconi, E. Fritsch, G. Calas and J. Petiau, *Phys. Rev. B*, 1985, **32**, 4292-4295.

(3) V. P. Santos, B. van der Linden, A. Chojecki, G. Budroni, S. Corthals, H. Shibata, G. R. Meima, F. Kapteijn, M. Makkee and J. Gascon, *ACS Catal.*, 2013, **3**, 1634-1637.

(4) A. Andersen, S. M. Kathmann, M. A. Lilga, K. O. Albrecht, R. T. Hallen and D. Mei, *J. Phys. Chem. C*, 2012, **116**, 1826-1832.

(5) V. S. Dorokhov, D. I. Ishutenko, P. A. Nikul'shin, K. V. Kotsareva, E. A. Trusova, T. N. Bondarenko, O. L. Eliseev, A. L. Lapidus, N. N. Rozhdestvenskaya and V. M. Kogan, *Kinet. Catal.*, 2013, **54**, 243-252.

(6) D. C. Koningsberger and R. Prins, *X-ray absorption: principles, applications, techniques of EXAFS, SEXAFS, and XANES, John Wiley and Sons, New York, NY, Calgary, United States*, 1988.

CHAPTER 3

INSIGHT INTO REACTION PATHWAYS IN CO HYDROGENATION REACTIONS OVER K/MoS_2 SUPPORTED CATALYSTS VIA ALCOHOL/OLEFIN CO-FEED EXPERIMENTS

This Chapter was adapted from Taborga Claure, M. et al., Catal Sci Technol, 2016,6, 1957-1966 by permission from The Royal Society of Chemistry. DOI**:** 10.1039/C5CY01587A

Mo-support interactions can directly affect the product distribution, as discussed in Chapter 2.[1-3] At low Mo and K loadings, carbon (C) supports yield high hydrocarbon selectivity due to weak Mo-support interactions that facilitate formation of single MoS_2 layers (without K intercalation). In contrast, hydrotalcite-derived mixed MgAl oxide (MMO) supports yield high $C_{2+}OH$ selectivity. It was hypothesized that the intimate contact between K/MoS_2 domains and MMO (due to strong Mo-MMO interactions resulting in predominant double MoS_2 layer formation over MMO) has a synergistic effect in the formation of higher alcohols. It is also thought that MMO may facilitate Guerbet coupling reactions due to its surface acid-base pairs that catalyse aldol condensations and related reactions.[4]

The current state of knowledge regarding reaction pathways for carbon-carbon bond formation for production of higher alcohols over K/MoS_2 based catalysts is limited. The most frequently discussed mechanisms for carbon-carbon bond formation are CO insertion and Guerbet coupling pathways, as discussed in Chapter 1. Whereas there has been some effort into investigating reaction pathways to higher alcohols over K_2CO_3 promoted bulk MoS_2 catalysts[5-7], reaction pathways over supported K/MoS_2 catalysts remain relatively poorly elucidated,

where Mo-support interactions have been shown to affect alcohol product distributions.[1-3]

In this Chapter, K/MoS_2 catalysts supported on MMO and C (similar to Chapter 2) and K/bulk MoS_2 are subject to methanol, ethanol and ethylene co-feed experiments to investigate the effect of the support on reaction pathways by evaluating changes in product distribution.[8-12] The MMO support is known to shift the product distribution from C_1-C_2 to C_2-C_4 alcohols and yield MoS_2 domains that are primarily selective towards alcohols,[1-3] therefore it is expected that the addition of an alcohol/ethylene co-feed would drive the reaction towards enhanced higher alcohol formation. Carbon (C) supported catalysts at low Mo, K loadings are primarily selective towards hydrocarbons.[1] Therefore, it is expected that alcohol/olefin co-feed experiments will influence primarily hydrocarbon formation over this catalyst. K/bulk-MoS_2 is used as a control catalyst, with an emphasis on understanding the role of K/MoS_2, and K/MoS_2-MMO sites on higher alcohol formation pathways.

3.1 Experimental Section

A new batch of MMO was prepared in a similar manner as described in Chapter 2 and in previous studies.[1-3] A new batch of mesoporous activated carbon (C) was obtained via collaboration with Oak Ridge National Laboratory (ORNL), which was prepared in a similar manner as described in Chapter 2.

MMO and C supported K/MoS_2 catalysts were prepared with an approximate Mo loading of 5 wt.%, K loading of 3 wt.%, and a molar ratio of Mo:K of 1, similar to the procedure described for the parent MoKMMO and MoKC in Chapter 2 (referred in the same way in this Chapter).

Bulk MoS_2 was prepared similar to methods described in the literature.[13] AMT was combined with $(NH_4)_2S$ (Alfa Aesar, 20-24 % aq.) and stirred for 1 h at 65 °C in an oil bath. Next, 25 mL of 25 wt.% acetic acid solution was added to the mixture to precipitate the thiomolybdate. The mixture was then washed and filtered with deionized water, and loaded into a quartz tube, whereby the thiomolybdate decomposed to the MoS_2 phase by heating to 450 °C for 2 h at 5 °C/min under 40 mL/min of flowing N_2. The resulting bulk MoS_2 was then passivated with 1% O_2 in He (Matheson Trigas, UHP) flow at 40 mL/min for 8 h at room temperature. K was added to the synthesized bulk MoS_2 with a molar ratio of Mo:K of 1, referred as K/bulk-MoS_2. Both supported and unsupported precatalysts were physically ground for 15 min with K_2CO_3 (Aldrich, 99%, stored in an oven at 105 °C). [14] Additionally, Mo-free MMO/K-3 and C/K-3 (used as a control catalyst with a K loading of 3 wt.%) was prepared similarly by grinding the bare MMO, and C support, respectively, with K_2CO_3 for 15 min.

The prepared K/bulk-MoS_2, MoKMMO, and MMO/K-3 catalysts were then pelletized, crushed, and sieved through a 20-40 mesh prior to loading in the reactor. Similar to Chapter 3, MoKC was mixed (without grinding) with silicon carbide (Alfa Aesar, 46 grit SiC) with a mass ratio of 5:1 SiC:catalyst ratio prior to loading in the reactor to minimize plugging and hot spots (self-supporting pellets cannot be made with carbon supported catalysts). SiC was previously shown to be inert under the reaction conditions used here.[1]

The precatalysts were then loaded into a 6.35 mm steel tube reactor (1 g for MoKMMO and MMO/K-3, 0.4 g for MoKC and C/K-3, 0.1 g for K/bulk-MoS_2) and pretreated with 10% H_2S/H_2 (Matheson Tri-Gas, UHP) at 450 °C for 2 h at a heating rate of 5 °C/min and a flow rate of 20 mL/min to reduce, in situ, the precatalyst oxide phase of MoKMMO and MoKC, and surface oxidized K/bulk-

MoS_2. The reactions with syngas, 45% H_2, 45% CO, 10% N_2, and 50 ppm H_2S were carried out at 310 °C and 1500 psig after in situ sulfidation, as described in Chapter 2.

The syngas flowrate was adjusted between 10-25 mL/min to reach pseudo steady state at 8% conversion. Once the reaction reached 8% conversion after ~3 days of reaction, the alcohol (methanol (Sigma Aldrich, 99.8%), ethanol (Sigma Aldrich, 99.5%)) or the olefin (ethylene (Matheson, 99.95%)) co-feed was introduced into the reactor using a 500D Isco pump, and a 100DX Isco pump, respectively. Alcohol co-feeds were heated to 200 °C (to convert the liquid phase to vapour phase) and pressurized to 1500 psig before introduction into the reactor at 1 and 2 μL/min, making a 0-6 mol% composition with the syngas feed. The ethylene co-feed was pressurized to 1500 psig and introduced into the reactor at 3 and 4 μL/min, making a 0-9 mol% composition with the syngas feed. The alcohol or olefin co-feed was fed into the reactor at the first flowrate set point until the reaction reached pseudo steady state. The flowrate was then increased to the second flowrate set point to measure the effect of co-feed mol fraction on the reactivity. After the reaction reached pseudo steady state a third time, the co-feed was shut off until the product selectivity returned to its original state. It is important to note that similar product distributions as obtained initially were observed after returning to the original state, suggesting that the co-feeds did not cause any significant changes in the catalyst.

An Agilent 7890 gas chromatograph was used to quantify the main reaction products (carbon dioxide, methane, ethane, ethylene, propane/propylene, C_1-C_6 linear alcohols) using single point calibration curves. Other oxygenates quantified in this Chapter include isobutyl alcohol, aldehyde, acetate, and propionate species. The productivity of reacting CO and the distribution of products were

calculated in terms of moles C per g of Mo per hour from pseudo-steady-state data. These units were chosen to enable a direct comparison of reaction components that are being produced and consumed by the catalysts. At the completion of the reactions, all catalysts were passivated, in situ, with 1% O_2 in He for 8 h at room temperature at 20 mL/min, as described in Chapter 2. Catalysts were then removed from the reactor and placed in a vial under argon and stored in a dessicator.

The reaction-aged catalysts were characterized, ex situ, via nitrogen physisorption and X-ray diffraction (XRD). Nitrogen physisorption isotherms were collected at -196 °C using a Micromeritics Tristar II after being heated to 200 °C under vacuum for 10 h prior to the analysis. XRD was performed using a Philips X-pert diffractometer using Cu-Kα radiation.

3.2 Results and Discussion

3.2.1 XRD Patterns of Reaction Aged Catalysts

Figure 3.A.1 shows the XRD patterns of the reaction-aged catalysts after passivation. All reaction-aged catalysts show small, relatively broad peaks for the MoS_2 [100] (33°) and [110] (58°) planes. Predominantly single layer formation is typically observed over the MoKC catalyst by high resolution scanning transmission electron microscopy (HRSTEM), which was previously correlated with high hydrocarbon selectivity (Figure 3.1), as discussed in Chapter 2. However, large K/MoS_2 domains are also formed (with 3+ layers), similar to the K/bulk-MoS_2 catalyst due to weak Mo-C interactions.[1, 14] Therefore, the MoKC catalyst showed the [002] MoS_2 plane at 14°, (indicative of MoS_2 stacking)[15] analogous to the K/bulk-MoS_2 catalyst. The absence of the [002] plane over the MoKMMO catalyst indicates a low degree of stacking, as it was previously

determined that double layers were predominantly formed over the MMO catalyst by HRSTEM in Chapter 2, with fewer 3+ layer structures compared to the MoKC catalyst.[1] The MoKMMO catalysts show diffraction lines characteristic of MgO at 44° and 64°. As previously discussed in Chapter 2, the MoKC catalyst exhibited diffraction lines at 26°, 37°, 44°, and 53°, characteristic of MoO_2 domains, likely attributed to incomplete conversion during in situ sulfidation.[1]

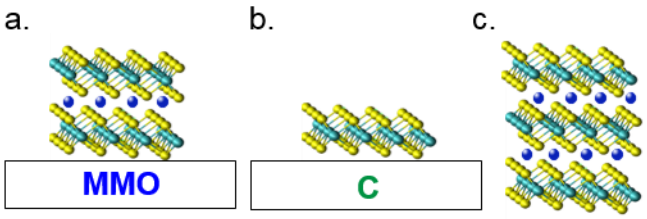

Figure 3.1: Important or predominant K/MoS_2 domains in catalysts, with turquoise spheres representing Mo atoms, yellow spheres representing sulfur atoms and blue spheress representing K^+ over (a) MoKMMO (b) MoKC and (c) K/bulk-MoS_2 catalysts.

3.2.2. N_2 Physisorption of Reaction-aged Catalysts

The Brunauer-Emmett-Teller (BET) surface areas calculated from N_2 physisorption data (P/P^o of 0.06-0.2) for the catalysts studied are shown in Table 3.A.1. The BET surface area for the reaction-aged MoKC catalyst after methanol, ethanol, ethylene co-feed experiments varies between 985 m^2/g -1378 m^2/g, similar to the reaction-aged MoKC catalyst run without any co-feed (1155 m^2/g). Similarly, the BET surface areas for the reaction-aged MoKMMO catalysts vary between 52 m^2/g -56 m^2/g for the co-feed experiments, while the reaction-aged catalyst without exposure to a co-feed has a BET surface area of 62 m^2/g. The reaction-aged K/bulk-MoS_2 catalyst did not exhibit any measurable porosity, similar to the pre-catalyst (as synthesized material). The textural properties after

exposure to co-feeds did not differ significantly from the properties of catalysts exposed only to normal syngas hydrogenation conditions.

3.2.3 Carbon Balances

Carbon distributions for methanol, ethanol, and ethylene co-feed experiments for the (a) MoKMMO, (b) MoKC and (c) K/bulk-MoS_2 catalysts are shown in Figure 3.B.1, Figure 3.B.2 and Figure 3.B.3, respectively. Inlet and outlet carbon distributions are shown in terms of productivity, in units of moles of carbon per gram of molybdenum per hour. These units were chosen to enable a direct comparison between inlet and outlet carbon. The inlet carbon shown in Figure 3.B.1- 3.B.3, consists of the reacting CO productivity, and inlet co-feed (methanol, ethanol or ethylene) productivity. Reacting CO productivity was determined using N_2 (internal standard). Inlet co-feed "productivity" was estimated by doing blank reactions with SiC at the same flowrate conditions as the co-feed reactions with catalyst in the reactor, as these values cannot be directly measured during the course of the reaction. These productivities were then normalized by the mass of Mo in each catalyst. It is important to note that the estimation of inlet methanol and ethanol productivities may be relatively imprecise compared to CO conversion, as these co-feed experiments were operated near the low end of the flow range of the 500D Teledyne Isco Pump. Additionally, ethylene productivities may be relatively imprecise, as Isco pumps are designed for liquids. A 100 DX Teledyne Isco pump was used for ethylene co-feed experiments due to lower minimum flow range and better precision compared to the 500D Isco pump. Outlet carbon, shown in Figure 3.B.1-3.B.3 was quantified from the GC data. It is important to note that the productivity term for methanol, ethanol or ethylene during co-feed experiments accounts for both unreacted co-feed and the amount of methanol, ethanol or ethylene respectively produced by the catalyst during

reaction. As these reactions are run at fairly low conversions (~8 %), unreacted CO was omitted from the balance to emphasize the effect of co-feeds on the reaction products. The magnitude of the inlet carbon and outlet carbon should match if there is a closed carbon balance. The closer the carbon balance is to 100%, the more accurate the depiction of the product distribution.

The majority of carbon balances are within 10% of closure for the MoKMMO (99-110%) and MoKC (91-107%) catalysts. The K/bulk-MoS_2 catalyst showed deviations within 30% (67-120%). Deviations in the carbon balance are likely associated with the non-real-time determination of inlet C for alcohol and olefin co-feed experiments (as explained above), as well as with the use of N_2 (that varies ~5% during the reaction) as the internal standard for reacting CO productivity. Note that the carbon balance for the MoKC catalyst (that has high total hydrocarbon selectivity) is ~91-94% for ethanol and ethylene co-feeds, therefore it can be inferred that the balance may most likely be associated with the unquantified C_{4+}HC. Refer to the 3.B Appendix for further C_{4+}HC discussion. Carbon balance distributions shown in Figure 3.B.4 over the Mo-free MMO/K-3 are between 73-129% (Table 3.B.2); carbon balance distributions shown in Figure 3.B.5 over the Mo-free C/K-3 are between 120-127% (Table 3.B.2).

3.2.4 Methanol Co-feed

The major products distribution for the methanol (MeOH) co-feed for the (a) MoKMMO, (b) MoKC, and (c) K/bulk-MoS_2 catalysts is shown in Figure 3.2. All the catalysts show an increase of CO conversion with increasing methanol co-feed (Table 3.B.1). The methanol conversion decreases with increasing methanol in the syngas feed (Table 3.B.1), likely attributed to overpopulation of surface sites by adsorption of methanol. The selectivity towards total alcohols decreases with increasing co-feed over the MoKMMO catalyst (Table 3.B.1). Similar to the

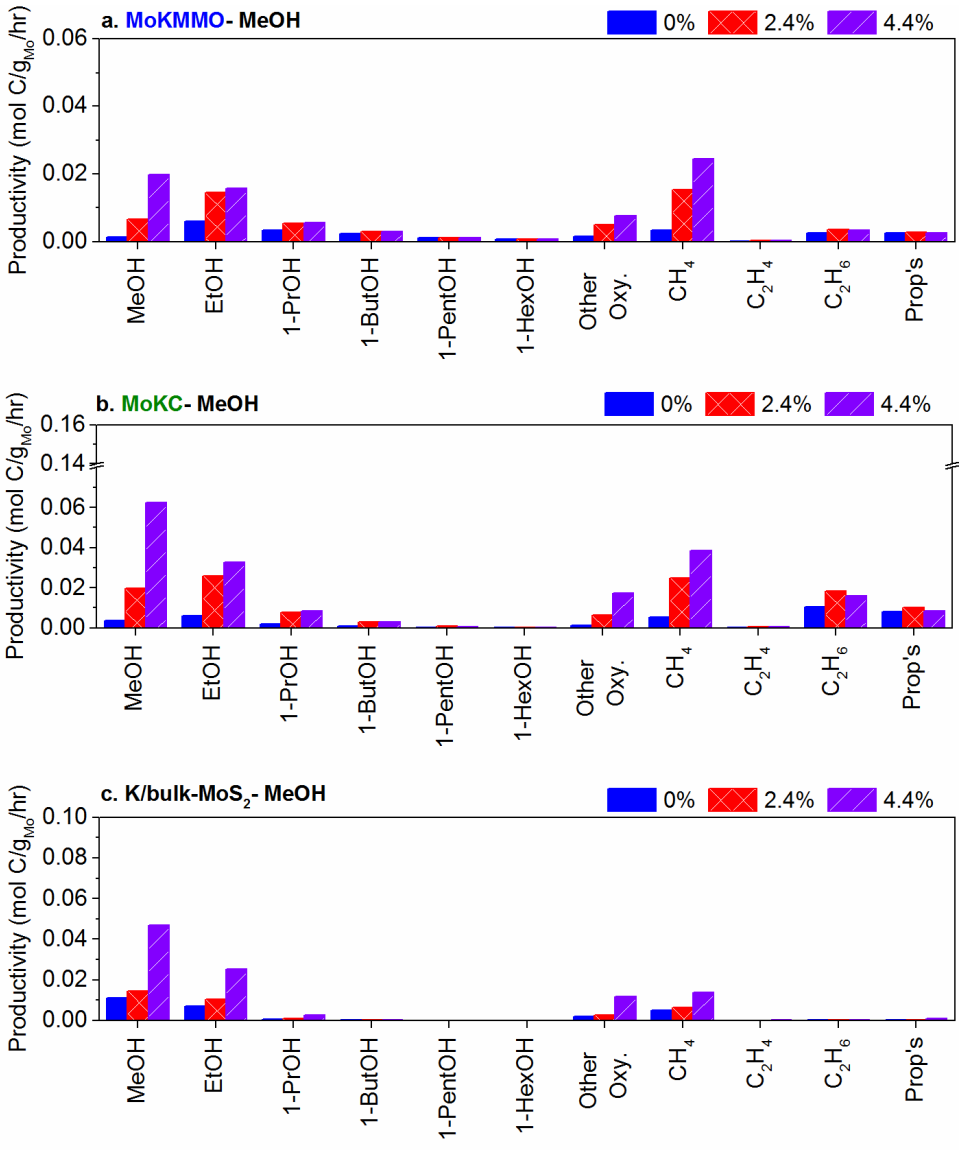

Figure 3.2: Major products for methanol co-feed experiments for the (a) MoKMMO, (b) MoKC, and (c) K/bulk-MoS_2 catalysts. Reaction conditions: 310 °C and 1500 psig.

MoKMMO catalyst, over the K/bulk-MoS_2 catalyst, the selectivity towards total alcohols decreases with increasing co-feed. The difference in the decrease in total alcohol selectivity between the MoKMMO and K/bulk-MoS_2 catalyst can be attributed to the difference in CO conversion (higher CO conversion yields lower selectivity towards total alcohols). In contrast, over the MoKC catalyst the selectivity towards total alcohols increases with increasing methanol co-feed, as

ethanol formation is favoured over ethane formation since ethyl species are not readily abundant, as explained below. All the catalysts show a significant increase in ethanol formation with increasing MeOH co-feed. Ethanol formation likely occurs through CO insertion into a methyl intermediate (CH_3*) to form an acetyl precursor (CH_3CO*) that is hydrogenated to ethanol (shown in Figure 3.3). The methyl species is likely formed via deoxygenation of a methoxy species (derived from co-fed methanol), as proposed by Santiesteban.[5] 1-propanol production slightly increased over the supported catalysts with increasing MeOH co-feed (ethanol to 1-propanol formation rate ratio is ~3-4, as shown in Table 3.B.1), as methanol primarily affects ethanol formation over C_{2+} alcohol formation. Over the K/bulk-MoS_2 catalyst, 1-propanol formation is negligible (ethanol to 1-propanol formation rate ratio is ~9). It is hypothesized that the formation of 1-propanol with a methanol co- feed is more favorable over small stacked K/MoS_2 domains (with more abundant edge sites) contained in the MoKMMO and MoKC catalysts than large stacked K/MoS_2 domains (with fewer edge sites) that dominate the K/bulk-MoS_2 catalyst.[1, 3, 14]

Santiesteban et al. also observed ethanol as the dominant product over a K/Co/MoS_2 catalyst with a methanol co-feed at 1200 psig and 304 °C, suggesting that the formation of C_3-C_4 alcohols is slower than the formation of ethanol.[5] In contrast, a recent work by Suárez París et al. reported that a methanol co-feed over K/MoS_2 at 1030 psig and 340 °C negatively affected the higher alcohol yield, and hydrocarbons were increased (with methane as the dominant product).[16] This observation is likely a result of the higher reaction temperature compared to this study (310 °C), which leads to higher hydrocarbon selectivity.[17, 18]

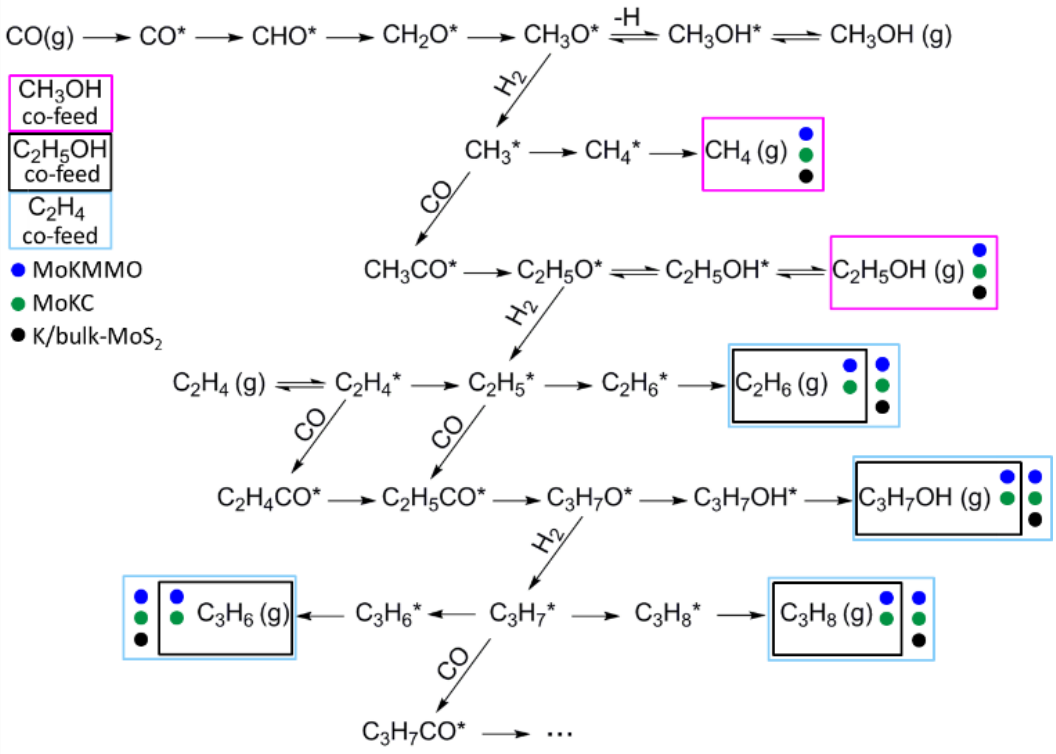

Figure 3.3: Proposed reaction pathway for higher carbon chain formation. The observed products are illustrated in boxes with each co-feed (methanol in magenta, ethanol in black, and ethylene in light-blue) for each catalyst shown in dots inside the corresponding boxes (blue for MoKMMO, olive for MoKC, black for K/bulk-MoS_2).

Methane formation is also observed to substantially increase over both supported (MoKMMO, MoKC) and K/bulk-MoS_2 catalysts with increasing methanol co-feed, indicating that methanol is a precursor of methyl species which are converted to methane. However, methane formation is suppressed over the K/bulk-MoS_2 catalyst compared to the supported counterparts. This is attributed to the relatively small increase in CO conversion with increasing methanol co-feed, which results in higher total alcohol selectivity (total hydrocarbon selectivity increases with increasing CO conversion). Ethane production is negligible with increasing methanol co-feed over the MoKMMO and K/bulk-MoS_2 catalysts, suggesting that the hydrogenation of the acetyl species to ethanol is favoured

over deoxygenation of ethoxy species to form ethyl species (intermediate to ethane formation). The increase in ethane production with increasing methanol co-feed over the MoKC catalyst may be associated with the acidic nature of the carbon support that may facilitate ethanol dehydration/hydrogenation reactions to produce ethane.[1]

3.2.4.1 Methanol Co-feed Minor Products

The distribution of other oxygenates is shown in Figure 3.B.6 for the (a) MoKMMO, (b) MoKC, and (c) K/bulk-MoS_2 catalysts. Methyl acetate is the main side product over all the catalysts during methanol co-feed experiments, suggesting that methanol itself is a building block for methyl acetate. Therefore, it is unlikely that the hydrogenolysis of methyl acetate to form ethanol and methanol is an alternate pathway to higher alcohols under the conditions employed.[19] Santiesteban et al. proposed that methyl acetate is formed via an acetyl precursor reacting with a methoxy anion, with both being intermediates in the CO insertion pathway shown in Figure 3.3.[5] Ethyl acetate, propyl acetate and methyl propionate are also observed in smaller quantities over all catalysts. Ethyl acetate and propyl acetate are likely formed through a similar pathway as methyl acetate and result from the increase of ethanol and 1-propanol production, respectively, associated with increasing methanol co-feeds. Methyl propionate is likely formed via esterification of propionate (produced in route to 1-propanol) with the co-fed methanol. Production of acetaldehyde increases over both supported and K/bulk-MoS_2 catalysts, likely derived from acetyl species (CH_3CO*).

Isobutyl alcohol is observed on the supported MoKMMO and MoKC catalysts. It is important to note that isobutyl alcohol productivity was measurably lower over the MoKC catalyst compared to the MoKMMO catalyst without any methanol co-feed,[1] but upon co-feeding methanol the production of isobutyl

alcohol significantly increases over the MoKC catalyst. Bifunctional acid-base pairs have been shown to be capable of Guerbet coupling reactions, with MgAl oxide (MMO) specifically being shown to facilitate ethanol coupling.[4] Therefore, the observation of isobutyl alcohol formation over MoKC suggests that this catalyst contains the necessary acid-base pairs to catalyse methanol coupling with 1-propanol. For both supported catalysts, 1-PrOH production increases with the 2.4 mol% methanol co-feed and remains constant with increasing methanol co-feed, whereas the isobutyl alcohol production continues to increase, suggesting that methanol coupling to 1-propanol may be occurring over both supported catalysts. Mo-free MMO/K-3 was also subjected to combined methanol and 1-propanol co-feed experiments with 1.4 mol% MeOH and 1.2 mol% 1-PrOH as a control experiment to investigate methanol coupling with 1-propanol. It can be observed in Figure 3.B.7c that the MMO/K-3 material indeed catalyses methanol to 1-propanol coupling, as speculated. In contrast, over Mo-free C/K -3 negligible isobutyl alcohol was observed (Figure 3.B.8), suggesting that Mo-K-C sites are needed to catalyse methanol coupling with 1-propanol over the MoKC catalyst.

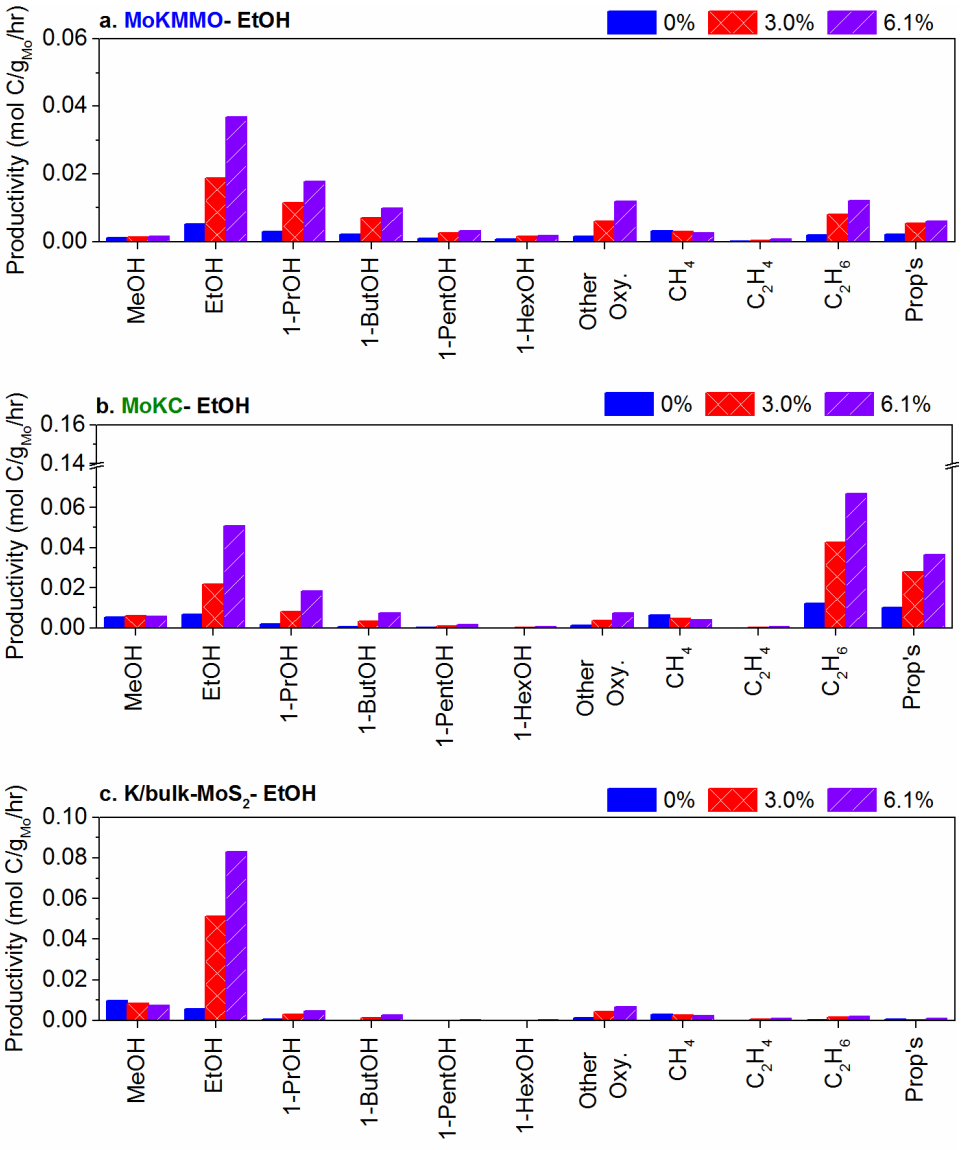

Figure 3.4: Major products for ethanol co-feed experiments for the (a) MoKMMO, (b) MoKC, and (c) K/bulk-MoS_2 catalysts. Reaction conditions: 310 °C and 1500 psig.

3.2.5 Ethanol co-feed

The major products distribution for the ethanol co-feed for the (a) MoKMMO, (b) MoKC, and (c) K/bulk-MoS_2 catalysts is shown in Figure 3.4. Both MoKMMO and MoKC catalysts show an increase of CO conversion with increasing ethanol co-feed (Table 3.B.1). Similar to the methanol co-feed, ethanol conversion decreases with increasing co-fed ethanol in the syngas feed (Table

3.B.1). The selectivity towards total alcohols decreases with increasing ethanol co-feed for all the studied catalysts (Table 3.B.1), as a result of higher formation of other oxygenates and in the case of the MoKC catalyst higher formation of other oxygenates and total hydrocarbons.

The MoKMMO catalyst shows the largest influence on C_{3+} alcohol formation (C_3-C_4 primarily) with increasing EtOH concentration in the syngas feed. The Anderson-Schulz-Flory distribution for linear alcohols, shown in Figure 3.B.9, supports this observation, as the probability for alcohol chain growth over MoKMMO (~0.5) is larger compared to that of MoKC (~0.3) and K/bulk-MoS_2 (~0.2) catalysts in ethanol co-feed experiments. The productivity of 1-propanol is higher than that of 1-butanol over the MoKMMO catalyst, suggesting that CO insertion is likely the predominant pathway to higher alcohols, as for CO insertion pathways the chain growth probability decreases with increasing carbon chain length. 1-propanol formation likely occurs through CO insertion into an ethyl species (C_2H_5*) to form a propionyl species (C_2H_5CO*) that can be hydrogenated to form 1-propanol (as shown in Figure 3.3). The ethyl species is likely formed via deoxygenation of an ethoxy species (derived from co-fed ethanol).

It is important to note that methanol production over the MoKMMO catalyst seems largely unaffected by increasing the ethanol co-feed, indicating that methanol-ethanol coupling to form 1-propanol is unlikely to occur to a significant extent. Similar to the 1-propanol formation pathway, 1-butanol is likely formed via hydrogenation of butanonyl species (C_3H_7CO*) after CO insertion into a propyl intermediate. Although the 1-butanol/1-propanol formation rate decreases from 0.72 to 0.55 (indicative of CO insertion), 1-butanol formation increases slightly with increasing ethanol co-feed over the Mo-free MMO/K-3 catalyst (indicative of ethanol self-coupling), shown in Figure 3.B.7b. This suggests that ethanol self-

coupling to 1-butanol over MoKMMO cannot be ruled out.[6] It is also observed that the MoKMMO catalyst gives a slight increase in 1-pentanol production. These observations may be associated with the inherent basic nature of the support that includes Mo-K-MMO sites that facilitate C_{3+}OH alcohol formation with an ethanol co-feed (total alcohol selectivity is higher than total hydrocarbon selectivity for this catalyst (Table 3.B.1)).

As expected, the ethanol co-feed over the MoKC catalyst favours C_{2+} hydrocarbon production over C_{3+} alcohol formation, with ethane being the dominant hydrocarbon product followed by propane/propylene (Table 3.B.1). The probability of hydrocarbon chain growth over the MoKC catalyst (~1.33-1.64) is significantly higher compared to the MoKMMO (~0.75-0.84) and the K/bulk-MoS_2 catalysts (~0.21-0.35) during ethanol co-feed experiments (Figure 3.B.9). The increase in ethane formation may be associated with the acidic nature of the carbon support[1] that likely facilitates ethanol dehydration-hydrogenation reactions to ethane with ethanol co-feed, unlike methanol co-feed, where this reaction is secondary. C_{3+}HC can be formed via alkyl intermediate, as proposed by Santiesteban et al.[5] However, it is also likely that the C_{3+}OH would be formed first and undergo dehydration/hydrogenation reactions to form the corresponding hydrocarbon, as the propane/propylene formation rate is significantly higher than the 1-PrOH formation rate. Propane/propylene productivity over the Mo-free C/K-3 catalyst was significantly increased with the mixed methanol, 1-propanol co-feed (Figure 3.B.8), supporting the notion that the carbon support facilitates acid catalysed hydrocarbon formation.

1-propanol productivity over the MoKC catalyst is higher than that of 1-butanol, suggesting that CO insertion is the predominant alcohol formation pathway. It is likely that 1-propanol is formed via CO insertion of ethylene species

(derived by ethanol dehydration) versus ethyl species (derived by deoxygenation of ethoxy species), as the carbon support is acidic in nature. In contrast to the MoKMMO catalyst, the 1-butanol over 1-propanol formation rate (0.36-0.4) is relatively unchanged over the MoKC catalyst with increasing co-fed ethanol, suggesting that ethanol favours dehydration-hydrogenation reactions to ethane over 1-propanol formation. This may be associated with the comparably inert support, in contrast to K/MoS_2 domains supported on MMO that allow more favourable sites (Mo-K-MMO sites) for 1-propanol formation with the ethanol co-feed.[1] In the case of the K/bulk-MoS_2 catalyst, the ethanol co-feed is largely unreactive (Table 3.B.1).

3.2.5.1 Ethanol Co-feed Minor Products

The selectivity towards other oxygenates is higher over the MoKMMO catalyst than over the MoKC catalyst. The distribution of other oxygenates is shown in Figure 3.B.10 for the (a) MoKMMO, and (b) MoKC catalysts. As can be observed, the MoKC catalyst shows no significant increase in any of the quantified side products. This further suggests that C_{2+}HC formation is the predominant reaction pathway over the MoKC catalyst, as adsorbed ethanol species readily dehydrate/hydrogenate to form ethane. In contrast, the MoKMMO catalyst shows a variety of important minor products. Both ethyl acetate and ethyl propionate formation increase with increasing ethanol feed, with ethyl propionate being the largest minor product formed. This observation suggests that ethanol is the precursor of these species (via an ethoxy intermediate). The increase in propyl acetate with increasing ethanol co-feed is likely a result of increasing 1-propanol production, as 1-propanol is a precursor of propyl acetate.

Isobutyl alcohol also increases over the MoKMMO catalyst with increasing ethanol co-feed, likely due to the increase in formation of 1-propanol derived

species (including propanal) that may undergo coupling with methanol. Similarly, 1-butanol derived species likely couple with methanol to form isoamyl alcohol. It is important to note that acetaldehyde and propanal production increases with increasing ethanol co-feed, as well. With ethanol co-feeds, acetaldehyde is likely formed via ethanol dehydrogenation instead of through an acetyl intermediate (CH_3CO^*) (as suggested for methanol co-feed experiments), as acetaldehyde formation is higher with ethanol co-feeds compared to methanol co-feeds. This is further supported by the increase in acetaldehyde over the K/bulk-MoS_2 catalyst with the ethanol co-feed, as ethanol is largely unreactive over this catalyst. Propanal is likely formed via a propionyl ($C_2H_5CO^*$) intermediate as a side reaction in the CO insertion pathway to 1-propanol.

Ethyl acetate and ethyl propionate productivity (Figure 3.B.10c) increases slightly over the K/bulk-MoS_2 catalyst with increasing ethanol co-feed. Ethyl acetate is likely formed via an acetyl precursor reacting with an ethoxy anion, similar to the reaction pathway to methyl acetate as explained above. Ethyl propionate is likely formed via esterification of propionate (produced in route to propanol) with the co-fed ethanol. However, the lack of 1-propanol formation suggests that ethanol may not be able to strongly adsorb on the unsupported K/bulk-MoS_2 catalyst and/or the formation of ethyl species is rate-controlling step(s) for 1-propanol formation. As discussed below under the ethylene co-feed section, 1-propanol formation significantly increases over the K/bulk-MoS_2 catalyst with increasing ethylene co-feed. This may be associated with readily abundant adsorbed ethylene or ethyl species that can undergo CO insertion to form propionyl species and further hydrogenation to form 1-propanol. It is hypothesized that small K/MoS_2 domains on the MoKC and MoKMMO catalysts allow more favoured and abundant sites for ethanol to adsorb and participate in the formation

of C_{3+} products. Even though the Mo-free MMO/K-3 catalyst can catalyse ethanol self-coupling to 1-butanol, it is produced in negligible amounts. This indicates that Mo-K-MMO sites are needed for enhancement of C_3-C_4 normalized alcohol productivity with ethanol co-feed (Figure 3.B.11).

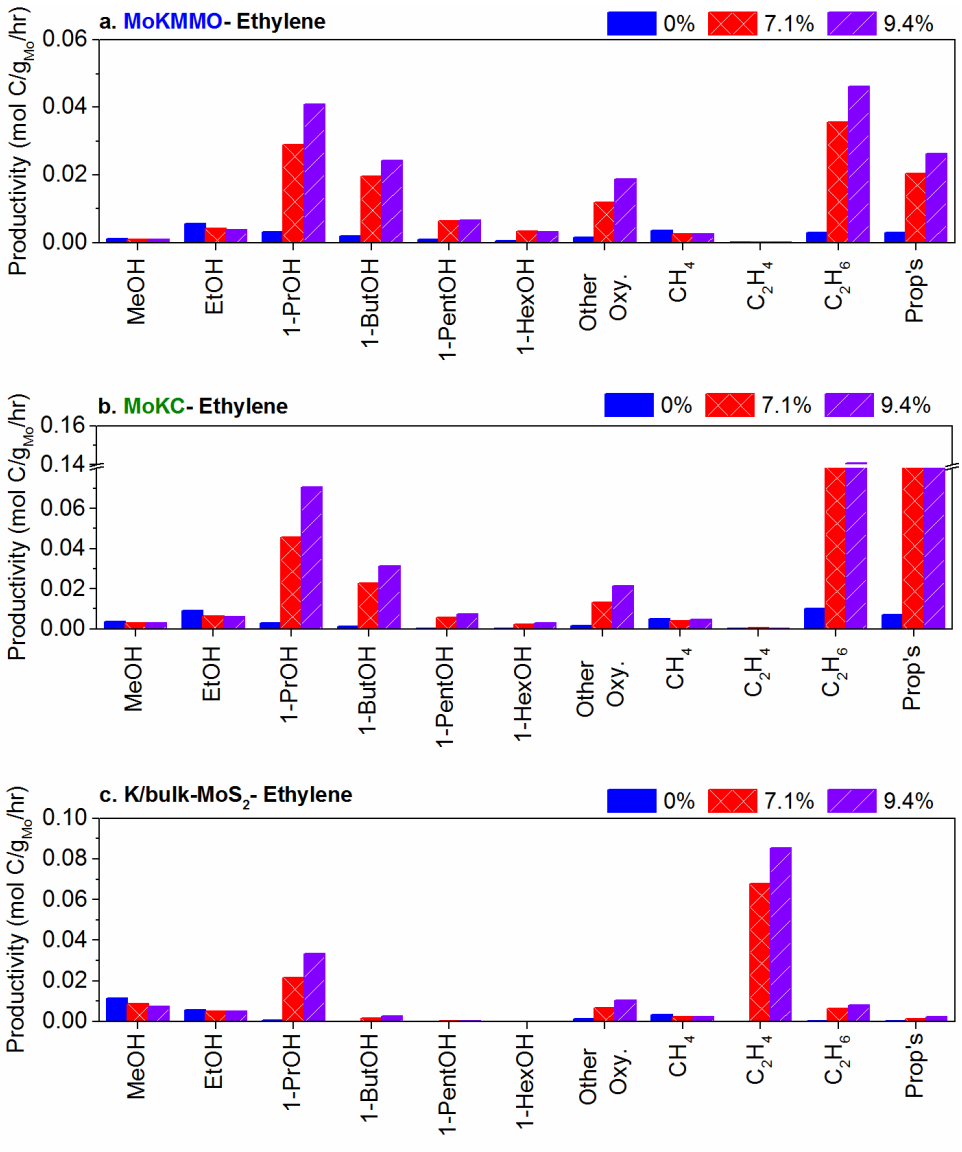

Figure 3.5: Major products for ethylene co-feed experiments for the (a) MoKMMO, (b) MoKC, and (c) K/bulk-MoS_2 catalysts. Reaction conditions: 310 °C and 1500 psig.

3.2.6 Ethylene Co-feed

The major products distribution for the ethylene co-feed reactions over the (a) MoKMMO, (b) MoKC, and (c) K/bulk-MoS_2 catalysts is shown in Figure 3.5. Both the MoKMMO and MoKC catalysts show an increase of CO conversion with increasing ethylene co-feed. Different from the methanol and ethanol co-feed experiments, the co-fed ethylene reaches 100% conversion with both 7.1 mol% and 9.4 mol% ethylene in the syngas feed (Table 3.B.1).

Both the MoKMMO and MoKC catalysts show increases in C_{3+} alcohols (C_3-C_4 primarily) with increasing ethylene concentration in the syngas feed (Figure 3.5), similar to the ethanol co-feed. Figure 3.6 shows the major products for MoKMMO normalized by mol C of co-feed for the cases of (a) ethanol and (b) ethylene co-feed. It can be observed that the normalized C_3-C_5 alcohol formation rate is similar for ethanol and ethylene co-feed experiments for the MoKMMO catalyst. This indicates that the increased C_{3+} alcohols observed with the ethylene co-feed are likely formed via the same pathway as with the ethanol co-feed. Tatsumi et al. also hypothesized that alcohol formation from CO-H_2 conversion proceeds via the same intermediates as olefin carbonylation over K-Mo supported on SiO_2.[20] CO is inserted directly into the ethylene species (C_2H_4*) or into an ethyl intermediate (C_2H_5*) to form a propionyl species (C_2H_5CO*). The propionyl species is then further hydrogenated to form 1-propanol (as shown in Figure 3). Similarly, 1-butanol is formed via hydrogenation of the butanonyl species (C_3H_7CO*) after CO insertion into a propyl (C_3H_7) intermediate, further supporting that ethanol self-coupling is a minor pathway for 1-butanol formation, as discussed above.

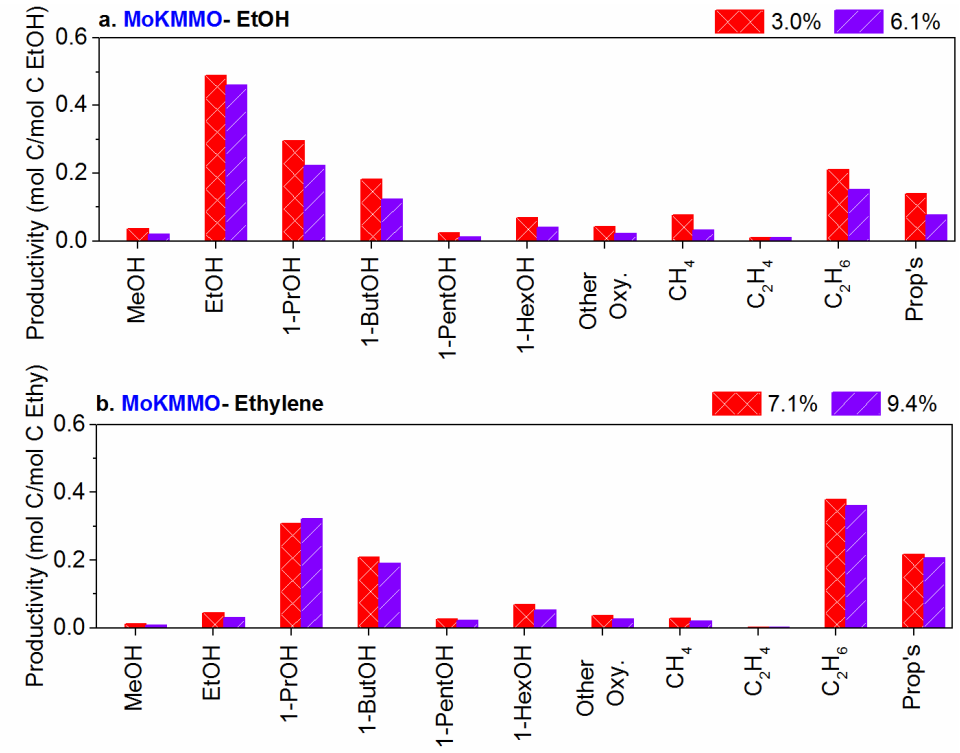

Figure 3.6: Normalized major products by co-feed mol of carbon via (a) ethanol, (b) ethylene co-feeds for the MoKMMO catalyst. Reaction conditions: 310 °C and 1500 psig.

There is an important difference in the C_{2+}HC formation over the MoKMMO catalyst compared to the ethanol co-feed case, resulting in comparable amounts of total alcohols and total hydrocarbons selectivity with the ethylene co-feed (Table 3.B.1). Ethane is the dominant product, which is likely formed by hydrogenation of ethylene. Propane/propylene productivity is the next dominant hydrocarbon product, likely derived from propyl species (C_3H_7*). However, it is also possible that chain propagation reactions are occurring, where CH_x (originating from CO) C-C couple with C_2H_4* or other alkyl species to form higher hydrocarbons with ethylene co-feed experiments, as discussed in Fischer Tropsch synthesis.[21] The normalized major products distribution for the MoKMMO catalyst for the ethylene co-feed (Figure 3.6b) shows that methane and methanol (derived

from CH_X* species) productivities are smaller compared to the ethanol co-feed case (Figure 3.6a). Therefore, CH_x* C-C coupling with C_2H_4* or other alkyl species to form higher hydrocarbons may be favoured over methane formation via CH_x intermediates during ethylene co-feed experiments. This pathway would be consistent with the increase in total hydrocarbon selectivity with an ethylene co-feed over the MoKMMO catalyst compared to the ethanol co-feed.

Similar to the ethanol co-feed, the MoKC catalyst favours formation of C_{2+} hydrocarbons over C_{3+} alcohols, with total hydrocarbon selectivity double that of total alcohol selectivity (Table 3.B.1). This is expected as the MoKC catalyst consists of primarily single MoS_2 layers that are selective towards hydrocarbons. Ethane is the dominant hydrocarbon product, followed by propane/propylene. As explained above for the MoKMMO catalyst, ethane is likely formed via hydrogenation of ethylene species and propane/propylene are likely formed via propyl intermediates (C_3H_7*). Similar to the MoKMMO catalyst, the normalized major products over the MoKC catalyst show that methane and methanol productivities are smaller with ethylene co-feeds (Figure 3.B.12b) compared to ethanol co-feeds (Figure 3.B.11b), suggesting that C-C coupling of CH_x* and C_2H_4* species may be occurring. In addition, ethane formation over the MoKC catalyst is smaller with ethylene co-feeds compared to ethanol co-feed, supporting the hypothesis that ethanol dehydration-hydrogenation reactions are favoured with ethanol co-feed.

The normalized major product distributions shown in Figure 3.B.11b and Fig. 3.A.13b demonstrate that C_3-C_4 alcohol productivities over the MoKC catalyst are higher for ethylene compared to ethanol co-feed experiments. In fact, the probability of chain growth doubles from ~0.3 with the ethanol co-feed to ~0.6 with the ethylene co-feed (Figure 3.B.9). With an ethylene co-feed, ethyl species are

readily abundant compared to the ethanol co-feed over the MoKC catalyst, supporting the argument that the formation of ethyl species is rate-controlling for the formation of 1-propanol. In contrast, ethyl species are readily abundant over the MoKMMO catalyst with both ethanol and ethylene co-feed, thereby suggesting that the nature of the support influences the formation of ethyl species. Specifically, ethyl species are readily formed on Mo-K-MMO sites, enhancing the normalized C_3-C_4 alcohol productivity with ethylene co-feed.

Although the ethylene co-feed does not affect the production of C_{3+} alcohols for the K/bulk-MoS_2 catalyst as significantly as for the MoKC catalyst, 1-propanol production significantly increases over the K/bulk-MoS_2 catalyst with increasing ethylene co-feed, unlike ethanol co-feed, which was largely unreactive. This suggests that ethylene has the propensity to adsorb on the catalyst surface and/or form ethyl adsorbed species that can then undergo CO insertion to form 1-propanol. Consistent with the ethanol co-feed results, smaller K/MoS_2 domains over the MoKMMO and MoKC catalysts provide more favoured and abundant sites for ethylene to form C_{3+} products compared to the K/bulk-MoS_2 catalyst, which produces 1-propanol exclusively amongst higher alcohol products. Additionally, over the K/bulk MoS_2 catalyst, the selectivity towards total hydrocarbons remains similar with increasing ethylene co-feed (Table 3.B.1), with ethane being the dominant product. This may be associated with small increases in CO conversion with increasing ethylene co-feed compared to the supported counterparts, which results in higher total alcohol selectivity.

Hofbauer et al. also observed over K/MoS_2 that ethylene in the syngas feed was responsible for build-up of higher alcohols, primarily 1-propanol.[22] They hypothesized that the formation of 1-propanol was due to hydroformylation of ethylene to propanal that was rapidly hydrogenated to 1-propanol. Propanal

formation is observed to increase over the MoKMMO, MoKC and K/bulk-MoS_2 catalysts with ethylene co-feeds (Figure 3.B.13), unlike during ethanol co-feeds (Figure 3.B.10), where propanal is primarily observed over only the MoKMMO catalyst. The increase in propanal formation with ethylene co-feeds over the MoKC and K/bulk-MoS_2 catalysts may be associated with the hydroformylation of ethylene.

3.2.6.1 Ethylene Co-feed Minor Products

The normalized major products show that isobutyl alcohol productivity over the MoKMMO catalyst is similar with ethanol (Figure 3.B.11) and ethylene (Figure 3.B.12) co-feeds. In contrast, over the MoKC catalyst, the isobutyl alcohol productivity significantly increases with the ethylene co-feed compared to the ethanol co-feed. This may be associated with increased propanal formation via ethylene hydroformylation that can undergo coupling with methanol to form isobutyl alcohol. This further indicates that the MoKC catalyst contains the acid-base pairs necessary for Guerbet coupling. Similar to the ethanol co-feed experiment over the MoKMMO catalyst, isoamyl alcohol production increases slightly in ethylene co-feed experiments (Figure 3.B.13), likely a result of 1-butanol derived species coupling with methanol to form isoamyl alcohol, as a result of increased 1-butanol formation with ethylene co-feeds.

For all the catalysts, propyl acetate and propyl propionate are the most significant minor products (Figure 3.B.13). For the MoKC catalyst, this observation suggests that ethanol adsorption and/or the formation of ethyl species are the controlling step(s) for the formation of acetate and propionate species, as the MoKC catalyst is readily able to form these species with ethylene but not with an ethanol co-feed.

3.3 Conclusions

Syngas conversion to higher alcohols was studied over three known catalysts using methanol, ethanol or ethylene co-feeds. The methanol co-feed resulted in increased ethanol, and methane production across all catalysts. However, methane formation is supressed over the K/bulk-MoS_2 catalyst compared to the supported counterparts, as it is comprised of primarily MoS_2 domains containing 3+ layers, different from the supported counterparts that include single MoS_2 layers that are selective towards hydrocarbons. The ethanol co-feed increased $C_{3+}OH$ and $C_{2+}HC$ over the supported catalysts, but did not yield any significant change in the product distribution over the K/bulk-MoS_2 catalyst. Similarly, an ethylene co-feed increased the $C_{3+}OH$ and $C_{2+}HC$ productivity over the supported catalysts. However, over the K/bulk-MoS_2 catalyst, a significant increase in only 1-propanol was observed, suggesting that ethanol adsorption and/or formation of ethyl species are likely rate-controlling for 1-propanol formation.

$C_{3+}OH$ productivity over the MoKC catalyst was more strongly affected by an ethylene compared to ethanol co-feed, indicating that ethanol adsorption and/or dissociation are also likely rate controlling steps for 1-propanol formation over this catalyst. In contrast, K/MoS_2 domains over MMO supports appear to provide more favourable and abundant Mo-K-MMO sites for the adsorption of ethanol or formation of ethyl species to undergo further reaction to higher chain products, as the normalized major $C_{3+}OH$ product distributions by co-fed ethylene and ethanol over the MoKMMO catalyst were similar. It can be therefore concluded that the alcohol formation likely proceeded via the same acyl intermediate as the olefin carbonylation over the MoKMMO catalyst.

Supports do have an influence on the reaction pathways to higher chain products. The acidity of the carbon support seems to facilitate alcohol dehydration/hydrogenation reactions to yield hydrocarbons. The MMO support influences methanol plus 1-propanol coupling to form isobutyl alcohol. The MoKC catalyst catalyses isobutyl alcohol formation, suggesting that it consists of the acid-base pairs needed for methanol plus 1-propanol coupling. Isobutyl alcohol formation over the MoKC catalyst significantly increased with an ethylene co-feed, likely associated with increased propanal productivity formed via ethylene hydroformylation.

3.4 References

(1) M. Taborga Claure, S.-H. Chai, S. Dai, K. A. Unocic, F. M. Alamgir, P. K. Agrawal and C. W. Jones, *J. Catal.*, 2015, **324**, 88-97.

(2) M. R. Morrill, N. T. Thao, P. K. Agrawal, C. W. Jones, R. J. Davis, H. Shou, D. G. Barton and D. Ferrari, *Catal. Lett.*, 2012, **142**, 875-881.

(3) M. R. Morrill, N. T. Thao, H. Shou, R. J. Davis, D. G. Barton, D. Ferrari, P. K. Agrawal and C. W. Jones, *ACS Catal.*, 2013, **3**, 1665-1675.

(4) J. T. Kozlowski and R. J. Davis, *ACS Catal.*, 2013, **3**, 1588-1600.

(5) J. G. Santiesteban, C. E. Bogdan, R. G. Herman and K. Klier, *in: M.J. Philips, M. Ternan (Eds.), vol. 2, 9th Annual Congress on Catalysis, Chemical Institute of Canada, Calgary, 1988, pp. 561-568.*

(6) J. M. Christensen, P. A. Jensen, N. C. Schiødt and A. D. Jensen, *ChemCatChem*, 2010, **2**, 523-526.

(7) V. P. Santos, B. van der Linden, A. Chojecki, G. Budroni, S. Corthals, H. Shibata, G. R. Meima, F. Kapteijn, M. Makkee and J. Gascon, *ACS Catal.*, 2013, **3**, 1634-1637.

(8) G. J. Quarderer, R. R. Stevens, G. A. Cochran and C. B. Murchison, *US Patent 4825013 A, to The Dow Chemical Company, 1989.*

(9) C. Murchison, M. Conway, R. Stevens and G. Quarderer, *Proc. 9th Intern. Congr. Catal*, 1988, **2**, 626.

(10) B. Temel, P. E. H. Nielsen and P. Beato, *US Patent 0225879A1, to Haldor Topsoe A/S*, 2013.

(11) P. E. H. Nielsen, B. Temel and P. Beato, *US Patent 8637580B2, to Haldor Toposoe A/S*, 2014.

(12) N. E. Kinkade, *US Patent WO1985003073 A1, to Union Carbide Corp*, 1985.

(13) J. Iranmahboob, H. Toghiani and D. O. Hill, *Appl. Catal., A*, 2003, **247**, 207-218.

(14) D. Ferrari, G. Budroni, L. Bisson, N. J. Rane, B. D. Dickie, J. H. Kang and S. J. Rozeveld, *Appl. Catal., A*, 2013, **462-463**, 302-309.

(15) K. S. Liang, R. R. Chianelli, F. Z. Chien and S. C. Moss, *J. Non-Cryst. Solids*, 1986, **79**, 251-273.

(16) R. Suárez París, M. Boutonnet and S. Järås, *Catal. Commun.*, 2015, **67**, 103-107.

(17) T. Toyoda, T. Minami and E. W. Qian, *Energy Fuels*, 2013, **27**, 3769-3777.

(18) T. Y. Park, I.-S. Nam and Y. G. Kim, *Ind. Eng. Chem. Res.*, 1997, **36**, 5246-5257.

(19) M. Xu and E. Iglesia, *Catal. Lett.*, 1998, **51**, 47-52.

(20) T. Tatsumi, A. Muramats and H.-o. Tominaga, *Chem. Lett.*, 1985, **14**, 593-594.

(21) F. Fischer and H. Tropsch, *Berichte Der Deutschen Chemischen Gesellschaft, vol. 59, 1926, p. 830*.

(22) G. Weber, R. Rauch and H. Hofbauer, *Biomass Conv. Bioref.*, 2015, **5**, 85-94.

APPENDIX 3.A

K/MOS_2 CATALYSTS CHARACTERIZATION

This appendix includes the supporting characterization of the reaction-aged supported K/MoS_2 catalysts via N_2 physisorption and X-ray Diffraction (XRD) discussed in this chapter.

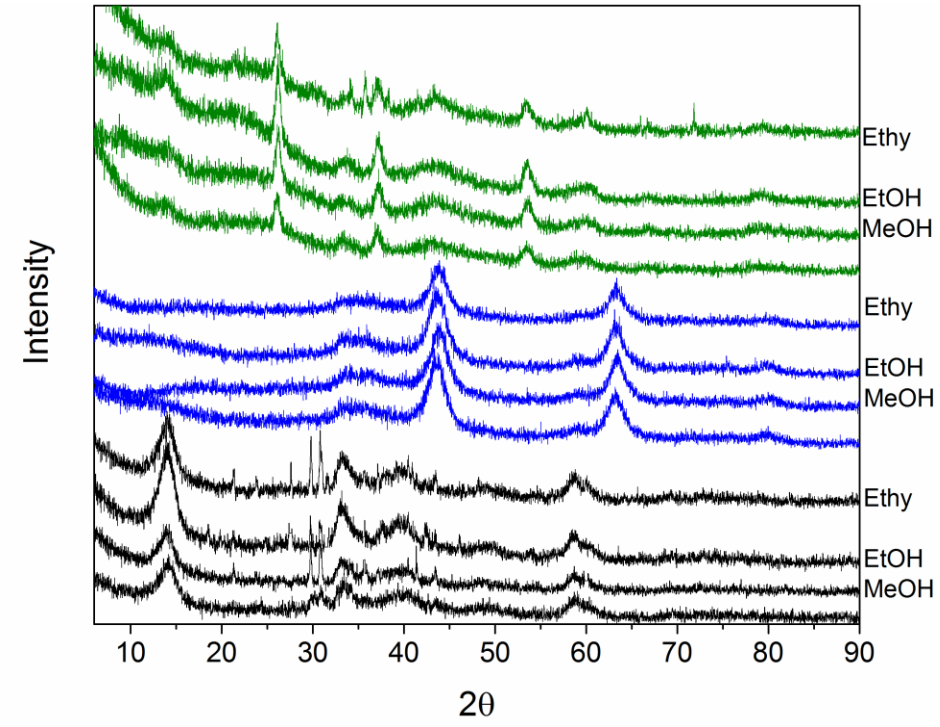

Figure 3.A.1: XRD patterns of reaction-aged K/bulk MoS_2 (black), MoKMMO (blue), MoKC (olive) catalysts from methanol, ethanol, and ethylene co-feed experiments.

Table 3.A.1: Brunauer-Emett-Teller (BET) surface areas for reaction-aged MoKMMO and MoKC catalysts.

Catalyst	Co-feed	BET SA (m^2/g)
MoKC	-	1155
MoKC	MeOH	1378
MoKC	EtOH	1374
MoKC	Ethy	985
MoKMMO	-	62
MoKMMO	MeOH	52
MoKMMO	EtOH	52
MoKMMO	Ethy	56

APPENDIX 3.B

K/MOS_2 CATALYSTS REACTIVITY DATA

This appendix includes the supporting reactivity data of supported K/MoS_2 catalysts discussed in this Chapter.

Note: 0%-B and 0%-A in Figure 3.B.1-3.B.5 attributes to the product distribution before and after co-feed, respectively. Linear Alcohols include C_1-C_6 linear alcohols, whereas hydrocarbons include methane, ethane, ethylene and propane/propylene. C_{4+}HC were not included in the carbon balance or product distributions as these products cannot be accurately quantified with the GC columns used for this study. Butane overlaps with methanol in the TCD column; therefore with methanol co-feed experiments, butane is embedded in the methanol peak. Pentane and Hexane are observed in the FID, but all hydrocarbons evolve in 0.4 min; making it difficult to accurately deconvolute these species.

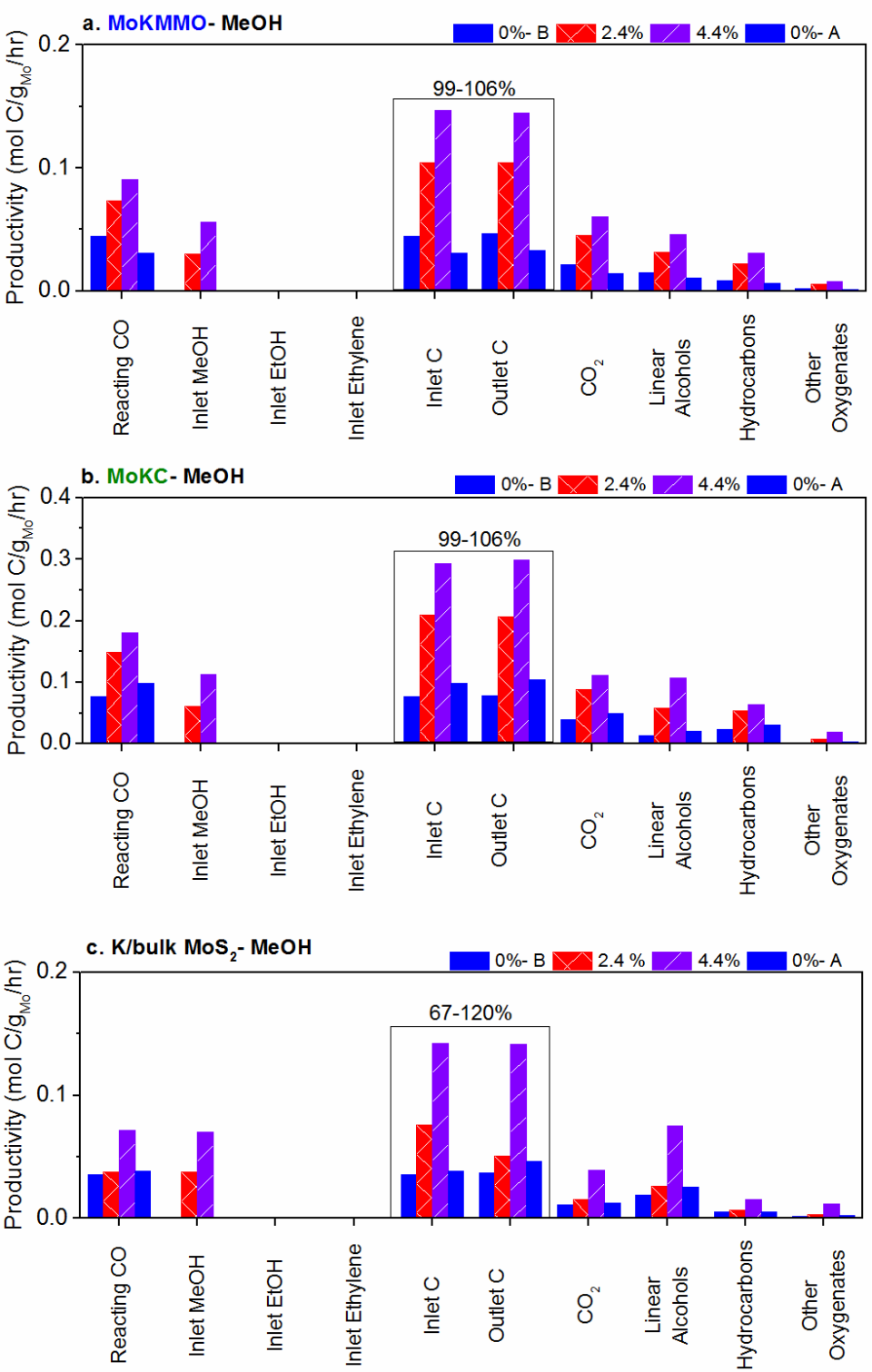

Figure 3.B.1: Carbon balance for methanol co-feed experiments for the (a) MoKMMO, (b) MoKC, and (c) K/bulk-MoS_2 catalysts.

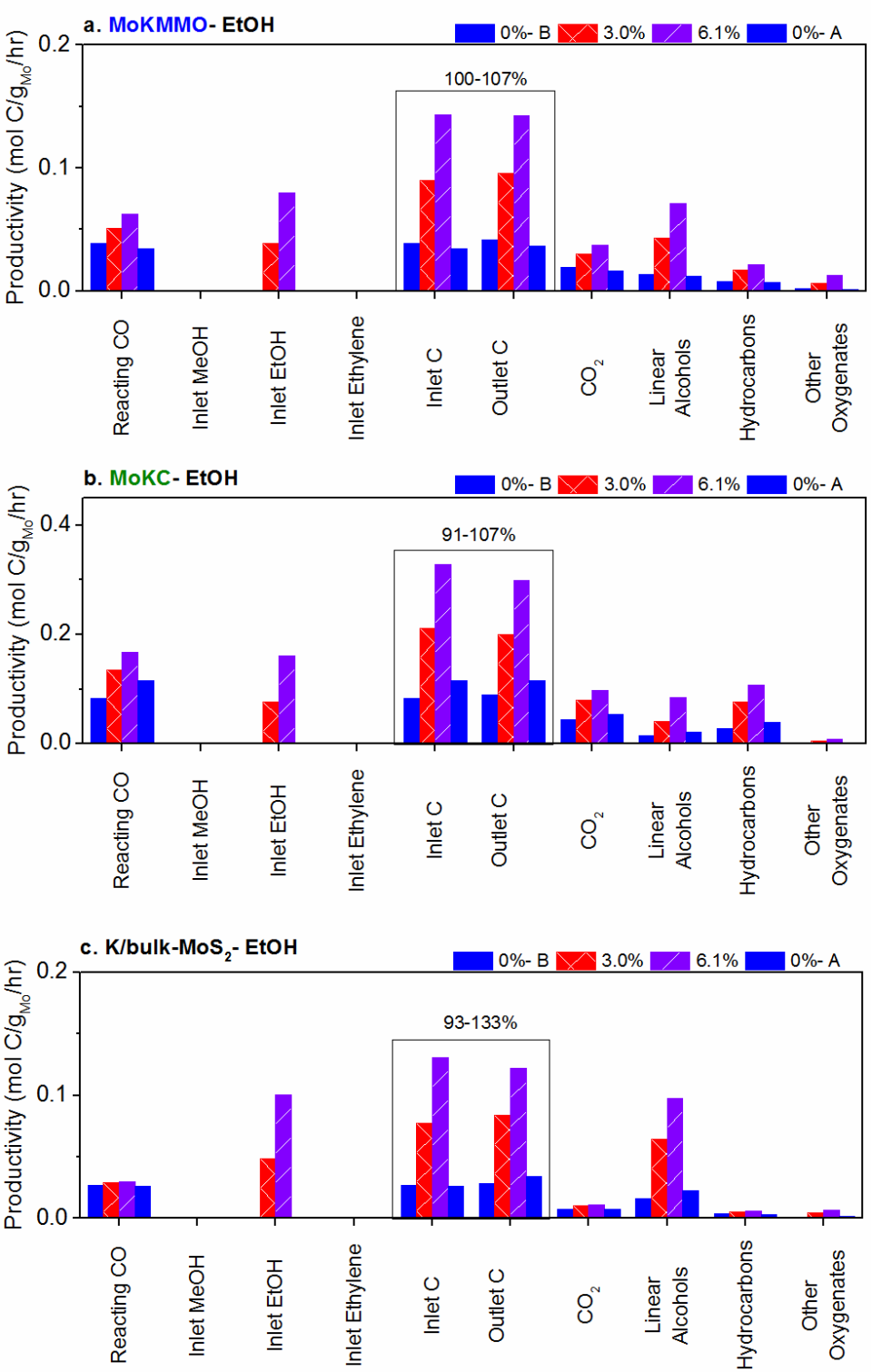

Figure 3.B.2: Carbon balance for ethanol co-feed experiments for the (a) MoKMMO, (b) MoKC, and (c) K/bulk-MoS_2 catalysts.

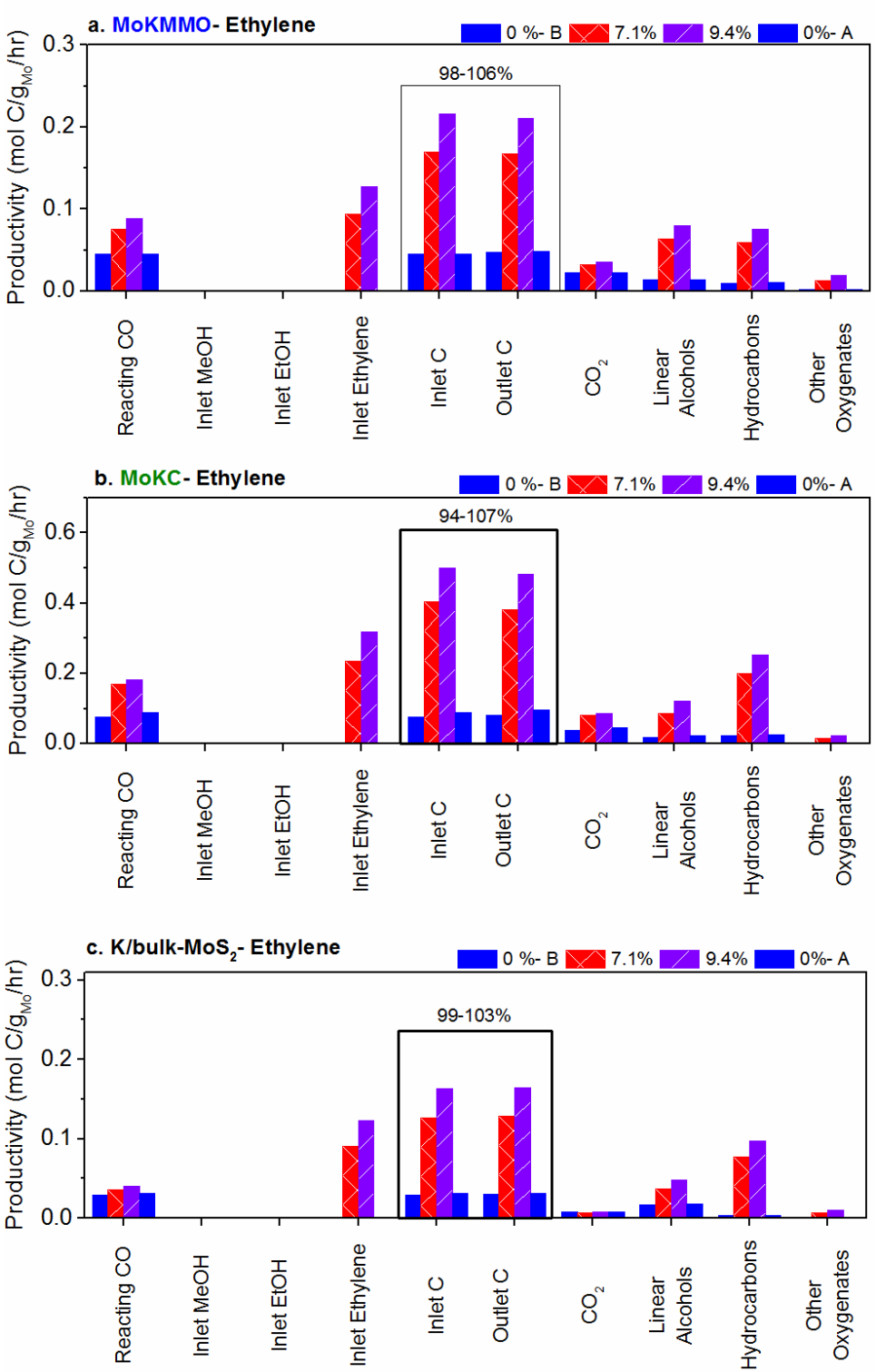

Figure 3.B.3: Carbon balance for ethylene co-feed experiments for the (a) MoKMMO, (b) MoKC, and (c) K/bulk-MoS_2 catalysts.

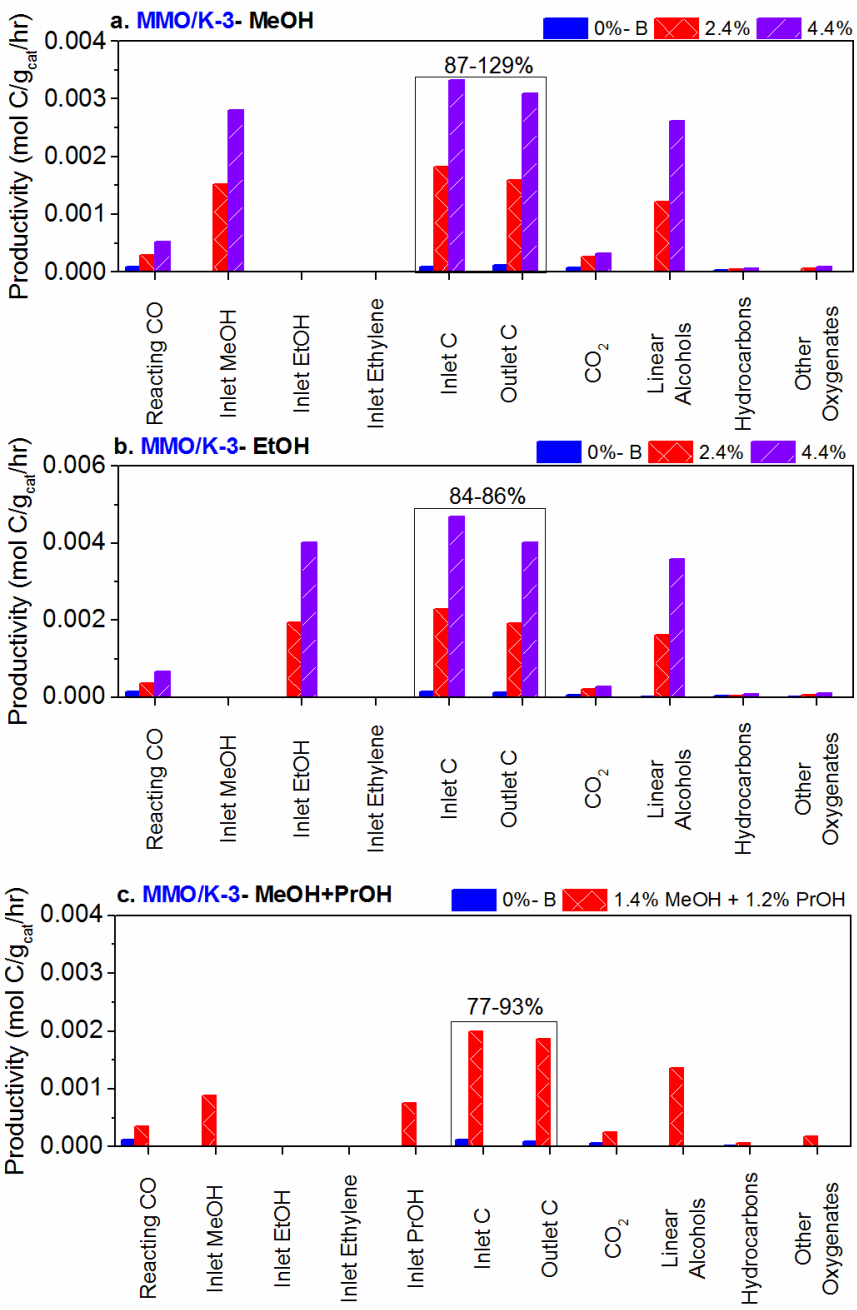

Figure 3.B.4: Carbon balance for the Mo-free MMO/K catalyst for (a) methanol, (b) ethanol, and (c) mixture of methanol and 1-propanol co-feed experiments.

Mo-free MMO/K was also subject to methanol co-feed experiments as a control experiment. The carbon balance shown in Figure 3.B.4 shows that CO conversion is largely unaffected by the introduction of methanol, ethanol and a mixture of methanol and 1-propanol; its minor increase may be associated with the water gas shift reaction to form CO_2.

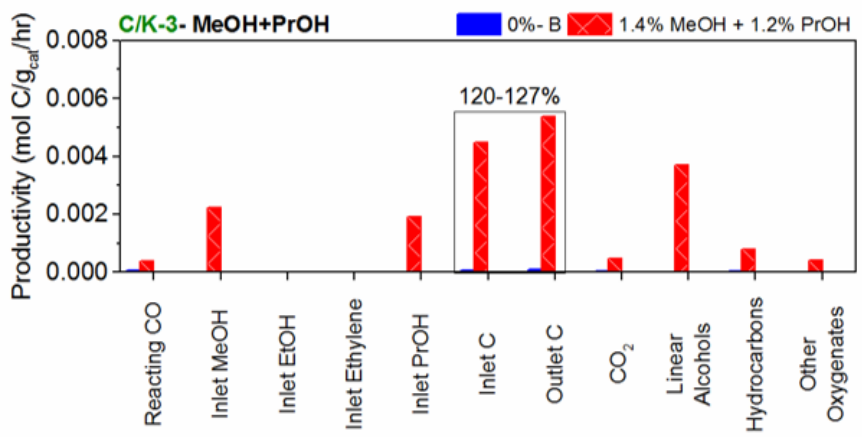

Figure 3.B.5: Carbon Balance for the Mo-free C/K catalyst for mixture of methanol and 1-propanol co-feed.

The carbon balance shows that CO conversion is largely unaffected; its minor increase may be associated with the water gas shift reaction to form CO_2, as explained for Fig. 3.B.4.

Table 3.B.1: Reactivity data for MoKMMO, MoKC and K/bulk-MoS_2 catalysts from methanol, ethanol, and ethylene co-feed experiments. Reaction conditions: 310 °C and 1500 psig.

Catalyst	Co-feed	Carbon Balance (%)	CO conv. (%)	Co-fed conv. (%)	Total OH Sel. (CO_2 Free) (%)	Total HC Sel. (CO_2 Free) (%)	1-EtOH/1-PrOH formation rate	1-ButOHl/1-PrOH formation rate
MoKMMO	0% -MeOH	104	8.2		59.1	33.8	1.8	0.7
MoKMMO	2.4%- MeOH	100	12.7	83.1	53.5	37.6	2.7	0.6
MoKMMO	4.4%- MeOH	99	15.2	67.4	54.4	36.2	2.8	0.5
MoKMMO	0%- MeOH	106	5.3		57.7	35.8	2.1	0.7
MoKC	0% -MeOH	101	8.4		33.7	62.6	2.9	0.4
MoKC	2.4%- MeOH	99	16.0	73.6	48.9	45.6	3.4	0.4
MoKC	4.4%- MeOH	102	19.0	47.8	56.8	33.8	3.9	0.3
MoKC	0%- MeOH	106	10.0		39.1	57.0	2.8	0.5
K/bulk-MoS_2	0% -MeOH	105	7.2		72.4	20.4	10.9	0.1
K/bulk-MoS_2	2.4%- MeOH	67	7.2	91.2	72.7	19.5	12.1	0.1
K/bulk-MoS_2	4.4%- MeOH	100	13.0	49.2	73.4	14.9	9.2	0.1
K/bulk-MoS_2	0%- MeOH	120	7.4		76.7	15.2	11.8	0.1
MoKMMO	0% -EtOH	107	8.5		58.8	33.4	1.8	0.72
MoKMMO	3%- EtOH	107	10.3	64.5	65.0	25.4	1.7	0.61
MoKMMO	6.1%- EtOH	100	12.4	60.5	67.5	20.5	2.1	0.55
MoKMMO	0%- EtOH	106	7.0		58.2	34.4	1.9	0.68
MoKC	0% -EtOH	107	7.4		33.4	63.8	3.4	0.4
MoKC	3%- EtOH	94	11.3	80.3	33.6	63.1	2.7	0.4
MoKC	6.1%- EtOH	91	14.0	72.5	42.2	54.0	2.8	0.4
MoKC	0%- EtOH	101	9.7		33.3	63.5	2.8	0.4
K/bulk-MoS_2	0% -EtOH	104	6.9		76.4	18.1	11.9	0.1
K/bulk-MoS_2	3%- EtOH	108	7.3	5.3	87.2	7.0	17.9	0.5
K/bulk-MoS_2	6.1%- EtOH	93	7.7	23.0	88.3	5.7	18.4	0.6
K/bulk-MoS_2	0%- EtOH	133	6.5		82.9	11.7	13.2	0.1
MoKMMO	0%- Ethy	104	8.3		54.2	38.6	1.8	0.7
MoKMMO	7.1%-Ethy	99	15.2	100.0	47.1	43.6	0.1	0.7
MoKMMO	9.4%-Ethy	98	18.1	100.0	45.8	43.0	0.1	0.6
MoKMMO	0%-Ethy	106	8.5		52.9	40.2	1.8	0.7
MoKC	0%- Ethy	105	8.2		42.3	53.9	3.1	0.4
MoKC	7.1%-Ethy	94	18.4	99.9	28.6	66.8	0.1	0.5
MoKC	9.4%-Ethy	96	19.6	100.0	30.6	63.9	0.1	0.4
MoKC	0%-Ethy	107	8.9		45.9	49.7	2.9	0.5
K/bulk-MoS_2	0%- Ethy	103	6.9		79.0	15.9	12.3	0.1
K/bulk-MoS_2	7.1%-Ethy	102	8.7	25.4	30.7	63.9	0.2	0.1
K/bulk-MoS_2	9.4%-Ethy	101	9.8	30.6	30.9	62.5	0.2	0.1
K/bulk-MoS_2	0%-Ethy	99	7.4		79.4	14.9	12.2	0.1

Total alcohol and hydrocarbon selectivity (CO_2 free) does not include unreacted co-feed carbon to better depict the selectivity of total alcohols and hydrocarbons with co-feed experiments. However, it is important to note that for instance in methanol co-feed experiments, methanol productivity is assumed to be the same as in the original state (at 0% co-feed) with increasing co-fed methanol. Similar assumptions were made for ethanol productivity with ethanol co-feed experiments, and ethylene productivity with ethylene co-feed experiments.

Total alcohol selectivity for K/bulk-MoS_2 is higher for all co-feed experiments compared to their supported counterparts. This is associated with the small increase in CO conversion with increasing co-feed compared to the supported counterparts that results in higher total alcohol selectivity. Hydrocarbons are formed by secondary reactions; therefore, the selectivity towards total hydrocarbons increases with increasing CO conversion

Table 3.B.2: Reactivity data for the MMO/K-3 catalysts from methanol, ethanol, and ethylene co-feed experiments. Reaction conditions: 310 °C and 1500 psig.

Catalyst	Co-feed	Carbon Balance (%)	CO conv. (%)
MMO/K-3	0% -MeOH	129	0.3
MMO/K-3	2.4%- MeOH	87	1.1
MMO/K-3	4.4%- MeOH	93	1.8
MMO/K-3	0% -EtOH	85	0.5
MMO/K-3	3%- EtOH	84	1.3
MMO/K-3	6.1%- EtOH	86	2.4
MMO/K-3	0% -MeOH + PrOH	77	0.4
MMO/K-3	1.4%- MeOH + 1.2 % PrOH	93	1.3
MMO/K-3	0% -MeOH + PrOH	127	0.1
MMO/K-3	1.4%- MeOH + 1.2 % PrOH	120	0.5

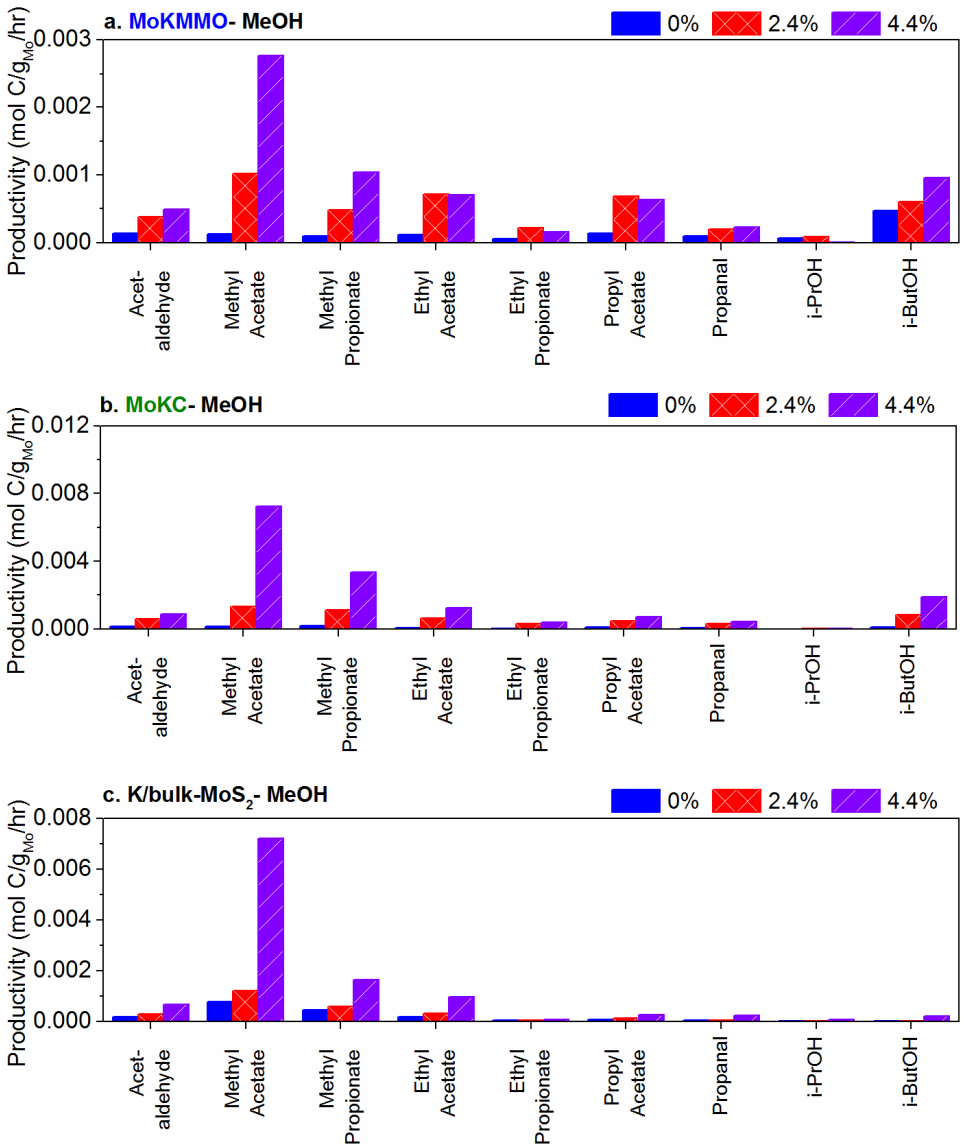

Figure 3.B.6: Minor products for methanol co-feed experiments for the (a) MoKMMO, (b) MoKC, and (c) K/bulk-MoS_2 catalysts.

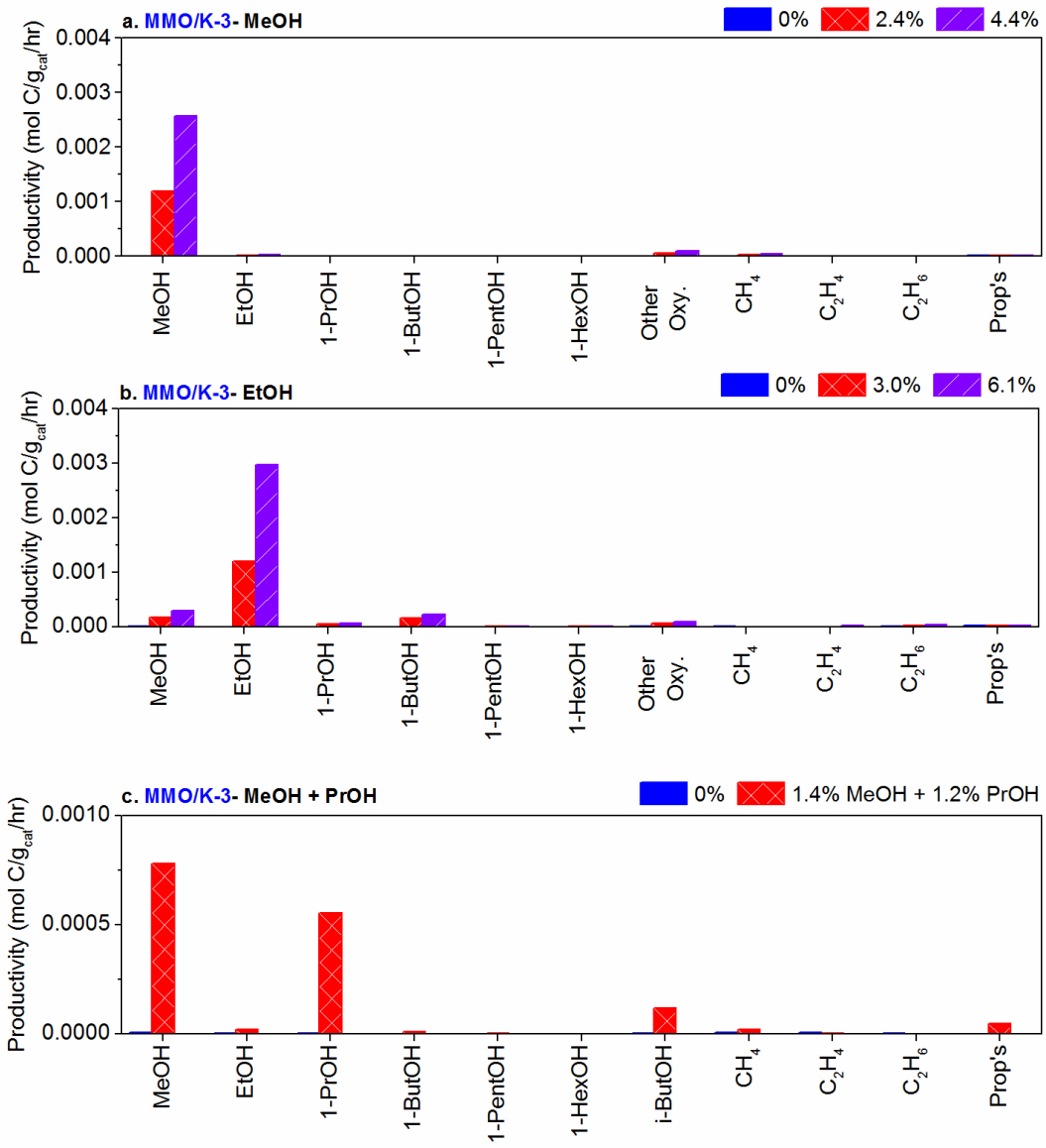

Figure 3.B.7: Major products for the Mo-free MMO/K material for (a) methanol (b) ethanol, and (c) methanol + ethanol co-feed experiments.

Note: The MeOH (a), and EtOH (b) co-feed experiments in Fig. 3.B.7 were run in succession over the same MMO/K-3 catalyst, therefore the small increase in MeOH formation with increasing ethanol co-feed is a result of leftover methanol in the co-feed line when running the ethanol co-feed. For all other experiments in this study, each co-feed experiment was conducted with a fresh catalysts.

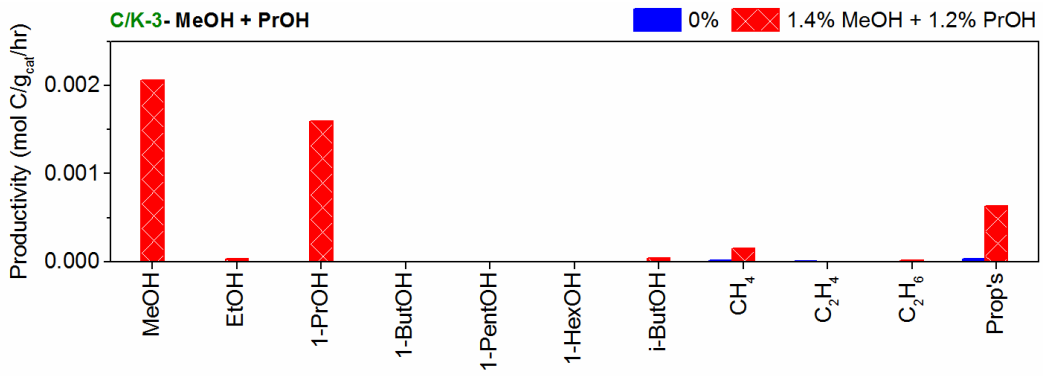

Figure 3.B.8: Minor products for the Mo-free C/K-3 material for mixed methanol, 1-propanol co-feed experiment.

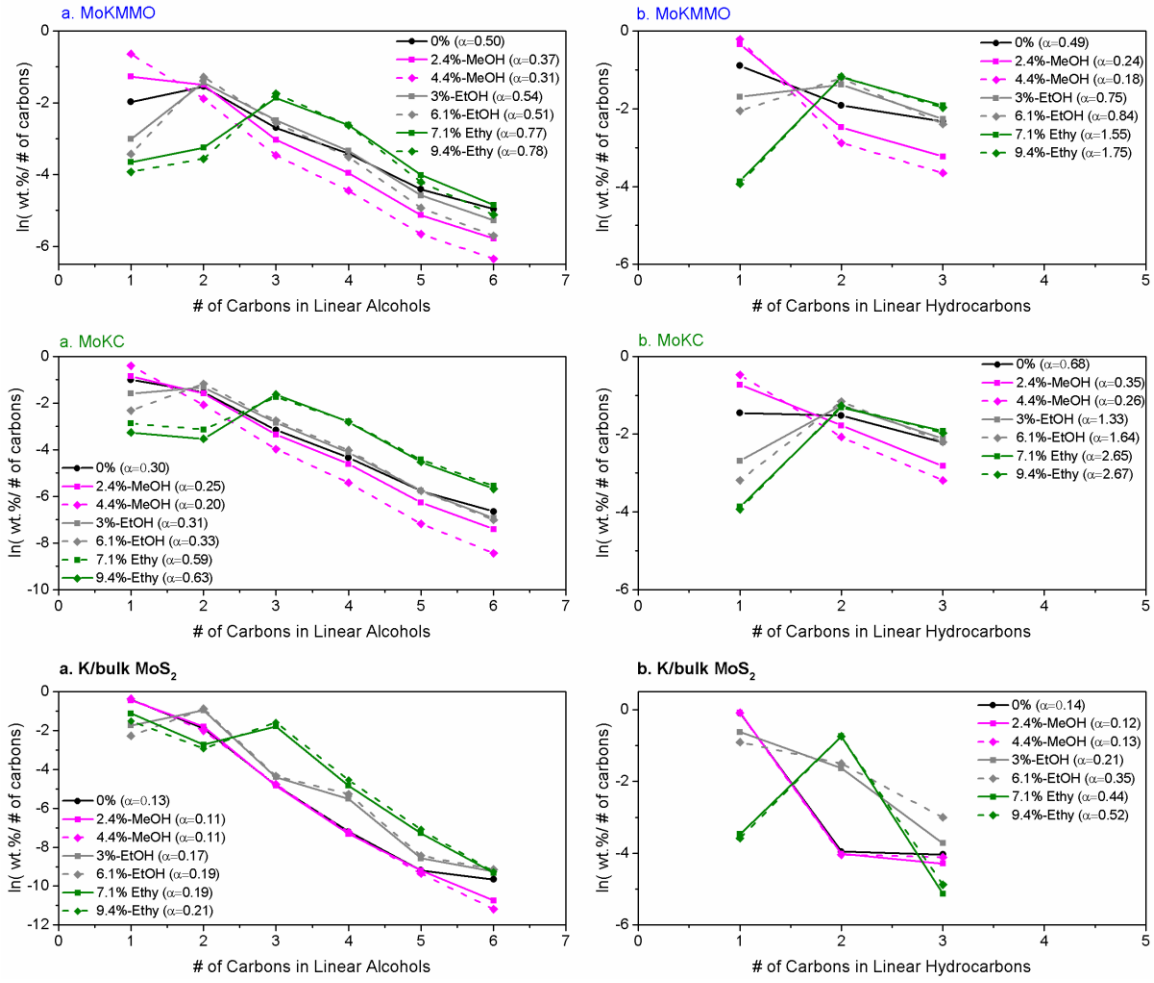

Figure 3.B.9: Anderson-Shulz Flory distribution for linear alcohols (a) and hydrocarbons (b) for the MoKMMO, MoKC, and K/bulk-MoS_2 catalysts.

Note: The probability of chain growth for linear alcohols includes unreacted co-fed methanol and ethanol for their respective co-feed experiments. Similarly, the probability of chain growth for linear hydrocarbons includes unreacted co-fed ethylene. Their inclusion does not greatly affect the probability of chain growth.

It is important to note that for ethanol and ethylene co-feed experiments, methane (produced in negligible amounts) strongly perturbs the ASF distribution, resulting in alpha values greater than one (which is physically impossible). The weight fraction for methane approaches zero and therefore makes the ln(methane wt.%/ 1) (where 1 is the # carbons in methane) a large negative number that does not follow the ASF distribution. However, if methane is not included in the probability of chain growth, the influence of co-feed on hydrocarbon product distribution would not be accurately represented.

The MoKMMO catalyst shows the largest influence in C_{3+} alcohol formation with methanol, ethanol, and ethylene co-feed experiments, as the probability of chain growth over the MoKMMO catalyst is larger than over the MoKC and K/bulk MoS_2 catalyst. This suggests that Mo-K-MMO sites facilitate higher alcohol formation. The probability of hydrocarbon chain growth over the MoKC catalyst is significantly higher compared to the MoKMMO and K/bulk MoS_2 catalysts with ethanol and ethylene co-feeds, suggesting that the MoKC catalyst favors C_{2+} hydrocarbon over C_{3+} alcohol formation.

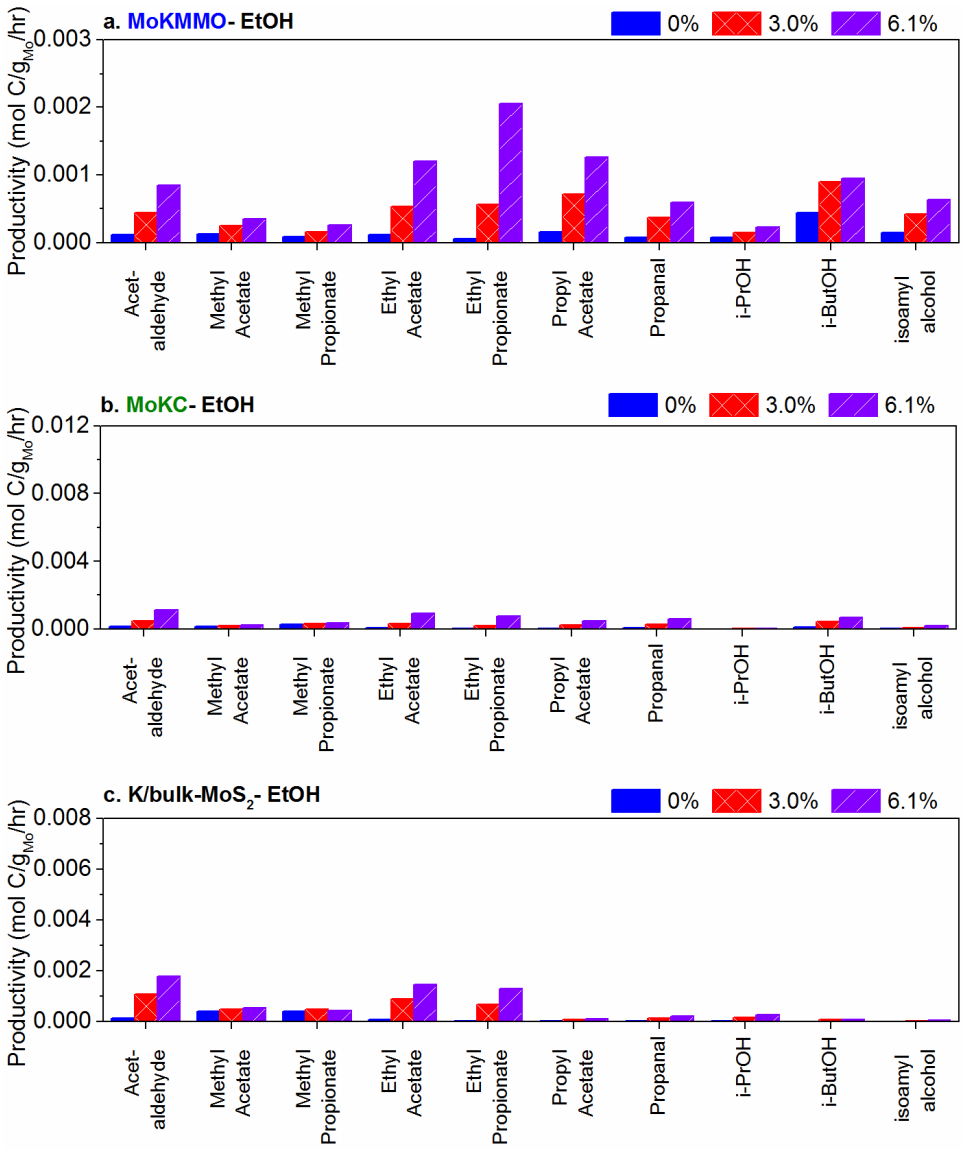

Figure 3.B.10: Minor products for ethanol co-feed experiments for the (a) MoKMMO, (b) MoKC, and (c) K/bulk-MoS_2 catalysts.

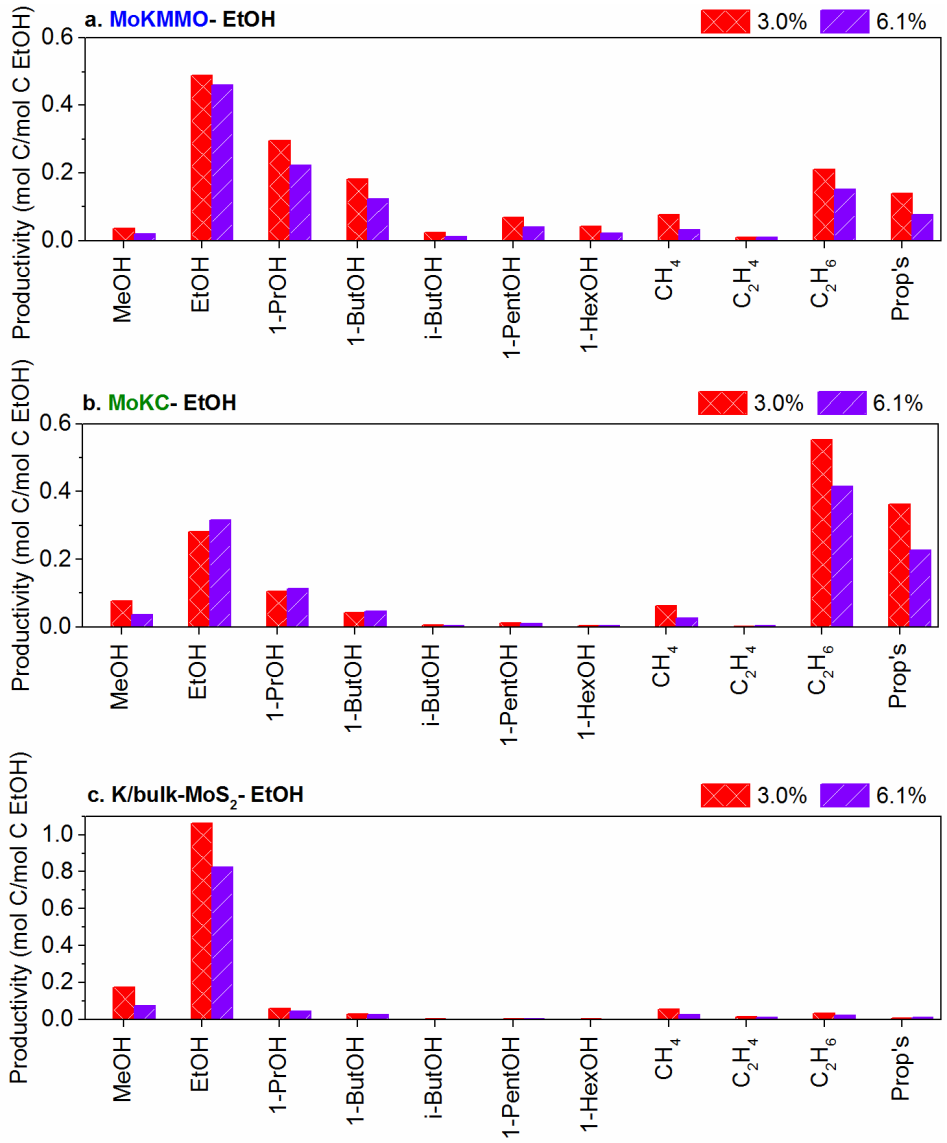

Figure 3.B.11: Normalized major products (by co-fed mol carbon from ethanol) for the (a) MoKMMO, (b) MoKC, and (c) K/bulk-MoS_2 catalysts.

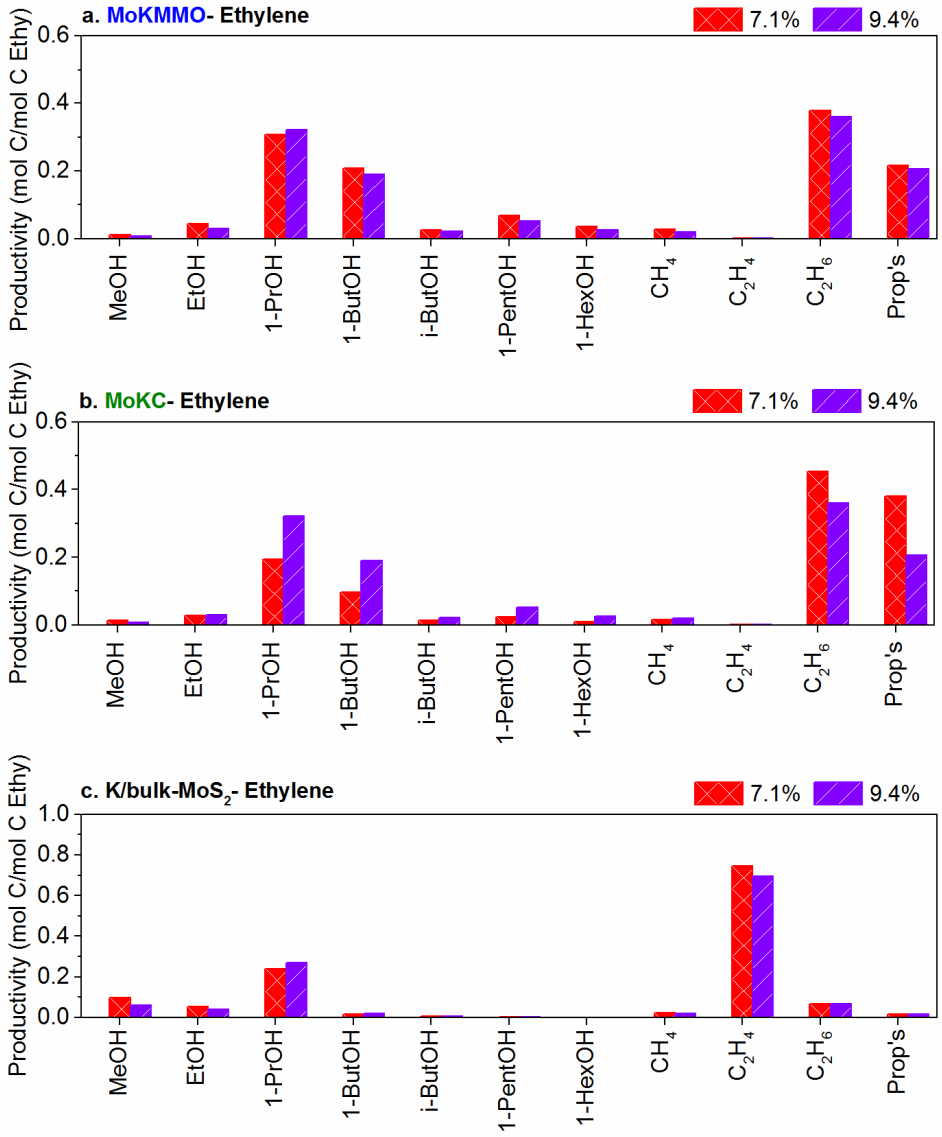

Figure 3.B.12: Normalized minor products (by co-fed mol carbon from ethylene) for the for (a) MoKMMO, (b) MoKC, and (c) K/bulk-MoS_2 catalysts.

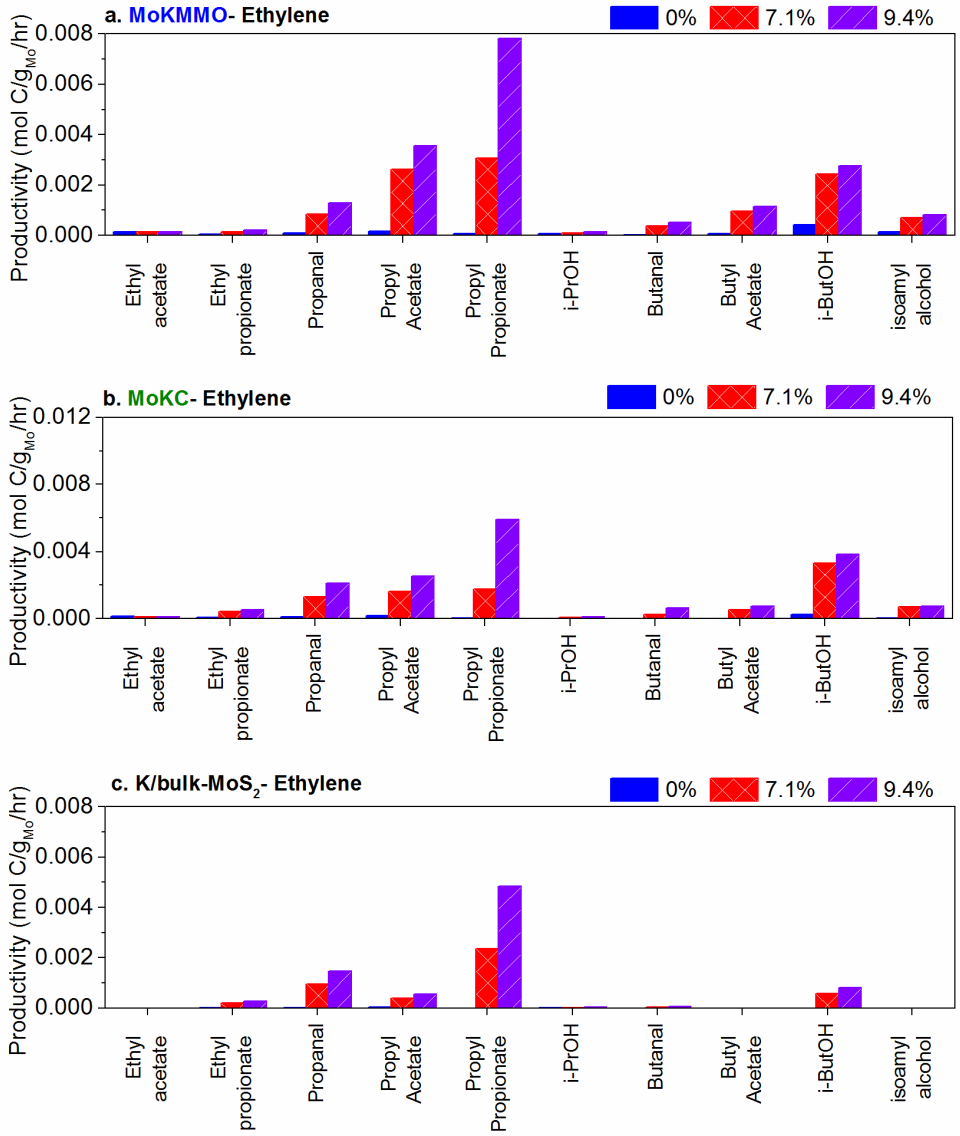

Figure 3.B.13: Minor products for ethylene co-feed experiments for the (a) MoKMMO, (b) MoKC, and (c) K/bulk-MoS_2 catalysts.

CHAPTER 4

ASSESING C_3-C_4 ALCOHOL SYNTHESIS PATHWAYS VIA $^{13}C_2$-ETHANOL AND $^{13}C_2$-ETHYLENE CO-FEEDS

4.1 Introduction

As explained above, the current state of knowledge regarding reaction pathways for carbon-carbon bond formation for higher alcohol production over supported K/MoS_2 catalysts is limited, where Mo-support interactions can directly affect the product distribution.[1-3] In Chapter 2, it was hypothesized that the intimate contact between K/MoS_2 domains and MMO has a synergistic effect in the formation of higher alcohols yielding high C_{2+}OH selectivity. In Chapter 3, MMO supported K/MoS_2 catalysts were subject to ethanol and ethylene co-feed experiments to evaluate changes in product distribution. It was hypothesized that CO insertion is the primary pathway to higher alcohols over MMO, as the alcohol chain growth probability decreased with increasing carbon chain length. Ethylene and ethanol co-feeds yielded similar production rates of C_{3+}OH over the MMO supported catalyst, indicating that alcohol formation likely proceeds primarily *via* the same acyl intermediate as olefin carbonylation.[4] Supports did seem to have an important influence on the reaction pathways. Specifically, MMO was thought to influence secondary reactions involving methanol plus 1-propanol coupling to form isobutyl alcohol and ethanol self-coupling to 1-butanol.

In this chapter, K/MoS_2 catalysts supported on MMO (studied in Chapters 2-3) were subjected to $^{13}C_2$-ethylene and $^{13}C_2$-ethanol co-feed experiments to elucidate the reaction pathways to higher alcohols over the MMO supported

K/MoS_2 catalyst by tracking the fate of ^{13}C in the products via ^{13}C-NMR and GC-MS analysis. K/bulk-MoS_2 was used as a control catalyst subject to 10% $^{13}C_2$-ethylene co-feed experiments, with an emphasis on understanding the role of K/MoS_2 and K/MoS_2-MMO sites on higher alcohol formation pathways. The K/bulk-MoS_2 catalyst was not subjected to reactions with $^{13}C_2$-ethanol, as the ethanol co-feed was found to be largely unreactive previously.[4] This study provides an unprecedented level of insight into the reaction pathways to higher alcohols from syngas over MMO supported K/MoS_2 catalysts.

4.2 Experimental Procedure

A new batch of MMO was prepared in a similar manner as described in Chapters 2-3.[1-3] MMO supported K/MoS_2 catalysts were prepared with an approximate Mo loading of 5 wt.%, K loading of 3 wt.%, and a molar ratio of Mo:K of 1, similar to the procedure described for the MoKMMO catalyst in Chapters 2-3 (referred in the same way in this Chapter). The same batch of bulk MoS_2 used for the study in Chapter 3 was used for the study in this Chapter. K was added to the synthesized bulk MoS_2 with a molar ratio of Mo:K of 1, with this sample referred to as K/bulk-MoS_2. Both supported and unsupported precatalysts were physically ground for 15 min with K_2CO_3 (Aldrich, 99%, stored in an oven at 105 °C).[5]

The prepared K/bulk-MoS_2 and MoKMMO catalysts were then pelletized, crushed, and sieved through a 20-40 mesh prior to loading in the reactor. The precatalysts were then loaded into a 6.35 mm steel tube reactor (1 g for MoKMMO and 0.15 g for K/bulk-MoS_2) and pretreated with 10% H_2S/H_2 (Matheson Tri-Gas, UHP) at 450 °C for 2 h at a heating rate of 5 °C/min and a flow rate of 20 mL/min to reduce, in situ, the precatalyst oxide phase of the MoKMMO and surface oxidized K/bulk-MoS_2 catalyst. The reactions with syngas,

45% H_2, 45% CO, 10% N_2, and 50 ppm H_2S were carried out at 310 °C and 1500 psig after in situ sulfidation, as described in Chapters 2-3.

The syngas flowrate was adjusted between 10-20 mL/min to reach pseudo steady state at 8% conversion. Once the reaction reached 8% conversion after ~3 days of reaction, an ethanol (Sigma Aldrich, 99.5%), 10% $^{13}C_2$-ethanol (Sigma Aldrich, 99 atom% ^{13}C), balanced with ethanol (Sigma Aldrich, 99.5%) (confirmed with GC-MS), ethylene (Matheson, 99.95%), or 10% $^{13}C_2$-ethylene (Cambridge Isotope, 99%), balanced with ethylene (Matheson, 99.95%) co-feed was introduced into the reactor using a 500D Isco pump for ethanol co-feeds and a 100DX Isco pump for ethylene co-feeds. Ethanol and ethylene co-feed experiments containing natural abundance (~1.1 atom%) ^{13}C were conducted as control experiments. Ethanol co-feeds were heated to 200 °C (to convert the liquid to the vapor phase) and pressurized to 1500 psig before introduction into the reactor at 1 and 2 μL/min, making a 0-6 mol% composition with the syngas feed. The ethylene co-feed was pressurized to 1500 psig and introduced into the reactor at 3 and 4 μL/min, making a 0-9 mol% composition with the syngas feed.

The ethanol and ethylene co-feeds were fed into the reactor at the first flowrate set point until the reaction reached pseudo steady state. Once pseudo steady state was reached, the liquid reaction products were collected for 18 hrs using a liquid nitrogen trap placed downstream from the backpressure regulator and subsequently transferred to NMR tubes for ^{13}C-NMR analysis. The flowrate was then increased to the second set point (2 μL/min for ethanol co-feed, 4 μL/min for ethylene co-feed). After the reaction reached pseudo steady state a third time, the same procedure as discussed above was used to collect liquid products. Additionally, gas-tight NMR tubes were used to collect a gas aliquot for subsequent ^{13}C-NMR and GC-MS analyses. It is important to note that similar

conversions and product distributions were observed before and after liquid product collection, as can be observed by the error bars in Figures 4.B.1-4.B.7 in Appendix 4.B. This suggests that the catalyst was stable during liquid product collection. Finally, the co-feed was shut off until the product selectivity returned to its original state (without co-feed). Similar product distributions as obtained initially were observed after returning to the original state (Figure 4.B.8-4.B.10), suggesting that the co-feeds did not cause any significant change in the catalysts.

An Agilent 7890 gas chromatograph (GC) was used to quantify the main reaction products (carbon dioxide, methane, ethane, ethylene, propane/propylene, C_1-C_6 linear alcohols) using single point calibration curves. Other oxygenates quantified for this Chapter include isobutyl alcohol, as well as various aldehyde, acetate, and propionate species. The productivity of reacting CO and the distribution of products were calculated in terms of moles C per g of Mo per hour from pseudo-steady-state data. These units were chosen to enable a direct comparison of reaction components that are being produced by the catalysts. At the completion of the reactions, all catalysts were passivated, in situ, with 1% O_2 in He for 8 h at room temperature at 20 mL/min, as described in Chapters 2-3. Catalysts were then removed from the reactor and placed in a vial under argon and stored in a desiccator.

The reaction-aged catalysts were characterized, ex situ, via nitrogen physisorption and X-ray diffraction (XRD). Nitrogen physisorption isotherms were collected at -196 °C using a Micromeritics Tristar II after being heated to 200 °C under vacuum for 10 h prior to the analysis. XRD was performed using a Philips X-pert diffractometer using Cu-Kα radiation.

^{13}C NMR liquid samples were prepared by adding reaction products (300 µL) into $CDCl_3$ (600 µL) with THF (50 µL) as the internal standard. ^{13}C NMR spectra were recorded at room temperature on a Bruker AVIII-400 spectrometer using broad band proton decoupling. All chemical shifts are reported in parts per million (ppm) with reference to the center $CDCl_3$ solvent peak at 77.0 ppm. Quantitative measurements were made by suppressing the Nuclear Overhauser Effect using an inverse gated decoupling pulse sequence (zgig) and utilizing a 90° pulse angle with a sufficiently long pulse delay of 200 sec to ensure complete recovery, as determined from an inverse recovery T_1 experiment. GC-MS liquid samples were prepared by adding reaction products and THF (internal standard) in the ratio of 10:1 into acetone (solvent). GC-MS analysis was conducted on a Shimadzu GCMS-QP2010 S. The MS absolute intensity for all *m/z* of EtOH, 1-PrOH, and 1-ButOH products was normalized by the highest THF absolute intensity at *m/z*=42.5 to compare unlabeled and labeled co-feed experiments.

^{13}C NMR gas samples were prepared by pressurizing gas-tight NMR tubes to 80 psig after pulling vacuum on the tubes. ^{13}C NMR spectra were recorded at room temperature on a Bruker AVIII-400 spectrometer using broad band proton decoupling. Measurements were made by suppressing the Nuclear Overhauser Effect using an inverse gated decoupling pulse sequence (zgig) and utilizing a 30° pulse angle with a pulse delay of 6 sec. GC-MS gas samples were prepared by pressurizing gas-tight NMR tubes to 70 psig after pulling vacuum on the tubes. An Agilent 6890 GC coupled with a Micromass AutoSpec mass spectrometer were used for GC-MS analysis. The mass spectrometer was set to a mass resolution of 3000. The GC column used was an Agilent DB-5. The column was held at 30 °C. Splitless injections were made, and the mass spectrometer was scanned from 10-110 Da at 0.5 sec/decade.

4.3 Results and Discussion

4.3.1 XRD Patterns and N_2 Physisorption of Reaction Aged Catalysts

The XRD patterns of the reaction-aged catalysts are shown in Figure 4.A.1 in Appendix 4.A. The diffraction peaks present in the reaction-aged K/bulk-MoS_2 catalysts can be indexed to the hexagonal MoS_2 phase (JCPDS: 00-037-1492). While the K/bulk-MoS_2 catalyst showed the [002] MoS_2 plane at 14° (indicative of MoS_2 stacking)[6], the [002] MoS_2 plane was negligible in the reaction-aged MoKMMO catalysts. This indicates a low degree of stacking associated with the predominant double MoS_2 layer formation over this catalyst, as discussed in Chapter 2. The reaction-aged MoKMMO catalysts do show relatively broad peaks for the MoS_2 [100] (33°) and [110] (58°) and peaks characteristic of MgO at 44° and 64°.

Table 4.A.1 shows the BET surface areas calculated from N_2 physisorption data (P/P^0 of 0.06-0.2) for the reaction-aged catalysts studied. The BET surface areas for the reaction-aged MoKMMO catalysts vary between 48 m^2g^{-1}-63 m^2g^{-1} for co-feed experiments, similar to the reaction-aged catalysts without exposure to a co-feed.[4] As observed in Chapter 3, the reaction-aged K/bulk-MoS_2 catalysts did not exhibit measurable porosity.[4] There is no measurable difference in the textural properties in the reaction-aged catalysts after co-feed exposure compared to those with only syngas hydrogenation exposure.

4.3.2 Carbon Balance

The carbon distributions shown in terms of productivity in units of moles of C per gram of Mo per hour quantified from the GC data for the MoKMMO catalyst for ethanol, and 10% $^{13}C_2$-ethanol co-feeds (Figure 4.B.8 in Appendix 4.B) and for ethylene, and 10% $^{13}C_2$-ethylene (Figure 4.B.9) co-feeds are within 20% of closure. The K/bulk-MoS_2 catalyst showed deviations within 10% of closure for 10% $^{13}C_2$-ethylene co-feed (Figure 4.B.10). Deviations in the carbon balance are likely attributed to the non-real-time

determination of the inlet co-feed, as explained in Appendix 4.B, and deviations of ~5% of the internal standard (N_2) during reaction.

4.3.3 $^{13}C_2$-Ethanol co-feed

The major product distribution quantified from the GC data for the ethanol (EtOH), and 10% $^{13}C_2$-ethanol ($^{13}C_2$-EtOH) co-feed for the MoKMMO catalyst is shown in Figure 4.B.1.The ethanol and $^{13}C_2$-EtOH co-feed strongly perturbed the product distribution toward C_3-C_4 alcohols from C_2-C_3 alcohols over the MoKMMO catalyst, similar to what has been previously observed with ethanol co-feed.[4] It was previously hypothesized that CO insertion is likely the predominant pathway to higher alcohols (Figure 4.1), as the chain growth probability decreased with increasing carbon chain length. It was also hypothesized that 1-propanol formation likely occurs through CO insertion into an ethyl species (C_2H_5*) (derived from co-fed ethanol) to form a propionyl species (C_2H_5CO*) that can be hydrogenated to form 1-propanol. Similarly, 1-butanol was hypothesized to be formed via hydrogenation of butanoyl species (C_3H_7CO*) after CO insertion into a propyl intermediate.

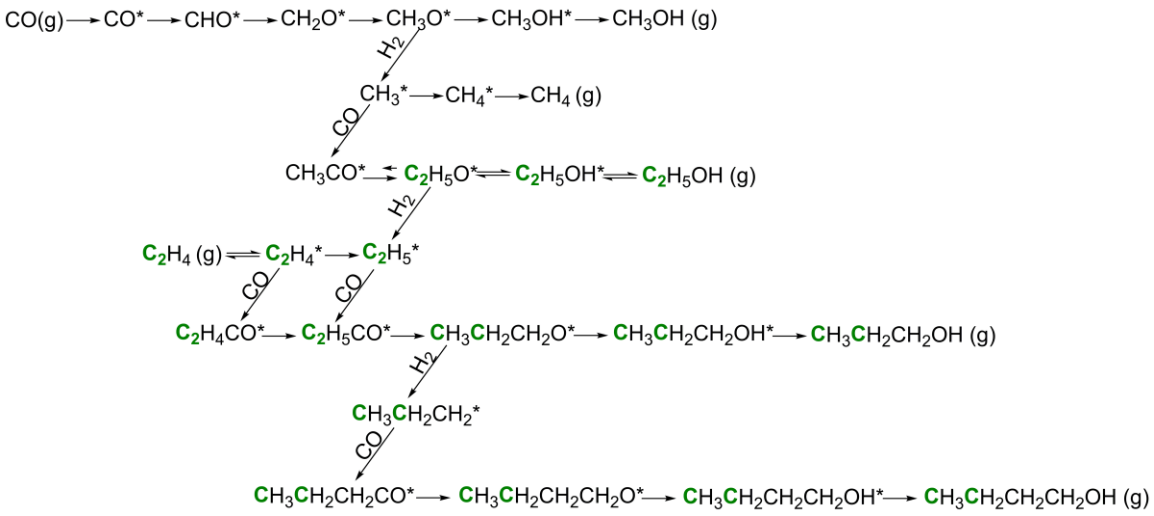

Figure 4.1: Proposed CO insertion reaction mechanism over unsupported and MMO supported K/bulk-MoS_2 catalysts. ^{13}C enriched carbons as a result of $^{13}C_2$-ethanol and $^{13}C_2$-ethylene co-feeds are labeled in green.

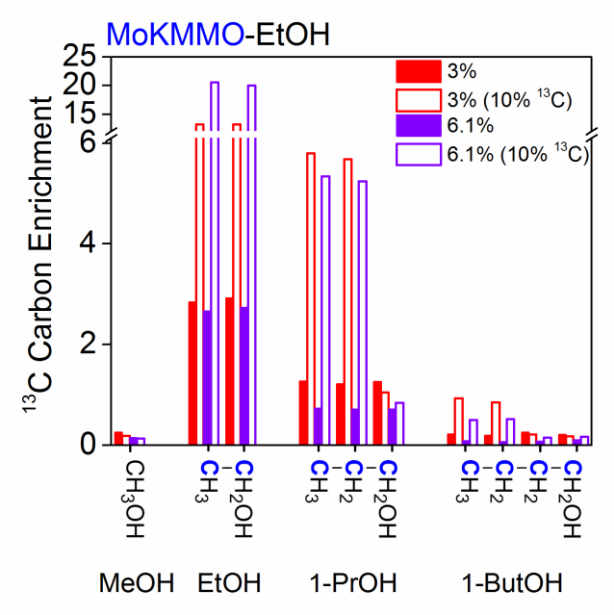

Figure 4.2: ^{13}C carbon enrichment of C_1-C_4 alcohols over the MoKMMO catalyst for EtOH (solid boxes) and $^{13}C_2$-EtOH (open boxes). Doublets are labeled in blue.

Figure 4.2 shows the ^{13}C carbon enrichment of major products for the $^{13}C_2$-EtOH co-feed. A carbon was determined to be enriched as a result of the $^{13}C_2$-EtOH co-feed (open boxes) if the enrichment factor was greater than that of the unlabeled ethanol co-feed (solid boxes). An example of ^{13}C carbon enrichment of 1-propanol over the MoKMMO catalyst for $^{13}C_2$-EtOH can be observed in Fig 4.C.1 in Appendix 4.C. All the carbons in 1-propanol include a center peak attributed to unlabeled 1-propanol, and a doublet attributed to J coupling with the adjacent labeled carbon. Note that the C_1 in 1-propanol is not enriched (Figure 4.2), and that the doublet observed for this carbon (C_1) is attributed to the significantly enriched adjacent C_2 carbon. For ^{13}C-NMR analysis, the methanol peak area was normalized to one, as a means to account for experimental error between unlabeled and labeled experiments, since methanol productivity is not influenced by ethanol nor ethylene co-feeds. The addition of the center peak and doublet areas normalized by the area of THF represents the ^{13}C carbon enrichment in Figure 4.2. It is important to note that only singlets (corresponding to the center peak in labeled

co-feed experiments) were observed for unlabeled co-feed experiments attributed to the natural ^{13}C abundance.

As expected, both carbons in ethanol were significantly enriched (also observed with GC-MS in Figure 4.D.1 in Appendix 4.D) when 10% $^{13}C_2$-EtOH was co-fed, as only ~56-67% of the ethanol is converted to higher chain products (Table 4.B.1). It is evident in Figure 4.2 that preferential enrichment of the terminal carbons of the C_3-C_4 alcohols occurred. This is further supported by MS analysis, where $^{13}C_2$-1-PrOH and $^{13}C_2$-1-ButOH where observed (Appendix 4.D). The MS spectrum of 1-PrOH for $^{13}C_2$-EtOH co-feed shows no ^{13}C enrichment of the C_1 carbon fragment ($[^{13}CH_3OH]^+$ with m/z=32) when compared to the unlabeled EtOH co-feed, further suggesting that the terminal carbon is not enriched (Figure 4.D.2). The terminal carbons in 1-butanol are preferentially enriched, suggesting that 1-butanol formation primarily occurs through CO insertion into a propyl intermediate (derived from a propoxy intermediate in the route to 1-propanol, as shown in Figure 4.1). These results elucidate that the findings by Santiesteban et al.,[7] suggesting that CO insertion is the primary pathway for higher alcohol synthesis over unsupported K_2CO_3/Co/MoS_2, extend to supported catalysts (i.e. MoKMMO). Specifically, 1-propanol and 1-butanol formation over the MoKMMO catalyst primarily proceeds through CO insertion into an alkyl intermediate to form an acyl precursor that can be hydrogenated to produce the corresponding alcohol (Figure 4.1).

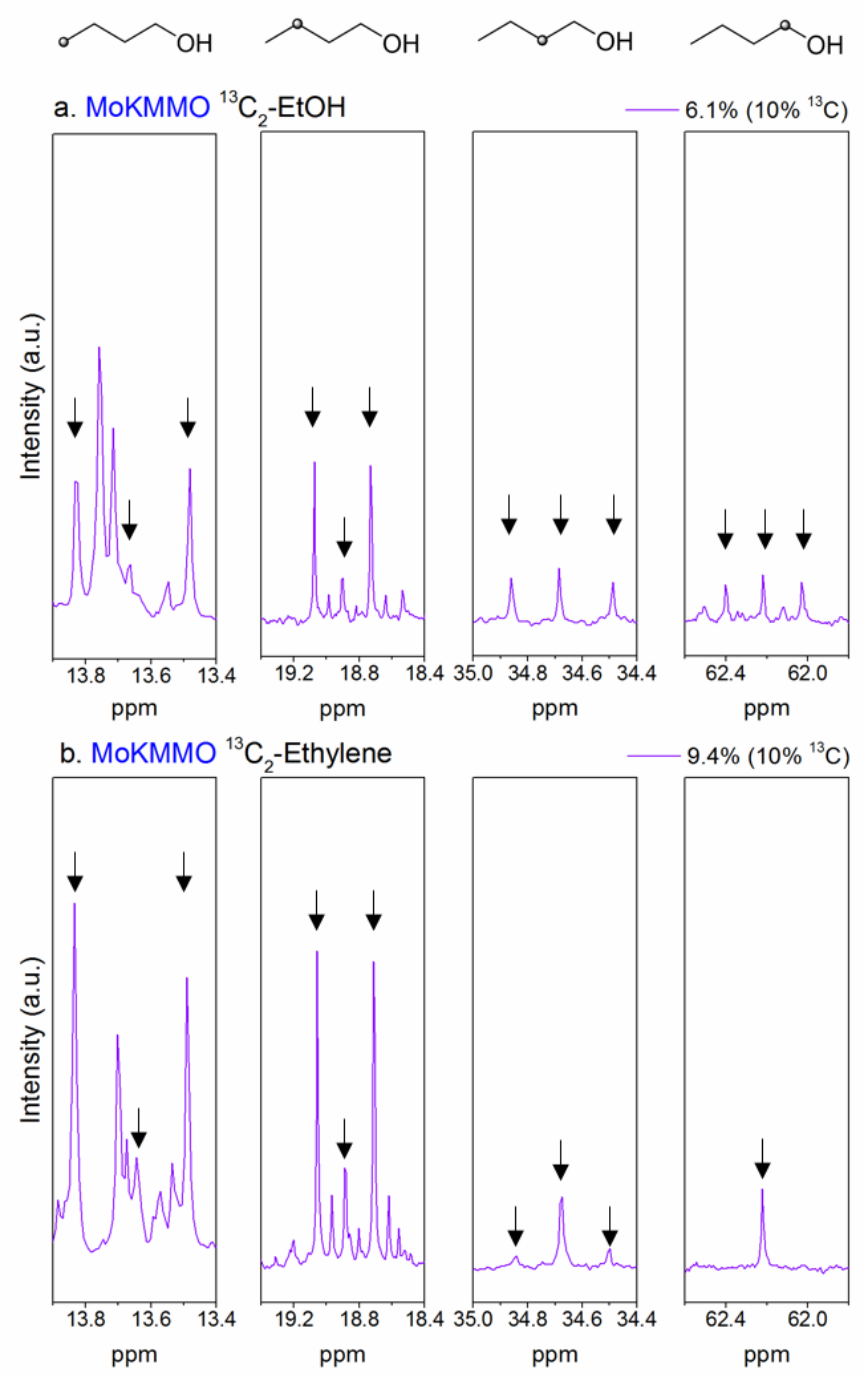

Figure 4.3: ^{13}C-NMR spectra for 1-ButOH over the MoKMMO catalyst for 6.1% $^{13}C_2$-EtOH (a) and 7.1% $^{13}C_2$-ethylene (b) co-feed experiments. Arrows denote the peaks assigned to 1-ButOH. Intensity scale is consistent across all graphs. Note: the other peaks present in the C_3 and C_4 graphs do not correspond to 1-butanol.

Even though the C_1 and C_2 ^{13}C carbon enrichment is subtle with increasing $^{13}C_2$-EtOH co-feed over the MoKMMO catalyst compared to the unlabeled ethanol co-feeds (Figure 4.2), the peaks in the NMR spectrum provide compelling evidence that $^{13}C_4$-1-butanol species, indicative of ethanol self-coupling, are present in experiments with the $^{13}C_2$-EtOH co-feed. A doublet is observed for the C_1 in 1-butanol for the $^{13}C_2$-EtOH co-feeds (Figure 4.3) in addition to the center peak attributed to unlabeled 1-butanol, indicating that the C_2 in 1-butanol is labeled. This is different from the 1-butanol ^{13}C-NMR spectrum with the 10% $^{13}C_2$-ethylene ($^{13}C_2$-ethylene) co-feed (discussed below), where no doublet could be observed for the C_1 in 1-butanol (in addition to the center peak attributed to unlabeled 1-butanol), indicating that the C_2 is not enriched. Therefore, the doublet observed for the C_2 for 1-butanol for $^{13}C_2$-ethylene co-feed experiments is attributed to J coupling with the significantly enriched C_3 in 1-butanol. The doublet observed for the C_2 in 1-butanol for the $^{13}C_2$-EtOH co-feed suggests that the adjacent C_1 or C_3 in 1-butanol are enriched. The MS spectrum of 1-butanol for the $^{13}C_2$-EtOH co-feed, shown in Figure 4.D.3, provides evidence that the C_1 in 1-butanol is enriched, as enrichment of the $[^{13}CH_3OH]^+$ fragment with *m/z*=32 was observed compared to the unlabeled EtOH co-feed (not observed with $^{13}C_2$-ethylene co-feed). The doublet observed for C_3 and C_4 and the ^{13}C enrichment in Figure 4.2 provide evidence that both C_3 and C_4 are labeled and preferentially enriched, as explained above.

In addition, Figure 4.C.2 shows that the ratio of doublet to the center peak increases for both C_1 and C_2 in 1-butanol for $^{13}C_2$-EtOH with increasing co-feeds, indicated by an increase in coupling between $^{13}C_1$ and $^{13}C_2$. The combination of these results elucidate the presence of $^{13}C_4$-1-butanol molecules with the $^{13}C_2$-EtOH co-feed, suggesting that ethanol or ethanol-derived species self-coupling to 1-butanol occurs, particularly with increasing $^{13}C_2$-EtOH co-feed. However, the preferential enrichment of the terminal carbons in 1-butanol indicates that ethanol or ethanol derived species self-coupling to 1-

butanol proceeds to a smaller extent as a secondary pathway compared to CO insertion over the MoKMMO catalyst. The work of Christensen et al. on K/$CoMoS_2$ and Santos et al. on K/MoS_2 catalysts previously suggested that higher alcohol formation proceeded not only through CO insertion, but also via aldol condensation of ethanol to 1-butanol with ethanol and nitrogen (syngas-free) co-feed experiments.[8, 9] The caveat of a syngas-free ethanol reaction is that it may facilitate the ethanol self-coupling reaction due to the presence of a nitrogen atmosphere that may not occur otherwise in a syngas atmosphere.[10] This observation highlights the importance of this work as the first study to conclusively show evidence for ethanol self-coupling to form $^{13}C_4$-1-butanol species in a syngas atmosphere over a K/MoS_2 based catalyst.

The product distribution of other oxygenates quantified from the GC data for the EtOH, and $^{13}C_2$-EtOH co-feed for the MoKMMO catalyst is shown in Figure 4.B.2. The MoKMMO catalyst shows a variety of important products, as observed before.[4] Ethyl acetate and ethyl propionate formation increases with increasing EtOH/$^{13}C_2$-EtOH co-feed, suggesting that ethanol is a precursor to these species.[4] Similarly, propyl propionate and propyl acetate increase with increasing EtOH/$^{13}C_2$-EtOH, likely a result of increasing 1-propanol formation, as 1-propanol is likely the precursor of these species.

Figure 4.4 shows the ^{13}C carbon enrichment of minor products for the $^{13}C_2$-EtOH co-feed. It can be observed that the ethoxy group (C_2H_5O) is preferentially enriched for ethyl acetate, suggesting that the ethoxy species derived from ethanol reacts with an acetyl species (CH_3CO) (not enriched at 3% $^{13}C_2$-EtOH). Similarly, the terminal carbons in the propoxy group (C_3H_7O) of propyl acetate are preferentially enriched, indicating that a propoxy intermediate (formed in the route to 1-propanol) reacts with an acetyl species to form propyl acetate. This is in agreement with the study by Santiesteban et al., where they observed that the methyl group of methyl acetate was preferentially enriched with a ^{13}C-MeOH co-feed experiment, suggesting that methanol is a building block for methyl

acetate, formed via an acetyl intermediate reacting with a methoxy anion.[7] With increasing $^{13}C_2$-EtOH co-feed (6.1% ^{13}C), the methyl carbon (CH_3) in the acetyl group (CH_3CO) of ethyl acetate becomes slightly enriched relative to the ^{13}C carbon enrichment of the propoxy group. No significant enrichment in the methyl carbon in the acetyl group of propyl acetate can be observed, as the increase in formation of ethyl acetate is significantly higher (~40%) than that of propyl acetate with increasing $^{13}C_2$-ethanol co-feed. Since the enrichment of the acetyl group is only apparent in ethyl acetate with abundant (6.1%) $^{13}C_2$-EtOH in the syngas feed, it can be concluded that hydrogenation of an acetyl species (CH_3CO^*) to the ethoxy intermediate ($C_2H_5O^*$) is largely irreversible under the conditions employed (Figure 4.1).

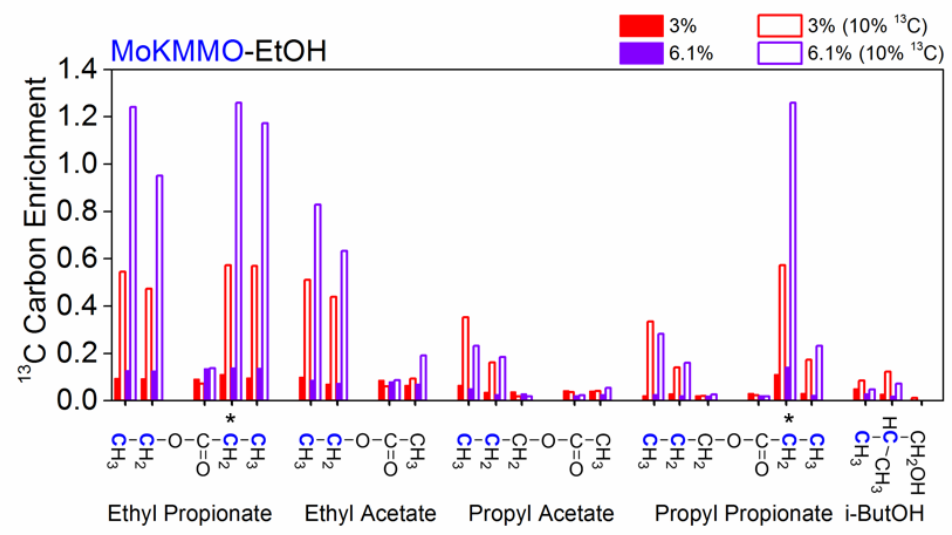

Figure 4.4: ^{13}C carbon enrichment of C_{2+} oxygenates over the MoKMMO catalyst for EtOH (solid boxes) and $^{13}C_2$-EtOH (open boxes) co-feed experiments. Doublets are labeled in blue.
Note that the methyl groups in isobutyl alcohol in ^{13}C-NMR are indistinguishable. The carbons denoted with an * have overlapping peaks for the open and solid boxes. For the carbons denoted with an *, the total peak area was attributed to both carbons. Therefore, the ^{13}C carbon enrinchment may be an overstimate, but does not significantly affect the results.

It was previously hypothesized that ethyl propionate is formed via esterification of propionate (produced in the route to 1-propanol) with the co-fed ethanol.[4] Figure 4.4 shows that both ethyl groups of ethyl propionate are preferentially enriched. Similarly, the terminal carbons in the propionate species and the propyl group are enriched in propyl propionate, suggesting that propyl propionate is formed via esterification of propionate with 1-propanol. These results elucidate that propionate species are formed via esterification of propionate with the corresponding alcohol. Additionally, it was hypothesized that the increase in 2-methyl-1-propanol formation observed over the MoKMMO catalyst with increasing ethanol co-feed was associated with the increase of 1-propanol derived species that coupled with methanol.[4] Even though it is not conclusive which of the methyl groups of 2-methyl-1-propanol is enriched, it can be concluded that only one of the methyl groups is labeled, as only a doublet is observed for the C_2 carbon in isobutyl alcohol (in addition to the center peak attributed to unlabeled isobutyl alcohol). Therefore, the preferential enrichment of terminal carbons of 2-methyl-1-propanol over the MoKMMO catalyst with $^{13}C_2$-EtOH indicates that 1-propanol is coupled with methanol to form isobutyl alcohol.

4.3.4 $^{13}C_2$-Ethylene co-feed

The major product distribution quantified from the GC data for the ethylene and $^{13}C_2$-ethylene co-feed for the MoKMMO catalyst is shown in Figure 4.B.3. Similar to the $^{13}C_2$-EtOH co-feed, the $^{13}C_2$-ethylene co-feed shifted the the product distribution toward C_3-C_4 alcohols from C_2-C_3 alcohols over the MoKMMO catalyst, as previously observed.[4] It was hypothesized that alcohol formation from ethanol co-feeds proceeds through the same intermediate as olefin carbonylation, as similar C_{3+}OH formation rates were observed for ethanol and ethylene co-feed experiments when the major products were normalized by mol C of co-feed (Figure 4.B.5).[4] This hypothesis was supported by the

work of Santiesteban et al. on a K_2CO_3/Co/MoS_2 catalyst, where they observed 1-propanol containing ^{13}C in two alternative positions ($^{13}CH_3CH_2CH_2OH$ and $CH_3{}^{13}CH_2CH_2OH$, but not $^{13}CH_3{}^{13}CH_2CH_2OH$) with a $^{13}CH_3OH$ co-feed suggesting that CO insertion could occur on symmetric ethylene species.[7]

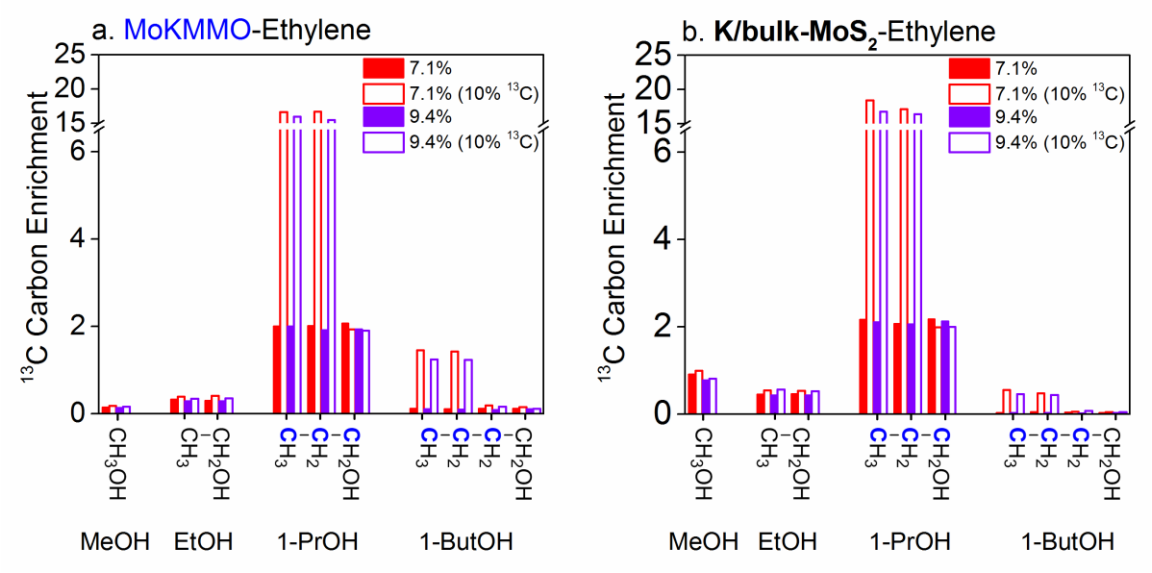

Figure 4.5: ^{13}C carbon enrichment of C_1-C_4 alcohols over the MoKMMO (a) and K/bulk-MoS_2 (b) catalysts for ethylene (solid boxes), and $^{13}C_2$-ethylene (open boxes) co-feed experiments. Doublets are labeled in blue.

Similar to the $^{13}C_2$-EtOH experiments, it is evident in Figure 4.5a that preferential enrichment of the terminal carbons of the C_3-C_4 alcohols occurred over the MoKMMO catalyst with $^{13}C_2$-ethylene co-feed experiments. This is further supported by MS analysis, where $^{13}C_2$-1-PrOH and $^{13}C_2$-1-ButOH were observed (Appendix 4.D). Figure 4.D.4 shows peaks for $[^{13}C_2\text{-M}]^{+\bullet}$ with *m/z*=62 for doubly label 1-PrOH, and its corresponding $[^{13}C_2\text{-M-H}]^+$ with *m/z*= 61. Even though no $[^{13}C_2\text{-M}]^{+\bullet}$ with *m/z*=76 was present for 1-butanol (Figure 4.D.5), the peak at m/z=58 attributed to $[^{13}C_2\text{-M-}H_2O]^+$ indicates the presence of doubly labeled 1-butanol. Note that this peak is only present in the $^{13}C_2$-ethylene co-feed experiment (not in the unlabeled ethylene co-feed). It can

therefore be concluded that alcohol formation from ethanol proceeds via the same acyl intermediate as olefin carbonylation over the MoKMMO catalyst. It is important to note that the C_1 in 1-propanol and C_2 in 1-butanol are not enriched (Figure 4.5) and the doublets observed for these carbons are attributed to J coupling with the significantly enriched C_2 carbon in 1-propanol and C_3 in 1-butanol, respectively.

It has been previously observed that an ethylene co-feed significantly enhances the 1-propanol formation over the K/bulk-MoS_2 catalyst, unlike an ethanol co-feed, which was largely unreactive.[4] However, the ethylene co-feed over the K/bulk-MoS_2 catalyst does not influence the product distribution to $C_{3+}OH$ as significantly as over the MoKMMO catalyst (Figure 4.B.5, and Figure 4.B.6), supported by significantly lower ethylene conversion (50-58%) over the K/bulk-MoS_2 catalyst compared to 100% ethylene conversion over the MoKMMO catalyst, as shown in Table 4.B.1. Similar to the MoKMMO catalyst, preferential enrichment of the terminal carbons of the C_3-C_4 alcohols over the K/bulk-MoS_2 catalyst was observed with $^{13}C_2$-ethylene co-feed experiments (Figure 4.5b). As discussed above, the doublet observed for the C_1 in 1-propanol and C_2 in 1-butanol is attributed to J coupling with the significantly enriched C_2 in 1-propanol and C_3 in 1-butanol, respectively. Relatively lower ^{13}C enrichment of the terminal carbons in 1-butanol was observed over the K/bulk-MoS_2 catalyst compared to that of the MoKMMO catalyst, consistent with the hypothesis that ethylene has the propensity to more favorably adsorb on smaller K/MoS_2 domains over the MoKMMO catalyst compared to large, multilayer K/MoS_2 domains over the K/bulk-MoS_2 catalyst.[4] Therefore, these observations provide support that intimate contact between K/MoS_2 domains and MMO has a synergistic effect in higher alcohol formation.

The distribution of other oxygenates quantified from the GC data for the ethylene, and $^{13}C_2$-ethylene co-feed over the MoKMMO catalyst is shown in Figure 4.B.4. As previously observed, propyl acetate and propyl propionate formation increases with

increasing ethylene/$^{13}C_2$-ethylene co-feed over the MoKMMO catalyst, suggesting that 1-propanol is a precursor to these species.[4] Similar to the $^{13}C_2$-EtOH co-feed over the MoKMMO catalyst, only the propoxy group in propyl acetate is preferentially enriched with $^{13}C_2$-ethylene (Figure 4.6a), providing further evidence that acetate species formation proceeds through the reaction of an alkoxy species and acetyl species (CH_3CO*). The propyl group and the terminal carbons in the propionate species are preferentially enriched in propyl propionate with $^{13}C_2$-ethylene, similar to $^{13}C_2$-EtOH. The terminal carbons of propanal can be observed to be enriched with $^{13}C_2$-ethylene over the MoKMMO catalyst (Figure 4.6a), as relatively more propanal is formed with ethylene co-feeds than ethanol co-feeds.[4] More apparent than with $^{13}C_2$-EtOH, the terminal carbons of 2-methyl-1-propanol were preferentially enriched with $^{13}C_2$-ethylene, indicating that the increased propanal formation, likely via ethylene hydroformylation, can likely undergo coupling with methanol to form isobutyl alcohol.

Although the productivity to other oxygenates is significantly smaller for the K/bulk-MoS_2 catalyst compared to the MoKMMO catalyst with ethylene co-feeds (Figure 4.B.3 and Figure 4.B.6), similar ^{13}C carbon enrichments in propanal, propyl acetate and propyl propionate were observed for both catalysts (Figure 4.6a and 4.6b). It is important to note that the K/bulk-MoS_2 catalyst does catalyze 1-propanol plus methanol coupling to isobutyl alcohol, as the terminal carbons of isobutyl alcohol were labeled with $^{13}C_2$-ethylene, similar to those over the MoKMMO catalyst. This suggests that the K/bulk-MoS_2 catalyst does contain the acid-base pairs necessary to catalyze isobutyl alcohol formation.

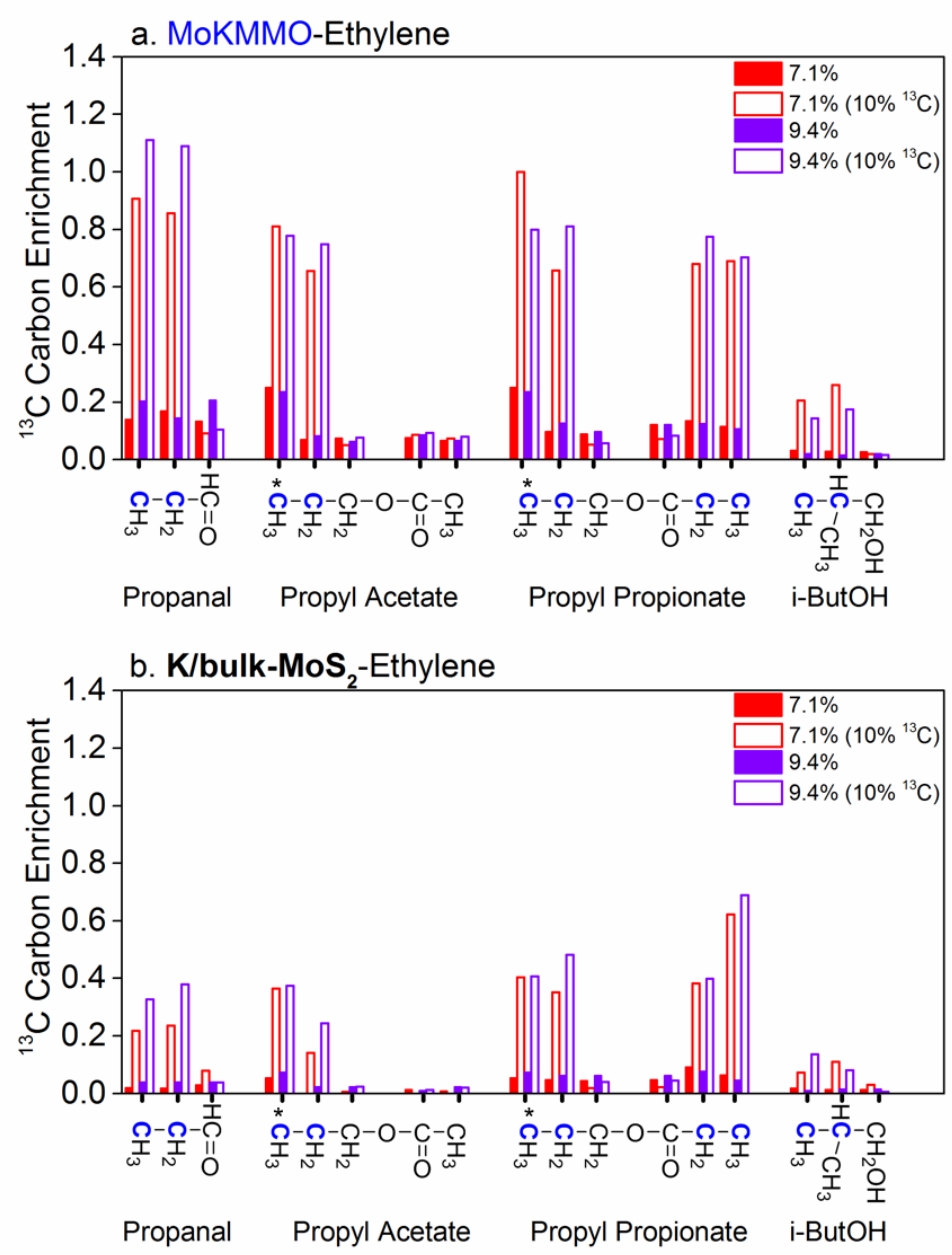

Figure 4.6: ^{13}C carbon enrichment of C_{2+} oxygenates over the MoKMMO (a) and K/bulk-MoS_2 (b) catalysts for ethylene (solid boxes) and $^{13}C_2$-ethylene (open boxes) co-feed experiments. Doublets are labeled in blue.
Note that the methyl groups in isobutyl alcohol in ^{13}C-NMR are indistinguishable. In plot (a) the carbons denoted with an * have overlapping peaks for the solid boxes. In plot (b) the carbons denoted with an * have overlapping peaks for the open and solid boxes. For the carbons denoted with an *, the total peak area was attributed to both carbons. Therefore, the ^{13}C carbon enrinchment may be an overstimate, but does not significantly affect the results.

4.3.4 Gas sample analysis for $^{13}C_2$-EtOH and $^{13}C_2$-ethylene co-feeds

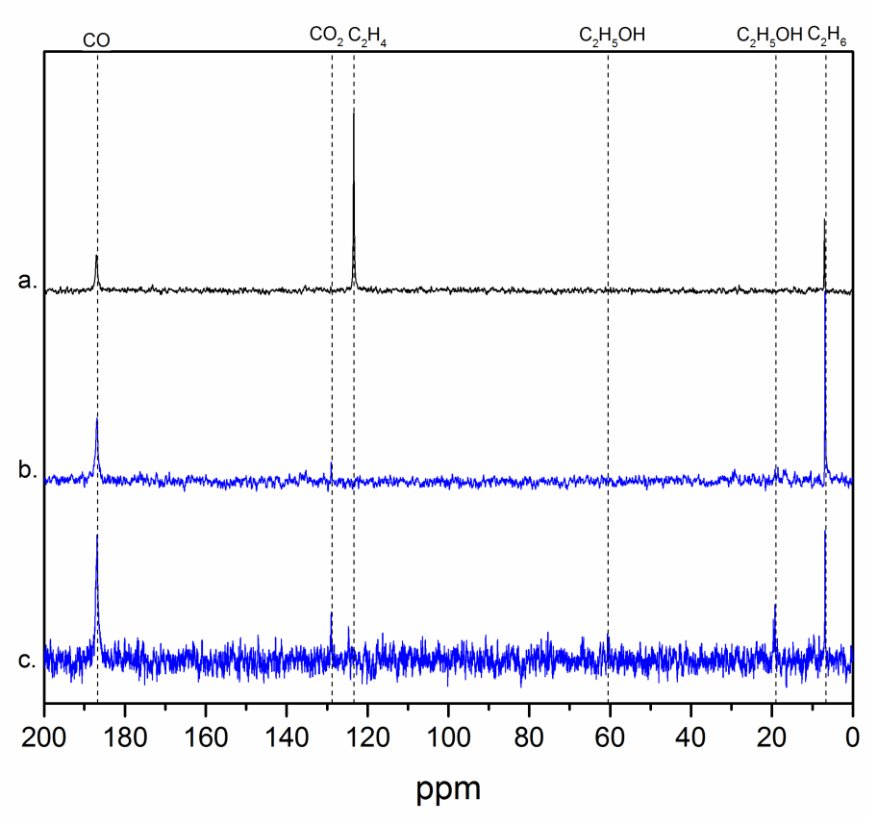

Figure 4.7: ^{13}C-NMR for gas samples pressurized to 80 psig in gas tight NMR tubes at 6.1% $^{13}C_2$-EtOH co-feed for the MoKMMO catalyst (a) and 9.4% $^{13}C_2$-ethylene co-feed for the MoKMMO (b) and K/bulk-MoS_2 catalyst (c). Note: no peaks were observed for the unlabeled co-feed experiments over these catalysts under identical reaction and ^{13}C-NMR conditions.

As previously observed, the co-fed ethylene more strongly enhanced the formation of ethane compared to the ethanol co-feed over the MoKMMO catalyst (Figure 4.B.5).[1] Consistent with the reaction productivity results, the ^{13}C-NMR spectrum for the gas sample for the $^{13}C_2$-ethylene co-feed over the MoKMMO catalyst showed a higher intensity singlet for C_2H_6 than the gas sample for $^{13}C_2$-EtOH co-feed (Figure 4.7). Similarly, a singlet is observed for C_2H_6 over the K/bulk-MoS_2 catalyst with $^{13}C_2$-ethylene co-feed. Even though it can be observed via ^{13}C-NMR that ethane is enriched over the MoKMMO and K/bulk-MoS_2 catalysts with $^{13}C_2$-EtOH and $^{13}C_2$-ethylene co-feed experiments, it cannot be determined whether singly and/or doubly labeled ethane

species are present. GC-MS was used to investigate this issue further. It was found that doubly labeled ethane is likely present in both $^{13}C_2$-EtOH and $^{13}C_2$-ethylene (Figure 4.D.8- 4.D.10), but it cannot be ruled out that singly labeled ethane is also present due to fragment analysis complexity (refer to Appendix 4.D for further discussion). However, the ^{13}C carbon enrichment observed for ethane, suggest that ethane formation occurred via an ethanol derived intermediate, suggesting that hydrocarbons are formed by secondary reactions involving alcohols, as previously hypothesized by Santiesteban et al. [7]

CO and CO_2 singlets were observed in the ^{13}C-NMR spectra of the MoKMMO catalyst with $^{13}C_2$-EtOH co-feed, while no peaks were observed for the unlabeled co-feed experiments over these catalysts under identical reaction and ^{13}C-NMR conditions, indicating the presence of ^{13}CO and $^{13}CO_2$. Additionally, $^{13}CH_4$ was observed with GC-MS analysis (not observed via ^{13}C-NMR) over the MoKMMO catalyst with $^{13}C_2$-EtOH (Figure 4.D.8). As discussed above, with increasing $^{13}C_2$-EtOH co-feed (6.1% ^{13}C), the methyl carbon (CH_3) in the acetyl group (CH_3CO) of ethyl acetate becomes slightly enriched, suggesting that the dehydrogenation of the ethoxy intermediate (C_2H_5O*) to an acetyl species (CH_3CO*) is reversible to a small extent. Therefore, it is likely that the step involving CO insertion to the acetyl species (CH_3CO*), shown in Figure 4.1, is also reversible, leading to the formation of ^{13}CO and $^{13}CH_4$, with $^{13}CH_4$ formed from an enriched methyl precursor ($^{13}CH_3$*). $^{13}CO_2$ is hypothesized to be formed over the MoKMMO catalyst through the water-gas shift (WGS) reaction, as K/MoS_2-based catalysts have a high WGS activity, which makes $^{13}CO_2$ an inevitable product.[11-13] With a $^{13}C_2$-ethylene co-feed the ^{13}CO and $^{13}CO_2$ singlet decreases in intensity over the MoKMMO catalyst compared to that of the $^{13}C_2$-EtOH co-feed. This observation indicates that the formation of ^{13}CO and $^{13}CH_4$ from $^{13}C_2$-ethylene is expected to occur to a lesser extent than with the $^{13}C_2$-EtOH co-feed, as the deoxygenation of the ethoxy species (C_2H_5O*) to form ethyl species (C_2H_5*) is likely largely irreversible in a reducing

syngas atmosphere. Consistently, negligible $^{13}CH_4$ is observed with GC-MS analysis over the MoKMMO catalyst with $^{13}C_2$-ethylene co-feed (Figure 4.D.9).

Less intense CO and CO_2 singlets were observed in the ^{13}C-NMR spectrum of the K/bulk-MoS_2 catalyst when compared with that of the MoKMMO catalyst for $^{13}C_2$-ethylene co-feeds, indicating that the formation of ^{13}CO and $^{13}CO_2$ with $^{13}C_2$-ethylene co-feeds is catalyst dependent, and; therefore, is unlikely to occur in the gas phase. It is thought that ethylene has the propensity to more favorably adsorb on smaller K/MoS_2 domains over the MoKMMO catalyst as compared to large, multilayer K/MoS_2 domains present in the K/bulk-MoS_2 catalyst, supporting the lower ^{13}CO and $^{13}CO_2$ formation over the K/bulk-MoS_2 catalyst.[4] Additionally, $^{13}CH_4$ is observed over the K/bulk-MoS_2 catalyst with a $^{13}C_2$-ethylene co-feed (Fig. S19), further supporting that ^{13}CO and $^{13}CH_4$ formation likely occurs via an enriched acetyl precursor ($^{13}CH_3CO$*).

Furthermore, it is important to note that the carbonyl groups of the acetate and propionate species were not enriched with $^{13}C_2$-EtOH nor $^{13}C_2$-ethylene co-feed over the MoKMMO catalyst, thus providing evidence that the carbonyl carbon for these species originated from syngas CO. Similarly, CO insertion of ^{13}CO originating from $^{13}C_2$-EtOH and $^{13}C_2$-ethylene likely occurs on a minor scale, as the C_1 carbon from 1-PrOH and 1-ButOH shows little to no enrichment with both ^{13}C-NMR and GC-MS analysis.

4.4. Conclusions

Syngas conversion to higher alcohols was studied over the known MoKMMO and K/bulk-MoS_2 catalysts using 10% $^{13}C_2$-ethanol and 10% $^{13}C_2$-ethylene co-feeds, as a means to elucidate the reaction pathways to higher alcohols. Analysis of the ^{13}C carbon enrichment via ^{13}C-NMR clearly showed that (i) preferential enrichment of terminal carbons in C_3-C_4 alcohols over the MoKMMO catalyst occurred, and (ii) $^{13}C_4$-1-butanol is observed during reaction over the MoKMMO catalyst with $^{13}C_2$-ethanol co-feed (not present with $^{13}C_2$-ethylene) providing conclusive evidence for ethanol self-coupling to 1-

butanol. It is concluded that higher alcohol formation over K/MoS_2 based catalysts primarily occurs through CO insertion, and the MMO support facilitates ethanol self-coupling to 1-butanol only to a small extent as a secondary pathway. Acetate species are formed via an acyl precursor reacting with an alkoxy anion, and propionate species are formed via esterification of propionate with the corresponding alcohol. $^{13}C_2$-ethanol co-feeds additionally showed that the hydrogenation of acetyl species (CH_3CO*) to ethoxy species is largely irreversible. It is also concluded that isobutyl alcohol formation observed over both the K/bulk-MoS_2 and the MoKMMO catalysts is via methanol coupling with 1-propanol or 1-propanol derived species. Formation of ^{13}CO and $^{13}CH_4$ over the MoKMMO and K/bulk-MoS_2 catalysts with $^{13}C_2$-ethylene co-feeds and over the MoKMMO catalyst with $^{13}C_2$-ethanol co-feed provides evidence that ^{13}CO and $^{13}CH_4$ formation likely occurs via an enriched acetyl precursor ($^{13}CH_3CO$*) derived from either a $^{13}C_2$-ethylene or $^{13}C_2$-ethanol.

4.5. References

(1) M. Taborga Claure, S.-H. Chai, S. Dai, K. A. Unocic, F. M. Alamgir, P. K. Agrawal and C. W. Jones, *J. Catal.*, 2015, **324**, 88-97.

(2) M. R. Morrill, N. T. Thao, P. K. Agrawal, C. W. Jones, R. J. Davis, H. Shou, D. G. Barton and D. Ferrari, *Catal. Lett.*, 2012, **142**, 875-881.

(3) M. R. Morrill, N. T. Thao, H. Shou, R. J. Davis, D. G. Barton, D. Ferrari, P. K. Agrawal and C. W. Jones, *ACS Catal.*, 2013, **3**, 1665-1675.

(4) M. Taborga Claure, M. R. Morrill, J. W. Goh, S.-H. Chai, S. Dai, P. K. Agrawal and C. W. Jones, *Catal. Sci. Technol.*, 2016, **6**, 1957-1966.

(5) D. Ferrari, G. Budroni, L. Bisson, N. J. Rane, B. D. Dickie, J. H. Kang and S. J. Rozeveld, *Appl. Catal., A*, 2013, **462-463**, 302-309.

(6) K. S. Liang, R. R. Chianelli, F. Z. Chien and S. C. Moss, *J. Non-Cryst. Solids*, 1986, **79**, 251-273.

(7) J. G. Santiesteban, C. E. Bogdan, R. G. Herman and K. Klier, *in: M.J. Philips, M. Ternan (Eds.), vol. 2, 9th Annual Congress on Catalysis, Chemical Institute of Canada, Calgary, 1988, pp. 561-568.*

(8) J. M. Christensen, P. A. Jensen, N. C. Schiødt and A. D. Jensen, *ChemCatChem*, 2010, **2**, 523-526.

(9) V. P. Santos, B. van der Linden, A. Chojecki, G. Budroni, S. Corthals, H. Shibata, G. R. Meima, F. Kapteijn, M. Makkee and J. Gascon, *ACS Catal.*, 2013, **3**, 1634-1637.

(10) V. S. Dorokhov, M. A. Kamorin, N. N. Rozhdestvenskaya and V. M. Kogan, *C. R. Chim.*, 2016, DOI: http://dx.doi.org/10.1016/j.crci.2015.11.018, . DOI: 10.1016/j.crci.2015.1011.0108.

(11) J. M. Christensen, P. A. Jensen and A. D. Jensen, *Ind. Eng. Chem. Res.*, 2011, **50**, 7949-7963.

(12) L. Gang, Z. Chengfang, C. Yanqing, Z. Zhibin, N. Yianhui, C. Linjun and Y. Fong, *Appl. Catal., A*, 1997, **150**, 243-252.

(13) G. J. Quarderer, R. R. Stevens, G. A. Cochran and C. B. Murchison, *US Patent 4825013 A, to The Dow Chemical Company, 1989.*

APPENDIX 4.A

K/MOS_2 CATALYSTS CHARACTERIZATION

This appendix includes the supporting characterization of the reaction-aged K/MoS_2 catalysts studied in this Chapter via N_2 physisorption and X-ray Diffraction (XRD).

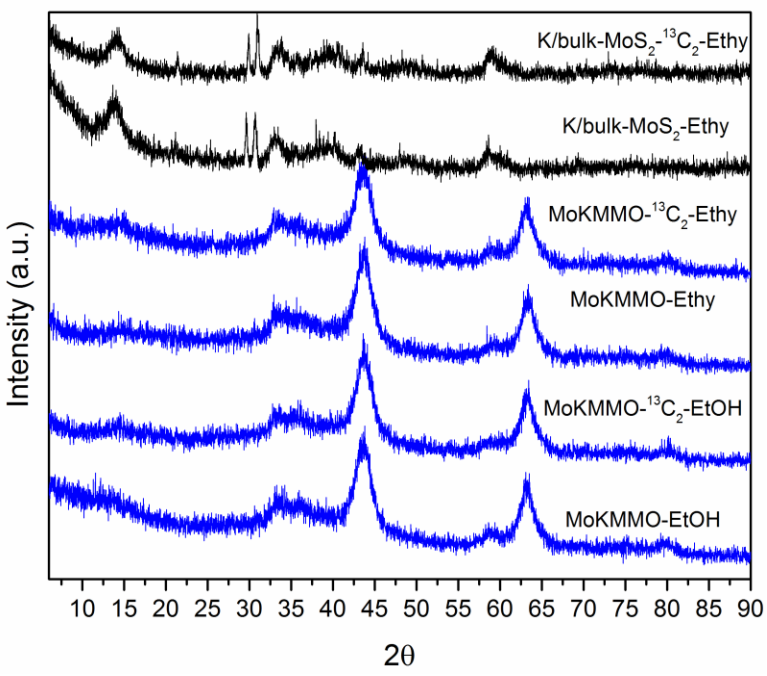

Figure 4.A.1: XRD patterns of the reaction-aged K/bulk-MoS_2 (black) and MoKMMO (blue) catalysts for ethanol, ethylene, $^{13}C_2$-ethanol, $^{13}C_2$-ethylene co-feed experiments.

Table 4.A.1: Brunauer-Emett-Teller (BET) surface areas for the reaction-aged MoKMMO catalyst.

	Co-feed	BET Surface area (m^2/g)
MoKMMO	EtOH	63
MoKMMO	$^{13}C_2$-EtOH	57
MoKMMO	Ethylene	48
MoKMMO	$^{13}C_2$-Ethylene	63

APPENDIX 4.B

K/MoS_2 CATALYSTS REACTIVITY DATA

This appendix includes the supporting reactivity data of the K/MoS_2 catalysts discussed in this Chapter.

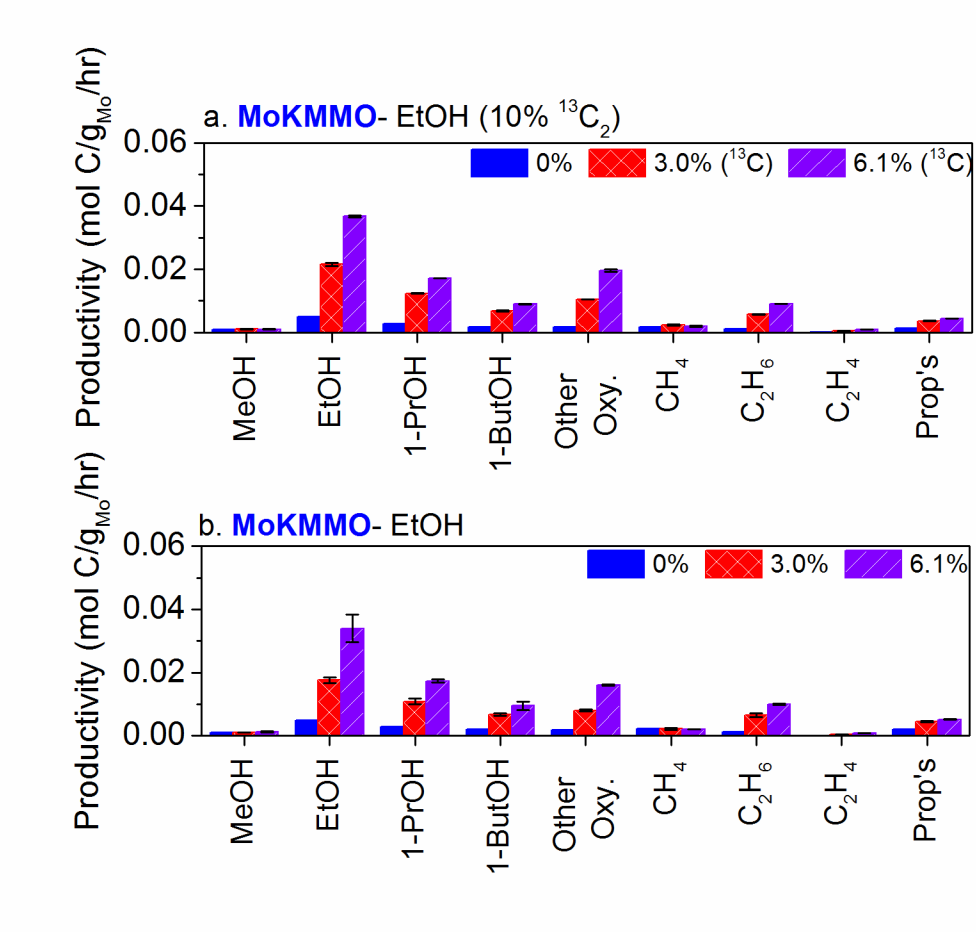

Figure 4.B.1: Major products for $^{13}C_2$-ethanol (a) and ethanol (b) co-feed experiments for the MoKMMO catalyst. The error bars indicate the standard deviation between the productivity before and after collection of liquid products. Reaction conditions: 310 ºC and 1500 psig.

Note: The productivity term for ethanol during co-feed experiments accounts for both unreacted co-feed and the amount of ethanol produced by the catalyst during reaction.

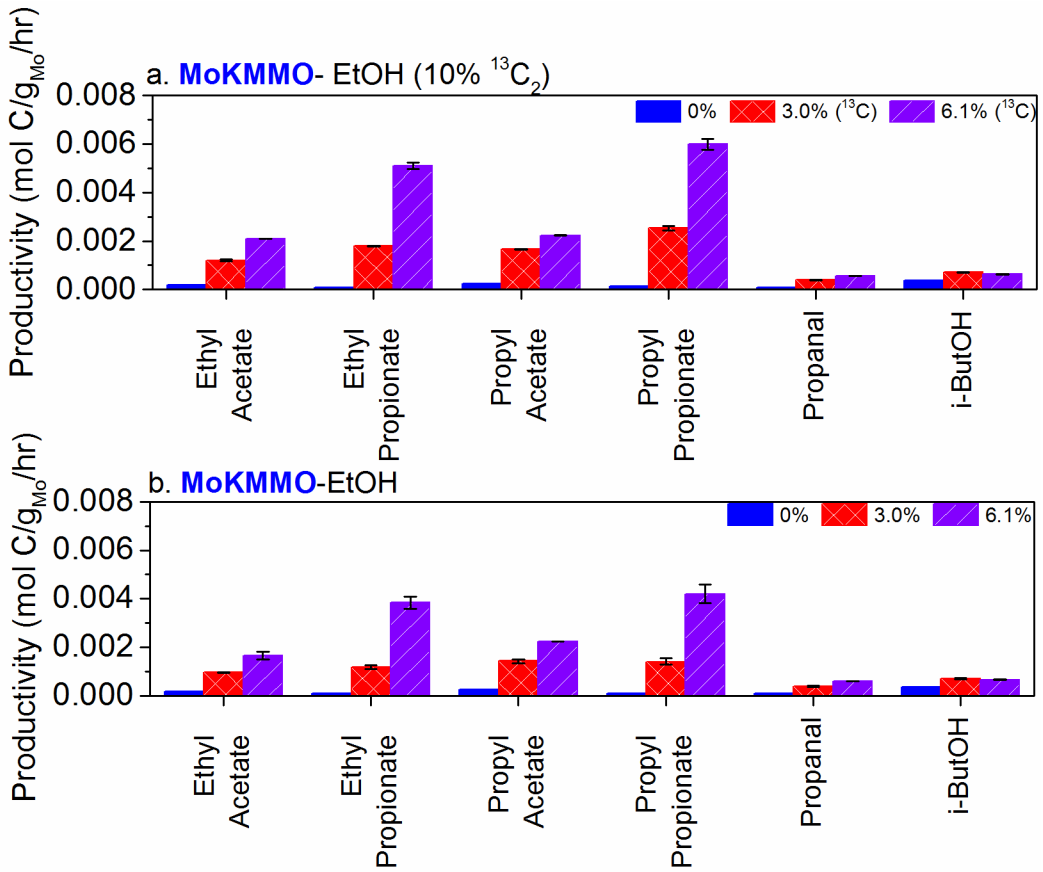

Figure 4.B.2: Minor products for $^{13}C_2$-ethanol (a) and ethanol (b) co-feed experiments for the MoKMMO catalyst. The error bars indicate the standard deviation between the productivity before and after collection of liquid products. Reaction conditions: 310 ºC and 1500 psig.

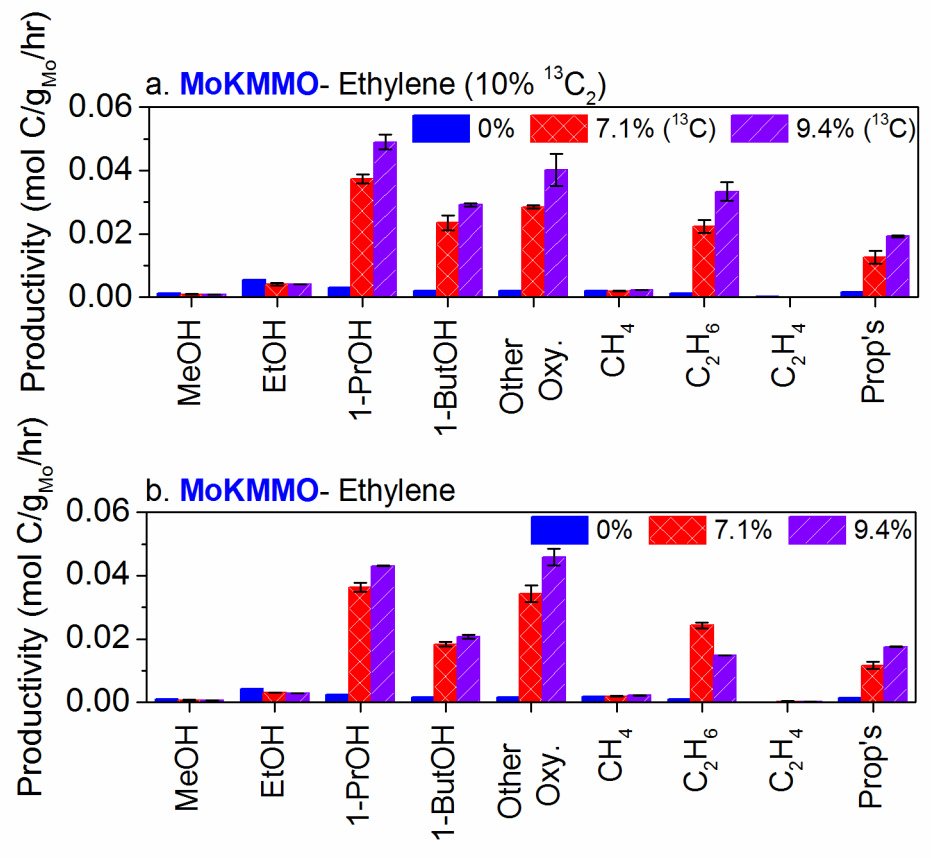

Figure 4.B.3: Major products for $^{13}C_2$-ethylene (a) and ethylene (b) co-feed experiments for the MoKMMO catalyst. The error bars indicate the standard deviation between the productivity before and after collection of liquid products. Reaction conditions: 310 ºC and 1500 psig.

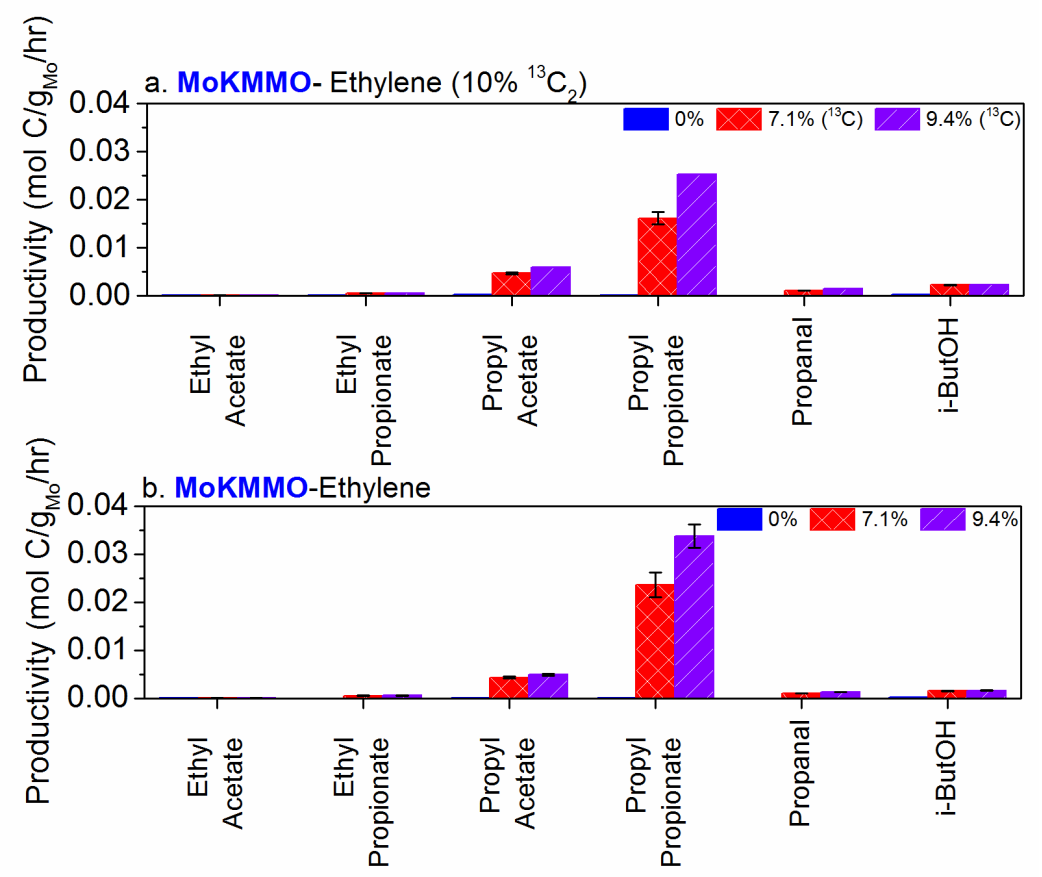

Figure 4.B.4: Minor products for $^{13}C_2$-ethylene (a) and ethylene (b) co-feed experiments for the MoKMMO catalyst. The error bars indicate the standard deviation between the productivity before and after collection of liquid products. Reaction conditions: 310 ºC and 1500 psig.

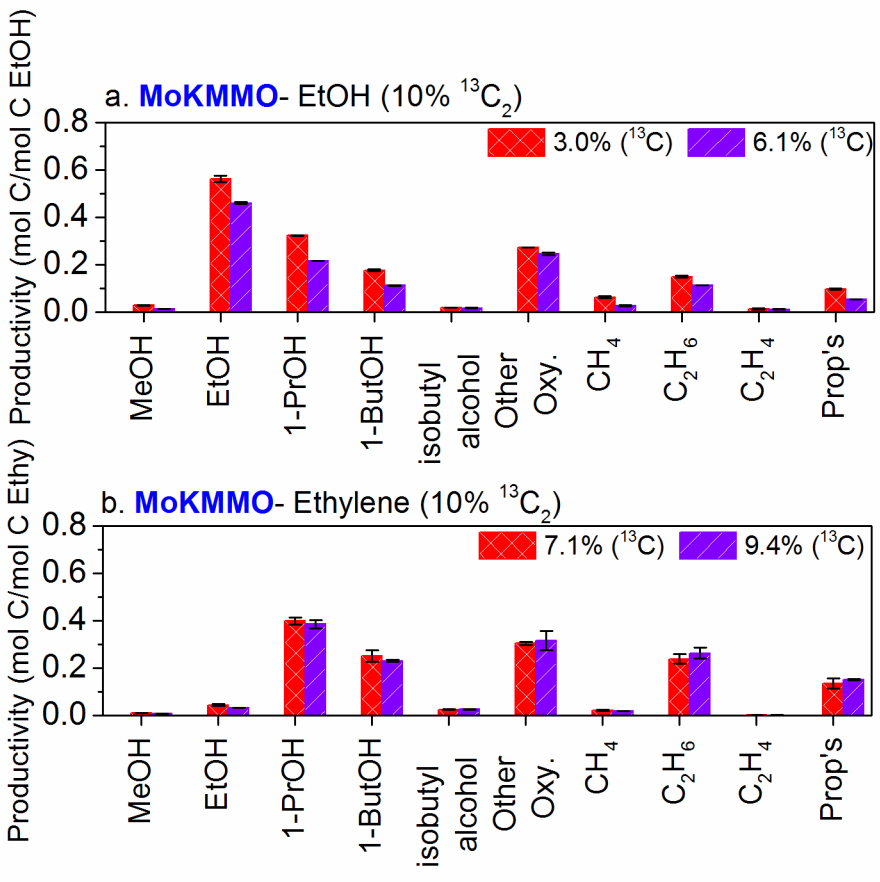

Figure 4.B.5: Normalized major products by co-feed mol of carbon for $^{13}C_2$-ethanol (a) and $^{3}C_2$-ethylene (b) co-feed experiments for the MoKMMO catalyst. The error bars indicate the standard deviation between the productivity before and after collection of liquid products. Reaction conditions: 310 ºC and 1500 psig.

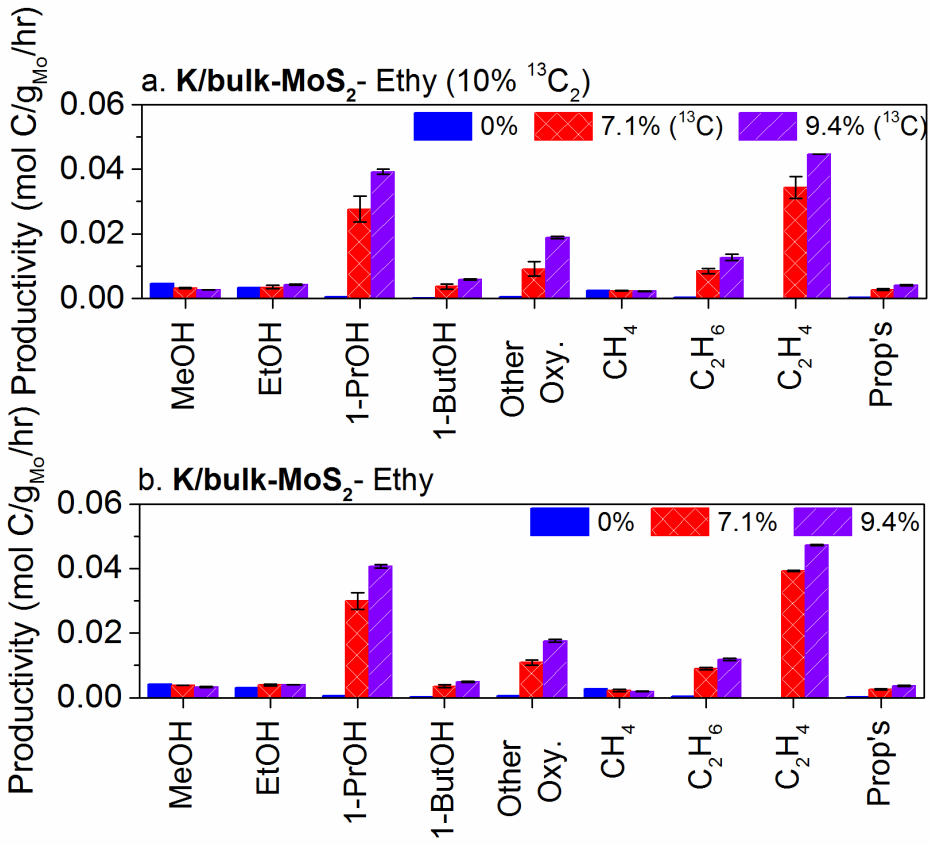

Figure 4.B.6: Major products for $^{13}C_2$-ethylene (a) and ethylene (b) co-feed experiments for the K/bulk-MoS_2 catalyst. The error bars indicate the standard deviation between the productivity before and after collection of liquid products. Reaction conditions: 310 ºC and 1500 psig.

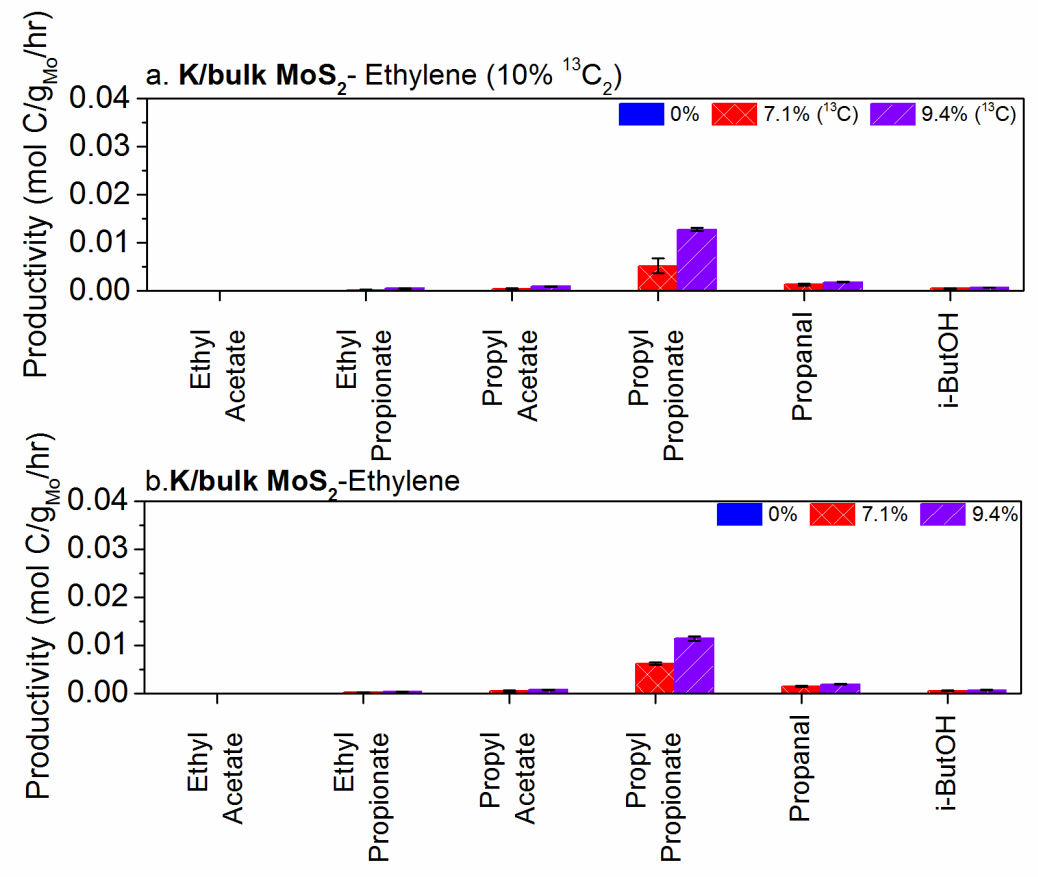

Figure 4.B.7: Minor products for $^{13}C_2$-ethylene (a) and ethylene (b) co-feed experiments for the K/bulk-MoS_2 catalyst. The error bars indicate the standard deviation between the productivity before and after collection of liquid products. Reaction conditions: 310 ºC and 1500 psig.

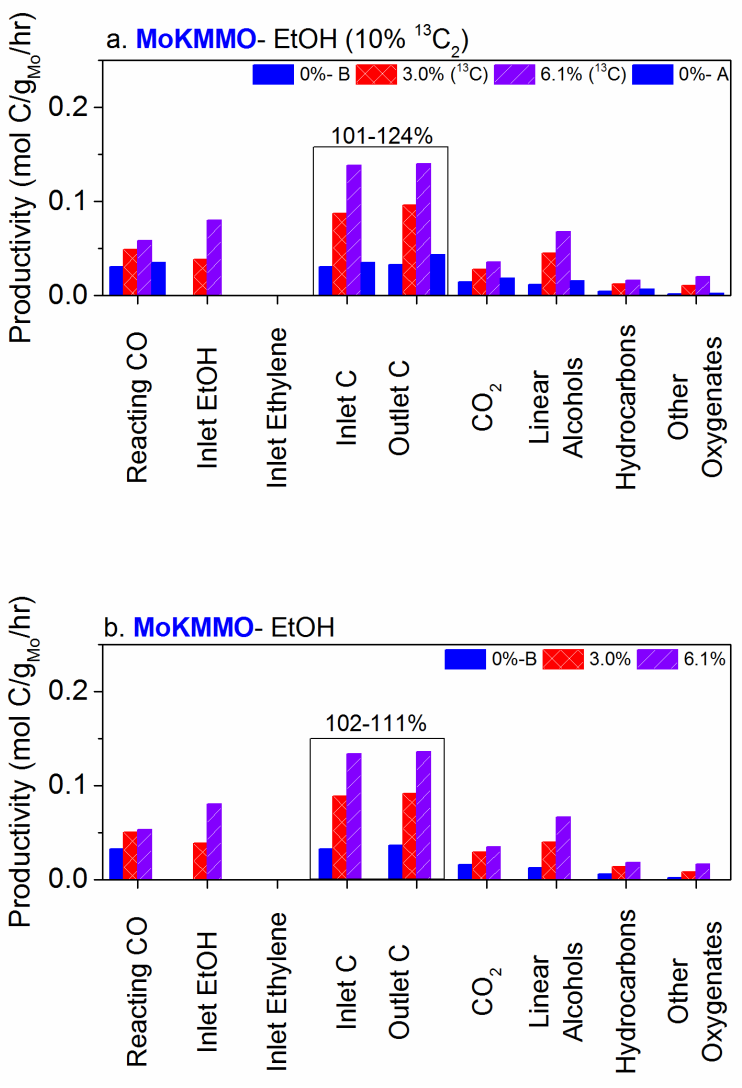

Figure 4.B.8: Carbon balance for $^{13}C_2$-ethanol (a) and ethanol (b) co-feed experiments for the MoKMMO catalyst. Reaction conditions: 310 ºC and 1500 psig. Note: 0%-B, 0%-A attributes to the product distribution before and after co-feed.

Inlet and outlet carbon distributions are shown in terms of productivity in units of moles of carbon per gram of Mo per hour. The inlet carbon consists of reacting CO productivity (determined from N_2 as the internal standard), and inlet co-feed "productivity" (ethanol, 10% $^{13}C_2$-ethanol, ethylene, 10% $^{13}C_2$-ethylene) estimated from blank reactions with SiC at similar reaction conditions. Unreacted CO was omitted from the carbon balance, as these reactions are run at fairly low conversions (~8%). The inlet co-feed "productivity" may therefore be relatively imprecise, as explained in a previous

study.[1] Outlet carbon was quantified from GC data. Linear alcohols include C_1-C_6 linear alcohols. Hydrocarbons include methane, ethane, ethylene and propane/propylene. C_{4+}HC were not included in the carbon balance or product distributions as these products cannot be accurately quantified in the system.[1] The closer the magnitude of the inlet C and outlet C in the carbon balance graphs (the closer the balance is to 100%), the more accurate the depiction of the product distribution is.

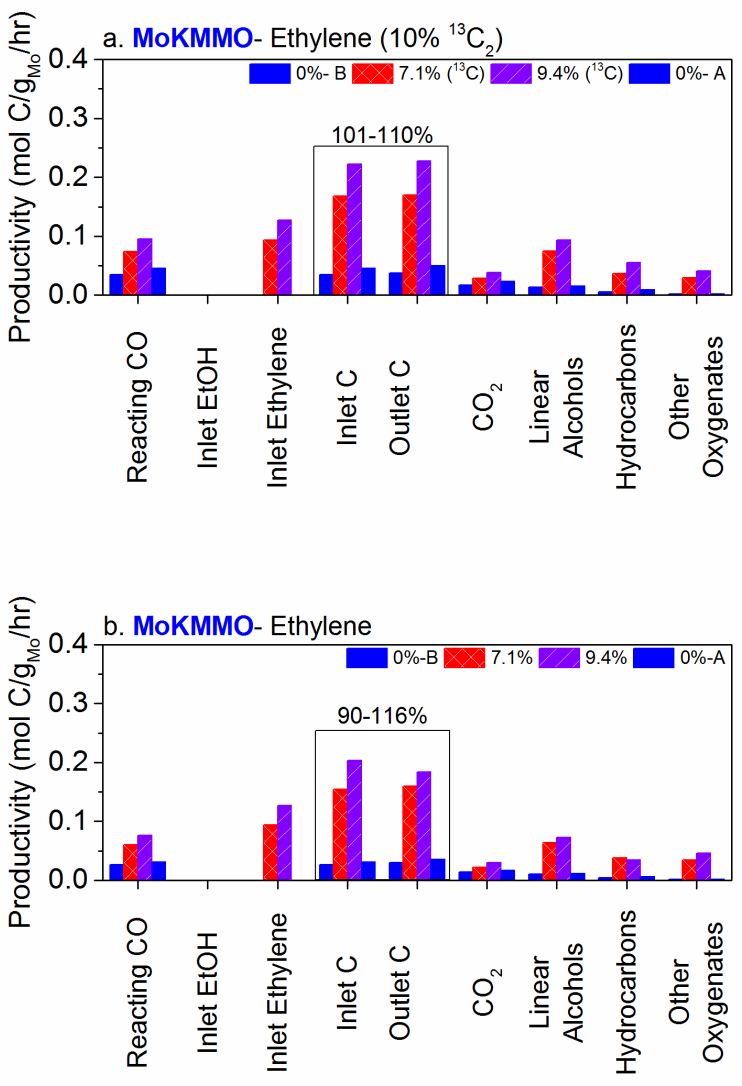

Figure 4.B.9: Carbon balance for $^{13}C_2$-ethylene (a) and ethylene (b) co-feed experiments for the MoKMMO catalyst. Reaction conditions: 310 ºC and 1500 psig. Note: 0%-B, 0%-A attributes to the product distribution before and after co-feed.

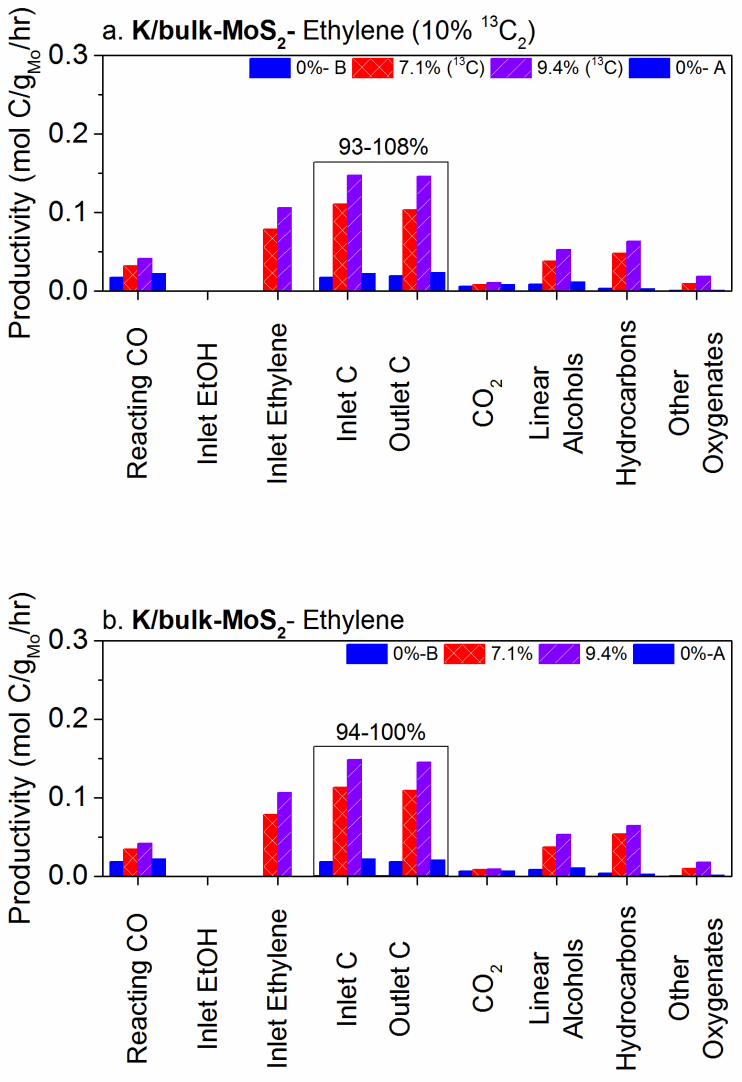

Figure 4.B.10: Carbon balance for $^{13}C_2$-ethylene (a) and ethylene (b) co-feed experiments for the K/bulk-MoS_2 catalyst. Reaction conditions: 310 ºC and 1500 psig. Note: 0%-B, 0%-A attributes to the product distribution before and after co-feed.

Table 4.B.1: Reactivity data for the MoKMMO and K/bulk-MoS_2 catalysts for ethanol, $^{13}C_2$-ethanol, ethylene, $^{13}C_2$-ethylene co-feed experiments. Reaction conditions: 310 ºC and 1500 psig.

Catalyst-Co-feed	Co-feed	Carbon Balance (%)	CO conv. (%)	Co-feed conv. (%)
MoKMMO-EtOH	0%	111	8.0	-
MoKMMO-EtOH	3%	103	11.3	67.3
MoKMMO-EtOH	3%	113	11.4	63.9
MoKMMO-EtOH	6.1%	102	14.1	64.0
MoKMMO-EtOH	6.1%	115	12.5	56.3
MoKMMMO-$^{13}C_2$-EtOH	0%	108	7.5	-
MoKMMMO-$^{13}C_2$-EtOH	3%	110	10.3	56.7
MoKMMMO-$^{13}C_2$-EtOH	3%	110	11.4	58.6
MoKMMMO-$^{13}C_2$-EtOH	6.1%	101	14.2	60.2
MoKMMMO-$^{13}C_2$-EtOH	6.1%	102	14.2	59.7
MoKMMMO-$^{13}C_2$-EtOH	0%	124	8.5	-
MoKMMO-Ethylene	0%	116	7.7	-
MoKMMO-Ethylene	7.1%	103	14.5	99.9
MoKMMO-Ethylene	7.1%	103	15.3	100.0
MoKMMO-Ethylene	9.4%	90	18.6	100.0
MoKMMO-Ethylene	9.4%	90	18.8	100.0
MoKMMO-Ethylene	0%	114	8.7	-
MoKMMO-$^{13}C_2$-Ethylene	0%	108	6.8	-
MoKMMO-$^{13}C_2$-Ethylene	7.1%	101	17.4	99.8
MoKMMO-$^{13}C_2$-Ethylene	7.1%	105	20.7	100.0
MoKMMO-$^{13}C_2$-Ethylene	9.4%	102	24.9	99.8
MoKMMO-$^{13}C_2$-Ethylene	9.4%	98	25.5	99.9
MoKMMO-$^{13}C_2$-Ethylene	0%	110	8.5	-
K/bulk-MoS_2-Ethylene	0%	100	7.4	-
K/bulk-MoS_2-Ethylene	7.1%	97	19.6	50.5
K/bulk-MoS_2-Ethylene	7.1%	100	21.2	50.0
K/bulk-MoS_2-Ethylene	9.4%	98	24.4	55.7
K/bulk-MoS_2-Ethylene	9.4%	98	25.3	55.3
K/bulk-MoS_2-Ethylene	0%	94	10.6	-
K/bulk-MoS_2-$^{13}C_2$-Ethylene	0%	108	6.8	-
K/bulk-MoS_2-$^{13}C_2$-Ethylene	7.1%	93	16.5	56.3
K/bulk-MoS_2-$^{13}C_2$-Ethylene	7.1%	105	17.6	50.3
K/bulk-MoS_2-$^{13}C_2$-Ethylene	9.4%	99	21.2	58.1
K/bulk-MoS_2-$^{13}C_2$-Ethylene	9.4%	97	21.8	58.0
K/bulk-MoS_2-$^{13}C_2$-Ethylene	0%	105	9.7	-

References

(1) M. Taborga Claure, M. R. Morrill, J. W. Goh, S.-H. Chai, S. Dai, P. K. Agrawal and C. W. Jones, *Catal. Sci. Technol.*, 2016, **6**, 1957-1966.

APPENDIX 4.C

^{13}C-NMR DATA

This appendix includes ^{13}C-NMR data and analysis discussed in this Chapter.

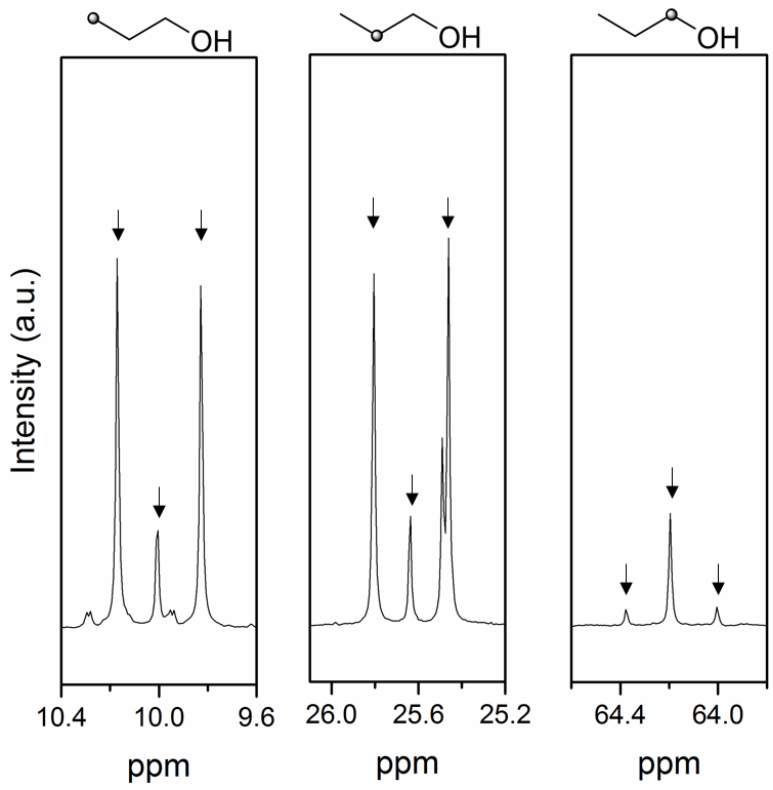

Figure 4.C.1: ^{13}C-NMR spectrum of 1-PrOH over the MoKMMO catalyst for 6.1% $^{13}C_2$-ethanol co-feed experiments. Arrows denote the peaks assigned to 1-PrOH. Intensity scale is consistent across all graphs.

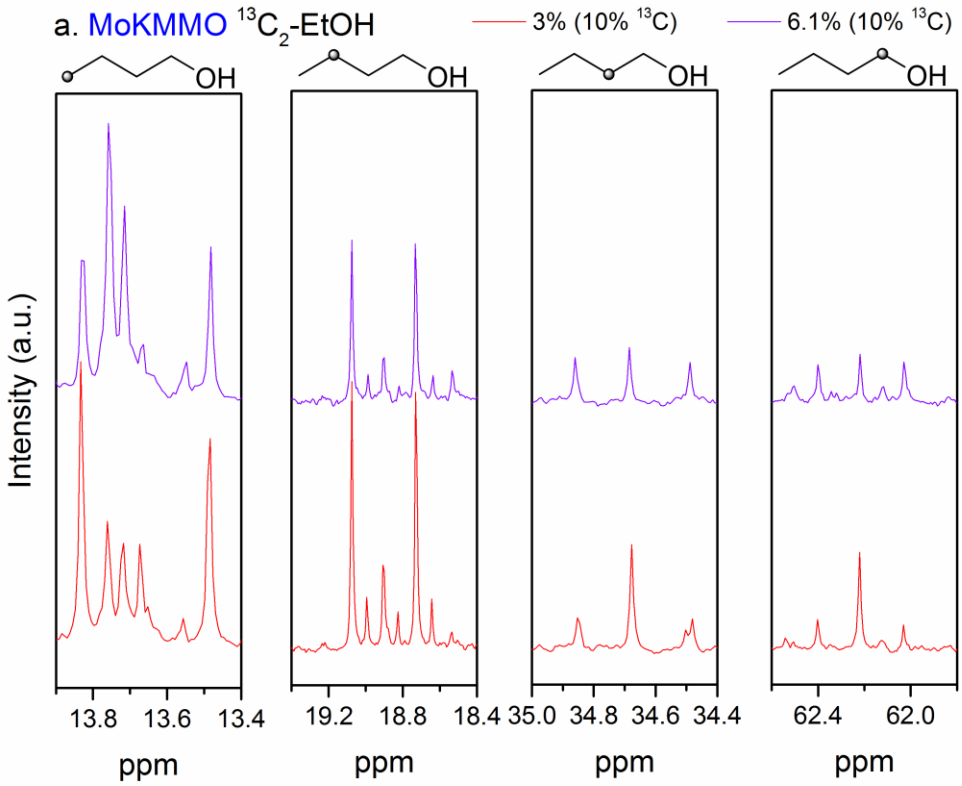

Figure 4.C.2: ^{13}C-NMR spectra of 1-ButOH over the MoKMMO catalyst for 6.1% $^{13}C_2$-ethanol and 7.1% $^{13}C_2$-ethylene co-feed experiments. Intensity scale is consistent across all graphs. The NMR spectrum for the 6.1% $^{13}C_2$-EtOH co-feed was shifted up.

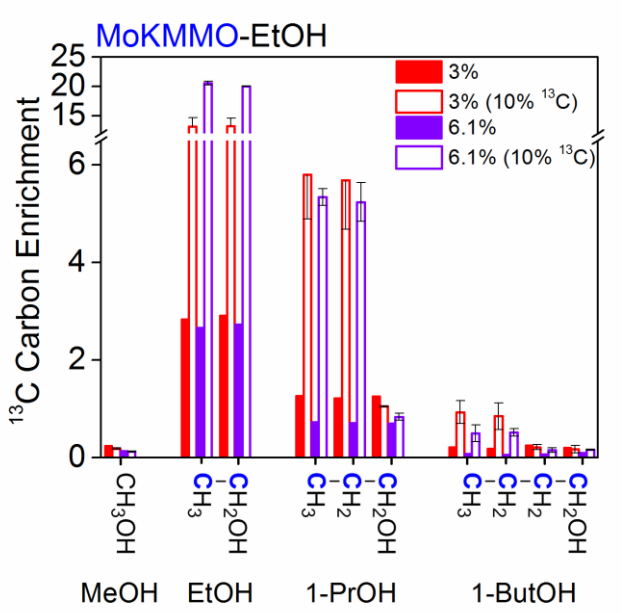

Figure 4.C.3: ^{13}C carbon enrichment of C_1-C_4 alcohols over the MoKMMO catalyst for EtOH (solid boxes) and $^{13}C_2$-EtOH (open boxes). Doublets are labeled in blue. Error bars show the standard deviation between two different $^{13}C_2$-ethanol co-feed experiments conducted for reproducibility purposes.

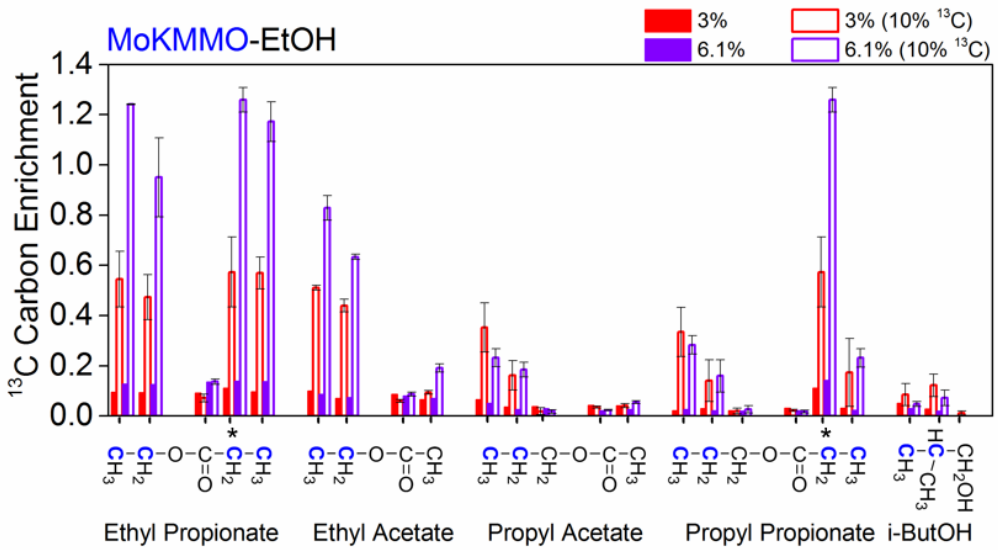

Figure 4.C.4^{13}C carbon enrichment of C_{2+} oxygenates over the MoKMMO catalyst for EtOH (solid boxes) and $^{13}C_2$-EtOH (open boxes) co-feed experiments. Doublets are labeled in blue.
Note that the methyl groups in isobutyl alcohol in ^{13}C-NMR are indistinguishable. The carbons denoted with an * have overlapping peaks for the open and solid boxes, and the total peak area was attributed to both carbons. Therefore, the ^{13}C carbon enrinchment may be an overstimate, but does not significantly affect the results. Error bars show the standard deviation between two different $^{13}C_2$-ethanol co-feed experiments conducted for reproducibility purposes.

APPENDIX 4.D

GC-MS DATA

This appendix includes GC-MS data discussed in this Chapter.

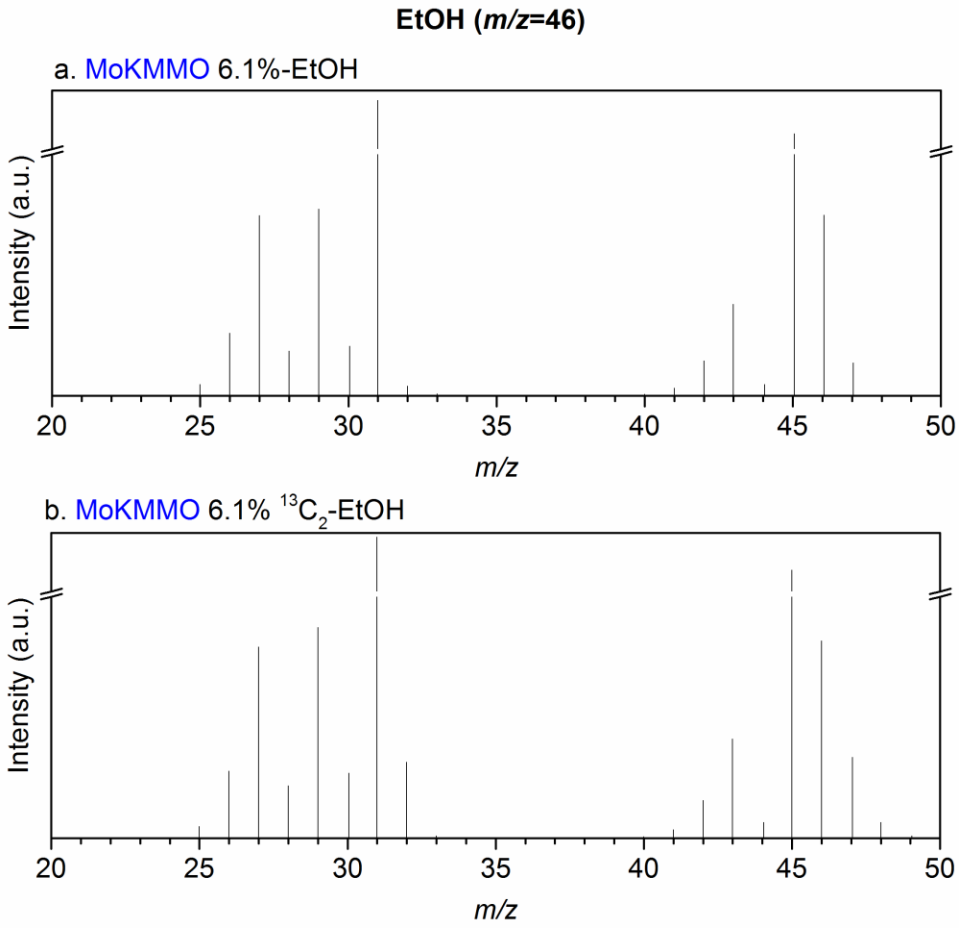

Figure 4.D.1: MS spectra of EtOH (*m/z*=46) for liquid products at 6.1% EtOH co-feed (a) and 6.1% $^{13}C_2$-EtOH co-feed (b) over the MoKMMO catalyst.

The MS spectrum of EtOH over the MoKMMO catalyst for $^{13}C_2$-EtOH co-feed (Figure 4.D.1) provides evidence of unreacted $^{13}C_2$ enriched ethanol, as peaks for $[^{13}C_2H_5OH]^{+\bullet}$ with m/z=48, $[^{13}C_2H_5OH\text{-}H]^+$ with *m/z*=47 and $[^{13}C_2H_5OH\text{-}^{13}CH_3]^+$ with *m/z*=32 are present.

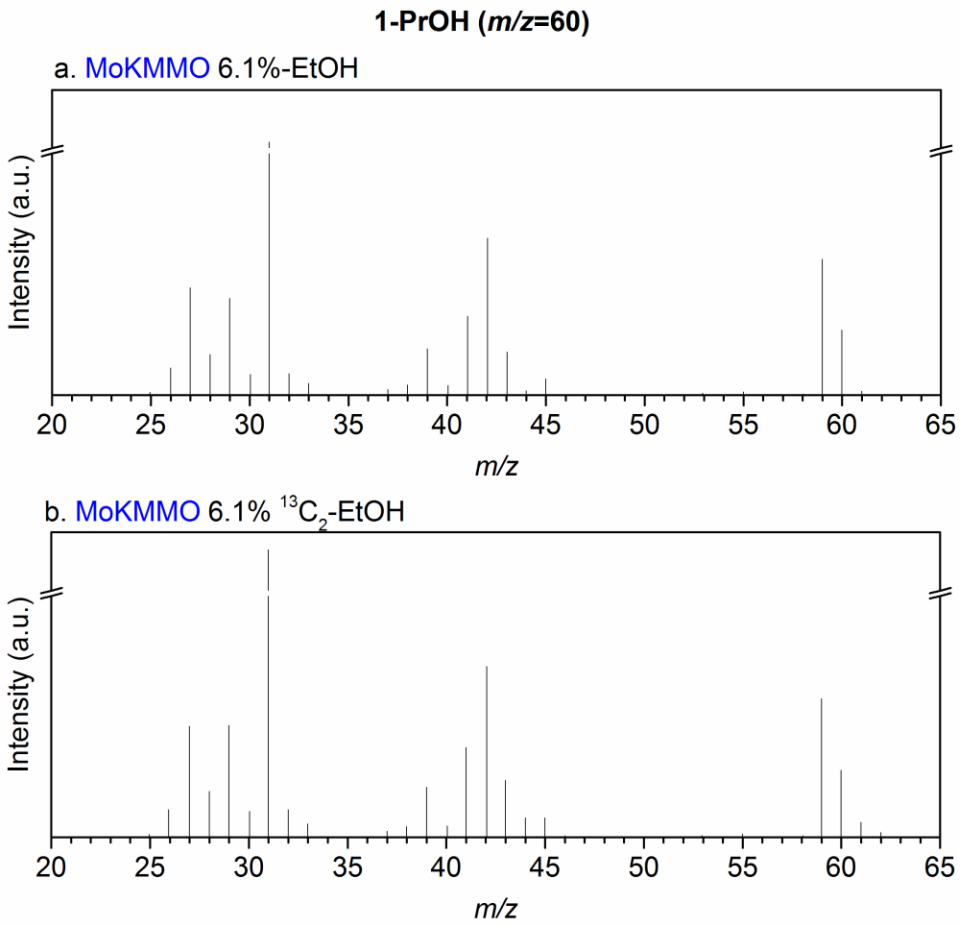

Figure 4.D.2: MS spectra of 1-PrOH (*m/z*=60) for liquid products at 6.1% EtOH co-feed (a) and 6.1% $^{13}C_2$-EtOH co-feed (b) over the MoKMMO catalyst.

The MS spectrum of 1-PrOH over the MoKMMO catalyst for $^{13}C_2$-EtOH co-feed (Figure 4.D.2) shows peaks for $[^{13}C_2\text{-M}]^{+\bullet}$ (where M is 1-PrOH) with *m/z*=62, and $[^{13}C_2\text{-M-H}]^+$ with *m/z*= 61, indicating that doubly labeled 1-PrOH is present.

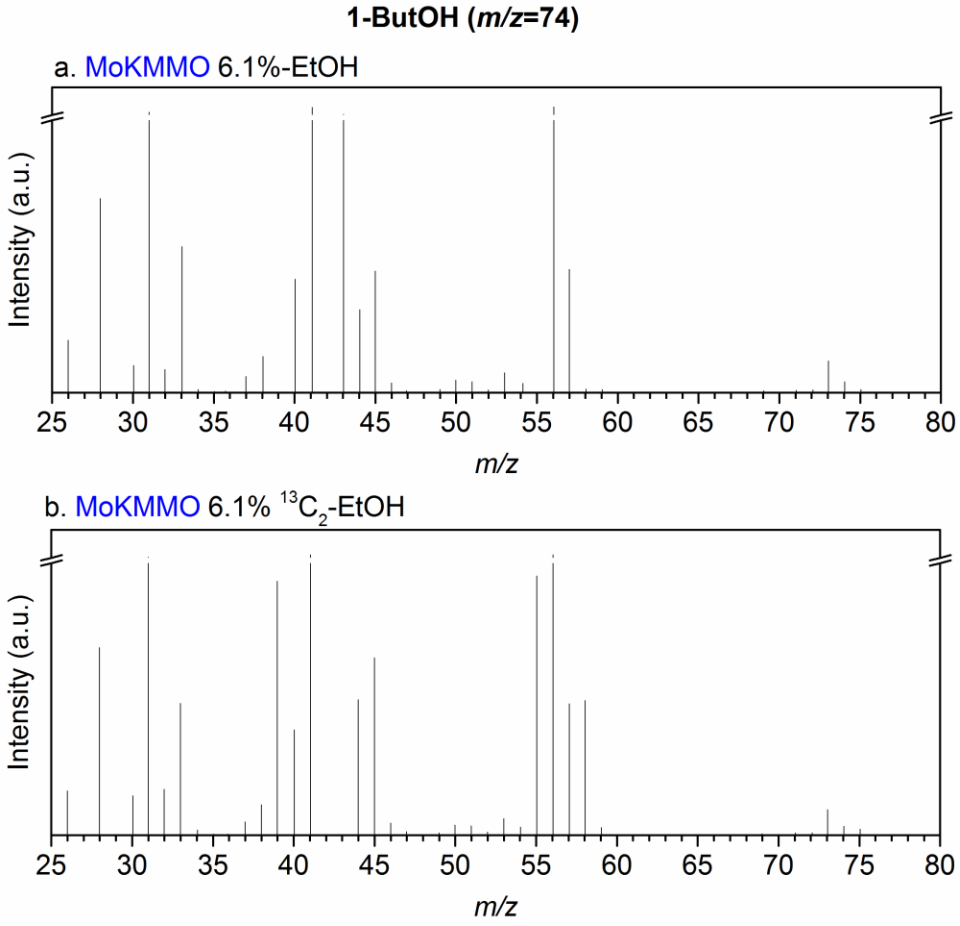

Figure 4.D.3: MS spectra of 1-ButOH (*m/z*=74) for liquid products at 6.1% EtOH co-feed (a) and 6.1% $^{13}C_2$-EtOH co-feed (b) over the MoKMMO catalyst.

The peak at *m/z*=58, attributed to $[^{13}C_2\text{-}M\text{-}H_2O]^+$, is only observed in the MS spectrum of 1-ButOH over the MoKMMO catalyst for the $^{13}C_2$-EtOH co-feed, shown in Figure 4.D.3 (not present for the EtOH co-feed), therefore indicating that doubly labeled 1-ButOH is present.

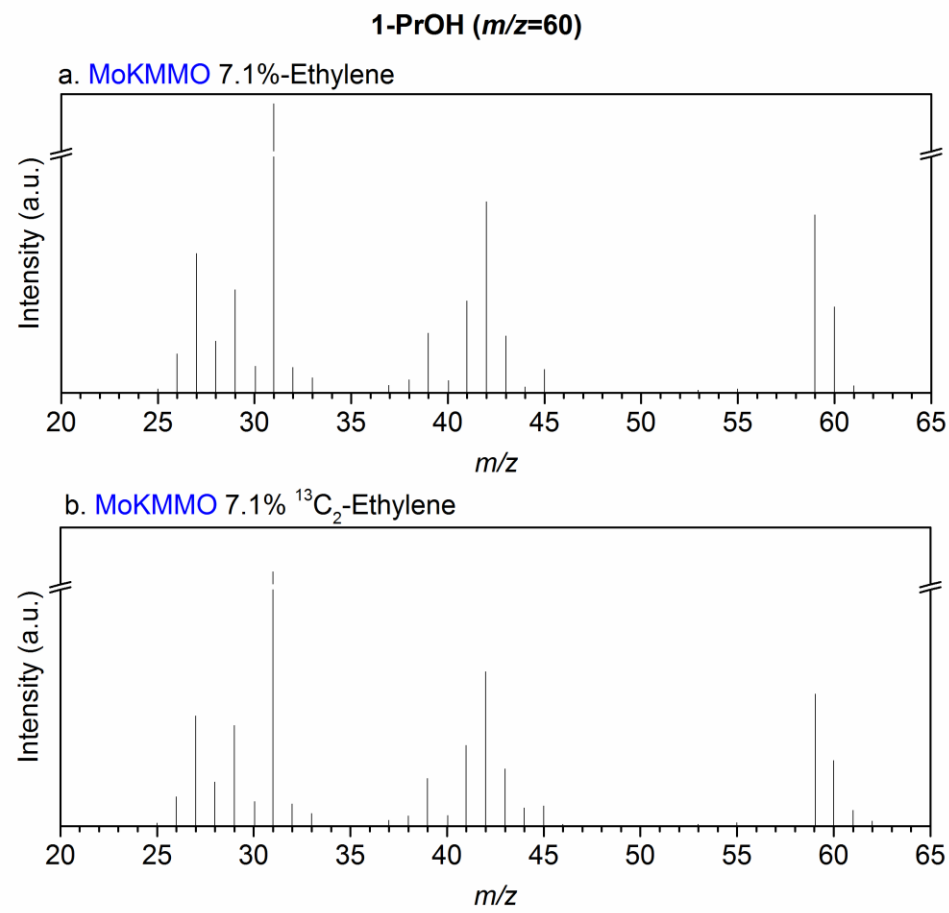

Figure 4.D.4: MS spectra of 1-PrOH (*m/z*=60) for liquid products at 7.1% ethylene co-feed (a) and 7.1% $^{13}C_2$-ethylene co-feed (b) over the MoKMMO catalyst.

The MS spectrum of 1-PrOH over the MoKMMO catalyst for the $^{13}C_2$-ethylene co-feed (Figure 4.D.4) shows peaks for $[^{13}C_2\text{-M}]^{+\bullet}$ (where M is 1-PrOH) with *m/z*=62, and $[^{13}C_2\text{-M-H}]^{+}$ with *m/z*= 61, indicating that doubly labeled 1-PrOH is present.

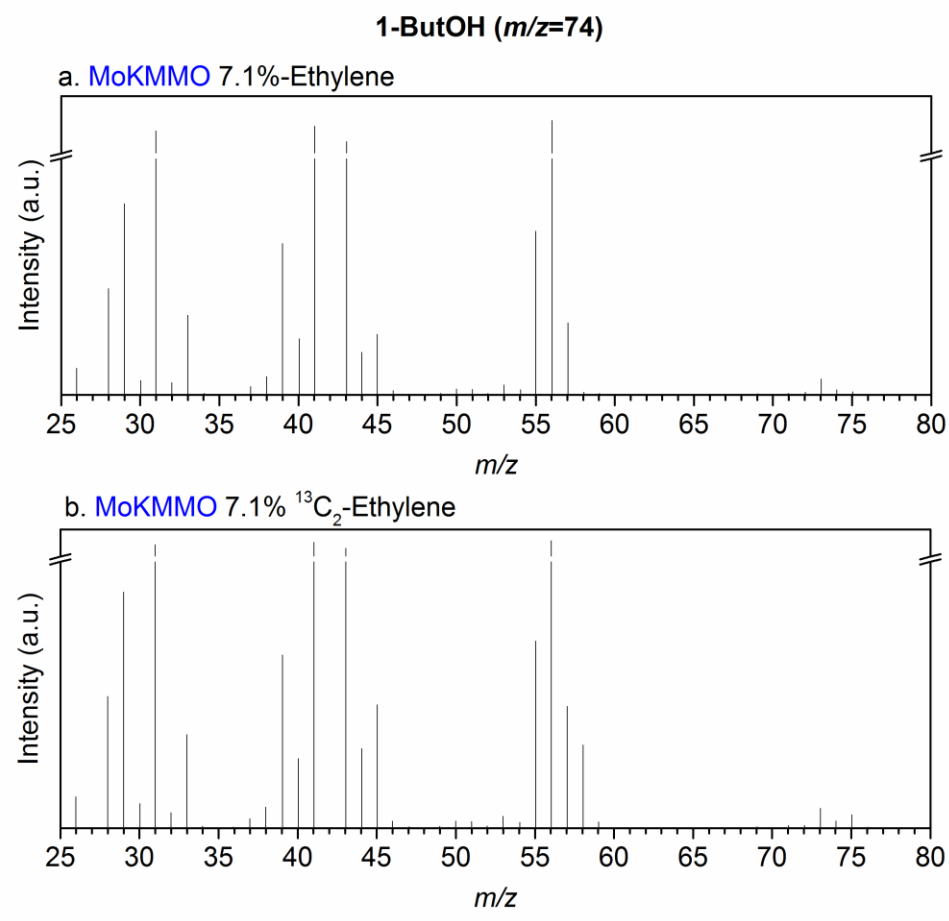

Figure 4.D.5: MS spectra of 1-ButOH (*m/z*=74) for liquid products at 7.1% ethylene co-feed (a) and 7.1% $^{13}C_2$-ethylene co-feed (b) over MoKMMO.

The peak at *m/z*=58, attributed to [$^{13}C_2$-M-H_2O] is only observed in the MS spectrum of 1-ButOH over the MoKMMO catalyst for the $^{13}C_2$-ethylene co-feed, shown in Figure 4.D.5 (not present for the EtOH co-feed), therefore indicating that doubly labeled 1-ButOH is present.

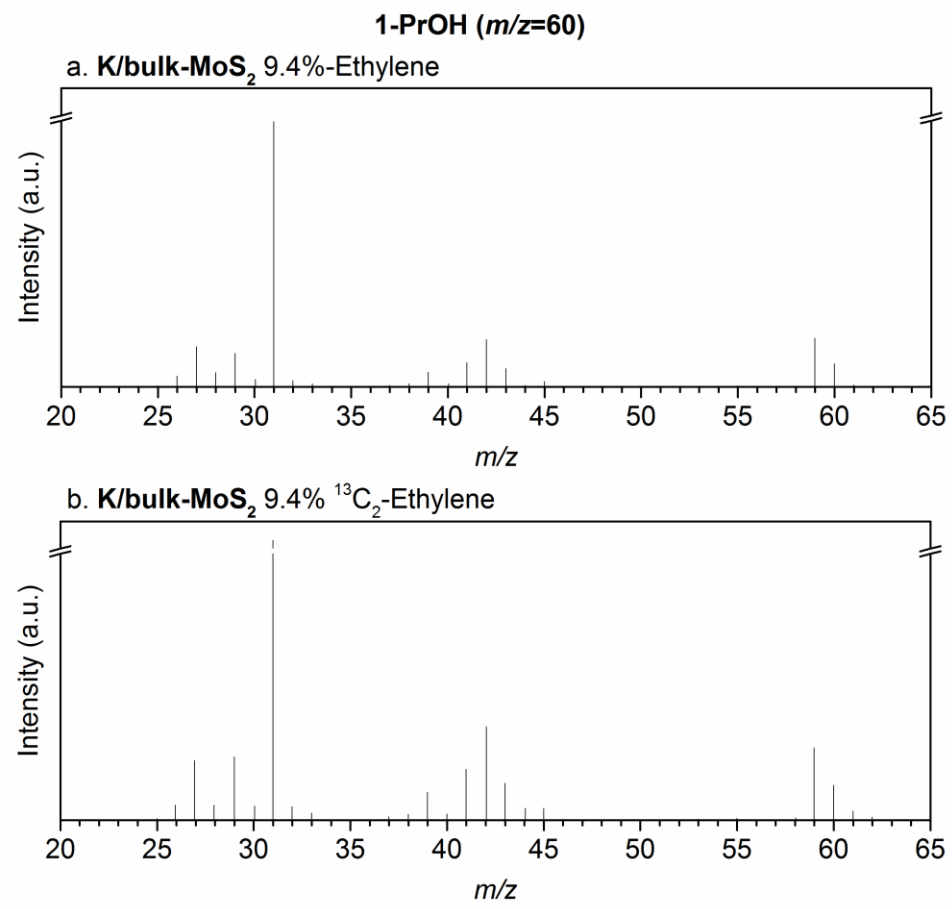

Figure 4.D.6: MS spectra of 1-PrOH (*m/z*=60) for liquid products at 9.4% ethylene co-feed (a) and 9.4% $^{13}C_2$-ethylene co-feed (b) over the K/bulk-MoS_2 catalyst.

The MS spectrum of 1-PrOH over the K/bulk-MoS_2 catalyst for the $^{13}C_2$-ethylene co-feed (Figure 4.D.6) shows peaks at m/z=61, likely attributed to $[^{13}C_2\text{-M-H}]^+$ with *m/z*= 61, indicating that doubly labeled 1-PrOH is present.

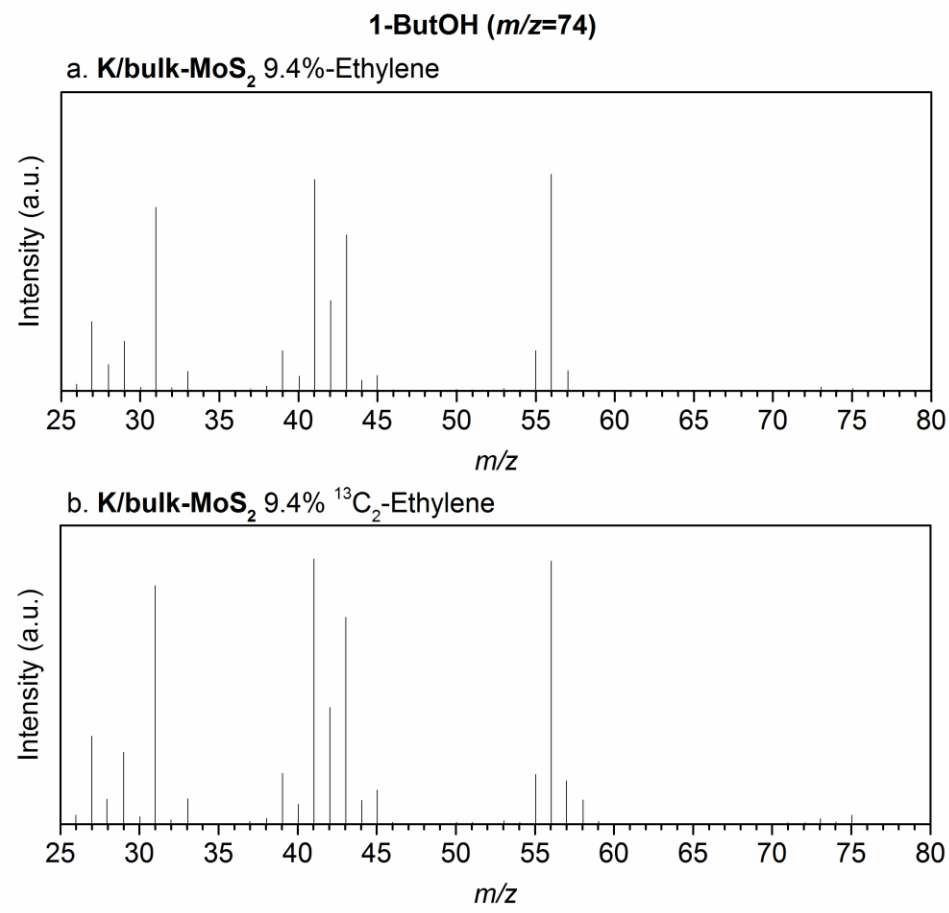

Figure 4.D.7: MS spectra of 1-ButOH (*m/z*=74) for liquid products at 9.4% ethylene co-feed (a) and 9.4% $^{13}C_2$-ethylene co-feed (b) over the K/bulk-MoS_2 catalyst.

The peak at *m/z*=58, attributed to [$^{13}C_2$-M-H_2O], is only observed in the MS spectrum of 1-ButOH the K/bulk-MoS_2 catalyst for the $^{13}C_2$-ethylene co-feed, shown in Figure 4.D.7 (not present for the ethylene co-feed), therefore indicating that doubly labeled 1-ButOH is present.

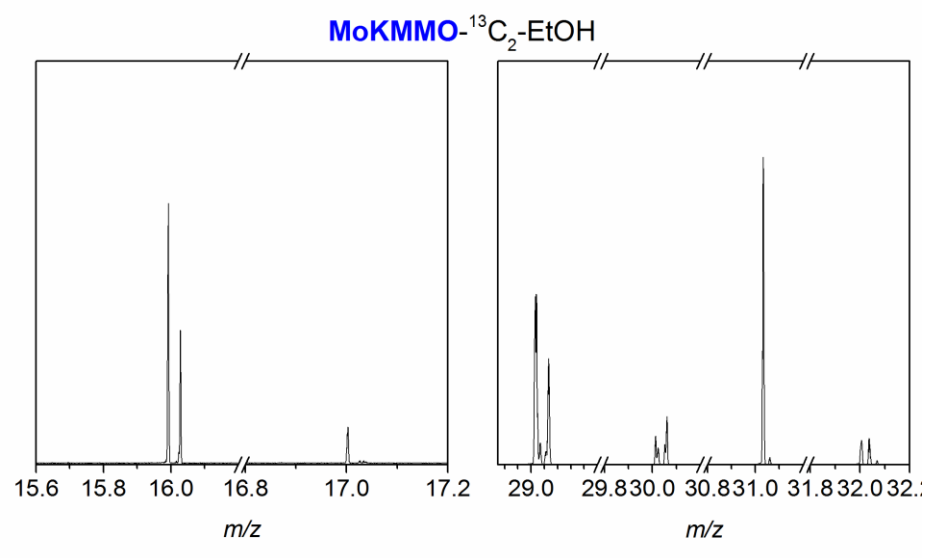

Figure 4.D.8: MS spectrum for gas samples for the MoKMMO catalyst at the 6.1% $^{13}C_2$-ethanol co-feed.

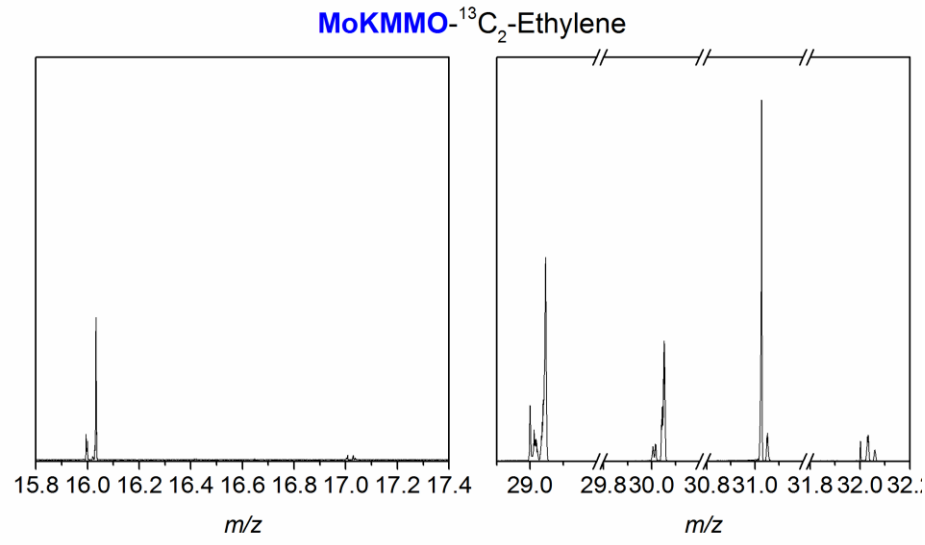

Figure 4.D.9: MS spectrum for gas samples for the MoKMMO catalyst at the 9.4% $^{13}C_2$-ethylene co-feed.

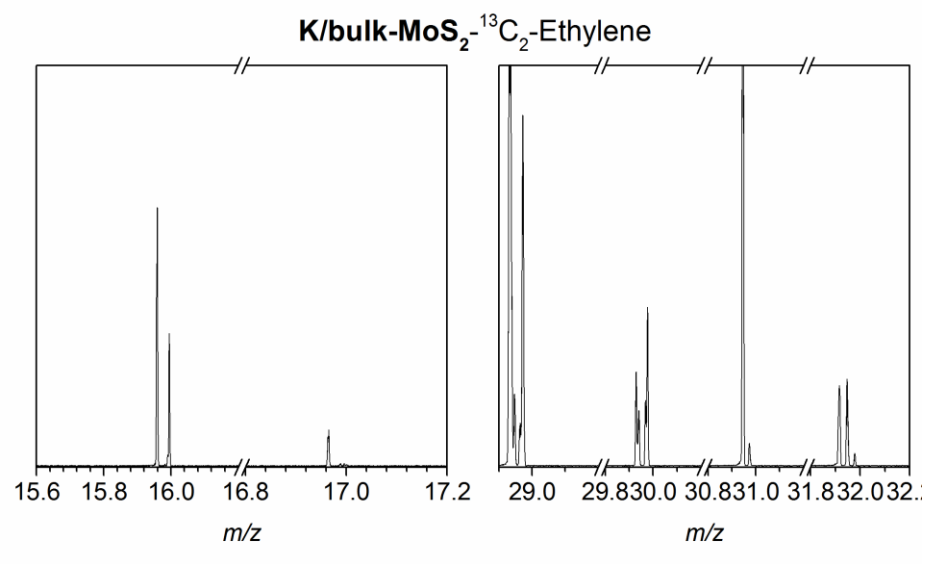

Figure 4.D.10: MS spectrum for gas samples for the K/bulk-MoS_2 catalyst at the 9.4% $^{13}C_2$-ethylene co-feed.

It is important to note that the peak intensities for Figure 4.D.8- 4.D.9 may not be comparable, as the GC-MS gas aliquot injections may be imprecise for the different samples. The $[C_2H_6]^{+\bullet}$ with *m/z*=30.047 and the $[M\text{-}H]^-$ with *m/z*= 29.039 are both likely present in the MS spectrum for MoKMMO-$^{13}C_2$-EtOH (Figure 4.C.1a) and MoKMMO-$^{13}C_2$-ethylene (Figure 4.C.2b). The three peaks observed at m/z= 32 in the MS spectrum over the MoKMMO and K/bulk-MoS_2 catalyst for $^{13}C_2$-EtOH and $^{13}C_2$-ethylene are likely associated with $[^{13}C_2H_6]^{+\bullet}$ with m/z 32.054, an alcohol fragment $[^{13}CH_2OH]^+$ with *m/z*=32.022, and $[O_2]^+$ with *m/z*=31.990. Two peaks are observed at m/z=31, likely attributed to $[^{13}C_2H_6\text{-}H]^+$ with *m/z*=31.046 and the common alcohol fragment $[CH_2OH]^+$ with *m/z*=31.0184. The *m/z* for singly labeled ethane $[^{13}CH_3CH_3]^{+\bullet}$ is 31.050 and the $[M\text{-}H]^+$ ion is 30.042. Since alcohol fragments also appear at *m/z*=30, it is not clear whether the extra peak at m/z=30 is attributed to singly labeled ethane or an alcohol fragment. Even though it appears that doubly labeled ethane is present in both the $^{13}C_2$-EtOH and $^{13}C_2$-ethylene co-feeds, it cannot be ruled out that singly labeled ethane is also present, as some of the peaks may be overlapping.

CHAPTER 5

CONCLUSIONS AND OUTLOOK

5.1 Conclusions

The work contained in this thesis focused on developing insight into the reaction pathways for higher alcohol synthesis from syngas over K/MoS_2 supported catalysts through alcohol, olefin, ^{13}C co-feed experiments and understanding of the structure-reactivity relationships through detailed catalyst characterization. The key findings in this work are:

(i) K/MoS_2 domain structure (MoS_2 stacking) was correlated with the selectivity of the catalyst. Specifically, single MoS_2 (002) layers (without K intercalation) were correlated with high hydrocarbon selectivity. Double MoS_2 (002) layers were correlated with high $C_{3+}OH$ selectivity.

(ii) Strong Mo-MMO interactions creating intimate contact between K/MoS_2 domains (consisted of mainly double layers) and MMO for the MMO supported K/MoS_2 catalyst result in the highest observed $C_{3+}OH$ selectivity over the catalysts studied.

(iii) Tuning of higher alcohol selectivity and productivity over K/MoS_2 catalyst supported on mixed C and MMO was demonstrated. The reactivity and structural data were consistent with the hypothesis that Mo had the ability to migrate from the carbon support (where mobility was high) to the MMO support (where mobility was lower), creating, in the case of the MoKC-MMO catalyst (where Mo was initially contained on the C and then ground with MMO), a hybrid catalyst that was both productive and selective towards higher alcohols.

(iv) A methanol co-feed resulted in increased ethanol and methane production across both supported and unsupported catalysts. An ethanol co-feed increased $C_{3+}OH$ and $C_{2+}HC$ over the C and MMO supported K/MoS_2 catalysts, but did not yield any significant change in the product distribution over the K/bulk-MoS_2 catalyst. Similarly, an ethylene co-feed increased the $C_{3+}OH$ and $C_{2+}HC$ productivity over the supported catalysts. However, over the K/bulk-MoS_2 catalyst, a significant increase in only 1-propanol was observed, suggesting that ethanol adsorption and/or formation of ethyl species are likely rate-controlling for 1-propanol formation.

(v) Supports do have an influence on the reaction pathways to higher chain products. The acidity of the carbon support seems to facilitate alcohol dehydration/hydrogenation reactions to yield hydrocarbons. The MMO support influences methanol plus 1-propanol coupling to form isobutyl alcohol.

(vi) Alcohol formation proceeded via the same acyl intermediate as olefin carbonylation. This is supported by similar normalized major $C_{3+}OH$ product distributions observed over the MMO supported K/MoS_2 catalyst with ethylene and ethanol co-feeds. ^{13}C co-feeds confirm this hypothesis as similar carbon enrichment in C_3-C_4 alcohols over the MMO K/bulk-MoS_2 catalyst is observed with $^{13}C_2$-ethanol and $^{13}C_2$-ethylene co-feed experiments.

(vii) Higher alcohols over the K/MoS_2 supported catalysts are primarily formed through a CO insertion pathway (similar to unsupported K/bulk-MoS_2), as only the terminal carbons of C_3-C_4 alcohols with $^{13}C_2$-ethanol, and $^{13}C_2$-ethylene co-feeds are preferentially enriched.

(viii) First study to conclusively show evidence for ethanol self-coupling to form $^{13}C_4$-1-butanol species during the CO hydrogenation reaction over the K/MoS_2

catalysts supported on MMO, demonstrating that the MMO support indeed facilitates ethanol self-coupling to 1-butanol as a secondary pathway.

(ix) Hydrogenation of an acetyl species (CH_3CO^*) to the ethoxy intermediate ($C_2H_5O^*$) is largely irreversible under the conditions employed as there is no preferential enrichment of the acetyl group in acetate species with either $^{13}C_2$-ethanol or $^{13}C_2$-ethylene co-feeds.

This research, focused on elucidation of higher alcohol synthesis and initial structure-reactivity relationships, provides a solid foundation for future work centered on fundamentally understanding the active sites as well as possible paths for creating more active Mo sites that may render a viable industrial catalyst.

5.2 Outlook

5.2.1 Elucidating Mo active sites

The reaction pathways involved in higher alcohol synthesis over K/MoS_2 based supported catalysts were elucidated in the work contained in this Thesis. Initial correlations between MoS_2 domain size and reactivity were provided in Chapter 1, where double MoS_2 (002) layers (with K intercalation) correlated with high $C_{3+}OH$ selectivity and single MoS_2 (002) layers (without K intercalation) correlated with high hydrocarbon selectivity. However, as discussed in the background, the nature of active sites of supported K/MoS_2 catalysts remains ill-defined. Therefore, future work should focus on elucidating the sites that activate H_2, CO and create new C-C bonds. To this end, MoKMMO should be characterized via techniques focused on elucidating the nature of active sites in combination with computational studies.

Gascon et al. conducted CO adsorption studies under IR spectroscopy after exposing K/bulk-MoS_2 to syngas for 3 h, at 30 bar and 350 °C. They determined that K is likely located at edge sites influencing an increase in corner Mo sites that poison the

hydrogenation ability of MoS_2. Additionally, it was determined that the transient period of CO hydrogenation reactions is associated with the spreading of K promoter on MoS_2 surface.[1] However, this study did not identify the association between v(CO) bands and CO adsorption on specific sites, nor quantify the number of Mo sites that adsorb CO. Oliviero et al. has recently demonstrated that low-temperature CO adsorption followed by infrared spectroscopy can be used to quantify the active sites of sulfide and metallic catalysts using specific molar extinction coefficients of CO adsorption for each type of site. It was also shown that citric acid can be used as a chelating agent to modify the MoS_2 morphology from a slightly truncated triangle with predominantly M-edge to a hexagon with both M- and S- edges and further understand the relationship between the M-edge and S-edge with the reactivity of the catalyst.[2]

To understand the nature of active sites on the MoKMMO catalyst and potentially quantify them, it is proposed to conduct low-temperature CO adsorption studies under IR after exposing the catalyst to syngas for 3 h, at 30 bar and 350 °C. Syngas exposure is key for accurate investigation of CO adsorption on M- and S- edges similar to those present under CO hydrogenation reaction. Preliminary CO adsorption studies conducted at ORNL for the MoKMMO catalyst at 1 atm and room temperature showed no CO bands. Therefore, at least moderate pressures (30 bar) are required to observe CO adsorption on M- and S- edges. It is important to note that the MoS_2 phase prepared from an oxide precursor is prone to oxidize after ex-situ sulfidation. Using sulfide precursors that can be decomposed in-situ prior to the gas adsorption experiments may be necessary to prevent this issue. The use of citric acid as a chelating agent can be used to increase the number of S-edged and investigate their effect on reactivity as means to elucidate the nature of M-edge and S-edges on CO hydrogenation reactions.[3] This experimental work should be supported with computational structural models of K/MoS_2 catalysts to assess adsorption and vibrational properties of CO. To this end,

computational models for MoS_2 catalysts capable of determining the preferred location of K in different MoS_2 domain sizes supported on MMO would be necessary.

5.2.2 Enhancing the MoKMMO catalytic reactivity

It has also been shown in this Thesis and previous work by our group that MMO supports over K/MoS_2 catalysts shift alcohol distribution from C_1-C_2 to C_2-C_4 alcohols, but generally yield low productivity.[4-6] In Chapter 2, double MoS_2 (002) layers over the MMO support were correlated with high C_{3+}OH selectivity. Therefore, it was hypothesized that the ideal MoKMMO catalyst would consist of highly dispersed double MoS_2 (002) layers over MMO support. Two distinct supports, a layered MMO material (that yields enhanced C_{3+}OH selectivity) and a mesoporous activated carbon (that offers high ethanol productivity) were combined to introduce a new catalyst composition with desirable reactivity. It was observed that over MoKC-MMO, whereby Mo is initially contained on the C support then ground with carbon, significant Mo migrates from the C to MMO during reaction, creating highly dispersed MoS_2 layers that are both selective and productive toward C_{3+}OH. Other methods that can be explored to enhance the productivity of MoKMMO catalysts include enhancing the properties of the MMO support to better disperse Mo, incorporating Co and Ni promoters in the MgAl oxide creating a similar synergistic effect to that of mixed Co-, Ni- MoS_2 catalysts, and enhancing the reactivity of MoS_2 based catalysts by synthetically modifying the Mo active phase.

5.2.2.1 Enhancing the properties of the MMO support

Ogino et al. showed that MgAl oxide prepared from MgAl hydroxide nanoscrolls from hydrotalcites has a high BET surface area of 509 m^2/g, which is among the highest in the reported Mg/Al mixed oxides derived from hydrotalcites.[7] The MMO used in this Thesis average a BET surface area of ~180 m^2/g. Therefore, using the MgAl oxide derived from MgAl hydroxide nanoscrolls would increase the surface area more than

two-fold from MMO used in this Thesis and likely result in higher Mo dispersion and in turn higher alcohol productivity.

Ordered mesoporous NiAl oxide, prepared through a soft template method using pluronic-F127 as a structure-directing agent by Suib et al., exhibited enhanced catalytic activity in Knoevenagel condensation reaction associated with higher pore accessibility compared to traditionally synthesized MgAl oxide.[8] Therefore, it is hypothesized that K/MoS_2 domains supported on a similar mesoporous MgAl oxide may result in higher number of accessible Mo sites that can result in higher alcohol productivity.

5.2.2.2 Incorporation of Ni, Co promoters in MgAl oxide

K/MoS_2 based catalysts achieve up to 30% conversion and 80% ethanol CO_2 free selectivity upon promoting the catalyst with transition metals (Ni, Co, Fe).[9-12] It is widely accepted that transition metals improve catalytic activity and selectivity to $C_{2+}OH$ due to hydrogenation ability and chain propagation enhancement.[12-14] To the best of our knowledge there are no reports that investigate the effect of incorporating the transition metal in the MgAl oxide on K/MoS_2 catalysts for CO hydrogenation reactions. Preliminary results on MoKNiMMO and MoKCoMMO (Figure 5.1), where Mg/Al^{3+} was kept constant at 2.33 but the $[M^{2+}Mg]/Al^{3+}$=2.66, show that the addition of Co leads to the highest observed EtOH selectivity over MMO supported catalysts and an increase in EtOH productivity compared to MoKMMO. The incorporation of Ni leads to the highest observed selectivity towards 1-PrOH and $C_{3+}OH$ productivity over MMO supported catalysts. It is important to note that for accurate comparison with MoKMMO, the $[M^{2+}Mg]/Al^{3+}$ should be kept constant at 2.33 (similar to previous Chapters) by partially substituting Mg^{2+} with M^{2+} (M^{2+}=Ni^{2+} or Co^{2+}) to maintain the ratio of 2^+ and 3^+ ions.[15] Further investigation of Ni and Co incorporation in the MgAl oxide with varying the Mg^{2+}/M^{2+} ratio should be performed to evaluate their effect on $C_{2+}OH$ reactivity. These NiMMO and CoMMO K/MoS_2 supported catalysts should be compared to Co-K/MoS_2

and Ni-K/MoS_2 catalysts supported on bare MMO to investigate the effect of the incorporation of the Ni and Co into the MgAl oxide structure. In depth characterization with EXAFS and STEM of the reaction-aged catalysts will be crucial for understanding the active phases in the reaction, as Ni and Co are likely to be reduced during CO hydrogenation.

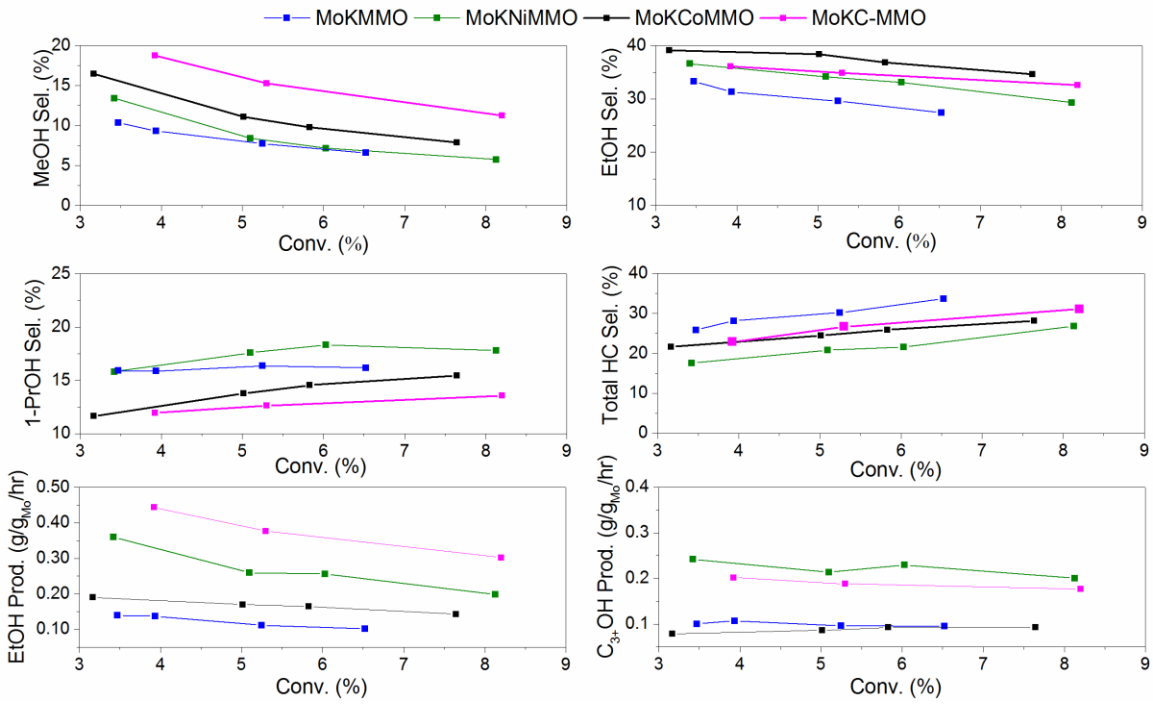

Figure 5.1: CO hydrogenation reactivity data of the MoKMMO, MoKC-MMO, MoKCoMMO, and MoKNiMMO catalysts at 310 °C and 1500 psig.

5.2.2.3 Enhancing Mo active sites

Mixed-metal catalysts are well known in higher alcohol synthesis over MoS_2 based catalysts with Ni, Co, K modifiers. However, there are limited studies with mixed-anion catalyst where synergistic effects (electronic and/or geometric) between sulfur and phosphorous, nitrogen or carbon could produce a more active catalyst phase than pure MoS_2 for CO hydrogenation reactions to higher alcohols. Jones et al. showed that at similar conditions Mo_2C produced more hydrocarbons than MoS_2 catalysts independent

of the support.[16] However, it was observed that the catalysts with different Mo precursor (Mo_2C or MoO_3 phase) after in situ sulfidation resulted in similar catalytic selectivities for CO hydrogenation reactions. It can be therefore hypothesized that the Mo_2C catalyst was decorated with MoS_2 domains on the surface creating a more active phase for higher alcohol formation while the bulk catalyst remained in the Mo_2C phase (supported by XRD). This hypothesis is supported by the work of Wand et al. that demonstrated that Mo_2C upon H_2S treatment resulted in a sulfur decorated Mo_2C by STEM, which significantly enhanced the hydrogen evolution reaction (HER) activity.[17]

In the HER literature, it has been demonstrated that modification of molybdenum phosphide (MoP) with surface sulfur by H_2S treatement produces a molybdenum phosphosulfide catalyst (MoP|S) with superb activity and stability, suggesting that S and P tune each other's electronic properties to produce an active catalyst phase.[18] Tour et al. have recently shown that phosphorous incorporation to a MoS_2 phase ($MoS_{2(1-x)}P_x$) leads to a more disordered structure with irregular morphology that may result in high HER performance as MoS_2 becomes surface active (not only edge active).[19] Additionally, a number of reports show that sulfur plays an important role in hydrodesulfurization (HDS) reactions over MoP and Ni_2P, as the HDS activity increases with time on stream, suggesting that the most active sites originate from surface phosphosulfide generated during HDS.[20-22] K/MoP subjected to CO hydrogenation reactions results in high C_2 oxygenates selectivities with low methanol and methane selectivity different from Mo-based CO hydrogenation catalysts where these C_1 products are important.[23, 24] Therefore, it is hypothesized that a K/MoP|S based catalyst may result in higher activity towards C_2 oxygenates in CO hydrogenation reactions by creating a more disordered structure and a hybrid phosphosulfide phase.

There are no reports of synthesis gas conversion at high pressures using Mo_2N. However, Zaman et al. recently suggested through DFT calculations that MoS_2 and

Mo_2N may have similar surface reaction features for CO hydrogenation reactions due to similar CO dissociation barriers.[25] Wang et al. synthesized a 3R-MoN_2, which has rhombohedral MoS_2 structure, which exhibits superior catalytic activities and high hydrogenation selectivity over MoS_2 in HDS.[26] Additionally, Zhang et al. showed that a MoS_2-MoN carbonitride catalyst exhibits remarkable HER and stability associated with increased structural and electronic modulations between MoS_2 and MoN.[27] Even though the supporting evidence is limited, a mixed K/MoS_2|N catalyst may also be interesting to investigate for CO hydrogenation reactions.

In-depth characterization of the proposed catalysts through elemental analysis, STEM and XAS will be crucial for determining the phases present in the catalyst. Different degrees of sulfidation would help determine the optimal phase for CO hydrogenation if a mixed-anion Mo catalyst family was found to be more active than the pure MoS_2 catalyst. Other methods have also been recently employed in HER to increase the number of Mo edge sites of the MoS_2 based catalysts, which may be applicable in CO hydrogenation reactions to higher alcohols.[28-31]

5.2.3 Alkylamine synthesis from syngas and ammonia over Mo based catalysts

The capacity for the production of methylamines exceeds 800,000 mt per year with dimethylamine having the highest demand. Alkyl amines (monomethylamine (MMA), dimethylamine (DMA), trimethylamine (TMA)) are used as feedstock for solvents, agricultural chemicals, surfactants, water treatment chemicals, animal feed supplements.[32] Methylamines are prepared commercially by the reaction of ammonia with methanol over solid acid catalysts (amorphous silica-alumina).[33] The selectivity of this reaction is determined by thermodynamics, with trimethylamine (TMA) being the main product. Other approaches to synthesis of methylamines from syngas have been investigated. Both methanol synthesis catalysts and Fischer-Tropsch catalysts have been extensively studied with high methylamine selectivities, as noted below. Therefore,

it is hypothesized that Mo based catalysts traditionally studied for higher alcohol synthesis (HAS) from syngas may also be active to alkylamine synthesis from syngas and ammonia. As noted below, no examples of HAS catalysts have been explored for synthesis of higher amines from ammonia and syngas. In particular, there are no reports of the use of molybdenum (sulfide, nitride, carbide, phosphide) based catalysts for alkylamine synthesis. Therefore, providing a unique opportunity to define an intellectual property position in this open area if a Mo based catalyst is found promising.

In the 1970s several families of catalysts were patented for the conversion of CO and H_2 in the presence of a nitrogen source (or ammonia) to methylamine and dimethylamine. These include, Hf, Zr, Ag-Zr alloy, U, Th, ZnO-Al_2O_3, FeO_4-Al_2O_3-BaO, and V_2O_5-BaO, CuO-ZnO.[34-36] It was proposed that a plausible reaction pathway involves the catalytic hydrogenation of carbon monoxide to methanol, followed by ammonolysis to the amine. Syngas is a well-known feedstock to alcohols (first step), the second step involves the dehydration reaction between alcohols and ammonia to give amines, therefore making Fisher-Tropsch catalysts a promising family. Olive et al. proposed one-step amination of the alkyl-metal bond, suggesting that this process would be competitive with CO insertion to alcohols and hydrocarbons.[37]

Methanol catalysts have also been investigated for syngas and NH_3 conversion to methylamines. The families studied are Cu/ZnO, ZnO/Al_20_3, Cu, Cr_2O_3/Al_2O_3 with amine selectivities 70-100%.[36] Recently, Baiker et al. demonstrated that methylamines can be directly produced in a continuous fixed-bed reactor from CO_2, H_2, and NH_3 (CO_2:NH_3:H_2= 1:1:3) over Cu/Al_2O_3 catalyst at 200-300 °C and 90 psig. [38, 39] Mono and dimethylamine (MMA and DMA) were the primary products. Reactions performed with CO instead of CO_2 resulted in slower reaction rates, but higher selectivity to MMA under similar reaction conditions. Baiker et al. further investigated various alumina-supported metal (Ni, Co, Fe, Pt, and Ag) catalysts showing little to no methylamine production.[40] Copper

(72% selectivity) and palladium (>80% selectivity) were the most selective and active catalysts for MMA production.[41, 42] The effect of various supports on reactivity was also studied. It was found that the activity for MMA formation decreased in the sequence CrO_3> ZrO_2>AL_2O_3>SiO_2>ZnO, MgO, with MMA being the dominant product for all catalysts, with lower amounts of DMA and TMA formed. [43] More recently, Baiker et al. developed CuMgAl oxides derived from hydrotalcite yielding MMA selectivity of 80%.[44]

Other families of catalysts studied for the conversion of CO, NH_3, H_2 include Zr, Zr/Ag, Mo/SiO_2 with amine selectivity of 50% with MMA and DMA being the major products produced.[36] Homogeneous catalysts have also been studied for synthesis of alkyl amines from syngas and ammonia.[34, 45, 46]

It is proposed that the molybdenum family of catalysts should be studied, including nitrides, carbides, sulfides, oxides and phosphides. It is possible that under reaction conditions, all the above families will evolve towards nitrides due to the ammonia used, though mixed phases or the other pure phases may prove to offer good performance as explained above in Section 5.2.2.3. K_2CO_3 has been shown to be crucial for shifting product distribution from hydrocarbons to higher alcohols for HAS reactions. It is hypothesized that the ability to synthesize higher alcohols is crucial for subsequent dehydration with NH_3 to form amines; therefore K should be used as the promoter. As explained above, Baiker et al. showed that a CuMgAl oxide is highly selective towards MMA. Therefore, it is hypothesized that Mo based catalysts supported on MgAl oxide (MMO), studied in this Thesis, would result in high alkylamine selectivity. In-depth characterization of the proposed catalysts through elemental analysis, STEM and XAS will be crucial to confirm the phases and structures present in the catalyst. This work should focus on screening reactivity of the above family of catalysts under a standard set of conditions: Syngas/NH_3 composition (CO:H_2:NH_3= 1:3:1), temperature (250-350 °C) and pressure (1-100 atm). If a promising family of catalysts is identified, it should be

further explored as a function of reaction conditions, while developing preliminary insight into reaction pathways important in higher amines synthesis from syngas.

5.2.4 CO_2 hydrogenation over MoS_2 based catalysts

K/MoS_2 based catalysts have not only been investigated for CO hydrogenation reactions, but also for CO_2 hydrogenation reactions. Lower productivities are observed over this catalyst in CO_2 hydrogenation reactions compared to CO hydrogenation reactions, with methanol and methane as the primary products. The deactivation of the catalyst observed during CO_2 hydrogenation reactions is thought to be a result of the water formation from the water gas shift reaction. Therefore, K/MoS_2 based catalysts are not considered to be promising for CO_2 hydrogenation reactions. Further discussion of these limitations can be found below.

Anderson et al. studied the effect of CO_2-containing syngas ($CO/H_2/CO_2/N_2$=1/1/0.5/0.08), relative to CO_2-free syngas ($CO/H_2/He/N_2$=1/1/0.5/0.08) over $K_2CO_3/Ni/MoS_2$ at 340 ºC, and 100 bar.[47] CO_2 addition was found to greatly decrease the organic products yield (-40%), as the CO conversion was significantly reduced. However, CO_2 addition led to significant change in the product distribution within alcohols and hydrocarbons. CO_2 addition leads to increased methanol selectivity (~+40%), while ethanol and $C_{3+}OH$ are significantly decreased. Also, Gang et al. have reported that the selectivity towards higher alcohols is lowered when CO_2 is added to the feed.[48] Methane selectivity is increased while $C_{2+}HC$ are decreased. It can be concluded that CO_2 addition greatly reduced C_{2+}/C1 alcohol ratio and product formation rate, which may be directly associated to CO_2 hydrogenation or indirectly to large amounts of water formed through the water-gas shift (WGS) reaction. The former is unlikely as CO_2 hydrogenation was determined to take place to a low extent compared to CO hydrogenation. This was shown by comparing the CO and CO_2 hydrogenation reactions with a mixture (H_2/CO_x= 3) at 340 °C and 71 bar (slightly different conditions).

Conversion to organic products dropped greatly (about 8 times) and the selectivity to methanol was strongly perturbed from 50 to 78%, while the selectivity to longer alcohols was decreased (e.g. ethanol selectivity from 28% to 9%).[47] It is difficult to establish whether CO_2 hydrogenation takes place at all, since this catalyst is highly active to WGS, suggesting that considerable amounts of CO_2 and H_2 are converted to CO and H_2O.

It was determined by XRD that the reaction-aged MoS_2 particle size was smaller than the as-synthesized MoS_2 particle size, which may be associated to K aggregation as a result of K_2SO_4 formation. Operation with elevated water levels (4.7%-13.4%) in the syngas feed with H_2S was observed by Christensen et al. to cause deactivation of a $K/Co/MoS_2$ catalyst and affect the chain growth over this catalyst.[49] Specifically, water lowers the synthesis activity and shifts the product toward methane and methanol, similar to the effect CO_2 in the syngas feed explained above. The deactivation of the catalyst caused by water is partially irreversible, which may be associated with MoS_2 undergoing partial oxidation in the presence of water as studied by Badawi et. al under high H_2O/H_2S ratios.[50] Additionally, Karolewski and Cavell suggested that the alkali metal promoted sulfide (Cs/MoS_2) could be more susceptible to oxidation by water than the bare sulfide.[51]

5.2.4 Outlook Summary

Several plausible future directions have been presented including elucidation of Mo active sites, catalyst design strategies to enhance the productivity of MoKMMO catalysts, alklyamine synthesis from syngas and ammonia over Mo based catalysts, and CO_2 hydrogenation over MoS_2 based catalysts. Elucidation of Mo active sites is contingent on DFT calculations to determine adsorption and vibrational properties of CO. It is not recommended to pursue CO_2 hydrogenation reaction over Mo based catalysts as this reaction is affected by the highly reactive water gas shift reaction. While improved catalyst design is a promising future direction path, alkylamine synthesis from syngas

and ammonia over Mo based catalyst is an open research area with potential to define an intellectual property position.

5.3 References

(1) V. P. Santos, B. van der Linden, A. Chojecki, G. Budroni, S. Corthals, H. Shibata, G. R. Meima, F. Kapteijn, M. Makkee and J. Gascon, *ACS Catal.*, 2013, **3**, 1634-1637.

(2) J. Chen, E. Dominguez Garcia, L. Oliviero and F. Maugé, *J. Catal.*, 2015, **332**, 77-82.

(3) N. Koizumi, G. Bian, K. Murai, T. Ozaki and M. Yamada, *J. Mol. Catal. A: Chem.*, 2004, **207**, 173-182.

(4) M. R. Morrill, N. T. Thao, P. K. Agrawal, C. W. Jones, R. J. Davis, H. Shou, D. G. Barton and D. Ferrari, *Catal. Lett.*, 2012, **142**, 875-881.

(5) M. R. Morrill, N. T. Thao, H. Shou, R. J. Davis, D. G. Barton, D. Ferrari, P. K. Agrawal and C. W. Jones, *ACS Catal.*, 2013, **3**, 1665-1675.

(6) M. Taborga Claure, S.-H. Chai, S. Dai, K. A. Unocic, F. M. Alamgir, P. K. Agrawal and C. W. Jones, *J. Catal.*, 2015, **324**, 88-97.

(7) I. Ogino, S. Kudo and S. R. Mukai, *24th Nam*, 2015, Pittsburgh, PA.

(8) M. N. Pahalagedara, L. R. Pahalagedara, C.-H. Kuo, S. Dharmarathna and S. L. Suib, *Langmuir*, 2014, **30**, 8228-8237.

(9) V. R. Surisetty, A. K. Dalai and J. Kozinski, *Appl. Catal., A*, 2010, **385**, 153-162.

(10) S. Zaman and K. J. Smith, *Cat. Rev.*, 2012, **54**, 41-132.

(11) C. B. Murchinson, M. M. Conway, R. R. Stevens and G. J. Quarderer, *In 9th Annual Congress on Catalysis, Calgary, Alberta, Canada*, 1988, 626-633.

(12) J. G. Santiesteban, C. E. Bogdan, R. G. Herman and K. Klier, *in: M.J. Philips, M. Ternan (Eds.), vol. 2, 9th Annual Congress on Catalysis, Chemical Institute of Canada, Calgary, 1988, pp. 561-568.*

(13) M. Xiang, D. Li, H. Xiao, J. Zhang, W. Li, B. Zhong and Y. Sun, *Catal. Today*, 2008, **131**, 489-495.

(14) M. Konarova, F. Q. Tang, J. L. Chen, G. Wang, V. Rudolph and J. Beltramini, *ChemCatChem*, 2014, **6**, 2394-2402.

(15) D. Bharali, R. Devi, P. Bharali and R. C. Deka, *New. J. Chem.*, 2015, **39**, 172-178.

(16) H. Okatsu, M. Morrill, H. Shou, D. Barton, D. Ferrari, R. Davis, P. Agrawal and C. Jones, *Catal. Lett.*, 2014, **144**, 825-830.

(17) C. Tang, W. Wang, A. Sun, C. Qi, D. Zhang, Z. Wu and D. Wang, *ACS Catal.*, 2015, **5**, 6956-6963.

(18) J. Kibsgaard and T. F. Jaramillo, *Angew. Chem. Int. Ed.*, 2014, **53**, 14433-14437.

(19) R. Ye, P. del Angel-Vicente, Y. Liu, M. J. Arellano-Jimenez, Z. Peng, T. Wang, Y. Li, B. I. Yakobson, S.-H. Wei, M. J. Yacaman and J. M. Tour, *Adv. Mater.*, 2016, **28**, 1427-1432.

(20) D. C. Phillips, S. J. Sawhill, R. Self and M. E. Bussell, *J. Catal.*, 2002, **207**, 266-273.

(21) J. Bai, X. Li, A. Wang, R. Prins and Y. Wang, *J. Catal.*, 2013, **300**, 197-200.

(22) S. T. Oyama, P. Clark, V. L. S. Teixeira da Silva, E. J. Lede and F. G. Requejo, *J. Phys. Chem. B*, 2001, **105**, 4961-4966.

(23) S. F. Zaman and K. J. Smith, *Catal. Commun.*, 2009, **10**, 468-471.

(24) R. Xu, Y. Li, Z. Cao, J. Zheng, N. Zhang, B. Chen and W. Wang, *Catal. Commun.*, 2014, **51**, 63-67.

(25) S. Zaman, *Bulg. Chem. Commun.*, 2015, **47**, 125-132.

(26) S. Wang, H. Ge, S. Sun, J. Zhang, F. Liu, X. Wen, X. Yu, L. Wang, Y. Zhang, H. Xu, J. C. Neuefeind, Z. Qin, C. Chen, C. Jin, Y. Li, D. He and Y. Zhao, *J. Am. Chem. Soc.*, 2015, **137**, 4815-4822.

(27) X. Dai, K. Du, Z. Li, H. Sun, Y. Yang, X. Zhang, X. Li and H. Wang, *Chem. Eng. Sci.*, 2015, **134**, 572-580.

(28) B. Guo, K. Yu, H. Li, H. Song, Y. Zhang, X. Lei, H. Fu, Y. Tan and Z. Zhu, *ACS Appl. Mater. Interfaces*, 2016, **8**, 5517-5525.

(29) G. Ye, Y. Gong, J. Lin, B. Li, Y. He, S. T. Pantelides, W. Zhou, R. Vajtai and P. M. Ajayan, *Nano Lett.*, 2016, **16**, 1097-1103.

(30) J. Kibsgaard, Z. Chen, B. N. Reinecke and T. F. Jaramillo, *Nat. Mater.*, 2012, **11**, 963-969.

(31) B. T. Yonemoto, G. S. Hutchings and F. Jiao, *J. Am. Chem. Soc.*, 2014, **136**, 8895-8898.

(32) K. S. Hayes, *Appl. Catal., A*, 2001, **221**, 187-195.

(33) A. Baiker and J. Kijenski, *Cat. Rev.*, 1985, **27**, 653-697.

(34) D. M. Roundhill, *Chem. Rev.*, 1992, **92**, 1-27.

(35) K. Klier, R. G. Herman and G. A. Vedage, *US4642381 A, to Lehigh University*, 1987.

(36) D. R. Corbin, S. Schwarz and G. C. Sonnichsen, *Catal. Today*, 1997, **37**, 71-102.

(37) G. Henrici-olivé and S. Olivé, *J. Mol. Catal.*, 1978, **4**, 379-383.

(38) B. Eliasson, P. Riemer and A. Wokaun, *Proceeding of the 4th Inter. Conf. on Greenhouse Gas Control Technologies, Interlaken, Switzerland*, 1999.

(39) S. V. Gredig, R. A. Koeppel and A. Baiker, *J. Chem. Soc., Chem. Commun.*, 1995, 73-74.

(40) S. V. Gredig, R. A. Koeppel and A. Baiker, *Appl. Catal., A*, 1997, **162**, 249-260.

(41) S. V. Gredig, R. A. Koeppel and A. Baiker, *Catal. Lett.*, 1997, **46**, 49-55.

(42) S. V. Gredig, R. Koeppel and A. Baiker, *Catal. Today*, 1996, **29**, 339-342.

(43) S. V. Gredig, R. Maurer, R. Koeppel and A. Baiker, *J. Mol. Catal. A: Chem.*, 1997, **127**, 133-142.

(44) S. M. Auer, S. V. Gredig, R. A. Köppel and A. Baiker, *J. Mol. Catal. A: Chem.*, 1999, **141**, 193-203.

(45) J. J. Lin and J. F. Knifton, *US4794199 A, to Texaco Inc.*, 1988.

(46) J. F. Knifton and J. J. Lin, *J. Mol. Catal.*, 1993, **81**, 27-36.

(47) R. Andersson, M. Boutonnet and S. Järås, *Fuel*, 2013, **107**, 715-723.

(48) L. Gang, Z. Chengfang, C. Yanqing, Z. Zhibin, N. Yianhui, C. Linjun and Y. Fong, *Appl. Catal., A*, 1997, **150**, 243-252.

(49) J. M. Christensen, P. A. Jensen and A. D. Jensen, *Ind. Eng. Chem. Res.*, 2011, **50**, 7949-7963.

(50) M. Badawi, S. Cristol, J.-F. Paul and E. Payen, *C. R. Chim.*, 2009, **12**, 754-761.

(51) M. A. Karolewski and R. G. Cavell, *Surf. Sci.*, 1989, **219**, 261-276.